

AD-A144 639

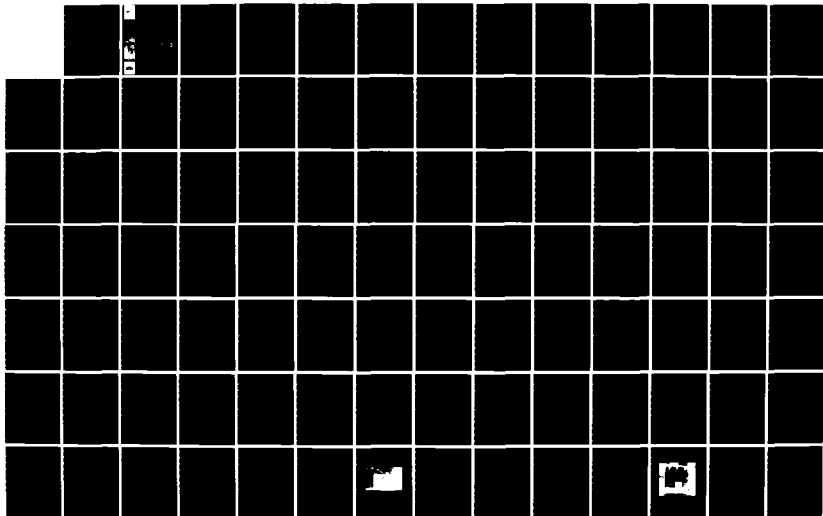
SCALE AND TIME EFFECTS IN HYDRAULIC FRACTURING (U)  
CALIFORNIA UNIV BERKELEY DEPT OF CIVIL ENGINEERING  
H WIDJAJA ET AL. JUL 84 DACW39-81-C-0024

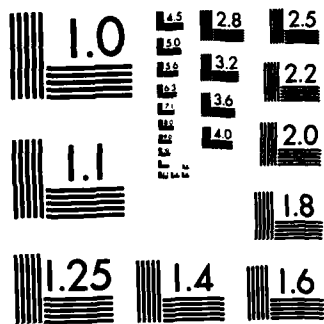
1/3

UNCLASSIFIED

F/G 20/11

NL





MICROCOPY RESOLUTION TEST CHART  
NATIONAL BUREAU OF STANDARDS-1963-A

12

MISCELLANEOUS PAPER GL-84-10

# SCALE AND TIME EFFECTS IN HYDRAULIC FRACTURING

by

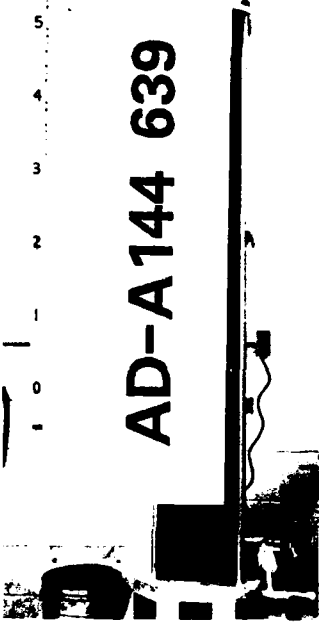
Hadi Widjaja, James Michael Duncan, H. Bolton Seed

Department of Civil Engineering  
University of California  
Berkeley, California 94720



US Army Corps  
of Engineers

AD-A144 639



DTIC FILE COPY



July 1984  
Final Report

Approved For Public Release. Distribution Unlimited

DTIC  
ELECTE  
AUG 15 1984  
B

Prepared for DEPARTMENT OF THE ARMY  
US Army Corps of Engineers  
Washington, DC 20314

Under Contract No. DACW39-81-C-0024  
(CWIS Work Unit 31211)

Monitored by Geotechnical Laboratory  
US Army Engineer Waterways Experiment Station  
PO Box 631, Vicksburg, Mississippi 39180

84 08 13 011

Destroy this report when no longer needed. Do not  
return it to the originator.

The findings in this report are not to be construed as an  
official Department of the Army position unless so  
designated by other authorized documents.

The contents of this report are not to be used for  
advertising, publication, or promotional purposes.  
Citation of trade names does not constitute an  
official endorsement or approval of the use of such  
commercial products.

Unclassified

SECURITY CLASSIFICATION OF THIS PAGE (When Data Entered)

REPORT DOCUMENTATION PAGE		READ INSTRUCTIONS BEFORE COMPLETING FORM
1. REPORT NUMBER Miscellaneous Paper GL-84-10	2. GOVT ACCESSION NO. <b>AD-A144639</b>	3. PRECISENT'S CATALOG NUMBER
4. TITLE (and Subtitle) SCALE AND TIME EFFECTS IN HYDRAULIC FRACTURING	5. TYPE OF REPORT & PERIOD COVERED Final Report	
7. AUTHOR(s) Hadi Widjaja, James Michael Duncan, and H. Bolton Seed		6. PERFORMING ORG. REPORT NUMBER
9. PERFORMING ORGANIZATION NAME AND ADDRESS University of California Department of Civil Engineering Berkeley, California 94720		8. CONTRACT OR GRANT NUMBER(s) Contract No. DACW39-81-C-0024
11. CONTROLLING OFFICE NAME AND ADDRESS DEPARTMENT OF THE ARMY US Army Corps of Engineers Washington, DC 20314		10. PROGRAM ELEMENT, PROJECT, TASK AREA & WORK UNIT NUMBERS CWIS Work Unit 31211
14. MONITORING AGENCY NAME & ADDRESS (if different from Controlling Office) US Army Engineer Waterways Experiment Station Geotechnical Laboratory PO Box 631, Vicksburg, Mississippi 39180		12. REPORT DATE July 1984
		13. NUMBER OF PAGES 205
		15. SECURITY CLASS. (of this report) Unclassified
16. DISTRIBUTION STATEMENT (of this Report) Approved for public release; distribution unlimited.		15a. DECLASSIFICATION/DOWNGRADING SCHEDULE
17. DISTRIBUTION STATEMENT (of the abstract entered in Block 20, if different from Report)		
18. SUPPLEMENTARY NOTES Available from National Technical Information Service, 5285 Port Royal Road, Springfield, Va. 22161.		
19. KEY WORDS (Continue on reverse side if necessary and identify by block number) Compaction                      Laboratory tests                      Tensile stress Cracking (fracturing)              Seepage                      Water content Dams                      Soil density                      Water pressure Erosion                      Tensile strength (soils) Hydraulic fracturing		
20. ABSTRACT (Continue on reverse side if necessary and identify by block number) - An experimental study was conducted to determine the effects of scale and time on hydraulic fracturing in compacted samples of Teton Dam silt and Pittsburg silty clay. A theory was developed to show how size of opening, time of pressurizing opening, and soil permeability are related to the occurrence of hydraulic fracturing. Finite element analyses were used to investigate the possible effects of nonlinear soil behavior. Both experimental and theoretical studies show that hydraulic fracturing can be initiated by seepage-induced forces without the presence of a preexisting flaw in the soil.		

## PREFACE

The work described in this report was performed under Contract No. DACW39-81-C-0024, dated 1 January 1981, as part of work being performed at the U. S. Army Engineer Waterways Experiment Station (WES), Vicksburg, Miss., on "Material Characterization and Analysis of Cracking in Embankment Dams," with funds provided by the Office, Chief of Engineers, U. S. Army, under CWIS Work Unit 31211. Technical monitor for OCE was Mr. Richard Davidson.

This report was prepared by Dr. Hadi Widjaja and Professors James Michael Duncan and H. Bolton Seed, University of California at Berkeley. The work was monitored by Dr. John F. Peters, Soil Research Center (SRC), Soil Mechanics Division (SMD), Geotechnical Laboratory (GL), under the general supervision of Mr. Gene P. Hale, Chief, SRC, Mr. Clifford L. McAnear, Chief, SMD, and Dr. William F. Marcuson III, Chief, GL.

GOL Tilford C. Creel, CE, was Commander and Director of WES during the period of study. Mr. F. R. Brown was Technical Director.

Accession For	
NTIS GRA&I	<input checked="" type="checkbox"/>
DTIC TAB	<input type="checkbox"/>
Unannounced	<input type="checkbox"/>
Justification	
By	
Distribution/	
Availability Codes	
Avail and/or	
Dist	Special
A-1	

## CONTENTS

		<u>Page</u>
PREFACE		1
CHAPTER I	INTRODUCTION	4
CHAPTER II	LITERATURE REVIEW	6
	Hydraulic Fracturing in Dams	6
	Hydraulic Fracturing for Petroleum Production	7
	Hydraulic Fracturing for Stress Measurement	8
	Experimental Studies of Size Effects	10
	Experimental Studies of Time Effects	20
	Experimental Studies of Permeability Effects	27
	Experimental Studies of Water Content and Density Effects	27
	Summary	29
CHAPTER III	THEORETICAL ANALYSES	31
	Review of Previous Hydraulic Fracturing Theories	31
	New Theory of Hydraulic Fracturing	40
	Finite Element Analyses	62
CHAPTER IV	EXPERIMENTAL STUDY	77
	Description of Soils	77
	Hydraulic Fracturing Equipment	82
	Preparation of Samples	90
	Types of Tests	95
	Testing Procedure	104
	Testing Program	104
CHAPTER V	PRESENTATION AND DISCUSSION OF TEST RESULTS	107
	Effect of Groove Size in Type I Tests	107
	Effect of Slot Size, Water Content, and Density in Type IV Tests	111
	Effect of Transition Material in Type V Tests	128
	Effect of Test Duration in Borehole Fracturing Tests	135

	<u>Page</u>
Effects of Borehole Length and Confining Pressures	149
Effect of Borehole Diameter	154
Effect of Water Content in Borehole Fracturing Tests	162
Effect of Density in Borehole Fracturing Tests	164
Summary	170
 CHAPTER VI	
COMPARISONS OF THEORETICAL WITH EXPERIMENTAL VALUES OF HYDRAULIC FRACTURING PRESSURES	173
Effect of Horizontal Stress	173
Effect of Test Duration	173
Effect of Borehole Diameter	175
A Note on the Effect of Rate of Pressurizing	179
 CHAPTER VII	
SUMMARY AND CONCLUSIONS	182
Prerequisite Conditions for Hydraulic Fracturing	182
Theoretical Studies	183
Experimental Study	186
 REFERENCES	189
 APPENDIX A	
DERIVATIONS OF EQUATIONS	A1
 APPENDIX B	
LIST OF SYMBOLS	B1

## SCALE AND TIME EFFECTS IN HYDRAULIC FRACTURING

### I. INTRODUCTION

Hydraulic fracturing can be defined as "a condition leading to the creation and propagation of a thin physical separation in a soil whenever the hydraulic pressure exerted on a surface of the soil exceeds the sum of the total normal stress on the surface and the tensile strength of the soil" (Seed et al, 1976).

Hydraulic fracturing has been suspected to be the cause of excessive leakage in a number of dams, e.g. Hyttejuvet Dam (Kjaernsli and Torblaa, 1968), Balderhead Dam (Vaughan et al, 1970), Viddalsvatn Dam (Vestad, 1976), and of the failure of Teton Dam (Independent Panel to Review Cause of Teton Dam Failure, 1976).

Hydraulic fracturing has occurred in boreholes in a number of dams, resulting in sudden losses of drilling mud, e.g., Djatiluhur Dam and Shek Pik Dam (Sherard, 1972), Akosombo and La Vallita Dam (Wilson and Squier, 1969). Hydraulic fracturing has also been observed to occur in boreholes during field permeability testing using very high pressures. (Bjerrum et al, 1972).

In the petroleum industry, hydraulic fracturing has been used for over 30 years as a means of "opening up" producing formations and thereby increasing oil production. This process consists of injecting a viscous liquid containing a granular material such as sand under high pressure to fracture the formation (Clark, 1949). The sand serves as a "propping agent," holding the fractures open. In the form of "mud-jacking," hydraulic fracturing has been used for many decades by geotechnical engineers to restore pavements and structural levels. In geotechnical exploration, it

has been used recently to determine the in-situ stresses (Bjerrum and Andersen, 1972; Bozozuk, 1974; Massarch and Broms, 1976).

It is apparent from the foregoing discussion that hydraulic fracturing is an important phenomenon in both soil and rock mechanics. Therefore, it has been the subject of a number of research studies in both fields. A number of these studies have employed laboratory samples with model boreholes drilled in the center to investigate the factors that control hydraulic fracturing. The studies have shown that the hydraulic fracturing pressure is dependent on parameters such as the initial stresses in the soil or rock around the borehole, the borehole size, the test duration, and the permeability of the soil.

These studies provide a good basic understanding of the phenomenon of hydraulic fracturing and a number of the factors that influence its occurrence. There are, however, a number of factors that are not sufficiently well understood to make it possible to understand fully how laboratory studies of hydraulic fracturing can be applied to full-scale field conditions. To determine more precisely how to assess the potential for hydraulic fracturing under field conditions, it would be very desirable to have a comprehensive theory capable of showing how time, scale, and permeability effects are related to the occurrence of hydraulic fracturing in the laboratory and the field. The studies described in the subsequent chapters were directed to the development of such a theory and to performing additional laboratory tests to provide a systematic basis for investigating its validity and effectiveness.

## II. LITERATURE REVIEW

A number of laboratory, field, and analytical studies of hydraulic fracturing in soil and rock have been conducted in recent years. These provide a basic understanding of the phenomenon. The findings of these studies are summarized in the following pages.

### HYDRAULIC FRACTURING IN DAMS

Löfquist, a Swedish engineer, was probably the first to point out that arching of the core of a dam may result in leakage and erosion. In 1951, he described earth pressure measurements made in the thin impervious cores of the 26 m (85 ft) high Hölle Dam and that of the 34 m (112 ft) high Harspranget Dam. Measured vertical pressures were as low as half the normal overburden pressures, and he commented that while the arching effects were favorable as regards the stability of the dams, one should question if it gave rise to a risk of horizontal cracks in the impervious layer which might have a detrimental effect on its ability to serve as a seepage barrier. In discussing a paper on arching theory by Trollope (1957), Löfquist re-emphasized this point and said "the case where the vertical pressure decreases to a value lower than the water pressure at the same level may also be considered as detrimental to the water tightness and performance of an earth core."

In 1968 for the first time the leakage of a dam was attributed to hydraulic fracturing. The incident which occurred at the 93 m (305 ft) high Hyttejuvet Dam in Norway, was reported by Kjaernsli and Torblaa

(1968); unexpected leakage occurred during the first filling of the reservoir.

Several other similar incidents were reported subsequently in the literature. Vaughan et al (1970) reported that unusual leakage occurred just before the reservoir became full during the initial filling of Balderhead Dam in England. Sherard et al (1972) investigated the failures of fourteen low flood control dams in Oklahoma and Mississippi, and concluded these failures could possibly be attributed to hydraulic fracturing. Sherard (1973) reported the failures of Stockton Creek Dam and Wister Dam, and the leakage at Yard's Creek Upper Reservoir Dam, which were also suspected to have suffered hydraulic fracturing. Vestad (1976) investigated the leakage that occurred at the Viddalsvatn Dam in Norway after its reservoir became full for the first time, and suggested that the leakage might be due to hydraulic fracturing. The independent panel to investigate the cause of the failure of Teton Dam in Idaho (1976), which failed completely during the first reservoir filling, identified hydraulic fracturing as a possible cause.

#### HYDRAULIC FRACTURING FOR PETROLEUM PRODUCTION

Hydraulic fracturing has been used since the 1940's in the oil industry as a method of enhancing the production of oil wells (Clark, 1949). The method consists of applying a sufficiently high hydraulic pressure to the walls of a sealed-off borehole section to cause hydraulic fracturing of the surrounding rock. The fractures are extended as far as possible to create new flow channels in the rock and increase production of crude oil. The fracturing medium is frequently a specially treated oil carrying a granular material (e.g. sand) in suspension. This so-called propping agent serves to hold the fractures open after the injection pressure is released.

## HYDRAULIC FRACTURING FOR STRESS MEASUREMENT

An analysis of the mechanics of hydraulic fracturing in rocks was published by Hubbert and Willis (1957). They assumed that the principal stresses at great depth were oriented vertically and horizontally, and that the two horizontal principal stresses were not necessarily equal. They suggested that a hydraulic fracture would propagate in a direction perpendicular to the smallest compressive principal stress, and that the magnitude of the fluid pressure required to propagate the fracture would be equal to or larger than that stress. They suggested that vertical fracture in a vertical borehole would occur by tensile rupture at the wall of the hole as the fluid pressure was increased. Assuming that the rock is elastic and isotropic, the borehole is very long, the tensile strength of the rock is negligible, and the fluid does not penetrate into the formation before fracture, they deduced that the pressure required to initiate a vertical fracture at the borehole wall would be equal to three times the smaller horizontal principal effective stress minus the other horizontal principal effective stress.

A study of the possibility of using hydraulic fracturing as a technique to determine the stresses in rocks was undertaken by Haimson (1968). The main purpose of his study was to verify his theoretical analysis of hydraulic fracturing for porous and non-porous rocks. He demonstrated that the fractures always occur perpendicular to the least compressive stress. He also investigated experimentally the effect of the borehole size and the rate of pressurizing the borehole. The results of these tests will be discussed more thoroughly later in this chapter.

Based on the method used by Haimson (1968), Bjerrum and Andersen (1972) developed a hydraulic fracturing procedure to determine the lateral pressure in clayey soils. This procedure employs a piezometer installed

in the soil at the location where the stresses are to be measured. After allowing the disturbed zone around the piezometer to consolidate, water pressure is applied through the piezometer into the clay until the soil around it fractures. The direction of the crack is dependent on the coefficient of earth pressure at rest,  $K_0$ . If the value of  $K_0$  is greater than one, a horizontal crack will develop. If  $K_0$  is less than one, the crack will be vertical.

Bjerrum et al (1972) indicated that the pressure to cause hydraulic fracturing around a piezometer was influenced by a number of factors, including (1) the initial state of stress and water pressure in the ground, (2) the changes in these stresses arising from the installation of the piezometer and any other disturbance of the soil, (3) the magnitude of the pressure increments and the time increments, (4) the deformation characteristics and the degree of homogeneity of the soil around the piezometer, and (5) the geometry of the piezometer tip. To avoid the uncertainties concerning these factors that influence when a fracture opens, Bjerrum and Andersen (1972) related the pressure at which the crack closes to the in-situ stress. To measure the pressure using their procedure, the water pressure is decreased after a fracture has developed, allowing the crack to close. When the crack closes, the flow rate of water decreases abruptly. Bjerrum and Andersen (1972) suggested that the pressure at which the flow rate of water decreases abruptly was close to the minor principal stress. A laboratory experiment using triaxial samples supported their concepts.

Massarch et al (1975) compared the measurements of in-situ horizontal stress at five sites in Sweden using the hydraulic fracturing method and Glötzl earth pressure cells. The agreement between the two methods was found to be poor. In a later paper, Massarch (1978) stated that the

hydraulic fracturing test was complex and difficult to analyze. He suggested that the factors that can be of significance in hydraulic fracturing were: (1) effect of piezometer installation, (2) initial stress conditions and changes of stress due to fracturing, (3) local inhomogeneities and prescribed fracture planes (e.g. due to compaction of an earth dam), (4) time after installation of piezometer and duration of tests, (5) applied maximum pressure and volume of water pumped into the soil, (6) effect of repetitive loading (number of tests performed in the same borehole), (7) effect of arching around the cylindrical piezometer, (8) number of fractures and their extension from the piezometer, and (9) the possibility of arching along irregularly shaped cracks.

#### EXPERIMENTAL STUDIES OF SIZE EFFECTS

##### Effect of Borehole Diameter

Haimson (1968) performed borehole hydraulic fracturing tests on five rock types in the laboratory. The samples were either cubical or cylindrical. The cubical samples were 12.7 cm X 12.7 cm (5 in X 5 in) in horizontal cross section and 14.0 cm (5.5 in) in height. The cylindrical samples were 12.7 cm (5 in) in diameter and 15.2 cm (6 in) in height.

The cylindrical samples were tested in a standard pressure jacket through which a hydrostatic horizontal loading was applied. The cubical samples were subjected to horizontal stresses from flat jacks which were independently controlled, allowing non-hydrostatic triaxial loading. The vertical stresses were generated by loading a steel platen with a compression testing machine. A channel in this platen was used to transmit pressurized fluid to a vertical borehole in the center of the samples. Seven types of oils were used as pressurizing fluid. The viscosity of the oils varied from 64 to 2100 centipoises at room temperature (75°F = 24°C).

The tests were performed by pressurizing the fluid in the borehole while the external loads were kept constant. The borehole fluid pressure was increased until a fracture was initiated, which was indicated by a sudden drop in the internal pressure and a sharp increase in the compressive load acting perpendicular to the fracture plane.

Haimson (1968) investigated the effect of borehole diameter on Tennessee marble and hydrostone. The Tennessee marble was described as a fine crystalline limestone containing mainly calcite. It was fairly uniform in texture and composition, with no preferred orientation in its crystals; therefore, it was considered isotropic and homogeneous. The hydrostone samples were prepared in the laboratory by mixing fixed quantities of water and a gypsum cement known commercially as Hydrostone. Three mixes were used: 30/100 (30 parts water to 100 parts Hydrostone, by weight), 32/100, and 35/100.

Ten tests were performed by Haimson to investigate the effect of borehole diameter on hydraulic fracturing pressure in Tennessee marble. The length of the borehole was 5.1 cm (2 in) in all of the tests. Five of the tests were run with a vertical pressure of  $281 \text{ kg/cm}^2$  (4000 psi) and a horizontal pressure of  $105 \text{ kg/cm}^2$  (1500 psi). The other five were tested with a vertical pressure of  $70 \text{ kg/cm}^2$  (1000 psi) and a horizontal pressure of  $141 \text{ kg/cm}^2$  (2000 psi). The rate of pressurizing was  $1.05 \text{ kg/cm}^2/\text{sec}$  (15 psi/sec). The diameter of the borehole varied from 0.79 cm (5/16 in) to 2.86 cm (1-1/8 in); therefore, the ratio of sample diameter to borehole diameter varied from 4 to 16.

The results of the tests are shown in Figure 2.1. It can be seen that the hydraulic fracturing pressure decreases as borehole diameter increases. Haimson attributed this behavior to a size effect on the tensile strength value.

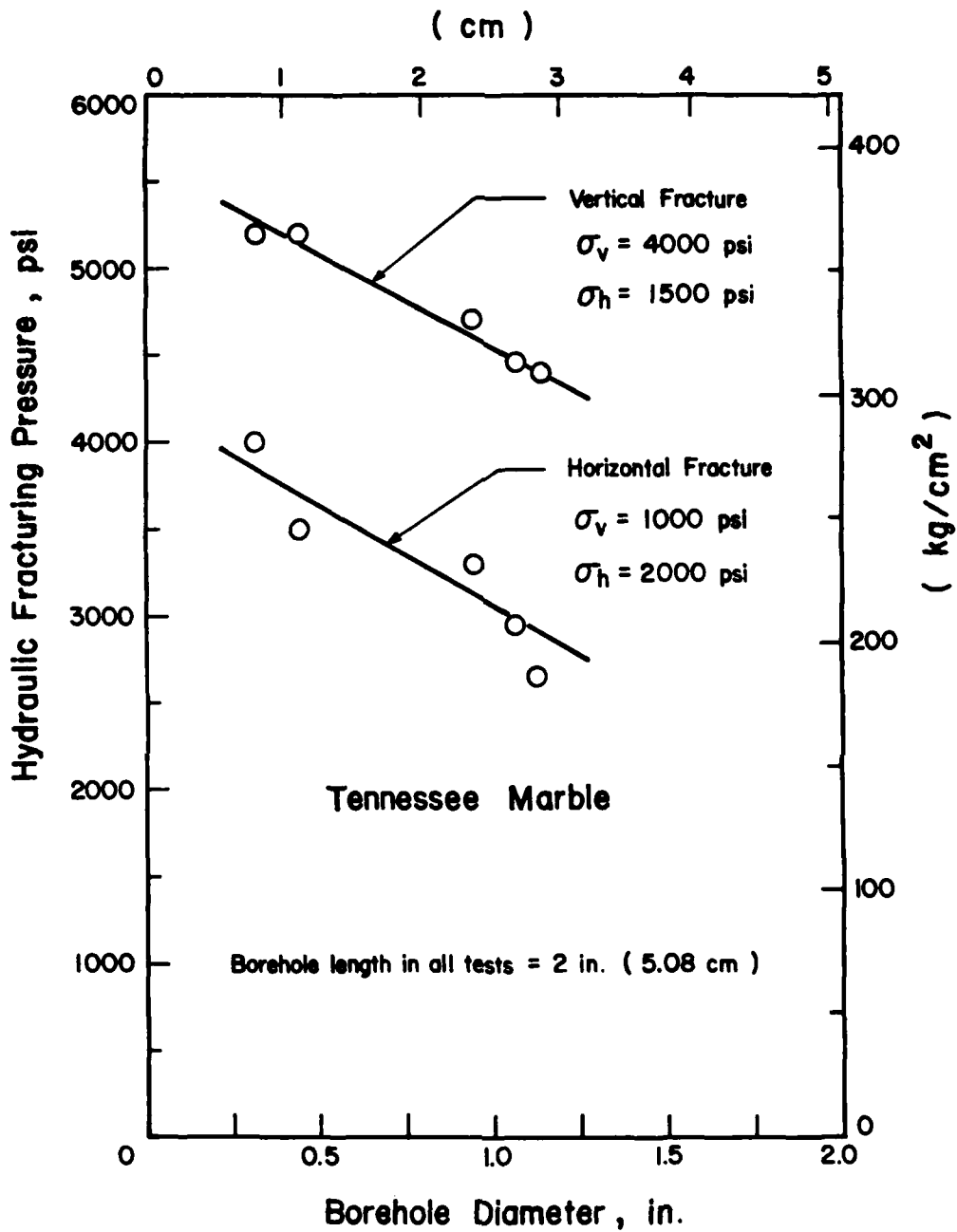


Figure 2.1 Effect of borehole diameter on hydraulic fracturing pressure in Tennessee Marble (after Haimson, 1968)

Haimson (1968) also studied the effect of borehole diameter on hydraulic fracturing pressure in Hydrostone. In one test series, the borehole length was kept constant at 5.1 cm (2 in); in another series, the ratio of the borehole length to its diameter was kept constant at 2. The tests were performed using four diameters ranging from 0.79 cm (5/16 in) to 3.49 cm (1-3/8 inch).

The tests with constant borehole length were carried out in two groups. In the first group, confining pressures were applied in three principal directions, while in the second group, the horizontal stress was zero. Therefore, in the second group, the fracturing pressure was a measure of the apparent tensile strength of the rock. The results of these tests are shown in Figure 2.2. The results showed that the hydraulic fracturing pressure decreased as the borehole diameter increased. Haimson attributed this behavior to a decrease in the "apparent tensile strength" of the hydrostone as the diameter increased.

The results of the tests where the ratio of the borehole length to its diameter was kept constant are shown in Figure 2.3. Again it can be seen that the hydraulic fracturing pressure decreased as the borehole diameter increased. Haimson suggested that the larger the borehole size, the larger the fluid to rock contact area, and the greater the number of weak points in the rock that would be exposed to the high pressure, leading to a greater likelihood of failure at lower pressure.

Von Schonfeldt (1970) conducted an experimental study of the use of hydraulic fracturing as a technique for stress measurement. He also investigated the effect of borehole diameter on hydraulic fracturing pressure. The rock he used was a pink granite, described as coarse grained, with feldspar crystals ranging up to 2.5 cm (1 in) in size. Although these crystals contained many fissures, the material exhibited only a

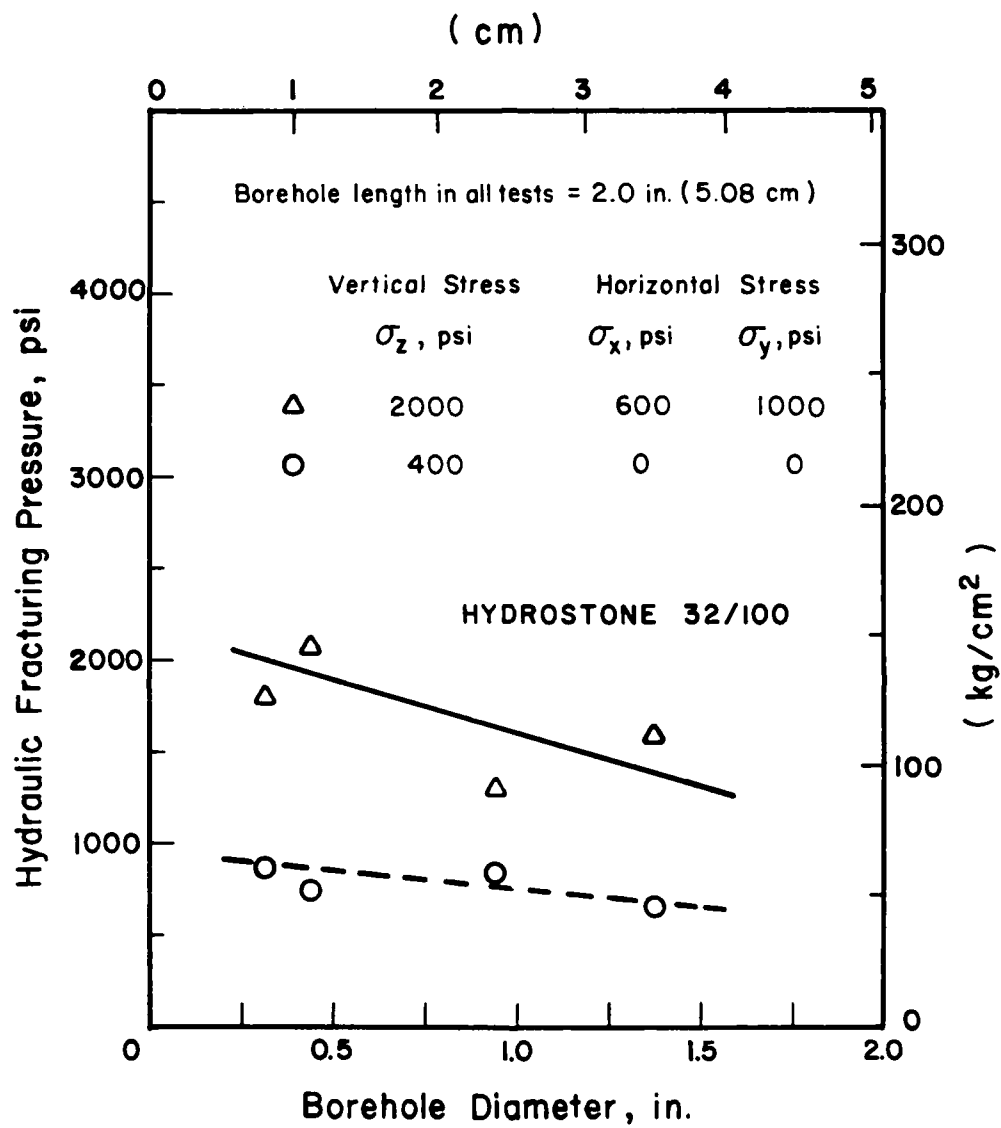


Figure 2.2 Effect of borehole diameter on hydraulic fracturing pressure in hydrostone 32/100 (after Haimson, 1968)

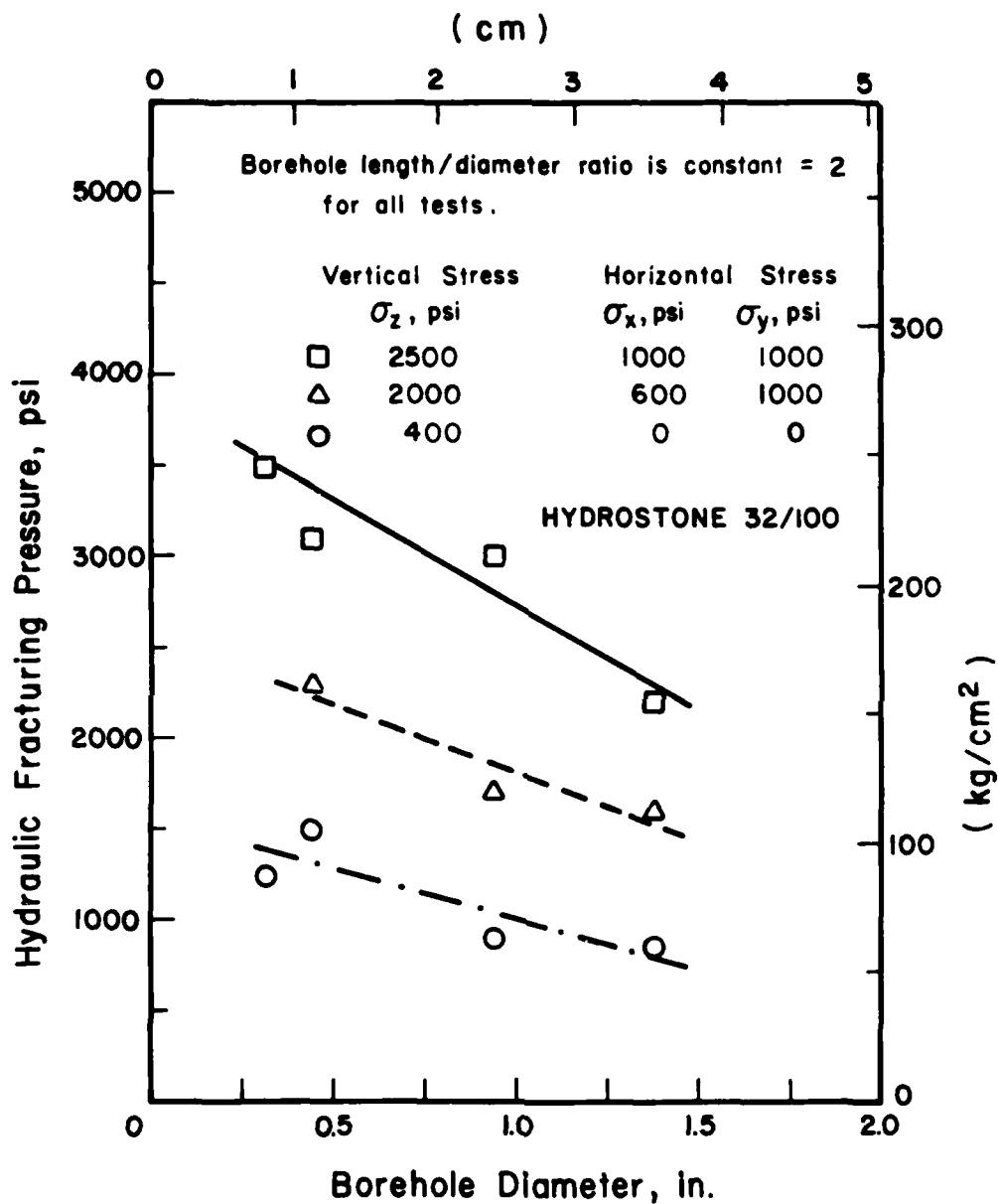


Figure 2.3 Effect of borehole size on hydraulic fracturing pressure in hydrostone 32/100 (after Haimson, 1968)

small amount of inelastic behavior.

Two sizes of samples were tested by Von Schonfeldt. The smaller were 20.3 cm (8 in) in diameter. The diameters of the boreholes in these samples were 1.1 cm (7/16 in); thus the ratio of the sample diameter to borehole diameter was 18. The large size samples were 160 cm (63 in) in diameter. The diameters of the boreholes in these samples were 5.7 cm (2-1/4 in); thus the ratio of the sample diameter to borehole diameter was 28. The rate of loading was  $42 \text{ kg/cm}^2/\text{sec}$  (600 psi/sec) for the small samples and  $70 \text{ kg/cm}^2/\text{sec}$  (1000 psi/sec) for the large samples. The average fracturing pressure of the small samples was  $246 \text{ kg/cm}^2$  (3505 psi) and that of large samples was  $258 \text{ kg/cm}^2$  (3675 psi). Thus the average fracturing pressures for the small and the large samples were within about 5 percent, even though the size of the boreholes differed by a factor of more than 5. Von Schonfeldt (1970) concluded that the size of a borehole does not affect the hydraulic fracturing pressure as long as the sample dimensions are large relative to the borehole diameter.

#### Effect of Borehole Length

Haimson (1968) performed 15 tests to investigate the effect of borehole length on the hydraulic fracturing pressure in Hydrostone 35/100. He kept the borehole diameter constant at 0.79 cm (5/16 in) and varied the length from 0.64 cm (1/4 in) to 5.1 cm (2 in). The results of these tests are shown in Figure 2.4. The results showed that the hydraulic fracturing pressure decreased as the borehole length increased. Haimson suggested that the decrease in tangential stress produced by pressurized fluid at the borehole wall is lower when the borehole length is smaller; therefore, higher pressure was required to fracture the sample with a shorter borehole.

Lefebre et al (1981) conducted field hydraulic fracturing tests using piezometers at the Gloucester test site near Ottawa, Ontario. The soils

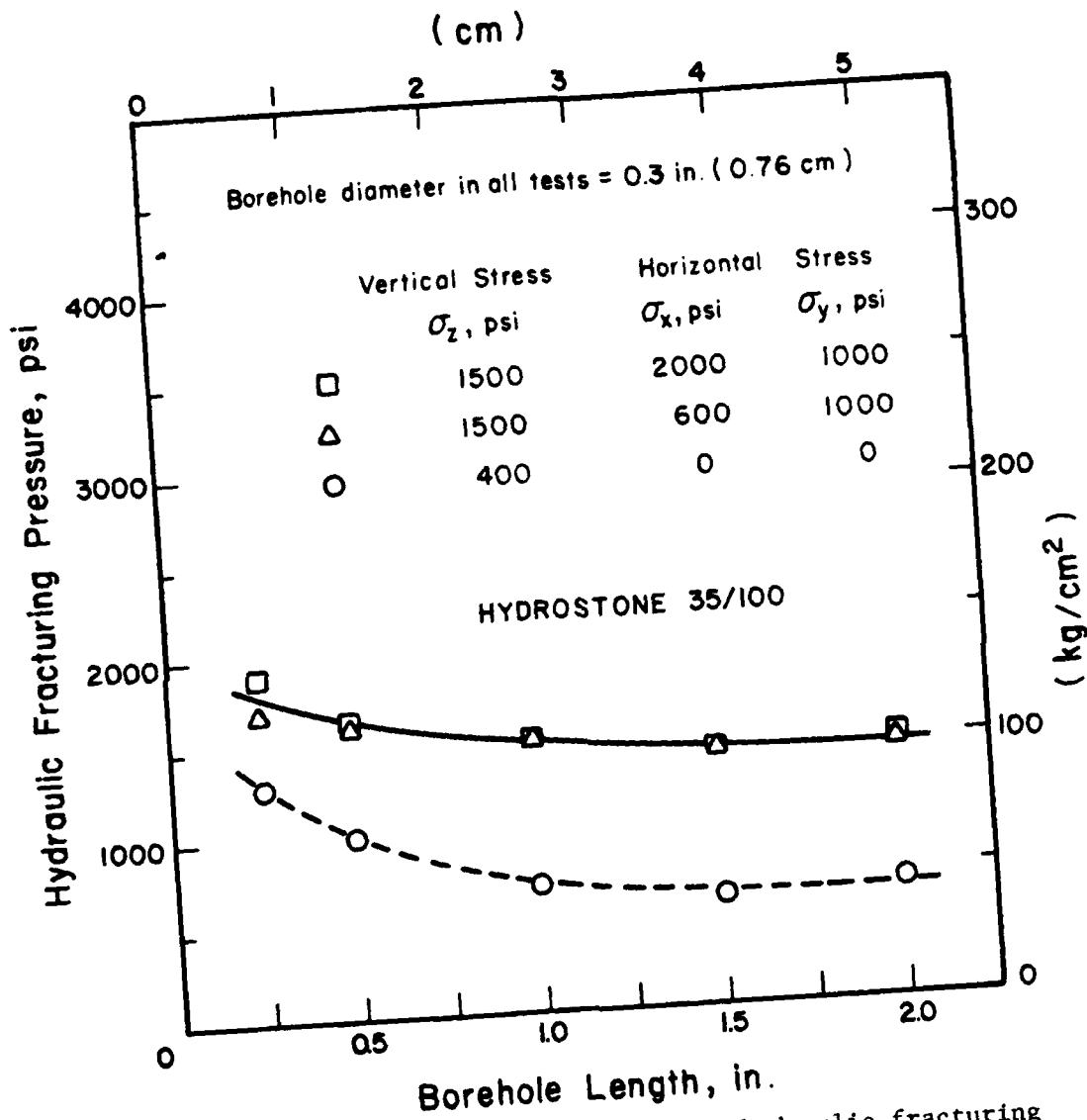


Figure 2.4 Effect of borehole length on hydraulic fracturing pressure in hydrostone 35/100 (after Haimson, 1968)

at Gloucester are marine clay deposits of the Champlain Sea. At the 4 m (13.1 ft) depth, where the hydraulic fracturing tests were conducted, the clay was normally consolidated, the water content was 75%, the liquid limit was 52%, and the sensitivity measured in-situ varied from 70 to 100.

Geonor piezometers made of porous bronze and 3.3 cm (1.3 in) in diameter were used to apply and measure water pressures on the sides of the holes surrounding the piezometers. Three lengths of piezometer were installed: 30 cm (11.8 in), 10 cm (3.9 in), and 0 cm. The piezometer tips of zero length were made from a porous bronze plate. After the piezometer tips had been saturated with deaired water, "E" size steel rods (O.D. about 3.6 cm) were fitted to them and jacked continuously into the ground until the desired depths were attained. The pressure in the piezometer was then built up gradually until fracturing occurred.

The fracturing tests were performed following the procedure developed by Bjerrum and Andersen (1972), except that a pressure transducer was used instead of a mercury manometer for measuring the pressure. The fractured clay was recovered using a large diameter block sampler. The fracturing pressures were not discussed by Lefebvre et al. However, the closing pressures, expressed as values of  $K_0$ , the coefficient of earth pressure at rest, are shown in Figure 2.5. The measured value increased from 0.68 for the longest piezometer to 0.91 for the zero length piezometer. Lefebvre et al (1981) suggested that the variation in measured value of  $K_0$  was due to the fracture mode around the piezometer tips. The longest piezometer produced the longest vertical fractures, the medium length piezometer produced shorter vertical fractures, and there were no vertical fractures around the piezometer of zero length. The fractures around the zero length piezometer were inclined, forming an inverted cone. Lefebvre et al

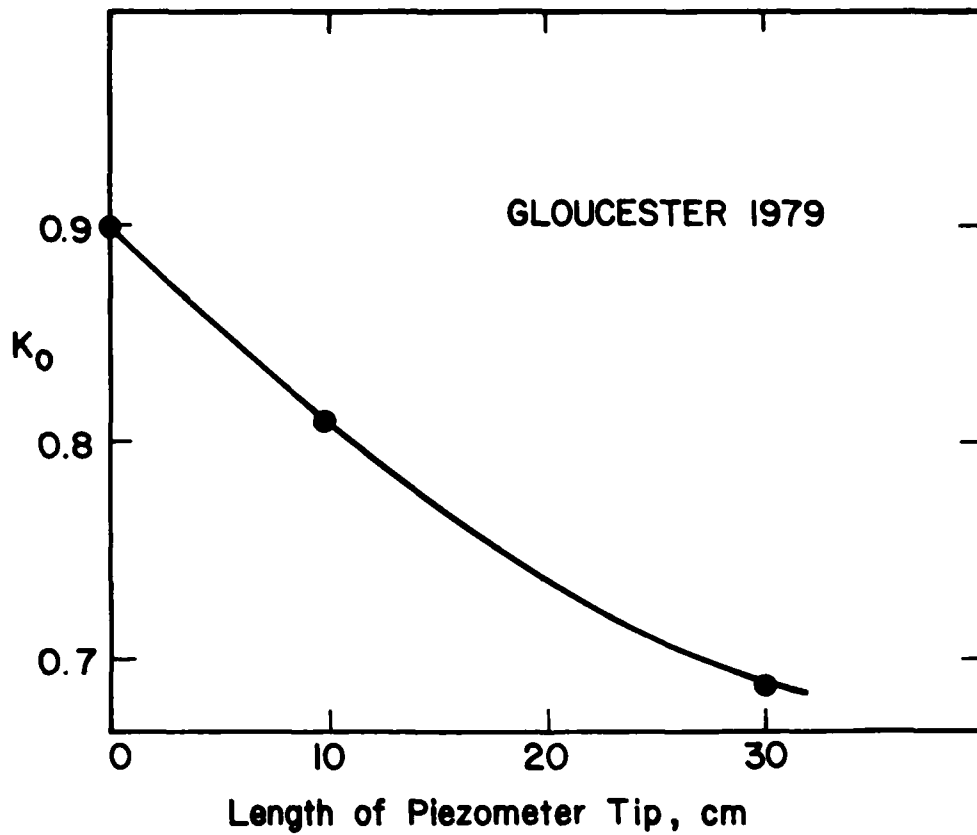


Figure 2.5 Influence of the length of piezometer tip on the calculated value of  $K_0$  (after Lefebvre et al., 1981)

(1981) suggested that the test with the longest piezometer was most influenced by the horizontal pressure, and the test with the zero length piezometer was strongly influenced by the vertical overburden pressure.

#### EXPERIMENTAL STUDIES OF TIME EFFECTS

Haimson (1966) investigated the effect of test duration on the hydraulic fracturing pressures in Tennessee marble, charcoal granite, and Hydrostone 32/100. The Tennessee marble and Hydrostone were described in the previous section. The charcoal granite used in the tests was a fine-grained granodiorite with abundant dark gray hornblende and biotite-rich inclusions. It also contained gray quartz and feldspar; it was uniform in texture and considered fairly isotropic.

The tests were carried out at three rates of loading:  $0.42 \text{ kg/cm}^2/\text{sec}$  (6 psi/sec),  $4.22 \text{ kg/cm}^2/\text{sec}$  (60 psi/sec), and  $42.20 \text{ kg/cm}^2/\text{sec}$  (600 psi/sec). The time to fracture varied from 2 to 500 seconds.

The results of these tests are shown in Figures 2.6 through 2.8. The results clearly showed that the longer the time to fracture, the lower was the fracturing pressure. Haimson attributed this result to the effect of rate of loading on the tensile strength. In the case of Hydrostone, Haimson also suggested that different degrees of fluid penetration into the rock, caused by different rates of loading, affected the test results. In tests where the rate was higher, the penetration of fracturing fluid was less, and Haimson suggested that the pressure required to fracture the sample was higher when the fluid penetration was less.

Kennard (1971) conducted a few tests to study the effect of test duration on hydraulic fracturing pressure in a silty clay material. The soil, called Harmondsworth brickearth, had the following properties: the liquid limit was 40%, the plastic limit was 18%, and the undrained strength was  $0.05 - 0.10 \text{ kg/cm}^2$  (100 - 200 psi).

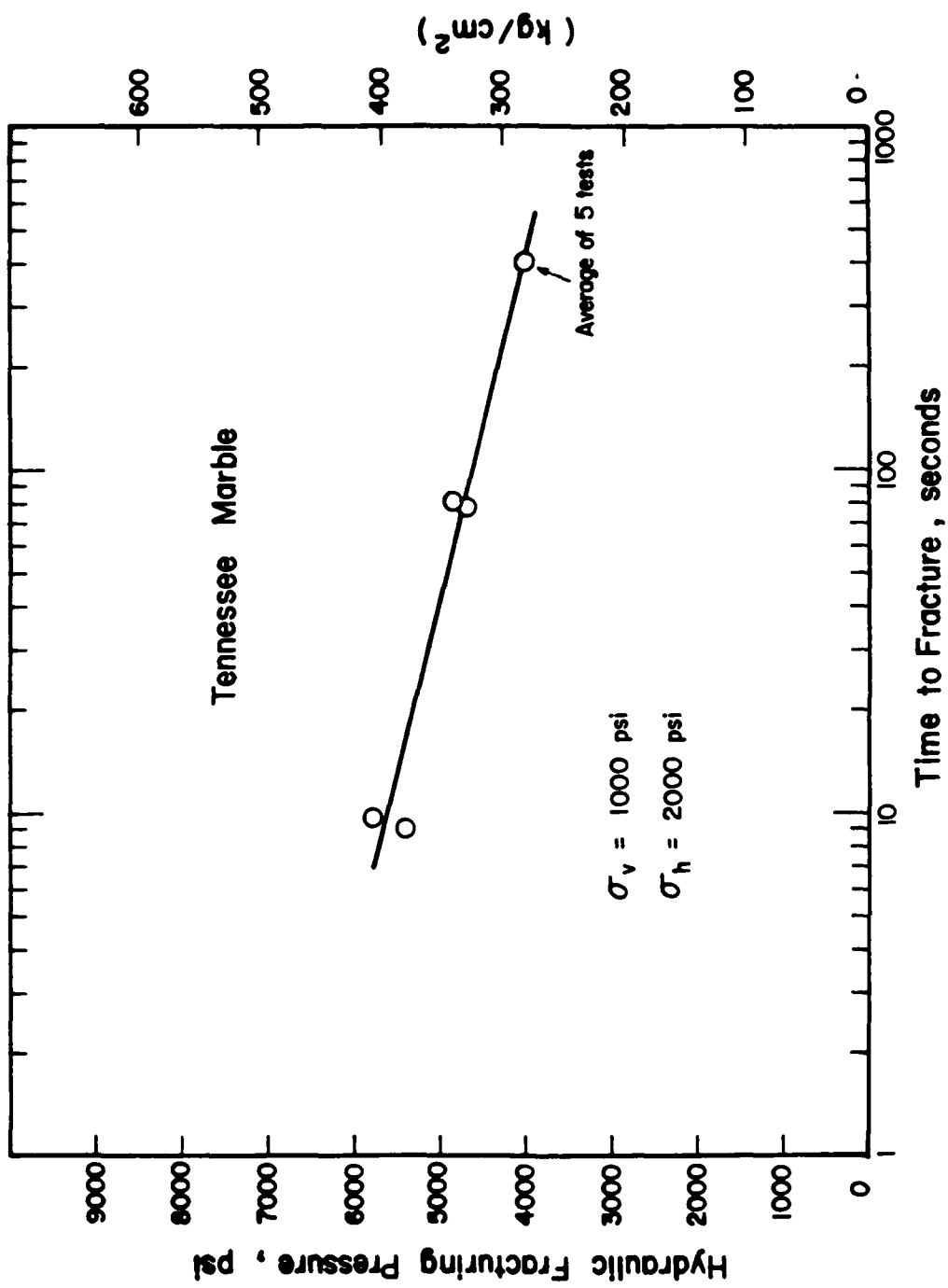


Figure 2.6 Effect of test duration on fracturing pressure in Tennessee Marble (after Haimson, 1968)

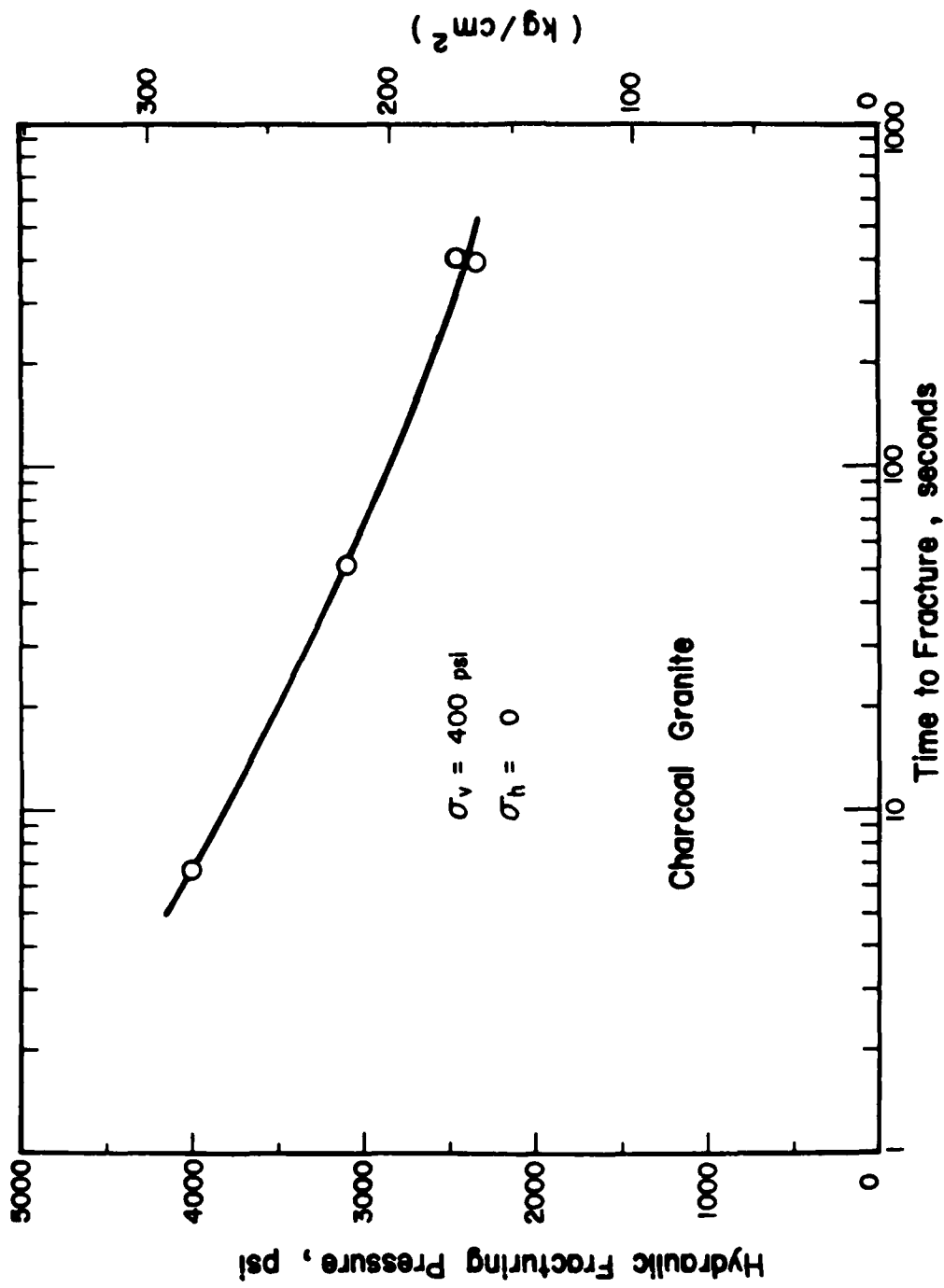


Figure 2.7 Effect of test duration on fracturing pressure in charcoal granite (after Haimson, 1968)

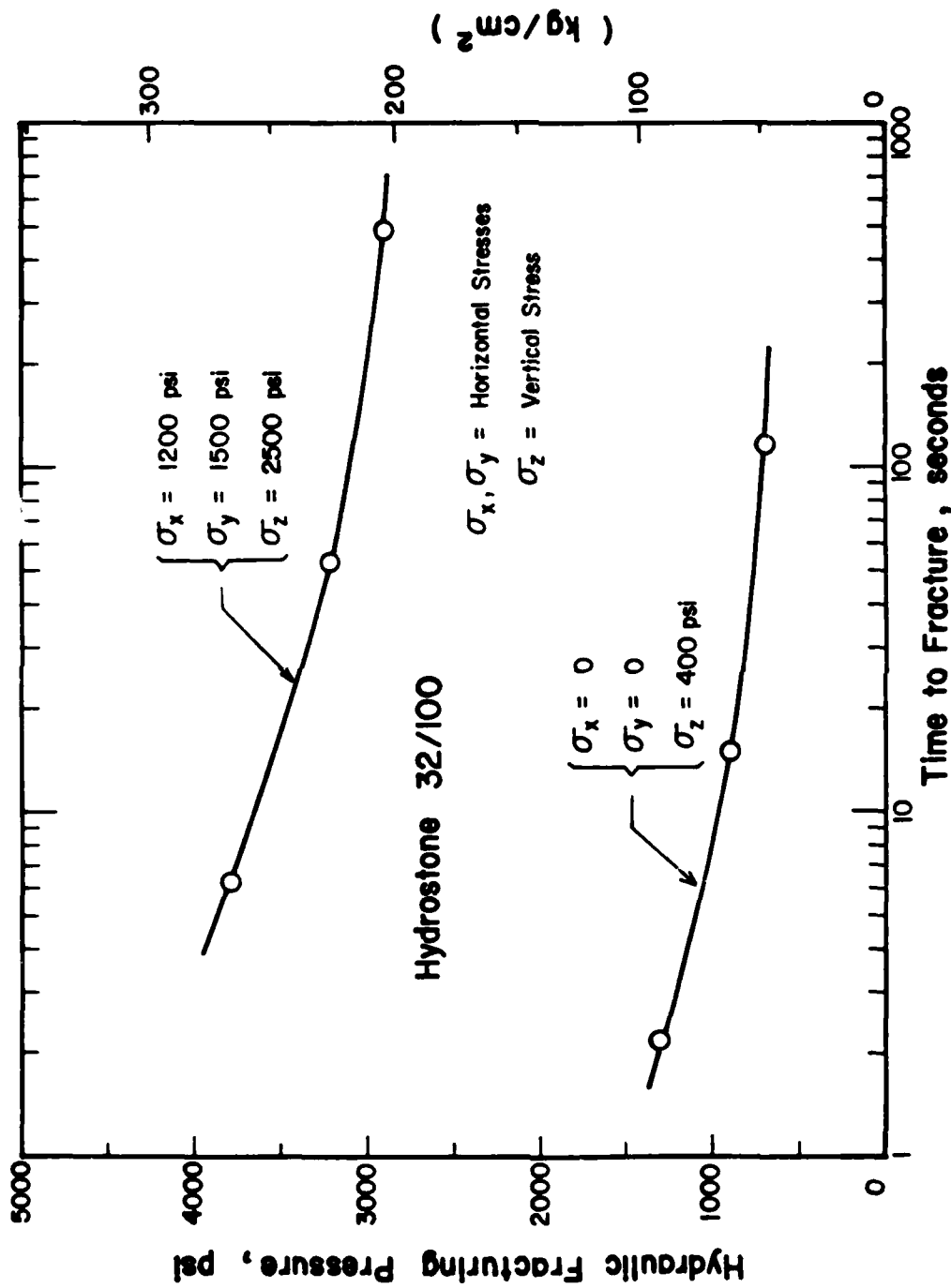


Figure 2.8 Effect of test duration on fracturing pressure in hydrostone 32/100 (after Haimson, 1968)

The pressure head was applied through a 0.63 cm (1/4 in) diameter piezometer, installed in the 25 cm (10 in) cubical samples. The head was raised in increments of 210 cm (82.7 in) until the measured flow rate showed a fundamental change. The time increments corresponding to each pressure increment varied from 10 minutes to 1 day. The results of the tests are shown in Figure 2.9. It may be seen that the fracturing pressure decreases as the time to fracture increases.

Jaworski et al (1979) conducted tests to investigate the effect of test duration on hydraulic fracturing pressure. The soil was obtained from the core of the remainder of Teton Dam after its failure. This material consisted primarily of aeolian silt, with some particles of caliche. The liquid limit varied from 28 to 32%, and the plasticity index from 3 to 6%.

The samples were compacted in a 19.1 cm (7.5 in) cubical mold. After compaction, the sample was placed in a 20.3 cm (8 in) cubical apparatus and the small gap around the sample was filled with soil of the same origin. The vertical confining pressure was  $4.0 \text{ kg/cm}^2$  ( $4.10 \text{ t/ft}^2$ ) and the horizontal confining pressure was  $2.0 \text{ kg/cm}^2$  ( $2.05 \text{ t/ft}^2$ ). A 0.48 cm (3/16 in) diameter uncased borehole, 5.1 cm (2 in) long, was drilled in the center of the sample one day after the confining pressures were applied. Times to fracture varied from several hours to 12 days.

In the tests of longer duration, the borehole water pressure was increased gradually each day. Later in the test, the rate of pressurizing was increased until the samples fractured. In the tests of shorter duration, the borehole water pressure was increased at an approximately constant rate until the samples fractured.

The results of the tests are shown in Figure 2.10. It can be seen that the fracturing pressures were higher in the long term tests. Jaworski

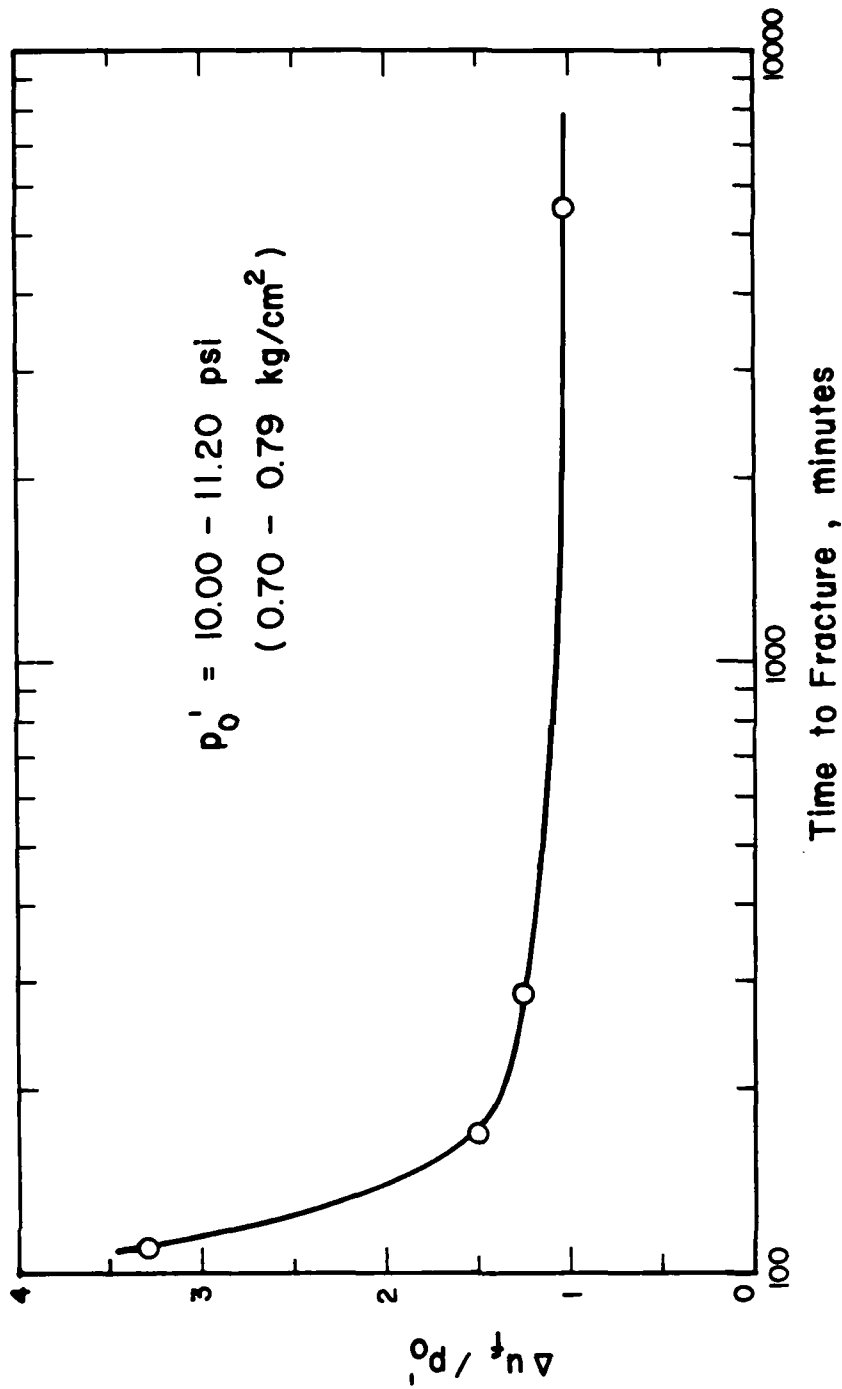


Figure 2.9 Effect of test duration on hydraulic fracturing pressure in Harmondsworth Brickearth (after Kennard, 1970)

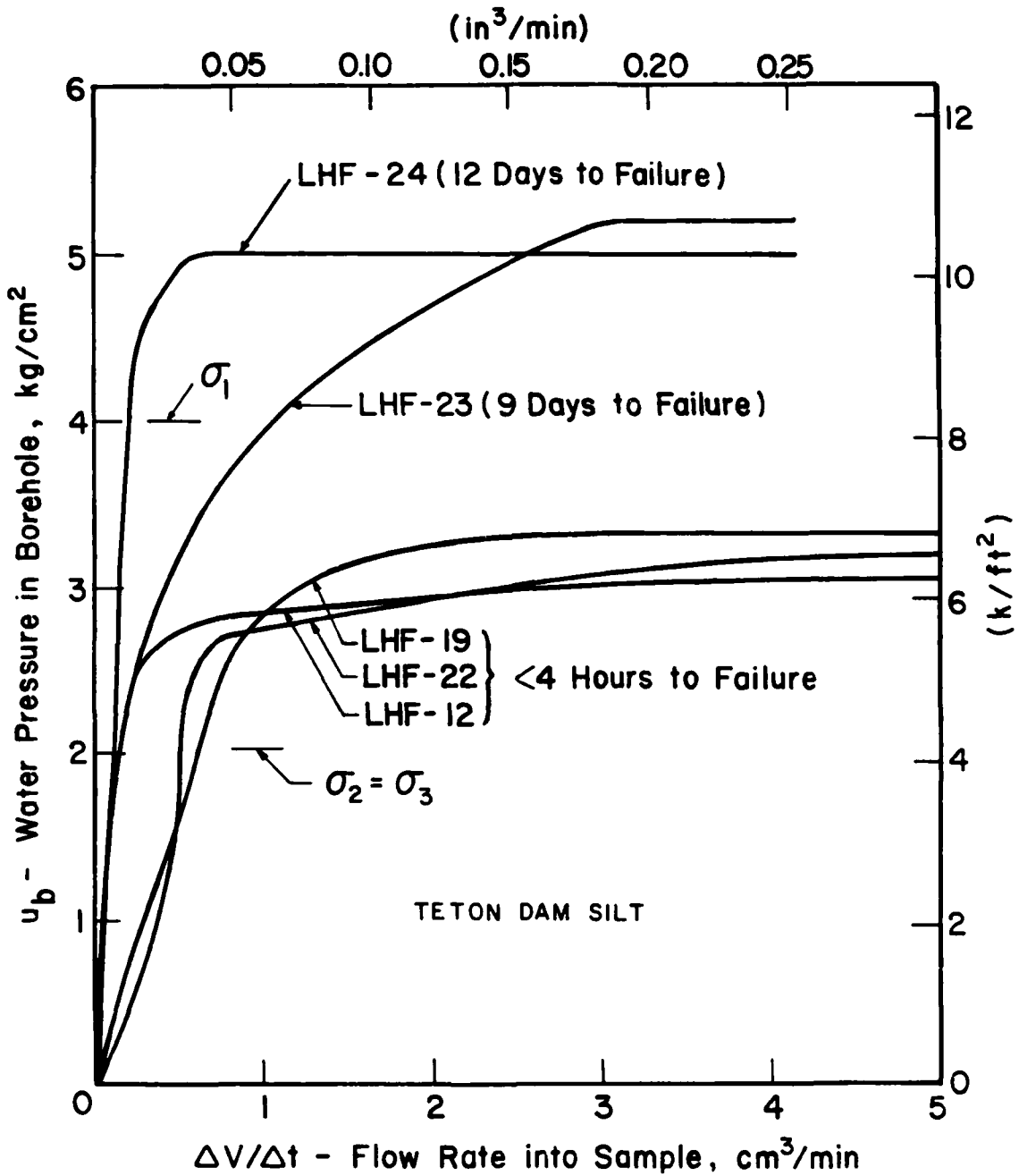


Figure 2.10 Effect of test duration on hydraulic fracturing pressure (after Jaworski et al., 1979)

et al (1979) attributed this behavior to the increase in strength (thixotropy) of the soil in the long term tests and greater ductility under slower loading.

#### EXPERIMENTAL STUDIES OF PERMEABILITY EFFECTS

Haimson (1968) performed 16 tests on Hydrostone to investigate the effect of the viscosity of the fracturing fluid on the fracturing pressure. This would appear to be a very good way of studying the effect of permeability, because the other properties of the rock remained the same.

Three types of Hydrostone were tested by Haimson: 30/100, 32/100, and 35/100. In the first two series of tests, 12.7 cm (5 in) cubical samples were tested, whereas in the last two 12.7 cm (5 in) cylindrical samples were tested. The borehole diameter was 0.79 cm (5/16 in) and the length was 5.1 cm (2 in). The viscosity of the oils ranged from 64 to 2100 centipoises at room temperature (75°F = 24°C).

The results of the tests are shown in Figure 2.11. Although there was some scatter in the results, it can be seen that the hydraulic fracturing pressures in the tests conducted with oil of higher viscosity were higher than those in tests conducted with oil of lower viscosity. This indicates that the hydraulic fracturing pressure decreased as the permeability increased.

#### EXPERIMENTAL STUDIES OF WATER CONTENT AND DENSITY EFFECTS

Jaworski et al (1981) also investigated the effects of water content and density on hydraulic fracturing pressures in Teton Dam silt. The soil was prepared by remolding and recompacting the material from block samples. The compaction water contents of the samples were about 2% dry of optimum. It was found that the samples with lower water contents generally fractured at higher pressure.

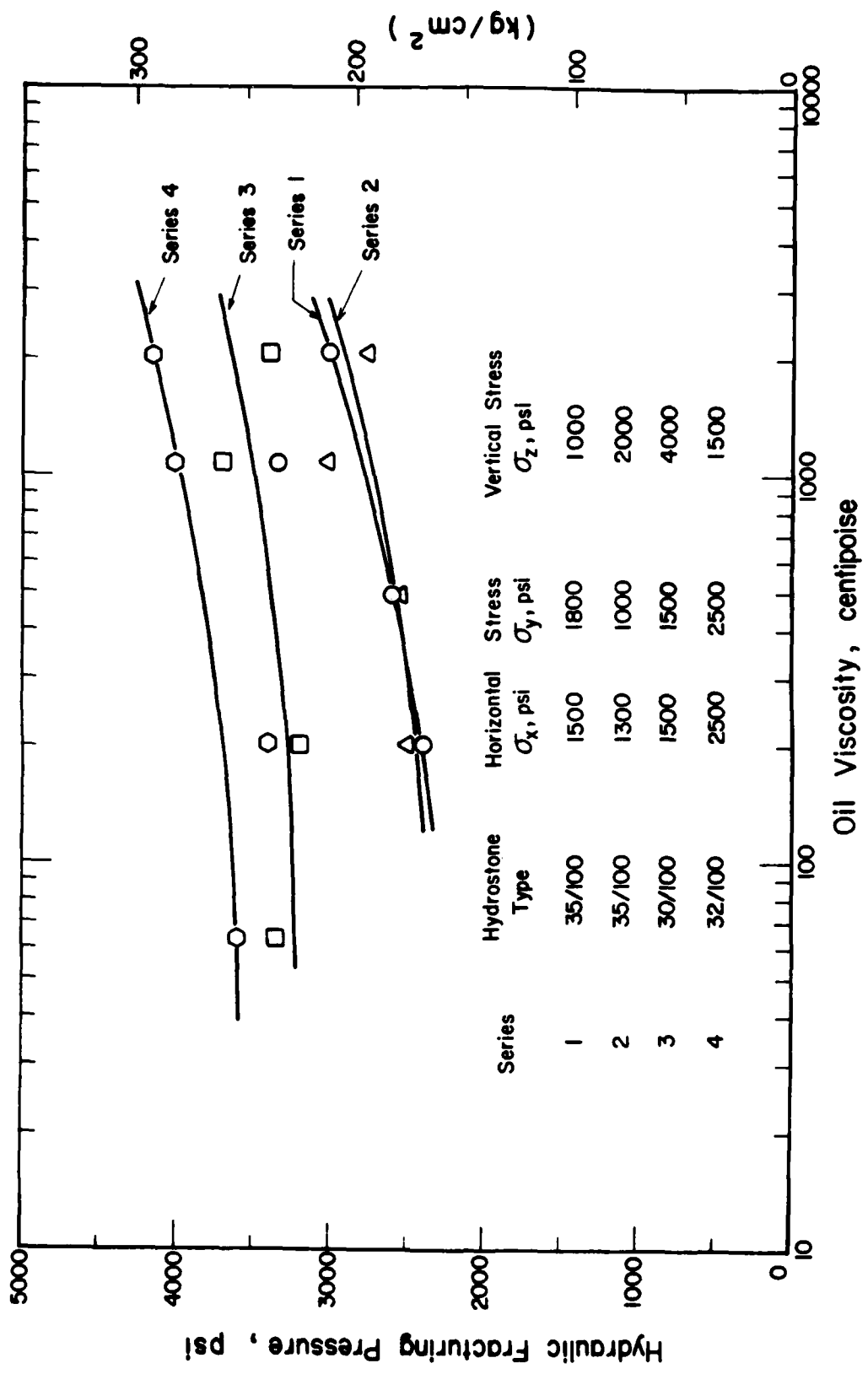


Figure 2.11 Effect of oil viscosity on hydraulic fracturing pressure in hydrostone (after Haimson, 1968)

The effect of density was examined by performing tests on samples with different compactive efforts. The results are summarized in Table 2.1. It may be seen that higher densities lead to higher hydraulic fracturing pressures.

#### SUMMARY

The results of previous studies on hydraulic fracturing can be summarized as follows:

- (1) The hydraulic fracturing pressure in rock samples was not influenced by borehole diameter if the ratio of sample diameter to borehole diameter was larger than about 15. The hydraulic fracturing pressure decreased as the borehole diameter increased if the sample diameter was kept constant and the ratio of sample diameter to borehole diameter was less than about 15.
- (2) The hydraulic fracturing pressures in rock samples and the closing pressure in a marine clay decreased as the borehole length increased.
- (3) It was generally found that the longer the test duration, the lower was the hydraulic fracturing pressure. The data from Jaworski et al (1979) showed an opposite trend.
- (4) Lower water contents in Teton Dam silt resulted in higher hydraulic fracturing pressures, as did higher dry densities.
- (5) The results of the tests using oil of varying viscosity for fracturing fluid indicated that the hydraulic fracturing pressure decreased as the permeability increased.

Table 2.1. Effect of Density on Hydraulic Fracturing Pressure  
(after Jaworski et al, 1981)

Test No.	Dry Density t/m <sup>3</sup>	Fracturing Pressure kg/cm <sup>2</sup>
LHF-7	1.74	6.9
LHF-10	1.67	4.5
LHF-12	1.55	3.1
LHF-19	1.53	3.3

Note: Water contents = 16.1 ± 1.2%

$$\sigma_v = 4 \text{ kg/cm}^2$$

$$\sigma_h = 2 \text{ kg/cm}^2$$

### III. THEORETICAL ANALYSES

A number of investigators have developed theories for hydraulic fracturing in rocks and soils for the purpose of isolating the effects of various factors that influence the magnitude of the hydraulic fracturing pressure. These theories are summarized briefly in the following section of this chapter.

Most of these theories assume either that the borehole water pressure acts with equal intensity throughout the surrounding mass, or that it acts only on the borehole wall as a boundary pressure, the surrounding mass being loaded in an undrained condition. Haimson (1968) considered seepage effects through a thermal analogy in his theory, but none of the previous theories have considered the actual mechanism involved in the gradual development of seepage in the mass around the borehole and the consequent gradual changes in effective stress and pore pressure.

A new theory will be presented following the review of previously published theories. The new theory considers the gradual advance of a seepage front from the borehole wall into the surrounding mass, and thus can be used to assess theoretically the effects of time and permeability as well as borehole size, initial stress, and tensile strength. The implications of the theory with regard to these factors will be examined, and a parameter study using finite element analyses will be presented.

#### REVIEW OF PREVIOUS HYDRAULIC FRACTURING THEORIES

##### Morgenstern and Vaughan (1963)

Morgenstern and Vaughan (1963) developed a theory of hydraulic fracturing to determine allowable grouting pressure. It was assumed that

the strength of the material being grouted was governed by Mohr-Coulomb failure criterion, and changes in stress due to drilling the borehole were ignored.

The pore pressure in the potential fracture zone was assumed to be equal to the water or grout pressure at the wall of the borehole. Hydraulic fracturing was analyzed in terms of the excess pore pressure required to displace the effective stress circle until it touched the Mohr-Coulomb strength envelope.

Based on the above assumptions, the excess pore pressure  $\Delta u_f$  to cause hydraulic fracturing was shown to be given by the following equation:

$$\Delta u_f = \frac{\sigma_1' + \sigma_3'}{2} - \frac{\sigma_1' - \sigma_3'}{2 \sin \phi'} + c' \cot \phi' \quad (3.1)$$

where

$\sigma_1'$  and  $\sigma_3'$  are the major and minor effective principal stresses, respectively

$c'$  is the effective stress cohesion intercept

$\phi'$  is the effective stress friction angle

The mechanism assumed implies shear failure of the soil around the borehole as the water pressure is increased. This mode of failure is different from the failure mechanism commonly assumed--that hydraulic fracturing occurs when the minor effective principal stress is reduced to the tensile strength of the soil.

For a specific case where:  $\sigma_1' = 4.00 \text{ kg/cm}^2$ ,  $\sigma_3' = 2.00 \text{ kg/cm}^2$ ,  $\phi' = 40^\circ$ , and  $c' = 0.15 \text{ kg/cm}^2$ , this theory predicts  $\Delta u_f = 1.62 \text{ kg/cm}^2$ . The predicted  $\Delta u_f$  is lower than  $\sigma_3'$ , and thus considerably smaller than values determined experimentally during this investigation.

Haimson (1968)

Haimson was interested in the determination of in-situ stresses in rocks by the hydraulic fracturing technique. He developed a theory of hydraulic fracturing and conducted an extensive laboratory test program.

In his analysis Haimson assumed that the rock was brittle elastic, homogeneous, isotropic, linear, porous, and that the fluid flowing through its pores obeyed Darcy's Law.

Haimson considered (1) anisotropic geostatic stresses, (2) the changes in stress due to the presence of a borehole, (3) the changes in stress due to water pressure acting as a boundary load on the borehole wall, and (4) the changes in stress due to fluid penetrating the rock and flowing through its pores. The initial stresses and the subsequent changes were superimposed and hydraulic fracturing was assumed to be initiated when the tangential stress at the borehole wall was equal to the tensile strength of the rock.

The changes in stress due to borehole and water pressure acting as a boundary load were analyzed using elasticity theory. The changes in stress due to fluid penetrating the rock were analyzed utilizing an analogy between thermoelasticity and elasticity for a hollow infinite cylinder.

For an infinite rock mass, the excess water pressure required to initiate a vertical fracture was expressed as:

$$\Delta u_f = \frac{\sigma_t + 3\sigma_3' - \sigma_2'}{2 - \alpha \frac{1-2\nu}{1-\nu}} \quad (3.2)$$

where

$\sigma_2'$  and  $\sigma_3'$  are the larger and the smaller effective horizontal stresses, respectively

$\sigma_t$  is the tensile strength of the rock

$\nu$  is Poisson's ratio of the rock

$\alpha$  is  $1 - C_r/C_b$

$C_r$  and  $C_b$  are the material matrix compressibility and the bulk compressibility of the rock, respectively.

According to Haimson the value of  $\alpha$  for rock is larger than the porosity and less than 1, and the value of Poisson's ratio lies between 0 and 0.5; therefore, the value of  $\alpha \frac{1 - 2\nu}{1 - \nu}$  lies between 0 and 1.

Even though Haimson appears to have considered seepage of water from the borehole, the equation for hydraulic fracturing pressure is independent of time, permeability, and borehole size; therefore, this equation cannot be used to assess the influence of these factors and sheds no light on the gradual evolution of seepage around the borehole.

For a specific case where:  $\sigma_2' = \sigma_3' = 2.00 \text{ kg/cm}^2$ ,  $\sigma_t = 0.10 \text{ kg/cm}^2$ ,  $\nu = 0.3$ , and  $\alpha = 0.8$ , Haimson's theory predicts  $\Delta u_f = 2.66 \text{ kg/cm}^2$ . This value is in reasonable agreement with the results of the tests conducted during this investigation.

When the fluid does not penetrate into the rock, Haimson found that the excess pressure required to initiate hydraulic fracturing was given by:

$$\Delta u_f = \sigma_t + 3\sigma_3' - \sigma_2' \quad (3.3)$$

In the case where  $\sigma_t = 0$ , this equation reduces to that obtained by Hubbert and Willis (1957) as discussed in Chapter II. For the case where:  $\sigma_2' = \sigma_3' = 2.00 \text{ kg/cm}^2$  and  $\sigma_t = 0.10 \text{ kg/cm}^2$ , Equation 3.3 results in  $\Delta u_f = 4.10 \text{ kg/cm}^2$ . This value is also in reasonable agreement with the results of the tests with high rates of pressurization conducted during this investigation.

#### Kennard (1970)

Kennard's study was concerned with the measurement of permeability by the constant head method using piezometers. Kennard observed that

the permeability increased abruptly when the soil around the piezometer fractured. He pointed out that the pressure used to perform the permeability test should be kept below the fracturing pressure to avoid erroneous results.

Kennard assumed that (1) the soil behaved elastically, (2) the piezometer was rigid and its length was great compared to its diameter, (3) the soil had complete freedom of movement in the vertical direction, and (4) the tensile strength of the soil was negligible.

The effect of the installation of the piezometer on the stresses was ignored. Two cases were analyzed--fully drained and fully undrained, and two boundary conditions were considered--fixed and free outer boundary. The criterion for vertical fracture employed in the theory was that fracturing would occur when the tangential stress at the borehole wall was zero.

For the fully drained case, it was found that the excess pressure  $\Delta u_f$  required to initiate a vertical fracture for the fixed outer boundary condition was:

$$\Delta u_f = \frac{2 \sigma_h'}{(1 + \nu) \left\{ 1 - \frac{1 - a^2/b^2}{2 \ln(b/a)} \right\}} \quad (3.4)$$

where

$\sigma_h'$  is the initial effective horizontal stress

a is the borehole radius

b is the sample radius

and for the free outer boundary condition:

$$\Delta u_f = \frac{2 \sigma_h'}{(1 + \nu) + (1 - \nu) \frac{1 - a^2/b^2}{2 \ln(b/a)}} \quad (3.5)$$

When the sample radius is large compared to the borehole radius

(b >> a), the two equations yield the same value for  $\Delta u_f$ :

$$\Delta u_f = \frac{2 \sigma_h'}{1 + \nu} \quad (3.6)$$

If the calculated value of  $\Delta u_f$  is higher than the overburden pressure  $p_o'$ , Kennard suggested that a horizontal fracture would result.

For a specific case where:  $\sigma_h' = 2.00 \text{ kg/cm}^2$ ,  $\nu = 0.3$ , and  $b \gg a$ , Kennard's "drained" theory predicts  $\Delta u_f = 3.08 \text{ kg/cm}^2$ . This is in reasonable agreement with the results of the tests conducted during this investigation.

In the undrained case, Kennard considered the piezometer as having a thin rubber membrane covering its surface. Water pressure acting inside the membrane was considered to generate excess pore pressure in the surrounding soil, which was calculated using Skempton's pore pressure parameters A and B, with  $B = 1.00$ .

For a finite soil mass with a fixed outer boundary, the excess pressure  $\Delta u_f$  required to induce fracturing was found to be:

$$\Delta u_f = \sigma_h' \left( 1 + \frac{1 + 3(a^2/b^2)}{2A} \right) \quad (3.7)$$

For  $b \gg a$  this equation reduces to:

$$\Delta u_f = \sigma_h' \left( 1 + \frac{1}{2A} \right) \quad (3.8)$$

For a finite soil mass with a free outer boundary, the excess pressure required to induce fracturing was found to be:

$$\Delta u_f = \sigma_h' \left( 1 + \frac{1 - (a^2/b^2)}{2A} \right) \quad (3.9)$$

For  $b \gg a$ , this equation reduces to Equation 3.8.

For a specific case where:  $\sigma_h' = 2.00 \text{ kg/cm}^2$ ,  $A = 0.70$ , and  $b \gg a$ , Kennard's "undrained" theory predicts  $\Delta u_f = 3.43 \text{ kg/cm}^2$ . This value is somewhat lower than the values of  $\Delta u_f$  determined experimentally during

this investigation with high rates of pressurization.

Bjerrum, Nash, Kennard, and Gibson (1972)

Bjerrum et al (1972) were interested in developing guide-lines for avoiding hydraulic fracturing in permeability tests, since hydraulic fracturing results in erroneous values of permeability for the soil tested.

The changes in the state of stress due to installation of a piezometer were considered by means of elastic theory. The installation was found to increase the radial effective stress in the soil next to the piezometer to  $(1 + \beta) \sigma_h'$ , while reducing the tangential effective stress to  $(1 - \alpha) \sigma_h'$ , where  $\alpha$  and  $\beta$  are functions of the compressibility ratio  $[E/(\sigma_h'(1+\nu))]$  of the soil. The value of  $\alpha$  determined by their analysis varies from 0.4 to -1.1, while the value of  $\beta$  ranges from 0.5 to 4.2. Typical values are listed in Table 3.1.

Bjerrum et al assumed plane strain condition in the vertical direction. The outer boundary of the soil was assumed fixed. Only the fully drained condition was analyzed. The criterion for hydraulic fracturing used was that fracturing would occur when the tangential stress in the soil next to the piezometer became equal to the tensile strength of the soil.

The analysis showed that the fracturing pressure depended on whether blow-off preceded cracking. Blow-off occurs when the radial effective stress in the soil next to the piezometer is reduced to zero; thereafter, any further increase of pressure head will have the effect of moving the soil away from the piezometer and creating a water-filled cavity around the piezometer tip.

If hydraulic fracturing occurs before blow-off, the excess pressure at which hydraulic fracturing is initiated was found to be:

Table 3.1 Values of  $\alpha$  and  $\beta$  (after Bjerrum et al, 1972)

Soil type	Range of compressibility ratio $E/[\sigma'_h(1+\nu)]$	Range of stress factors	
		$\alpha$	$\beta$
Highly compressible	1 to 3	0.4 to 0.2	0.5 to 1.1
Medium compressibility	3 to 10	0.2 to -0.2	1.1 to 2.0
Low compressibility	10 to 70	-0.2 to -1.1	2.0 to 4.2

$$\Delta u_f = \frac{1 - \nu}{\nu} \{(1 - \alpha) \sigma_h' + \sigma_t\} \quad (3.10)$$

where

$\alpha$  is a constant which varies with soil type, and ranges from 0.4 to -1.1 (see Table 3.1)

$\sigma_t$  is the tensile strength of the soil

This equation is only valid when fracturing occurs before blow-off, that is if:

$$\frac{1 - \nu}{\nu} \{(1 - \alpha) \sigma_h' + \sigma_t\} \leq (1 + \beta) \sigma_h' \quad (3.11)$$

If this equation is not satisfied, blow-off precedes fracturing, and the excess pressure required to induce fracturing was found to be:

$$\Delta u_f = (1 - \nu) \{(2 - \alpha + \beta) \sigma_h' + \sigma_t\} \quad (3.12)$$

For a specific case where:  $\sigma_h' = 2.00 \text{ kg/cm}^2$ ,  $\sigma_t = 0.10 \text{ kg/cm}^2$ ,  $\alpha = 0$ ,  $\beta = 1.5$ , and  $\nu = 0.3$ , the above equations show that hydraulic fracturing will occur before blow-off, and  $\Delta u_f$  calculated from Equation 3.10 is  $4.90 \text{ kg/cm}^2$ . This is considerably higher than the values of  $\Delta u_f$  determined experimentally in open boreholes (no piezometer).

Jaworski, Duncan, and Seed (1979)

Jaworski et al (1979) used an elastic analysis in terms of total stresses to analyze the changes in stress due to the presence of a borehole and water pressure acting on the borehole wall as a boundary pressure. They assumed that the soil behaved as an impermeable linear elastic material and ignored the influence of penetrating borehole water on the stresses. However, the pore pressure in the soil near the borehole was assumed equal to the borehole water pressure. Their criterion for hydraulic fracturing was that fracturing would occur when the tangential

stress in the soil at the borehole wall became equal to the tensile strength of the soil.

Based on those assumptions, they found that the hydraulic fracturing pressure was given by the following equation:

$$u_f = \sigma_h + \frac{\sigma_t}{2} \quad (3.13)$$

where  $\sigma_h$  is the initial total horizontal stress in the soil.

For a specific case where:  $\sigma_h = 2.00 \text{ kg/cm}^2$  and  $\sigma_t = 0.10 \text{ kg/cm}^2$ , the hydraulic fracturing pressure predicted by this theory is  $2.05 \text{ kg/cm}^2$ . This is lower than the values of  $u_f$  determined experimentally during this investigation.

#### NEW THEORY OF HYDRAULIC FRACTURING

The new theory presented here considers the gradual advance of a seepage front from a borehole into the surrounding mass. Therefore, this theory can be used to assess the effects of time and permeability as well as borehole size, initial stress, and tensile strength.

Generally, the horizontal stress in a soil is lower than the vertical stress. Therefore, in most conditions, vertical fracturing is more likely than horizontal fracturing. Accordingly, the proposed theory will consider only vertical fracturing.

The factors considered by this theory are:

- (1) the initial state of stress in the soil
- (2) changes in stress due to the presence of a borehole
- (3) changes in stress due to water pressure in the borehole
- (4) soil properties--Poisson's ratio, permeability, tensile strength, and porosity
- (5) borehole diameter and sample diameter
- (6) rate of pressurizing the borehole or test duration

### Conditions and Criteria Considered by the New Theory

The proposed criteria for hydraulic fracturing are as follows:

- (1) The soil must have cohesion and tensile strength.

This is important because without cohesion and tensile strength there can be no fracture plane. A condition where the effective stress is reduced to zero can be induced in a sand, but hydraulic fracturing cannot, because sand has no tensile strength.

- (2) Wedging is a necessary condition for fracturing.

Wedging is an action by the water pressure that produces extensional strain in the soil. Without wedging, no tensile stress can be induced in the soil mass, and fracturing cannot occur.

- (3) The tensile stress on a potential fracture plane must be equal to the soil tensile strength. The analysis presented here is focused on determining the magnitude of the change in water pressure required to produce a tensile stress equal to the tensile strength.

In this theory it is assumed that (1) the soil is elastic, homogeneous, and isotropic, (2) the shape of the sample is cylindrical, (3) a condition of plane strain exists in the vertical direction, (4) the outer boundary of the sample is free to move, and (5) the sample is drained at the outer boundary.

The steps in the analysis involve calculation of the changes in stress due to the presence of a borehole, water pressure in the borehole, and seepage from the borehole. These changes are superimposed on the initial stresses. When the tangential stress at the borehole wall is decreased (from compressive to tensile stress) to a value equal to

the tensile strength of the soil, hydraulic fracturing is initiated. Increasing the borehole water pressure further increases the radius of the crack. The analysis is continued until the fracture extends to the outer boundary of the sample.

Initial Stresses, and Changes Due to the Presence of a Borehole

The initial effective horizontal stress is assumed to be the same throughout the sample, and is equal to  $\sigma_h'$ .

Due to the presence of a borehole, the horizontal stress in the radial and tangential direction will be changed. The resulting stresses can be obtained from many textbooks on the theory of elasticity, e.g. Timoshenko and Goodier (1953). The stresses after the borehole has been made are:

$$\sigma_r' = \frac{1 - a^2/r^2}{1 - a^2/b^2} \sigma_h' \quad (3.14)$$

$$\sigma_\theta' = \frac{1 + a^2/r^2}{1 - a^2/b^2} \sigma_h' \quad (3.15)$$

where

$\sigma_r'$  and  $\sigma_\theta'$  are the effective radial and tangential stresses,  
respectively

a is the borehole radius

b is the sample radius

r is the radial distance from the center of the borehole

At the borehole wall, the effective tangential stress is:

$$\sigma_\theta' = \frac{2 \sigma_h'}{1 - a^2/b^2} \quad (3.16)$$

Due to the presence of a borehole, the effective radial stress at the borehole wall becomes zero, and the effective tangential stress at

the same location is approximately twice the initial effective stress. The distributions of radial and tangential stresses away from the borehole are shown in Figure 3.1 for a specific set of conditions listed in the figure.

#### Changes in Stress Due to Water Pressure in a Borehole

When the borehole is pressurized, water will seep radially into the sample. If the seepage zone extends to the outer boundary of the sample, a steady state flow condition is established.

As a general case it is assumed that for a particular borehole water pressure, water has not seeped to the outer boundary of the sample. In this case the sample can be divided into two zones--Cylinder 1 which is the seepage zone and Cylinder 2 which is outside the seepage zone. The radius of the boundary between the two cylinders is  $r_s$ , which is the radius of the seepage zone. Figure 3.2 shows the two zones in the sample.

Due to the seepage forces within Cylinder 1, this cylinder tends to expand. The expansion, however, is restricted by the presence of Cylinder 2. A restraint pressure will develop at the boundary of the two cylinders that maintains the same displacement at the boundary between them.

The method of superposition is utilized to calculate the restraint pressure as follows (Figure 3.3):

- (1) Calculate  $\delta_{1s}$  = displacement in the unrestrained Cylinder 1 due to seepage forces
- (2) Calculate  $\delta_{1p}$  = displacement in the same cylinder due to a restraint pressure  $p$  acting at the outer boundary
- (3) Calculate  $\delta_{2p}$  = displacement in Cylinder 2 due to the same restraint pressure  $p$  acting at the inner boundary.

The compatibility requirement of displacement at the boundary between the

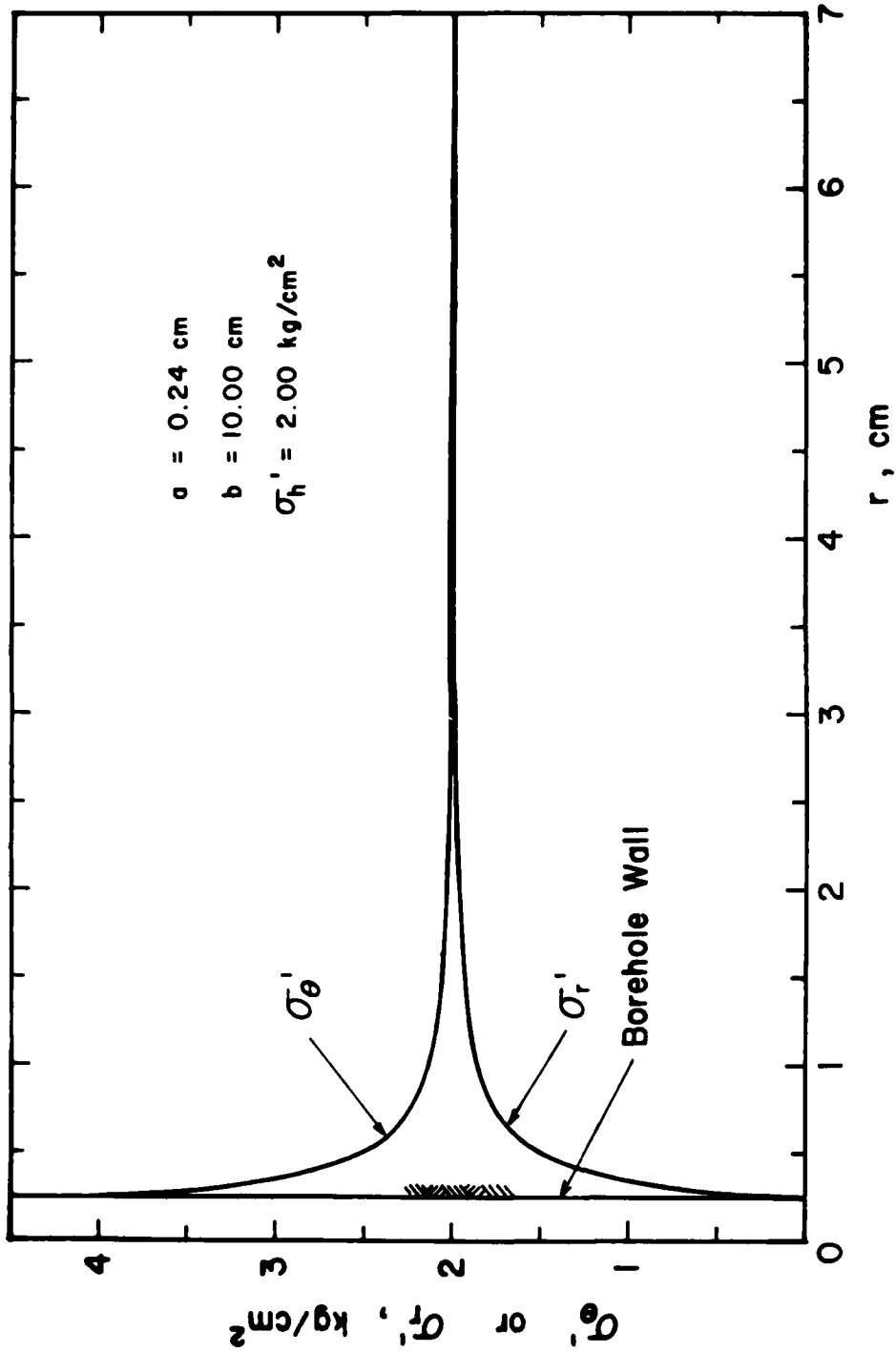
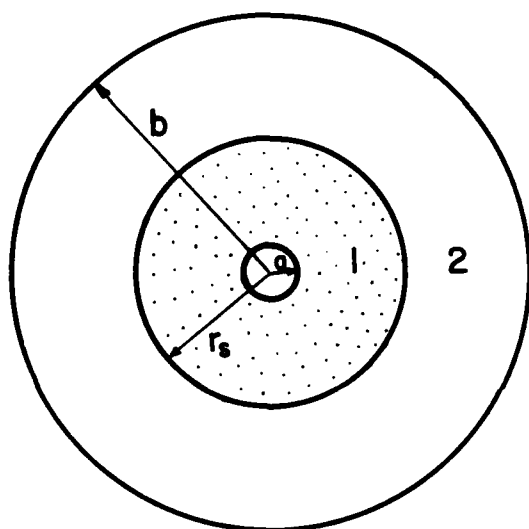


Figure 3.1 Distribution of tangential and radial stresses away from borehole



$a$  = borehole radius

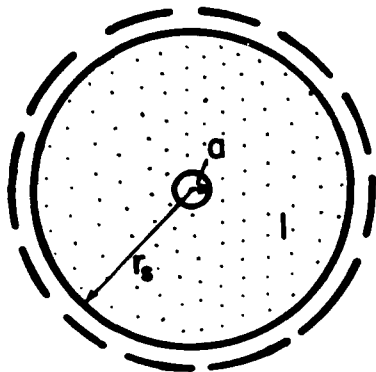
$r_s$  = seepage radius

$b$  = sample radius

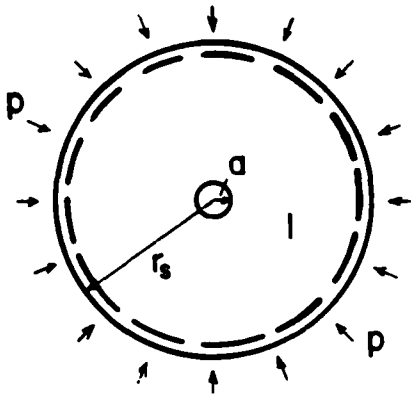
zone 1 = seepage zone

zone 2 = zone of no seepage

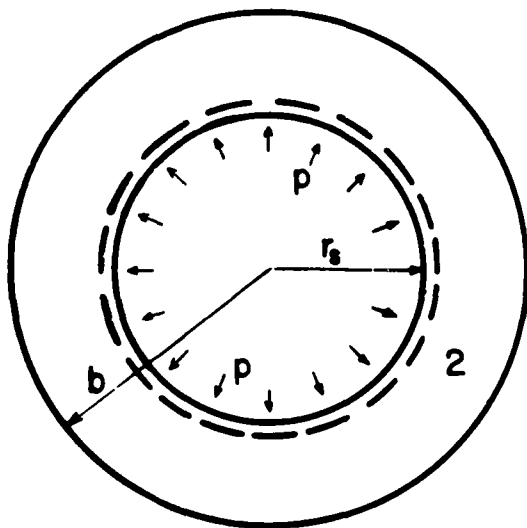
Figure 3.2 Cylindrical sample with seepage from central hole



Displacement due to seepage forces in cylinder 1



Displacement due to restraint pressure in cylinder 1



Displacement due to restraint pressure in cylinder 2

Figure 3.3 Displacements due to seepage forces and restraint pressure

two cylinders is:

$$\delta_{1s} + \delta_{1p} = \delta_{2p} \quad \text{at } r = r_s \quad (3.17)$$

The magnitude of the restraint pressure  $p$  can be obtained from Equation 3.17. If the seepage zone has extended to the outer boundary of the sample, the magnitude of restraint pressure  $p$  will be equal to the effective horizontal stress,  $\sigma_h'$ .

The changes in stress in Cylinder 1 due to water pressure in the borehole is obtained by superimposing the changes in stress due to the seepage forces in an unrestrained cylinder on the changes in stress due to restraint pressure  $p$ .

The radius of seepage  $r_s$  at a particular instant can be calculated by iteration using the following equation\*:

$$r_s^2 \{ \ln(r_s/a) - 0.5 \} - r_{so}^2 \{ \ln(r_{so}/a) - 0.5 \} - \frac{k}{n} \{ 2h_o(t-t_o) + m(t-t_o)^2 \} = 0$$

where (3.18)

- $r_s$  is the new seepage radius
- $r_{so}$  is the previous seepage radius
- $h_o$  is the previous pressure head
- $k$  is the permeability of soil
- $n$  is the porosity of soil
- $t-t_o$  is the elapsed time
- $m$  is the rate of pressurizing

Using elasticity theory, the changes in tangential stress in the sample and the displacement at the external boundary of unrestrained Cylinder 1 due to seepage forces can be shown to be\*:

$$\Delta\sigma_{\theta 1s}' = -\frac{1+a^2/r^2}{1-a^2/b^2} \sigma_h' - \frac{\Delta u(1+a^2/r^2)}{2(1-\nu)(1-a^2/r_s^2)} + \frac{\Delta u(1+\ln(r/a))}{2(1-\nu) \ln(r_s/a)} - \frac{\Delta u}{\ln(r_s/a)} \quad (3.19)$$

\*Derivation of these equations are presented in Appendix A.

$$(\delta_{1s})_{r_s} = \frac{r_s(1+\nu)(1-2\nu)}{E} \left\{ \frac{\sigma_h'}{1-a^2/b^2} + \frac{\Delta u}{2(1-\nu)(1-a^2/r_s^2)} + \frac{\sigma_h' a^2/r_s^2}{(1-2\nu)(1-a^2/b^2)} + \frac{\Delta u a^2/r_s^2}{2(1-\nu)(1-2\nu)(1-a^2/r_s^2)} - \frac{\Delta u}{2(1-\nu)} + \frac{\Delta u}{2 \ln(r_s/a)} \right\} \quad (3.20)$$

where

$\Delta u$  is the excess water pressure in the borehole

$E$  is the Young's modulus of the soil

The changes in tangential stress in the sample and the displacement at the external boundary of Cylinder 1 due to the restraint pressure  $p$  are as follows\*:

$$\Delta \sigma_{\theta'}'_{1p} = p \frac{1 + a^2/r_s^2}{1 - a^2/r_s^2} \quad (3.21)$$

$$(\delta_{1p})_{r_s} = - \frac{r_s(1+\nu)(1-2\nu)}{E} \left\{ \frac{p}{1-a^2/r_s^2} + \frac{p a^2/r_s^2}{(1-2\nu)(1-a^2/r_s^2)} \right\} \quad (3.22)$$

The changes in tangential stress in the sample and the displacement at the inner boundary of Cylinder 2 due to the restraint pressure  $p$  are as follows\*:

$$\Delta \sigma_{\theta'}'_{2p} = - \frac{r_s^2/b^2 + r_s^2/r^2}{1 - r_s^2/b^2} \left\{ p - \frac{1 - a^2/r_s^2}{1 - a^2/b^2} \sigma_h' \right\} \quad (3.23)$$

$$(\delta_{2p})_{r_s} = \frac{r_s(1+\nu)(1-2\nu)}{E} \left\{ \frac{1 + (1-2\nu) r_s^2/b^2}{(1-2\nu)(1-r_s^2/b^2)} p - \frac{1 + (1-2\nu) r_s^2/b^2}{(1-2\nu)(1-r_s^2/b^2)} \frac{1 - a^2/r_s^2}{1 - a^2/b^2} \sigma_h' \right\} \quad (3.24)$$

\*Derivations of these equations are presented in Appendix A.

Substituting Equations 3.20, 3.22, and 3.24 into Equation 3.17 gives the magnitude of restraint pressure  $p$ :

$$p = \frac{\frac{1-2\nu + a^2/r_s^2}{2(1-\nu)(1-a^2/r_s^2)} + \frac{1-2\nu}{2 \ln(r_s/a)} - \frac{1-2\nu}{2(1-\nu)}}{\frac{1-2\nu + a^2/r_s^2}{1-a^2/r_s^2} + \frac{(1-2\nu)r_s^2/b^2 + 1}{1-r_s^2/b^2}} \Delta u + \frac{1-a^2/r_s^2}{1-a^2/b^2} \sigma_h' \quad (3.25)$$

Combining Equations 3.19 and 3.21, the net changes in tangential stress in Cylinder 1 due to water pressure in the borehole is:

$$\Delta \sigma_{\theta}' = - \frac{1 + a^2/r^2}{1 - a^2/b^2} \sigma_h' - \frac{\Delta u(1+a^2/r^2)}{2(1-\nu)(1-a^2/r_s^2)} + \frac{\Delta u \{1 + \ln(r/a)\}}{2(1-\nu) \ln(r_s/a)} - \frac{\Delta u}{\ln(r_s/a)} + \frac{p(1+a^2/r^2)}{1-a^2/r_s^2} \quad (3.26)$$

where  $p$  is defined in Equation 3.25. Equation 3.26 is valid for  $a < r \leq r_s$ . For  $r_s < r \leq b$ , the changes in tangential stress are defined in Equation 3.23.

The changes in tangential stress in the sample due to water pressure in the borehole are illustrated in Figure 3.4 for two conditions where the seepage radii are 1 cm and 10 cm. The other parameters used in the analysis are listed in the figure. It can be seen from this figure that the larger the seepage radius, the larger is the decrease in tangential stress due to a given change in water pressure. A larger seepage radius can be caused by a higher permeability or by a slower rate of pressurizing the borehole. Larger seepage radius causes only a slight decrease in tangential stress at the borehole wall. Therefore, higher permeability or slower pressurization would be expected to have only minor influences on the tangential stress at the borehole wall and on the hydraulic fracturing pressure.

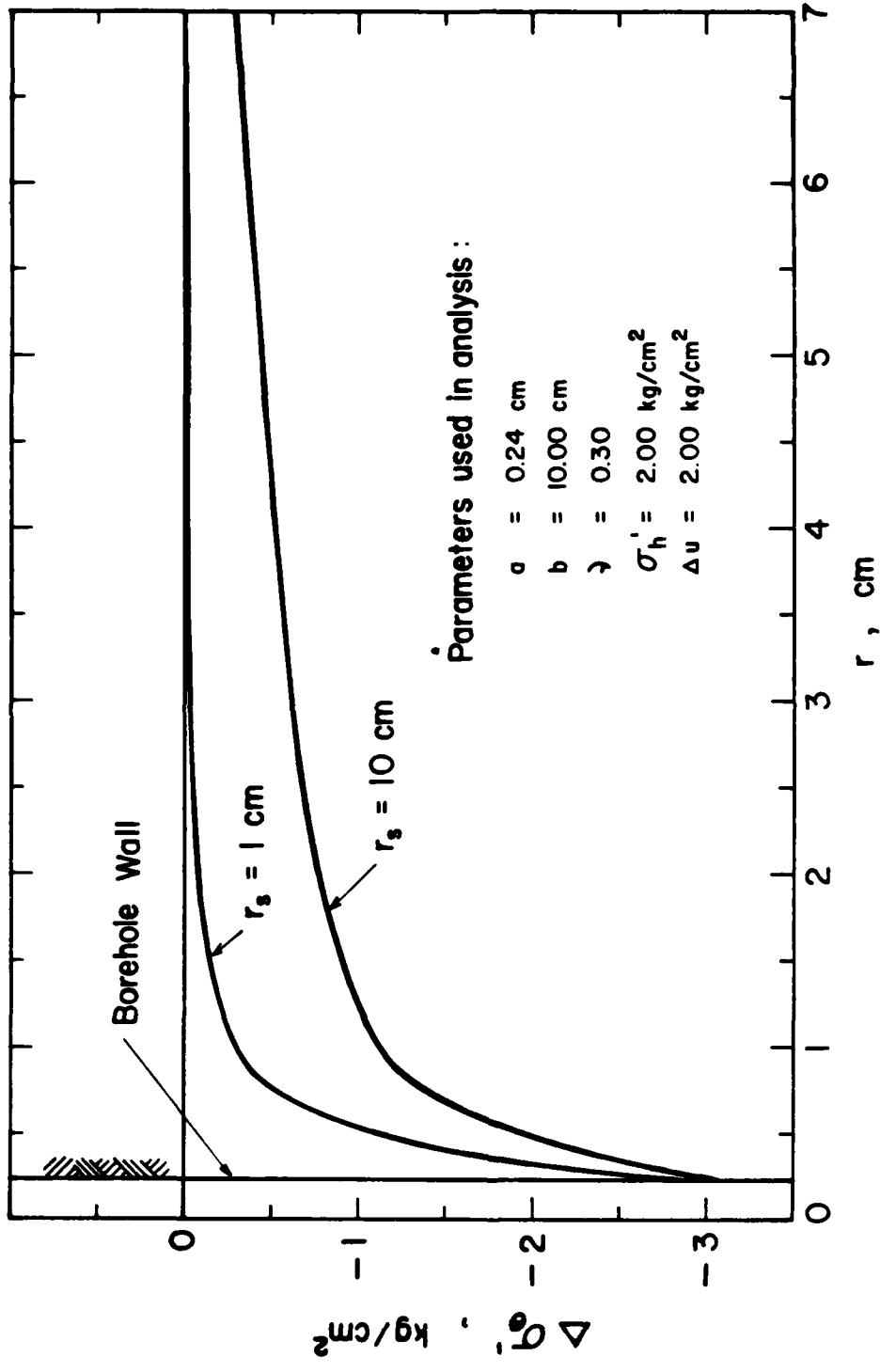


Figure 3.4 Effect of seepage radius on changes in tangential stresses

### Initiation and Propagation of a Hydraulic Fracture

The tangential stress in the soil after drilling the borehole is defined by Equation 3.15, whereas its changes due to water pressure in the borehole are defined by Equation 3.26. Combining these two equations, the tangential stress due to the presence of a borehole, the water pressure in it, and seepage into the surrounding soil is:

$$\sigma_{\theta}' = -\frac{\Delta u(1+a^2/r^2)}{2(1-\nu)(1-a^2/r_s^2)} + \frac{\Delta u\{1+\ln(r/a)\}}{2(1-\nu)\ln(r_s/a)} - \frac{\Delta u}{\ln(r_s/a)} + \frac{p(1+a^2/r^2)}{1-a^2/r_s^2} \quad (3.27)$$

At the borehole wall, the tangential stress can be obtained from the above equation by substituting  $r = a$ . The result is:

$$(\sigma_{\theta}')_a = -\frac{\Delta u}{(1-\nu)(1-a^2/r_s^2)} + \frac{\Delta u}{2(1-\nu)\ln(r_s/a)} - \frac{\Delta u}{\ln(r_s/a)} + \frac{2p}{1-a^2/r_s^2} \quad (3.28)$$

To illustrate how the tangential stresses vary as the borehole water pressure is increased, an analysis was performed using the set of parameters listed in Figure 3.5. The variation of tangential stress is shown for various values of borehole water pressure. It can be seen that the sample started to fracture ( $\sigma_{\theta}'$  became equal to the soil tensile strength) at an excess borehole water pressure of  $2.80 \text{ kg/cm}^2$ .

To summarize, the elements of the new theory are as follows:

- (1) From the pressure head vs time curve, the seepage radius is calculated using Equation 3.18. In the beginning, the value

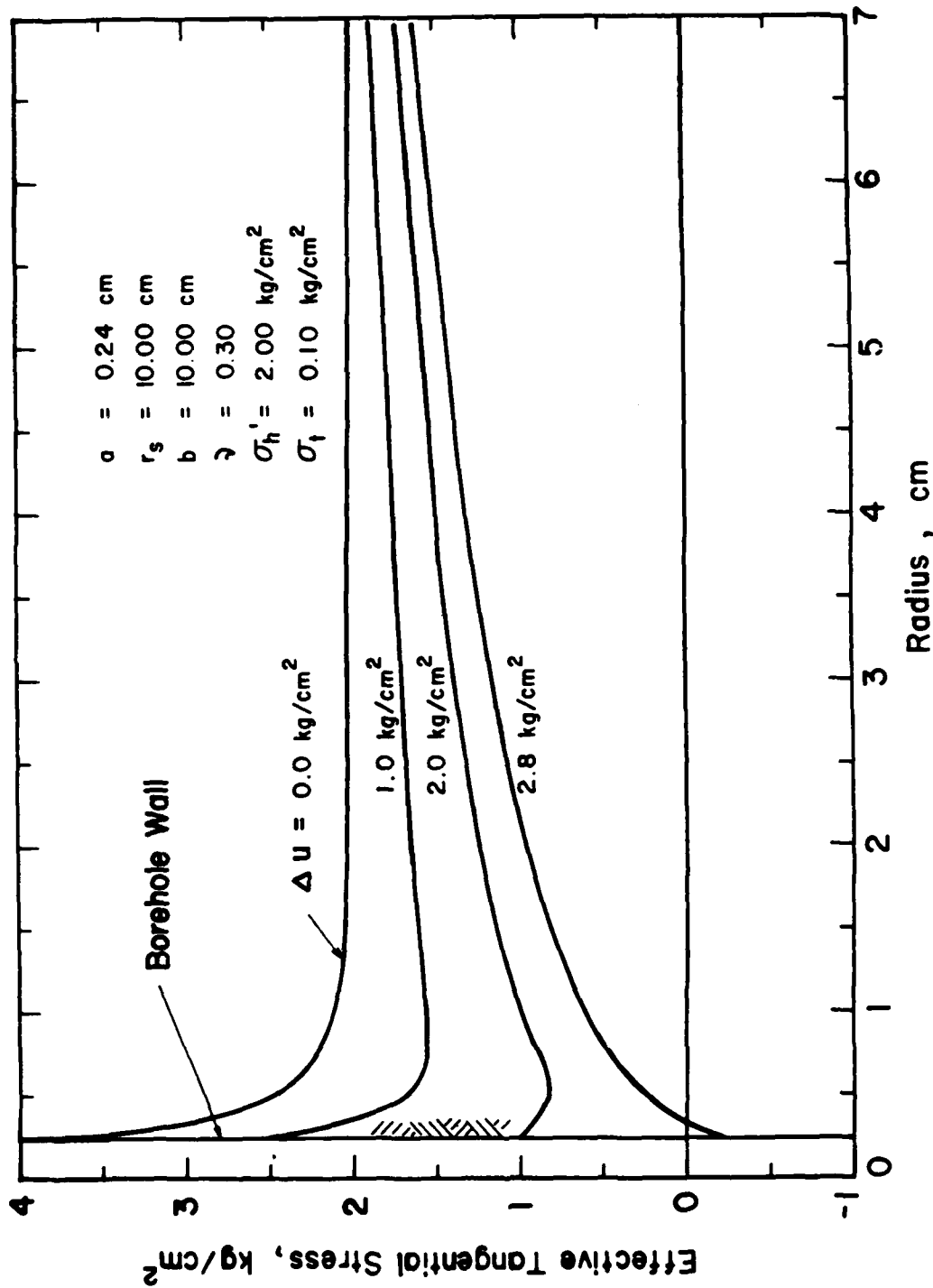


Figure 3.5 Distribution of tangential stress as borehole water pressure increases

of seepage radius ( $r_{so}$ ) is equal to the borehole radius  $a$ .

- (2) The restraint pressure  $p$  is calculated using Equation 3.25.
- (3) The effective tangential stress at the borehole wall  $(\sigma_{\theta}')_a$  is calculated using Equation 3.28 and is compared to the soil tensile strength.

If the calculated value of  $(\sigma_{\theta}')_a$  is higher (more compressive) than the tensile strength of the soil, fracture has not occurred. A new pressure head is determined from the pressure head vs time curve, and a new seepage radius is calculated. The process is continued until  $(\sigma_{\theta}')_a$  is equal to or less (more negative) than the soil tensile strength, in which case the sample has cracked. The radius of the crack is calculated by assuming that the crack extends to the radius where the tangential stress is exactly equal to the tensile strength of the soil.

After the sample has cracked, the permeability of the cracked portion increases substantially. Therefore, it is assumed that the pore pressure at the tip of the crack is equal to the borehole water pressure. Ignoring the cracked portion of the sample for the purpose of subsequent analysis, it is assumed that the new borehole radius is equal to the radius of the crack. The procedure is then repeated to calculate the radius of the subsequent crack and continued until the calculated crack radius is equal to the sample radius, at which point the sample is considered to be completely fractured.

#### Parameter Study

The effects of five parameters were studied using a computer program. These were horizontal stress, permeability, tensile strength, borehole diameter, and test duration. In all of the studies the initial pore pressure in the sample was assumed to be zero, and the borehole water pressure was increased in increments of  $0.10 \text{ kg/cm}^2$ , as shown in Figure 3.6.

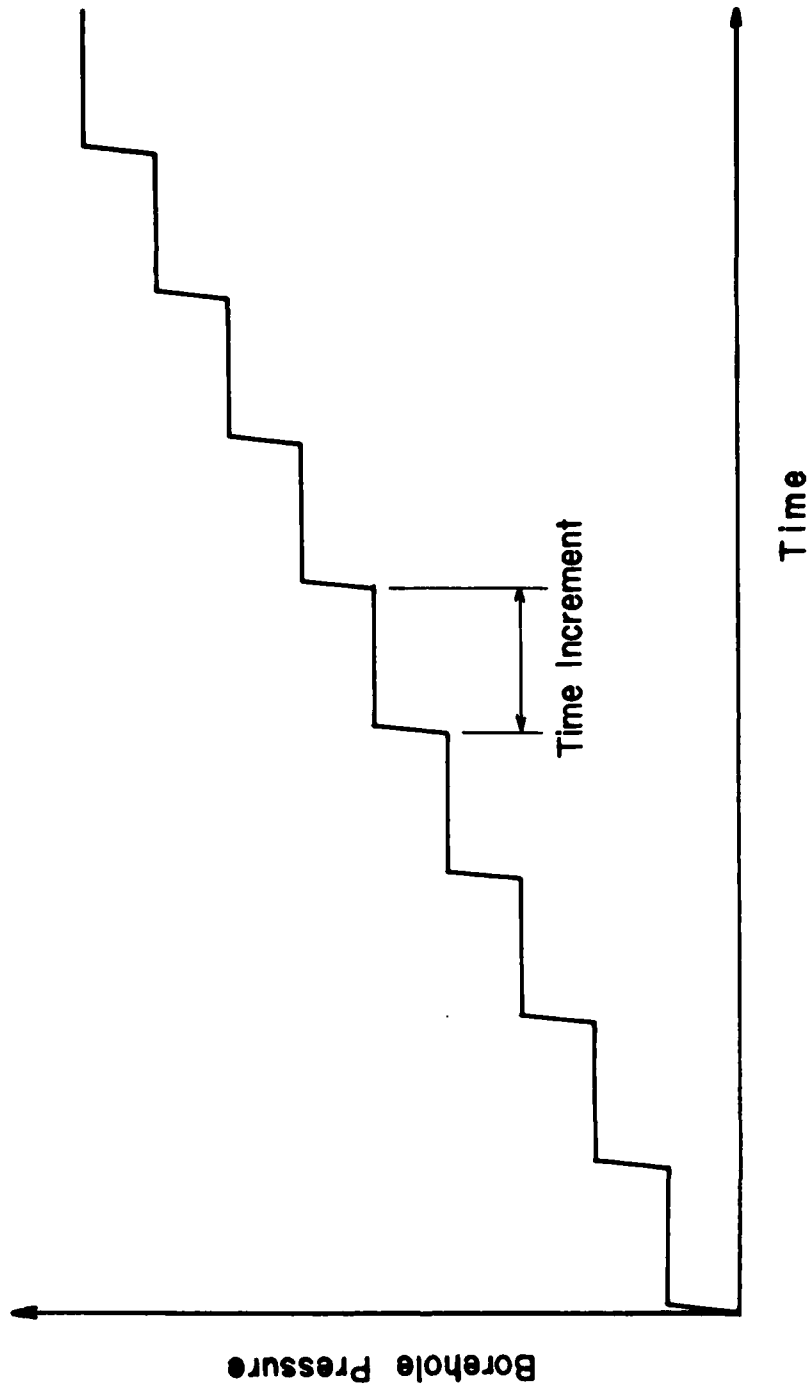


Figure 3.6 Typical borehole pressure vs time curve

The calculated values of fracturing pressure were found to be significantly influenced by the value of Poisson's ratio used in the analysis. The effect of Poisson's ratio is shown in Figure 3.7, where it can be seen that a decrease of 0.1 in the value of Poisson's ratio results in an increase of about  $0.4 \text{ kg/cm}^2$  in the calculated values of hydraulic fracturing pressure.

#### Effect of Horizontal Stress

The parameters used in this study correspond to the experimental conditions in the laboratory tests on Teton Dam silt. These parameters, along with the results of the analysis, are shown in Figure 3.8.

It can be seen from Figure 3.8 that hydraulic fracturing pressure increases with horizontal stress. The ratio of hydraulic fracturing pressure to the horizontal stress is about 1.5.

#### Effect of Borehole Diameter

The parameters used to study the effect of borehole diameter are listed in Figure 3.9. These parameters correspond to the experimental conditions in the laboratory tests on Teton Dam silt. The borehole diameter was varied from 0.48 cm (3/16 in) to 1.91 cm (3/4 in).

The results of the analysis are shown in Figure 3.9. According to the new theory, borehole diameter has practically no effect on hydraulic fracturing pressure. The difference between the highest and the lowest calculated values of hydraulic fracturing pressure is only  $0.03 \text{ kg/cm}^2$ , or about 1%.

These results conflict with Haimson's (1968) results for tests on marble. It is not understood why Haimson's tests do not agree with the theory or the tests on soil described in this report.

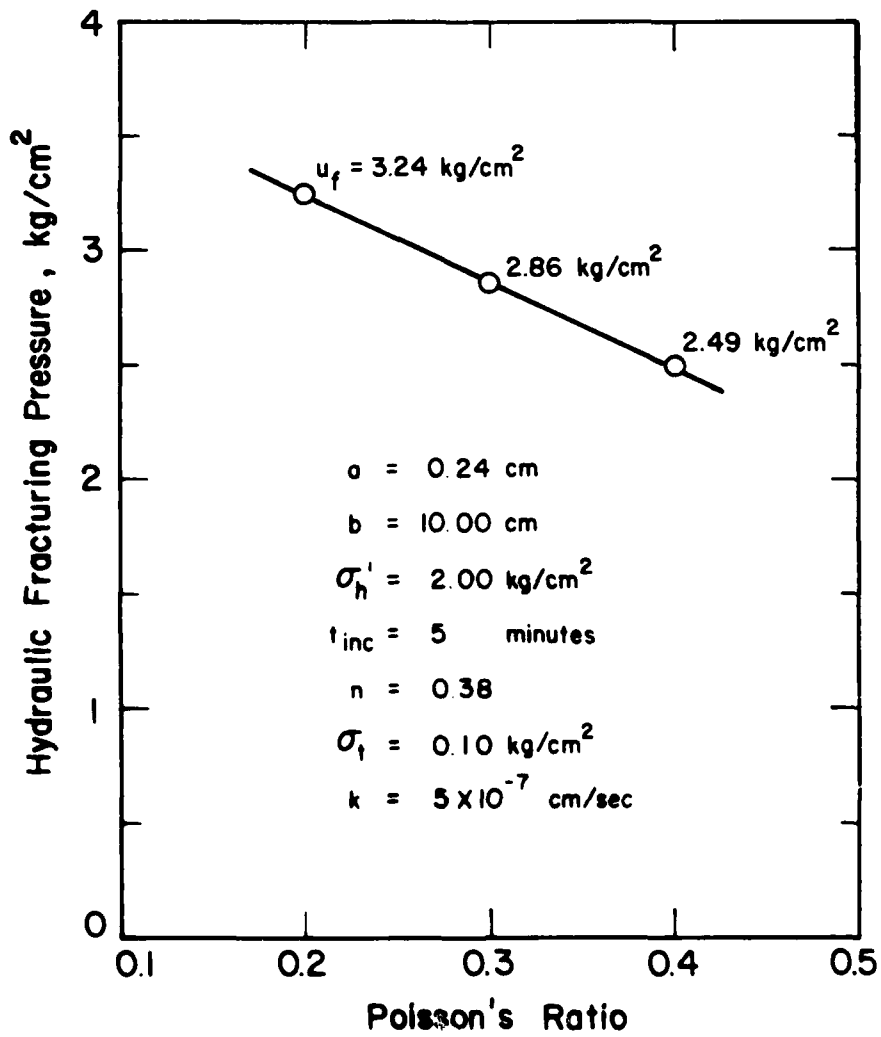


Figure 3.7 Effect of Poisson's ratio on prediction of hydraulic fracturing pressure by proposed theory

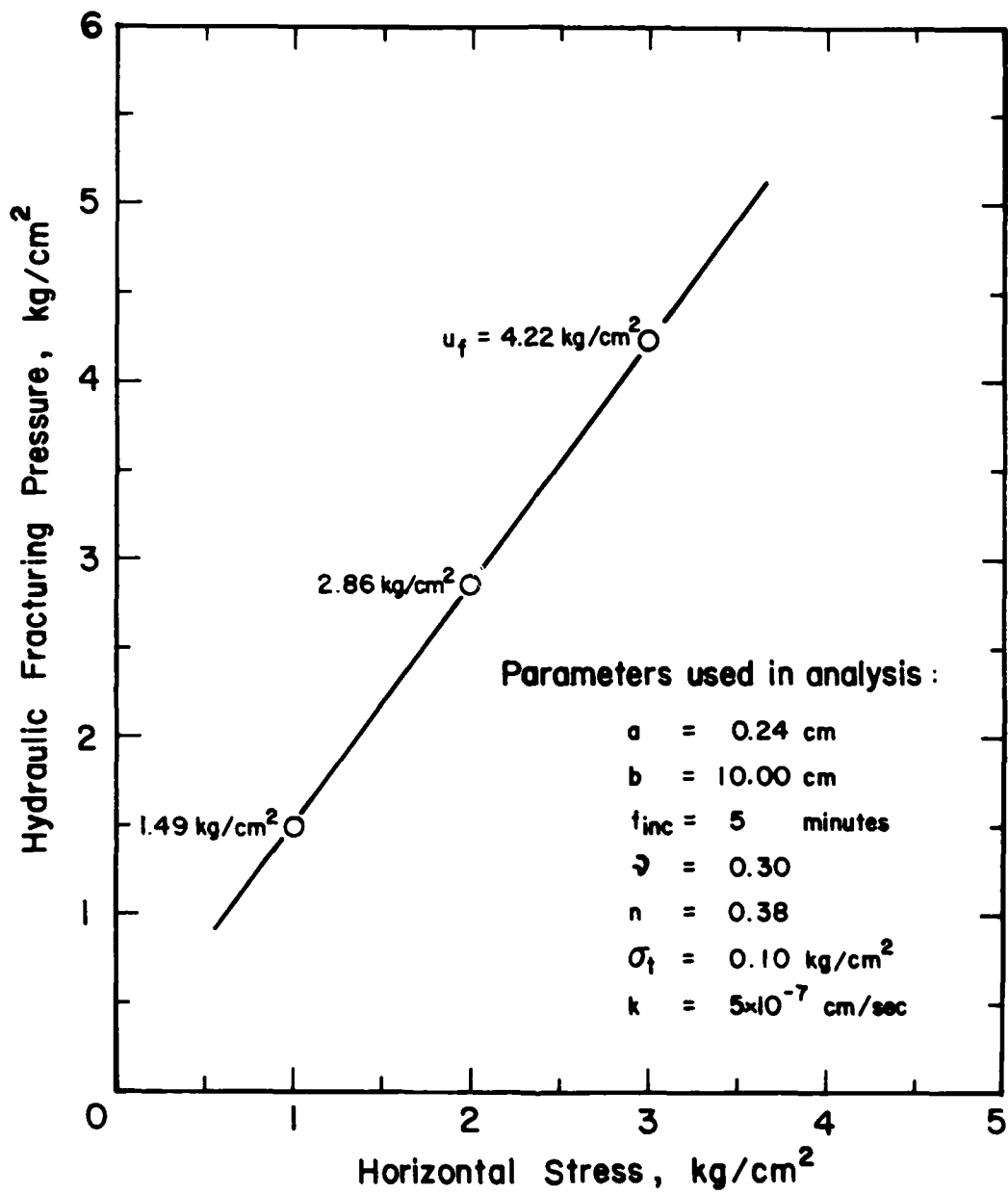


Figure 3.8 Effect of horizontal stress on prediction of hydraulic fracturing pressure by proposed theory

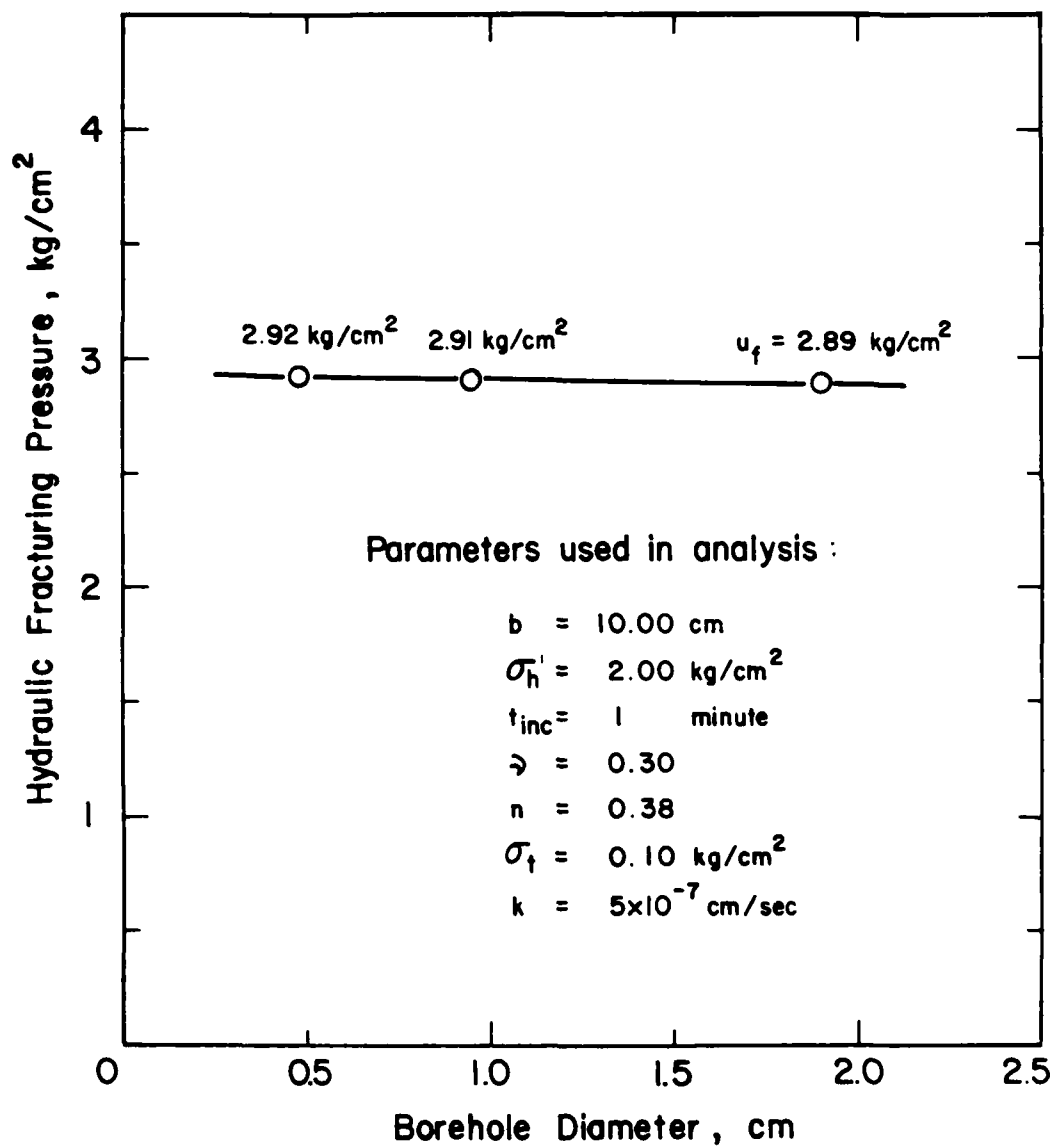


Figure 3.9 Effect of borehole diameter on prediction of hydraulic fracturing pressure by proposed theory

### Effect of Test Duration

The parameters used in this study are listed in Figure 3.10. These parameters correspond to the experimental conditions in the laboratory tests on Teton Dam silt. The time increment corresponding to an increase of  $0.1 \text{ kg/cm}^2$  in the borehole water pressure varied from 30 seconds to 6 hours.

It can be seen from Figure 3.10 that the longer the test duration, the lower is the calculated value of hydraulic fracturing pressure. In the two cases with slowest rates of pressurization, the calculated values of hydraulic fracturing pressure are the same.

When the rate of pressurization is lower, the seepage radius is larger. As shown in Figure 3.4, the larger the seepage radius, the larger is the decrease in tangential stress. Therefore, lower pressure is required to fracture a sample when the borehole is pressurized at a lower rate. The calculated values of fracturing pressure for the two cases with the largest time increments are the same because, as indicated by the computer output, the seepage zones in these cases had extended to the outer boundary of the sample before fracturing was initiated.

### Effect of Permeability

To study the effect of permeability, four analyses were performed using coefficients of permeability varying from  $1 \times 10^{-8}$  to  $1 \times 10^{-5}$  cm/sec. The values of other parameters are listed in Figure 3.11.

It can be seen from Figure 3.11 that the calculated value of hydraulic fracturing pressure decreases as the permeability increases. A ten-fold increase in permeability reduces the calculated value of fracturing pressure by about  $0.1 \text{ kg/cm}^2$ .

The higher the permeability of a soil, the larger is the seepage radius

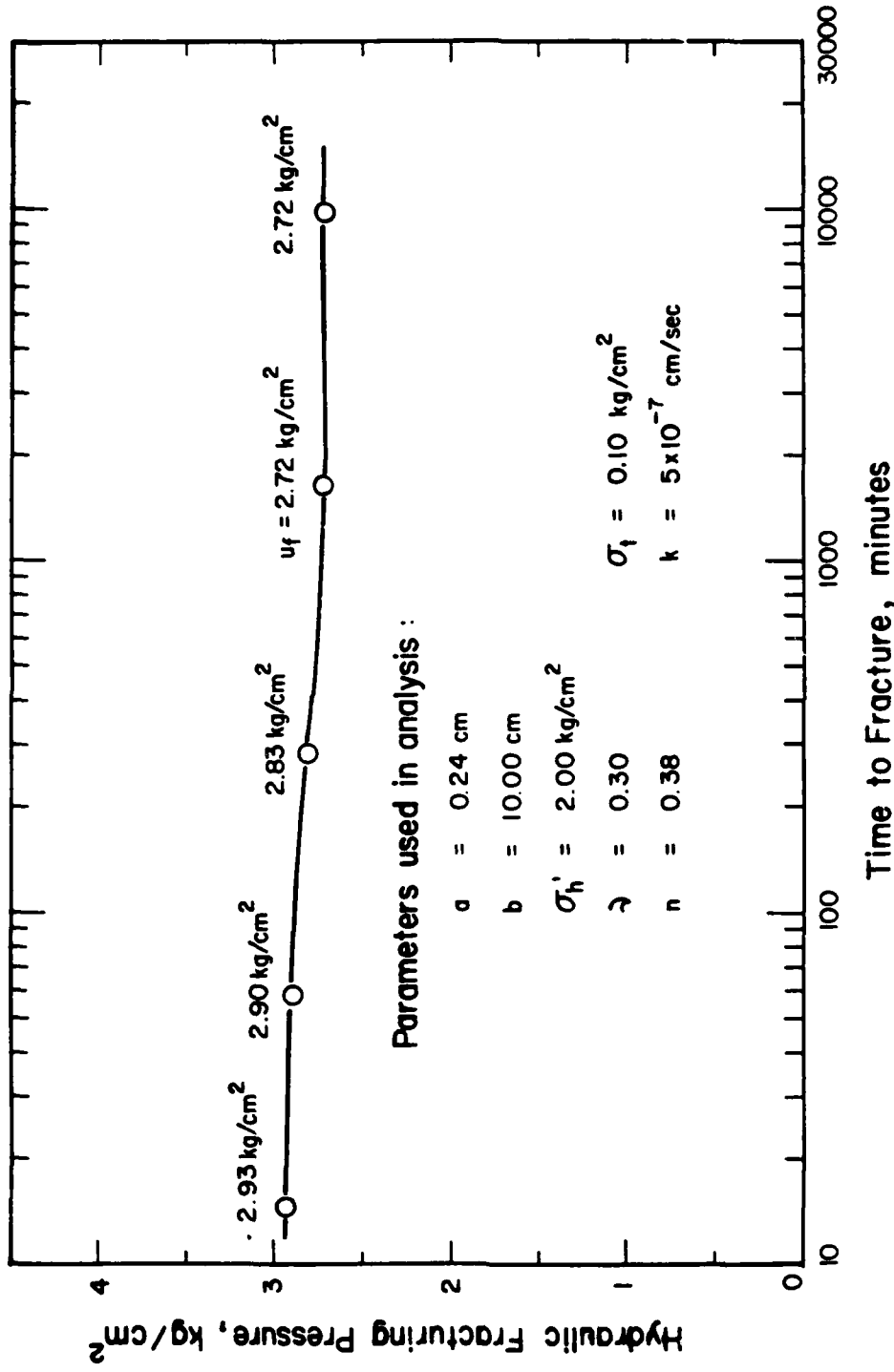


Figure 3.10 Effect of test duration on prediction of hydraulic fracturing pressure by proposed theory

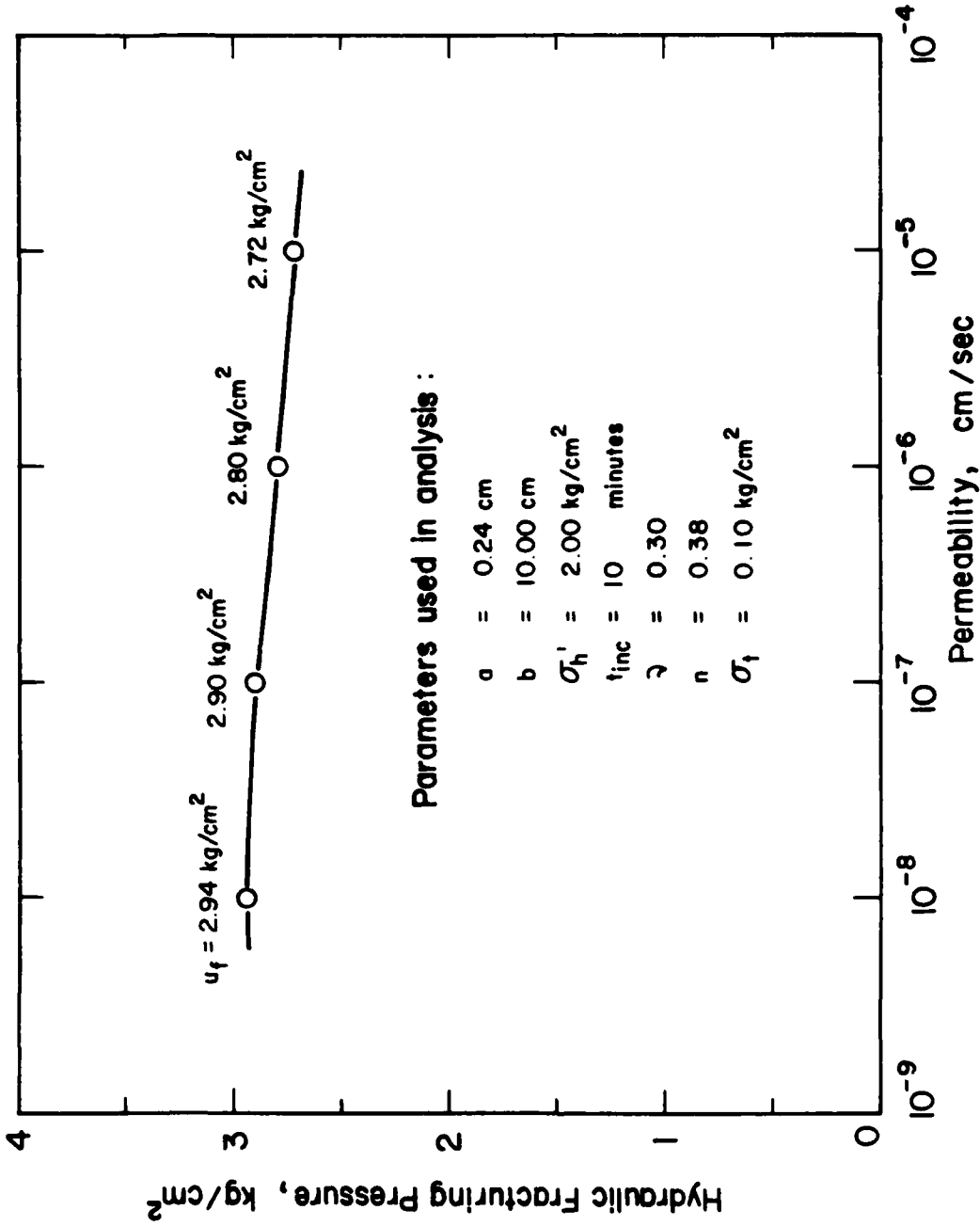


Figure 3.11 Effect of permeability on prediction of hydraulic fracturing pressure by proposed theory

at the same borehole water pressure. It was shown in Figure 3.4 that a larger seepage radius causes a larger reduction in tangential stress. Therefore, lower borehole water pressure is required to fracture a sample with higher permeability.

#### Effect of Tensile Strength

The parameters used to study the effect of tensile strength are listed in Figure 3.12. The values of tensile strength were varied from 0.2 to 0.6 kg/cm<sup>2</sup>.

The results of the analysis are shown in Figure 3.12, which indicates that the calculated value of hydraulic fracturing pressure increases with tensile strength.

#### Summary of Parameter Study

The results of the parameter study can be summarized as follows:

- (1) Calculated values of hydraulic fracturing pressure increase with increasing horizontal stress.
- (2) Borehole diameter has practically no effect on the calculated values of hydraulic fracturing pressure.
- (3) Longer test duration and higher permeability lead to slightly lower calculated values of hydraulic fracturing pressure.
- (4) The calculated values of hydraulic fracturing pressure increase with the tensile strength of the soil.
- (5) Calculated hydraulic fracturing pressure decreases with increasing value of Poisson's ratio.

#### FINITE ELEMENT ANALYSES

The finite element study described in the following pages was performed to investigate the effects of nonlinear soil behavior on the stresses required to initiate hydraulic fracturing around a borehole. The analyses were performed using a finite element computer program

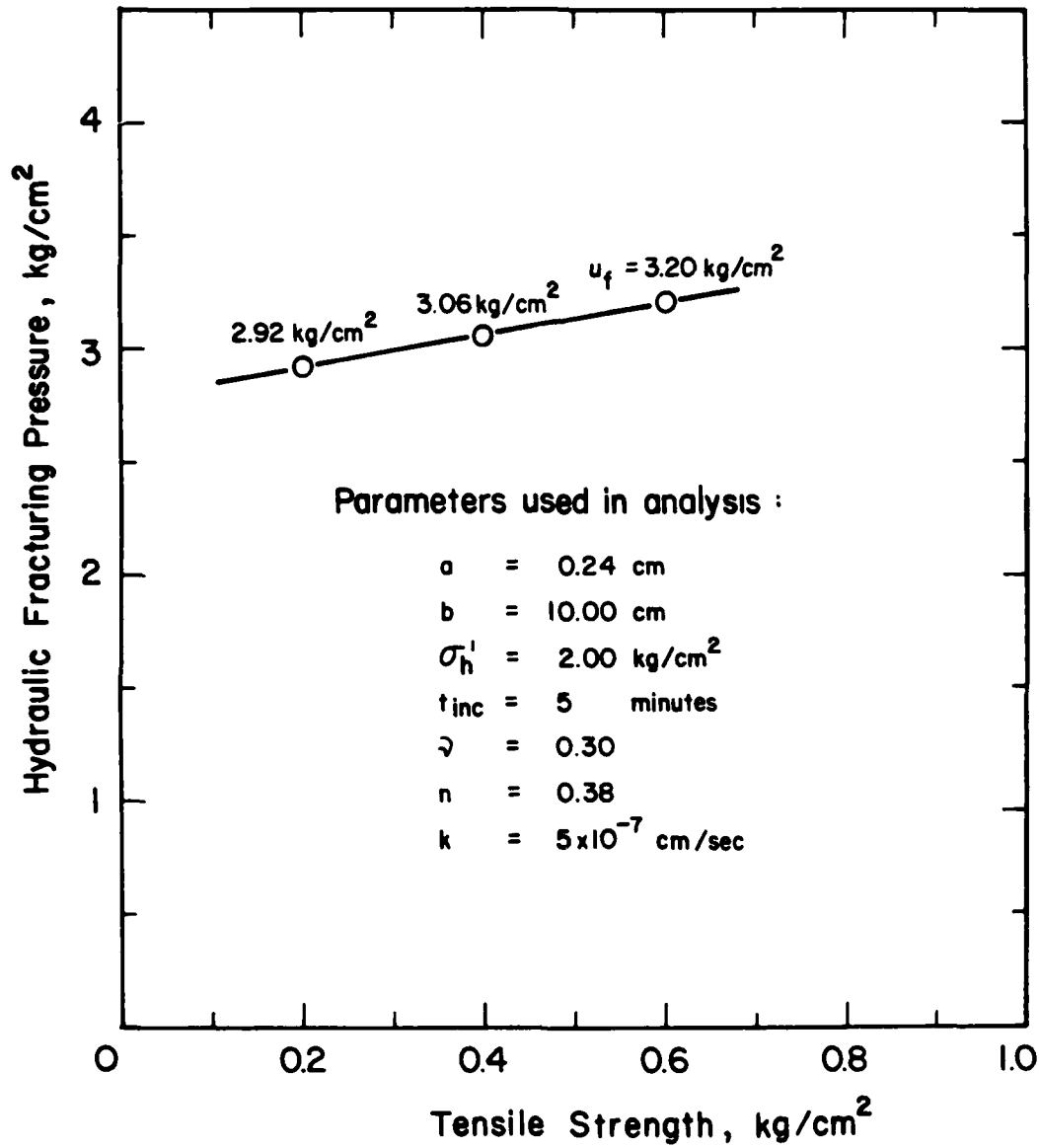


Figure 3.12 Effect of tensile strength on prediction of hydraulic fracturing pressure by proposed theory

called CONSAX. CONSAX is an axisymmetric finite element computer program, capable of treating the coupled problems of nonlinear soil deformation and fluid flow (D'Orazio and Duncan, 1982).

The finite element mesh used in the analyses is shown in Figure 3.13. The mesh consists of 12 six-node elements. The displacements of the nodal points were restricted in the vertical direction (plane strain condition). The pore pressures of the two nodal points at the outer boundary were assumed to be zero and the outer boundary points were free to move radially. The initial stresses in all of the elements were the same, with vertical stresses twice as large as the horizontal stresses. To model the excavation of a borehole, a negative change in radial stress, equal to the value of the initial horizontal stress, was applied at the borehole wall. Subsequently, the increase in borehole water pressure was modelled by incrementally applying positive changes in radial stress at the borehole wall, and simultaneously specifying pore pressures of the same magnitude at the two nodal points on the borehole wall.

The values of the material properties used in the finite element analyses were determined from drained tests on Teton Dam silt, using the procedure developed by D'Orazio and Duncan (1982). The values of the material properties are listed in Table 3.2.

Hydraulic fracturing was assumed to begin when the calculated value of effective tangential stress at the borehole wall became equal to the tensile strength of the soil. The theoretical studies described in the second part of this chapter indicated that only a very small additional pressure is required to extend a crack indefinitely once it forms, and that initiation of a fracture is thus practically coincident with complete fracture.

As a result of excavating the borehole, the finite element analyses indicated that the tangential stress at the borehole wall would be higher

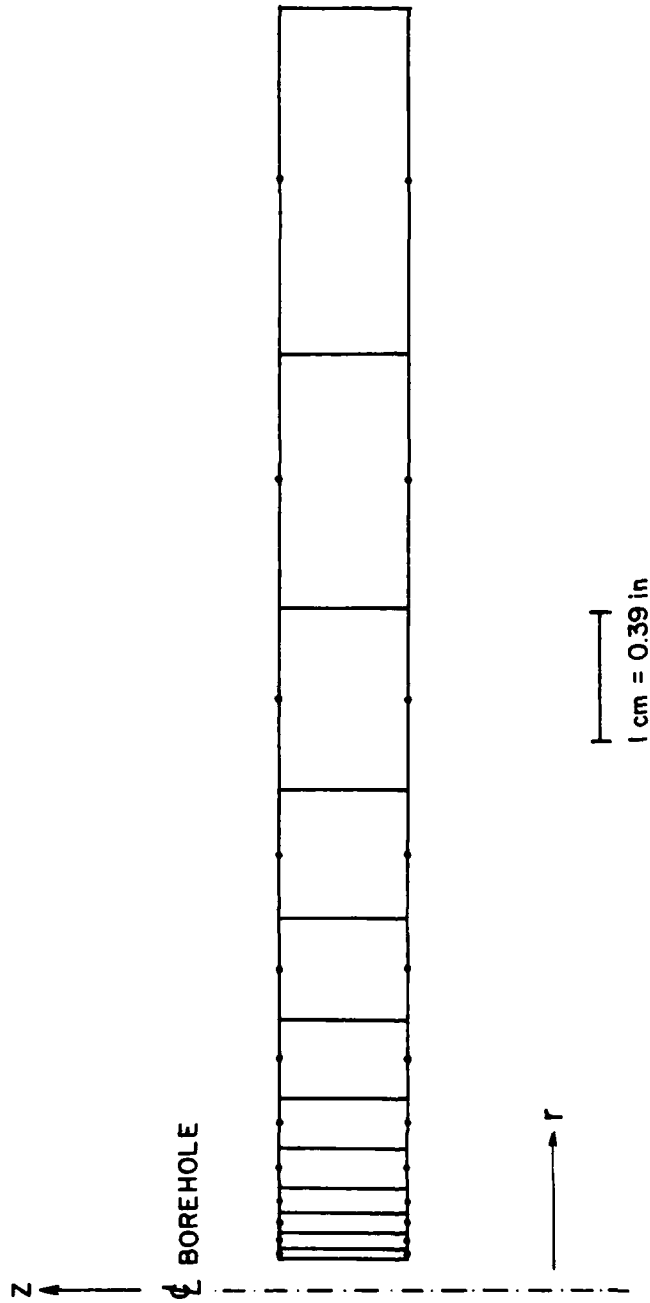


Figure 3.13 Axisymmetric finite element mesh

Table 3.2 Values of Material Properties Used in Finite Element Analyses

Parameter	Symbol	Value
Moist unit weight	$\gamma$	2.00 t/m <sup>3</sup>
Slope of recompression e vs ln p <sub>o</sub> ' curve	K	0.0048
Strength parameter	M	1.636
Intercept stress	p <sub>r</sub>	0.18 kg/cm <sup>2</sup>
Saturated permeability	k <sub>s</sub>	5X10 <sup>-7</sup> cm/sec
Degree of saturation at which water begins to move freely	S <sub>f</sub>	0.
Initial void ratio	e <sub>o</sub>	0.60
Initial degree of saturation	S <sub>o</sub>	0.85
Tensile strength	$\sigma_t$	0.10 kg/cm <sup>2</sup>
Poisson's ratio	$\nu$	0.40

Note: Values of P<sub>p</sub> were set equal to P<sub>o</sub>' for each element.

p<sub>o</sub>' vs  $\lambda$  Relationship

p <sub>o</sub> ', kg/cm <sup>2</sup>	$\lambda$
1.92	0.0119
4.15	0.0179
8.03	0.0214

Note:

M = Strength parameter, slope of line describing variation of effective mean normal stress, p', with value of generalized deviatoric stress at failure, q<sub>f</sub>

p<sub>r</sub> = Intercept stress, where the line describing variation of effective mean normal stress, p', with value of generalized deviatoric stress at failure, q<sub>f</sub>, intersects the p' axis

p<sub>o</sub>' = Effective stress where yield surface intersects the p' axis.

$\lambda$  = Slope of virgin isotropic consolidation curve

than the initial horizontal stress. However, unlike the result of the elastic theory, the value of the tangential stress at the borehole wall when calculated by the finite element method was found to be less than twice the initial horizontal stress. This appears to be due to nonlinear behavior; as the stresses in elements near to the borehole wall approach failure, the stiffnesses of these elements decrease, and stresses tend to be redistributed to elements further from the borehole. The strength of the soil need not be fully mobilized for this to occur, and, indeed, the finite element analyses indicated that the elements near the borehole walls were highly stressed, but were not in a state of failure.

As the borehole water pressure was increased, the calculated tangential stress in the soil decreased. The bulk modulus is a function of the effective stress, and its value decreased with decreasing tangential stress. In the nonlinear analyses, in which the values of the bulk modulus declined without limit as the tangential stress decreased (behavior typical of cohesionless soils), no tensile stress ever developed in the soil around the borehole. To model the behavior of cohesive soil more realistically, additional finite element analyses were performed considering that the soil immediately adjacent to the borehole wall was linear elastic at low effective stress. In these analyses, as the value of the tangential stress decreased to zero and negative values, the value of the bulk modulus of the soil was not permitted to decline below  $500 \text{ kg/cm}^2$ , a characteristic representative of soils with some cohesion. With this type of behavior, tensile stress could develop in the soil around the borehole. Thus it seems clear that some degree of cohesive behavior, at least at values of effective stress close to zero, is essential for hydraulic fracturing. Soils such as sands, gravels, and non-plastic silts, which do not exhibit

cohesive behavior near zero effective stress, could never undergo hydraulic fracturing.

A typical set of results for a finite element analysis is shown in Figure 3.14. The distribution of the tangential stress away from the borehole is shown for various values of borehole water pressures. It may be seen that the tangential stress at the borehole wall became equal to the tensile strength of the soil ( $\sigma_t = 0.10 \text{ kg/cm}^2$ ) when the borehole water pressure was about  $2.85 \text{ kg/cm}^2$ . The theory described in the previous section gave essentially the same result. Thus the finite element analyses indicated that the theory described previously is reasonable.

The results of the finite element analyses were found to be influenced by the values of Poisson's ratio used in the analyses, in the same way as were the results of the theory described earlier. As shown in Figure 3.15, the borehole water pressure required to initiate fracturing for the analysis conditions shown was  $2.43 \text{ kg/cm}^2$  when the value of Poisson's ratio used was 0.4; however, the calculated pressure was  $2.85 \text{ kg/cm}^2$  when the value of Poisson's ratio used in the analysis was 0.3.

The effects of borehole diameter, test duration, permeability, and tensile strength on the calculated hydraulic fracturing pressure are shown in Figures 3.16 through 3.19. It can be seen from these figures that the calculated fracturing pressure decreases with test duration and permeability, increases with tensile strength, and is independent of borehole diameter. Thus the results agree very well with those of the theory described in the previous section.

The effect of water content was studied by varying the values of the degree of saturation in the analyses. The finite element program CONSAX used Poiseuille's equation to calculate the permeability value for the partly saturated soil, i.e. the saturated permeability is multiplied by

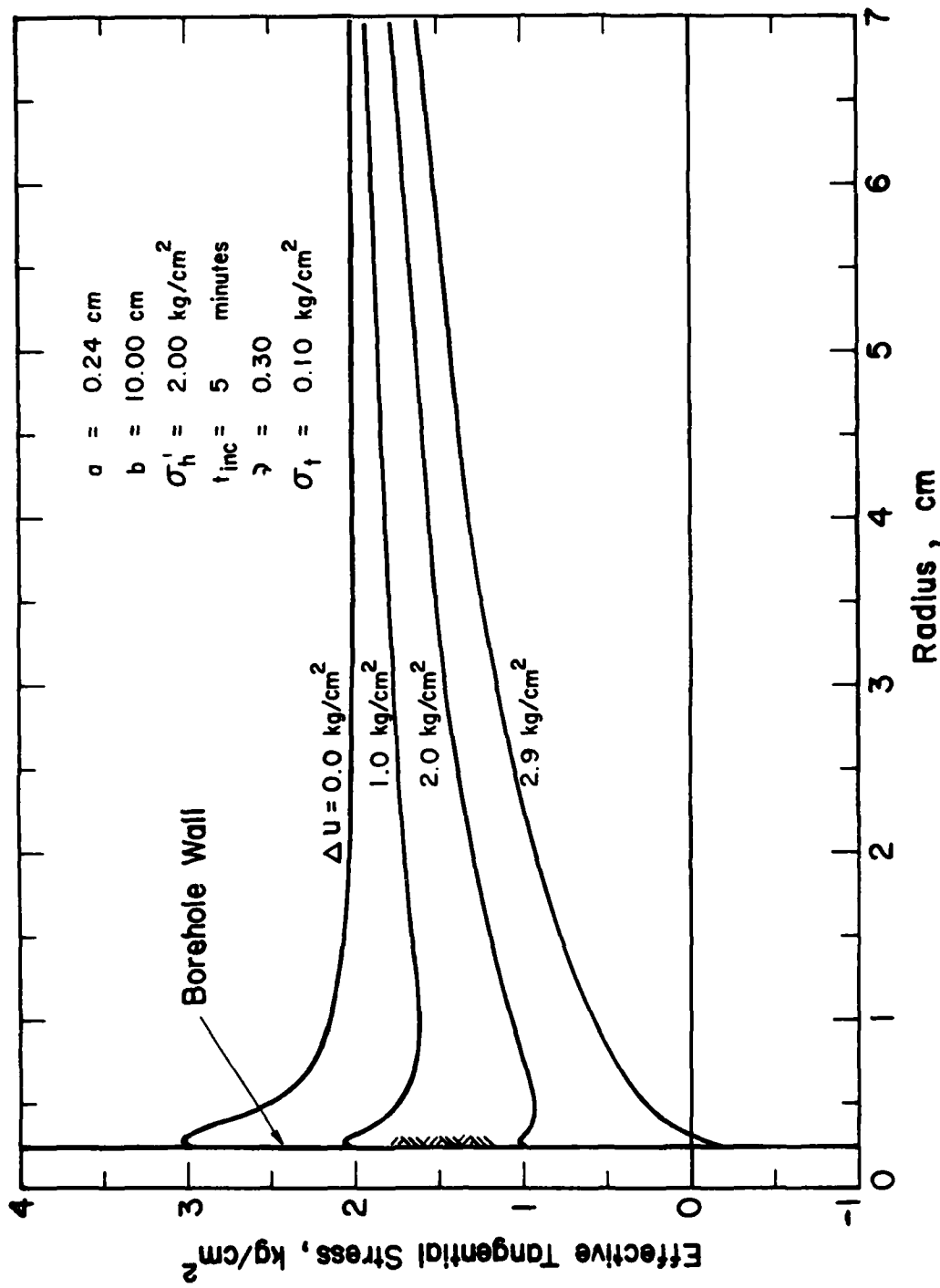


Figure 3.14 Distribution of tangential stress as borehole water pressure increases

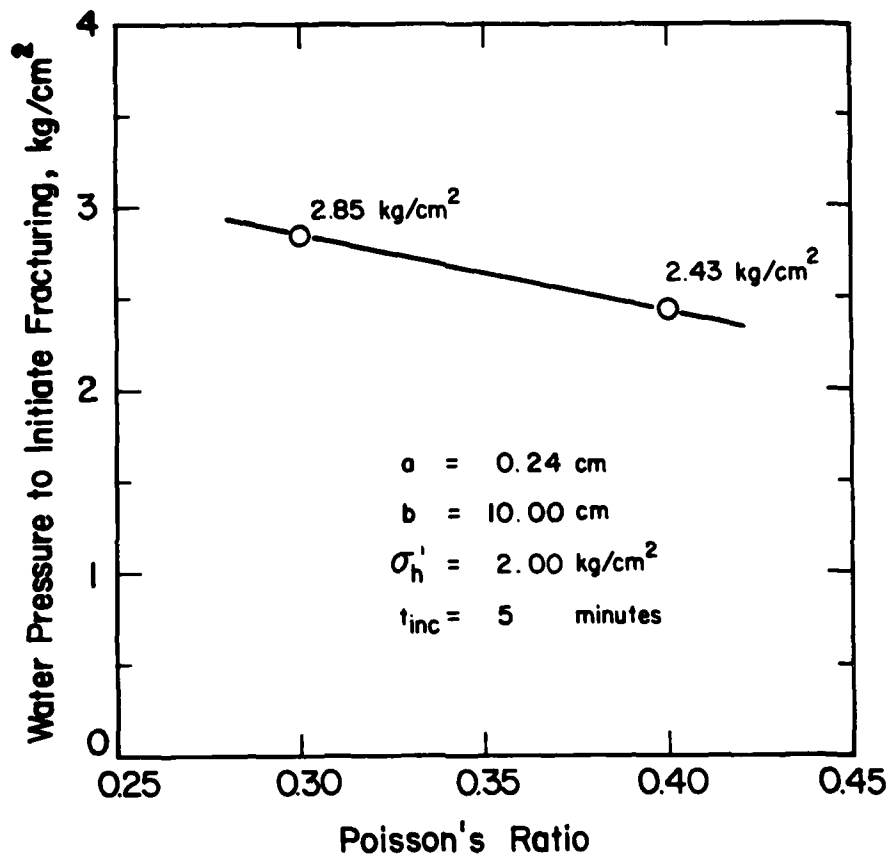


Figure 3.15 Effect of Poisson's ratio on prediction of water pressure required to initiate fracturing by finite element method

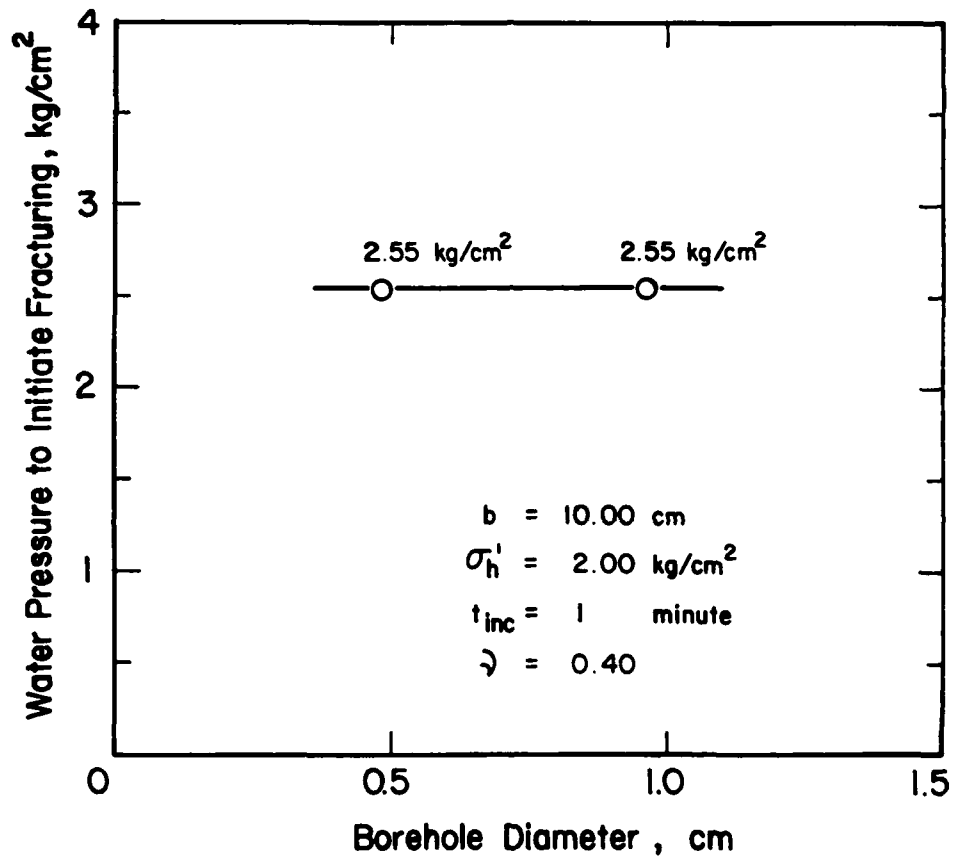


Figure 3.16 Effect of borehole diameter on prediction of water pressure required to initiate fracturing by finite element method

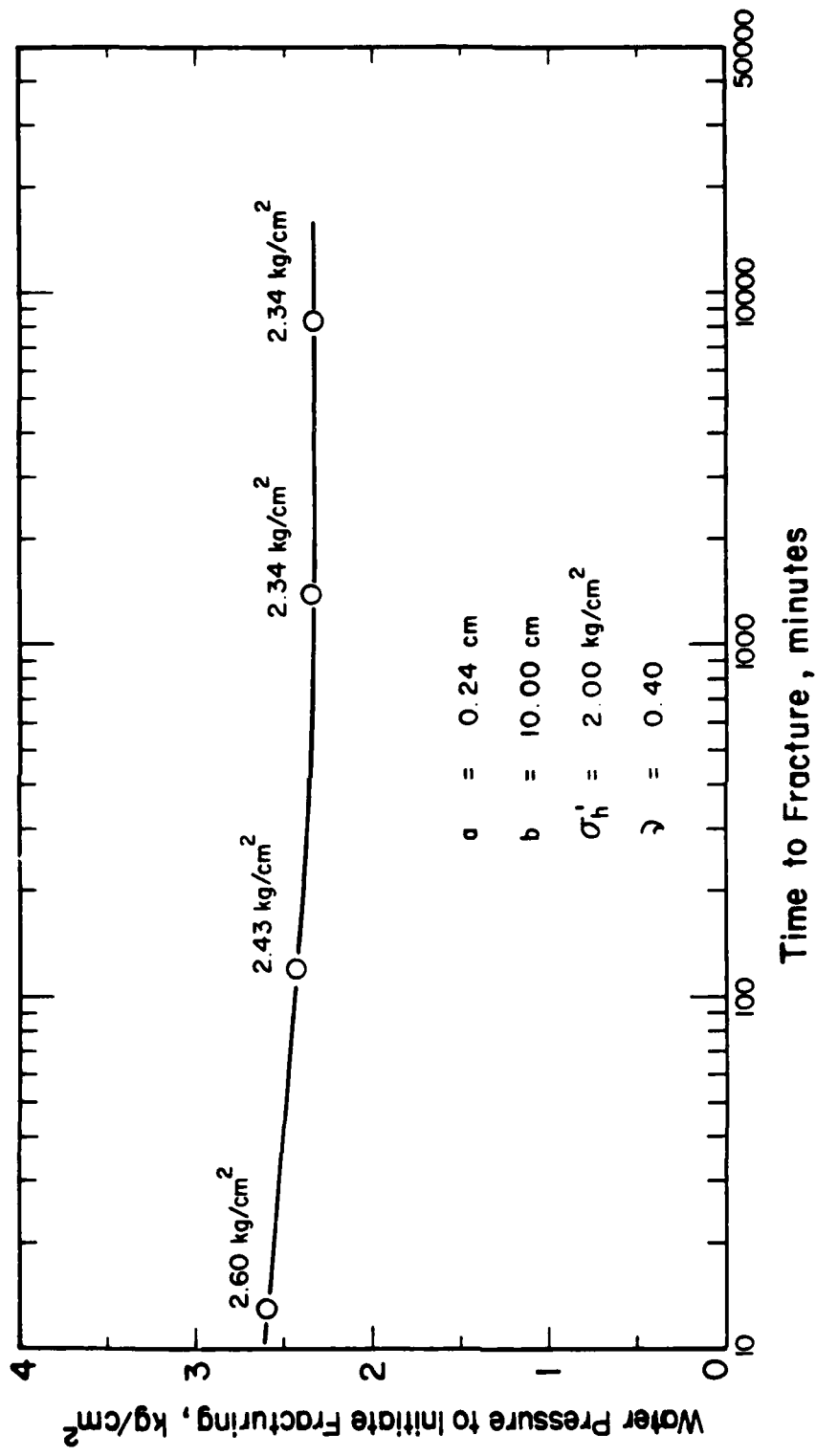


Figure 3.17 Effect of test duration on prediction of water pressure required to initiate fracturing by finite element method

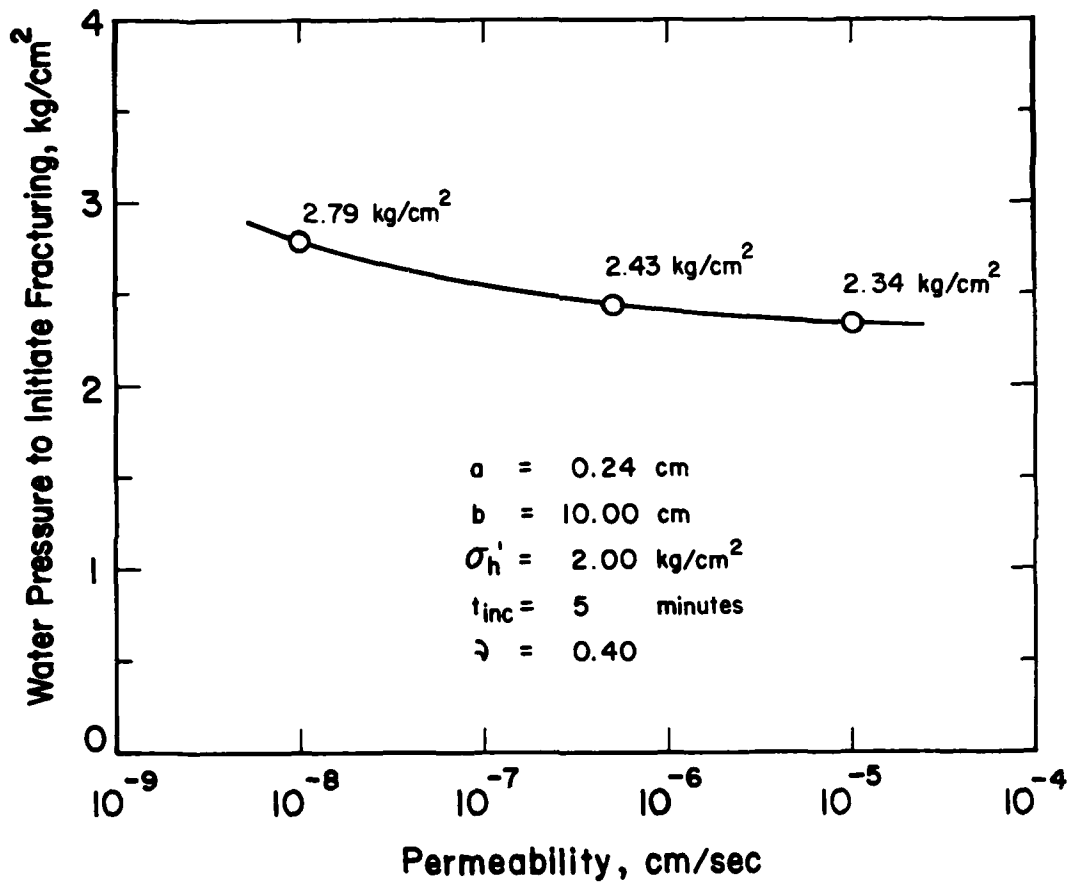


Figure 3.18 Effect of permeability on prediction of water pressure required to initiate fracturing by finite element method

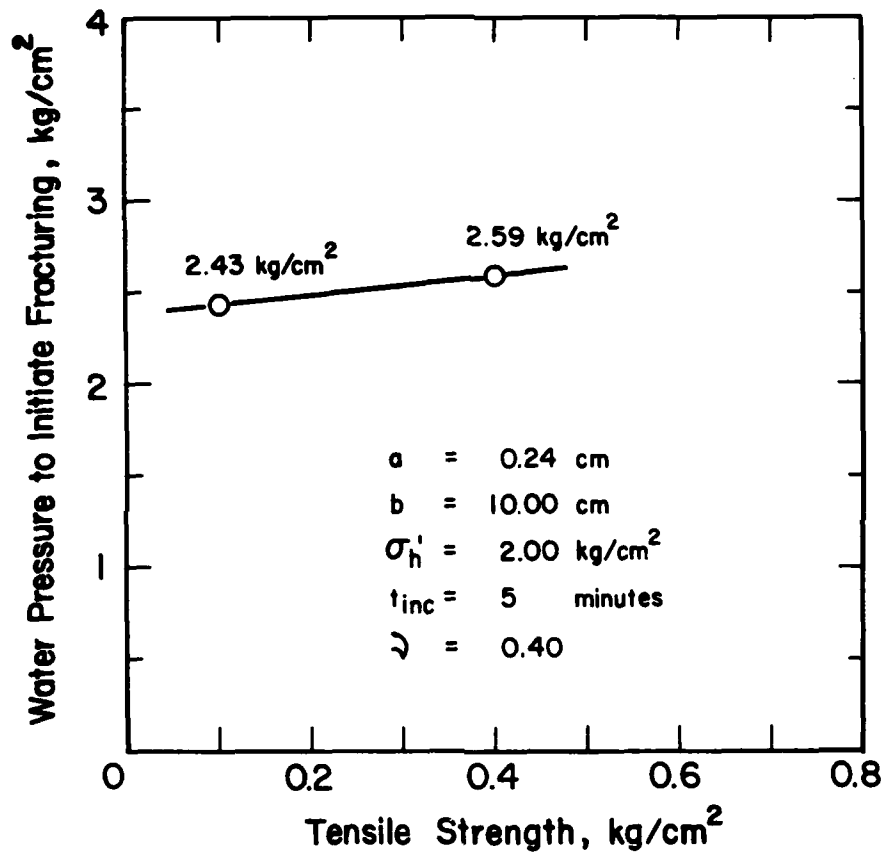


Figure 3.19 Effect of tensile strength on prediction of water pressure required to initiate fracturing by finite element method

$S^3$ , where  $S$  is the degree of saturation, to obtain the value of permeability for partially saturated soil. Thus the lower the degree of saturation, the lower is the calculated permeability. Lowering the water content would be expected to reduce the permeability by reducing the degree of saturation and thus the permeability, thereby leading to higher fracturing pressures. This is confirmed by the results of the analyses shown in Figure 3.20, which indicated that the lower the water content, the higher was the calculated pressure at which fracturing began. It is important to note that the values of the other properties employed in the analyses were not changed when the water content was varied. In reality, changing the compaction water content might affect other soil properties, most notably the tensile strength and the saturated permeability, which could in turn affect the hydraulic fracturing pressure.

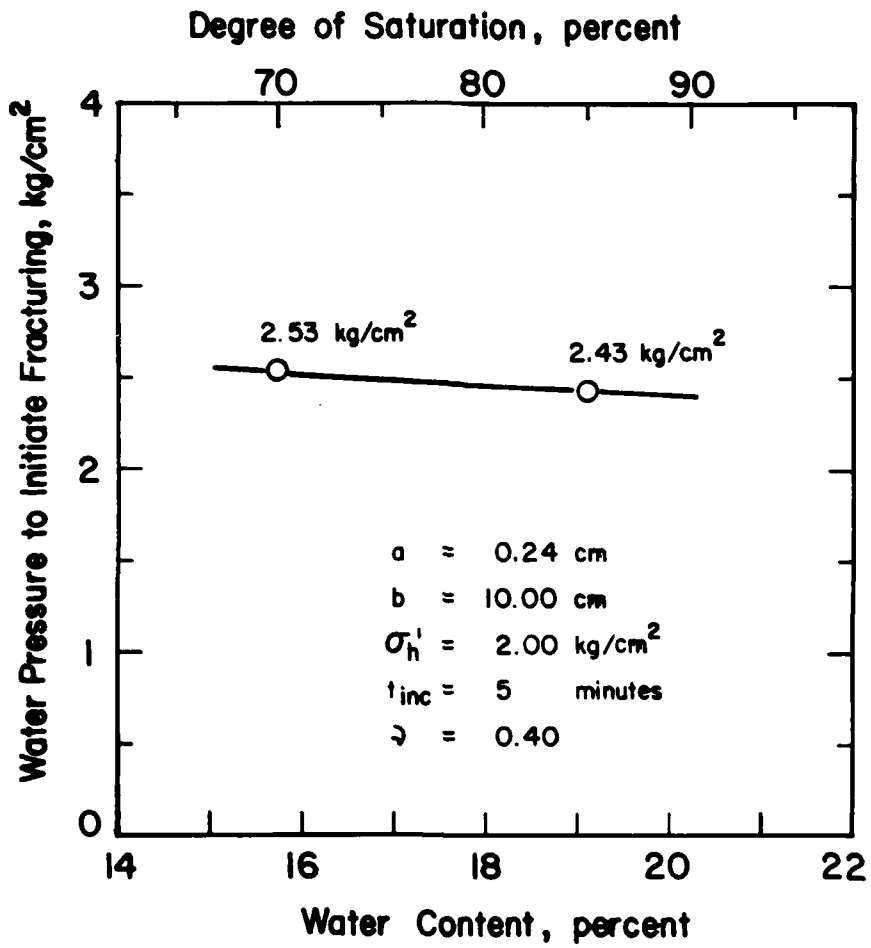


Figure 3.20 Effect of water content on prediction of water pressure required to initiate fracturing by finite element method

#### IV. EXPERIMENTAL STUDY

The purpose of this experimental study was to investigate the effects of scale, time, and permeability through hydraulic fracturing tests on compacted samples.

The tests were conducted on two types of soils--Teton Dam silt and Pittsburg silty clay. The equipment used for this study was basically the same as that used by Jaworski et al (1979). Four types of hydraulic fracturing tests were conducted in the laboratory. The total number of tests completed was 84.

#### DESCRIPTION OF SOILS

##### Teton Dam Silt

The Teton Dam silt was derived from undisturbed block samples obtained from the core of the remainder of Teton Dam after its failure. The soil consisted primarily of aeolian silt, with small particles of caliche (a soil inclusion formed by cementation of calcium carbonate).

The liquid limit of the Teton Dam silt was about 28% and the plastic limit was about 26%. According to the Unified Soil Classification System, the soil is classified as ML.

Grainsize distribution curves for the silt are shown in Figure 4.1, together with that for Monterey sand, which was used as "transition material" in some of the tests. About 90% of the silt by weight passed the No. 200 sieve. About 15% was clay size (finer than 2 microns).

Compaction curves for the Teton Dam silt are shown in Figure 4.2. The optimum water content in the Standard Proctor compaction test was

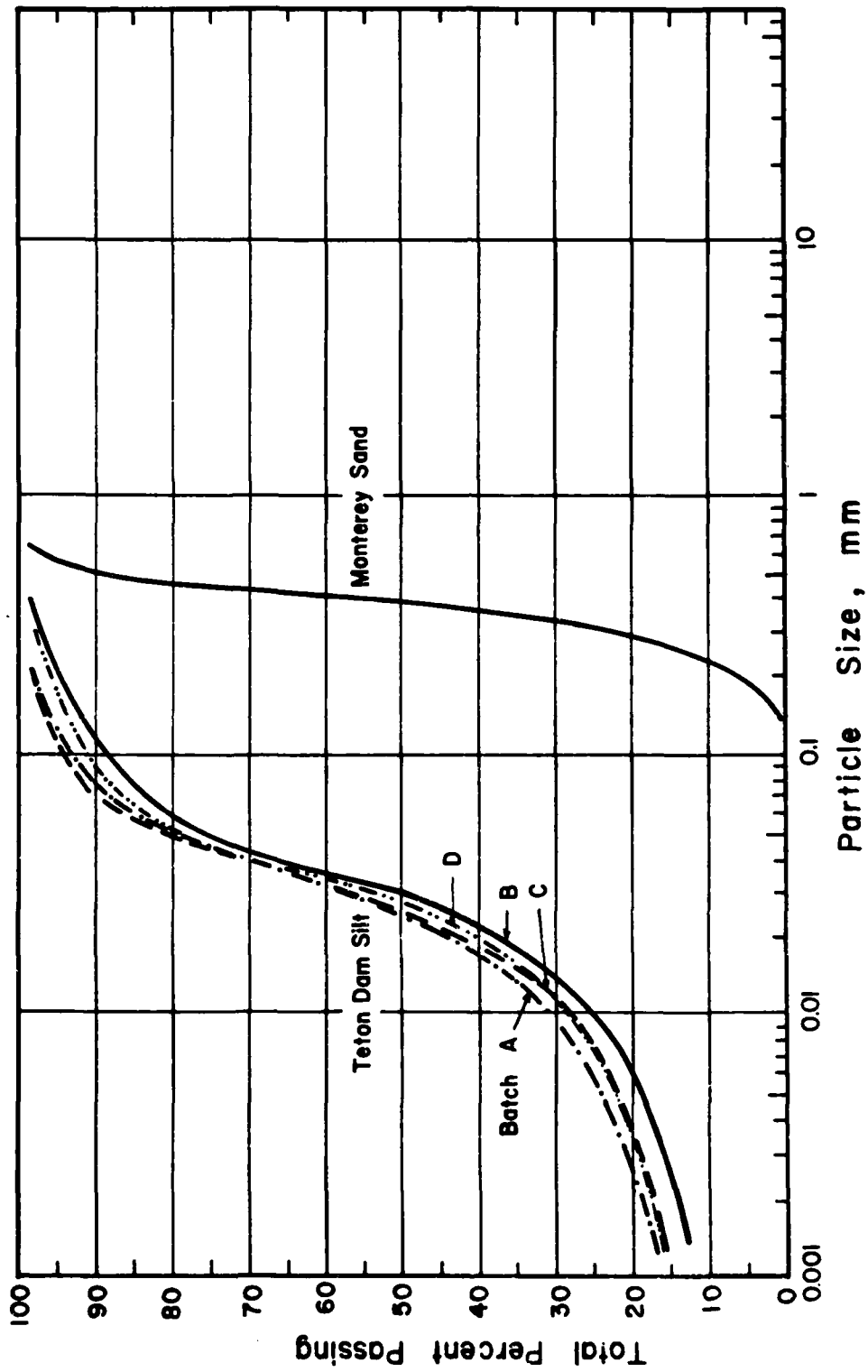


Figure 4.1 Grainsize distribution curves for Teton Dam silt and Monterey sand

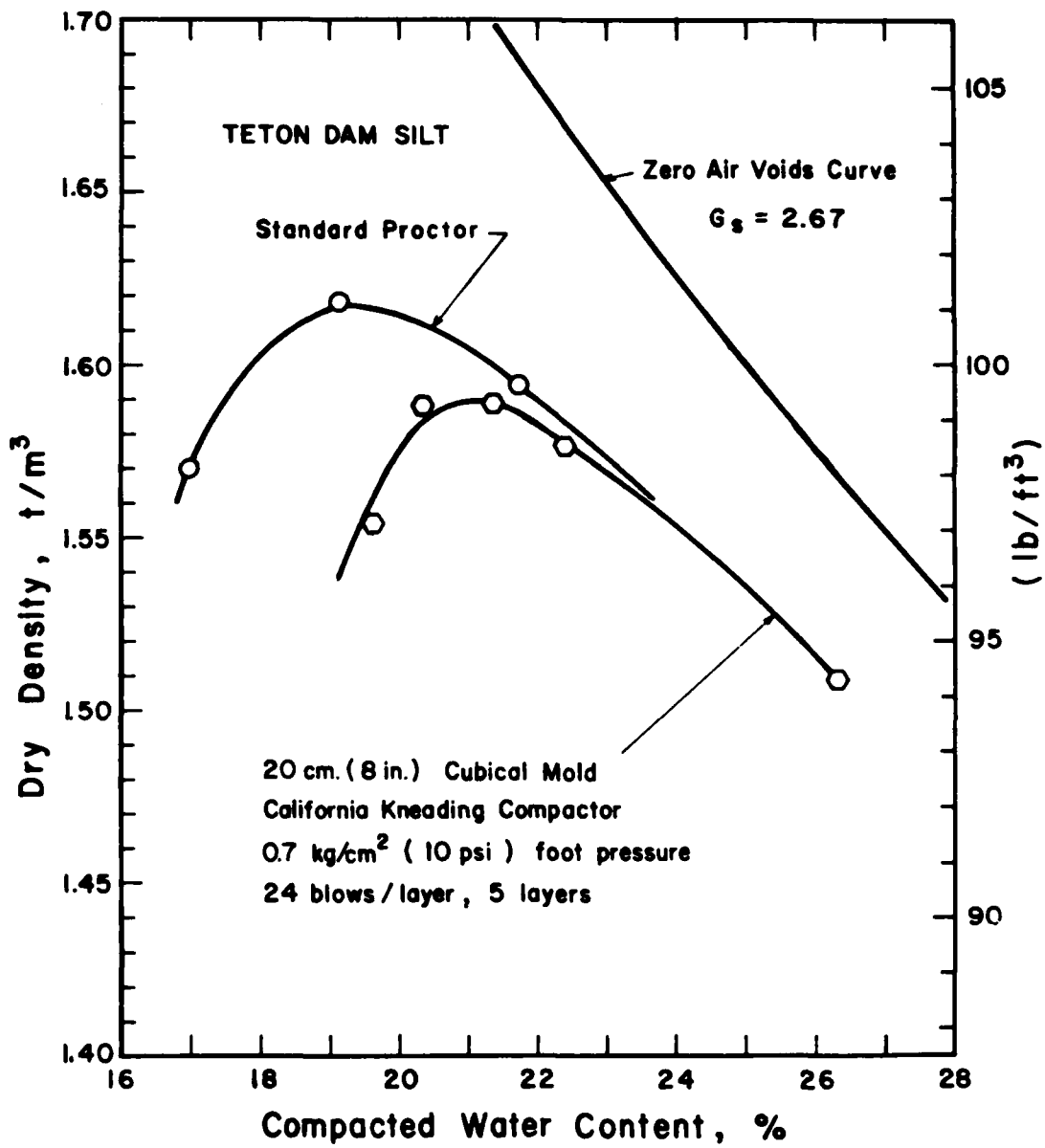


Figure 4.2 Compaction curves for Teton Dam silt, Batch A

about 19%. With the lower compactive effort used in preparing samples for hydraulic fracturing tests, using a kneading compaction procedure, the optimum water content was about 21%.

The tensile strength of Teton Dam silt, compacted to a dry density of  $1.59 \text{ t/m}^3$  (99.1 pcf) at a water content of 23.1%, was determined using diametral compression tests. The average of 3 tests was  $\sigma_t = 0.125 \pm 0.005 \text{ kg/cm}^2$ . These are total stress values and likely to be larger than the effective stress tensile strength values, considering that it is likely that the tensile test induced negative pore pressures. It is not possible to estimate how great the difference might be, however, because no data were obtained concerning pore pressures at failure during the tensile tests. For purposes of analysis, it was assumed that the total stress and effective stress values were equal; thus the value used in the analyses, which was an effective stress value, may be viewed as an upper bound on the actual effective tensile strength of the soil.

Two series of triaxial compression tests were conducted to determine the strength characteristics of the Teton Dam silt. These were consolidated-drained tests performed using confining pressures of 0.5, 1, and  $2 \text{ kg/cm}^2$  (0.5, 1, and 2 tsf) on 3.56 cm (1.4 in) diameter specimens, 8.89 cm (3.5 in) long. The density and water contents of the specimens used in the CD tests were chosen to be within the range of those of the hydraulic fracturing samples. Results are shown in Figure 4.3. The results of the tests with the two compaction conditions were very similar; the average effective cohesion intercept was  $0.14 \text{ kg/cm}^2$  (0.14 tsf) and the average effective friction angle was  $39.6^\circ$ .

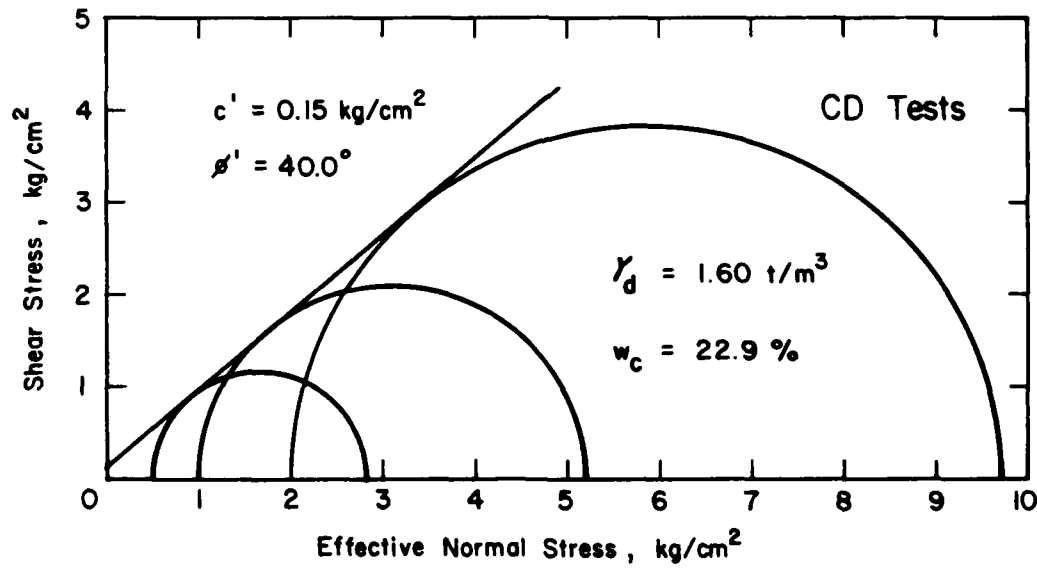
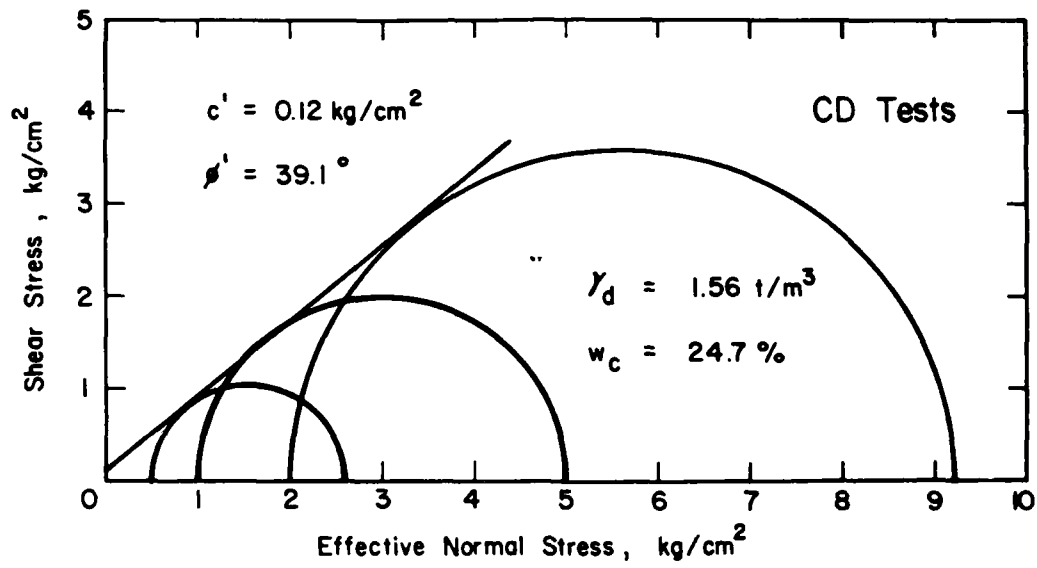


Figure 4.3 Results of consolidated drained triaxial tests on Teton Dam silt

### Pittsburg Silty Clay

The Pittsburg silty clay tested during this investigation was obtained from Pittsburg, California. The soil had a liquid limit of 45% and a plastic limit of 22%. It classifies as CL according to the Unified Soil Classification System.

The grain-size distribution curve of the clay is shown in Figure 4.4, where it can be seen that the clay size content was about 35%. The optimum water content in the Standard Proctor compaction test was about 19%, as shown in Figure 4.5.

A series of triaxial compression tests were performed to determine the strength characteristics of this material. These were consolidated-undrained tests performed using confining pressures of 0.5, 1, and 2 kg/cm<sup>2</sup> (0.5, 1, and 2 tsf) on 3.56 cm (1.4 in) diameter specimens, 8.89 cm (3.5 in) long. The density and water contents of the specimens used in the CD tests were chosen to be within the range of those of the hydraulic fracturing samples. The results, shown in Figure 4.6, showed that the effective stress cohesion intercept was 0.10 kg/cm<sup>2</sup> (0.10 tsf) and the effective friction angle was 23.4°.

## HYDRAULIC FRACTURING EQUIPMENT

### Cubical Stress Apparatus

The cubical stress apparatus used for this study was basically the same as that used by Jaworski et al (1979) except for minor modifications.

The apparatus was designed to test 20.3 cm (8 in) cubical soil samples. Three independent perpendicular stresses can be applied to the samples by water pressures acting on the latex membrane which covered three sides of the apparatus, as shown in Figure 4.7. The other three sides were solid aluminum.

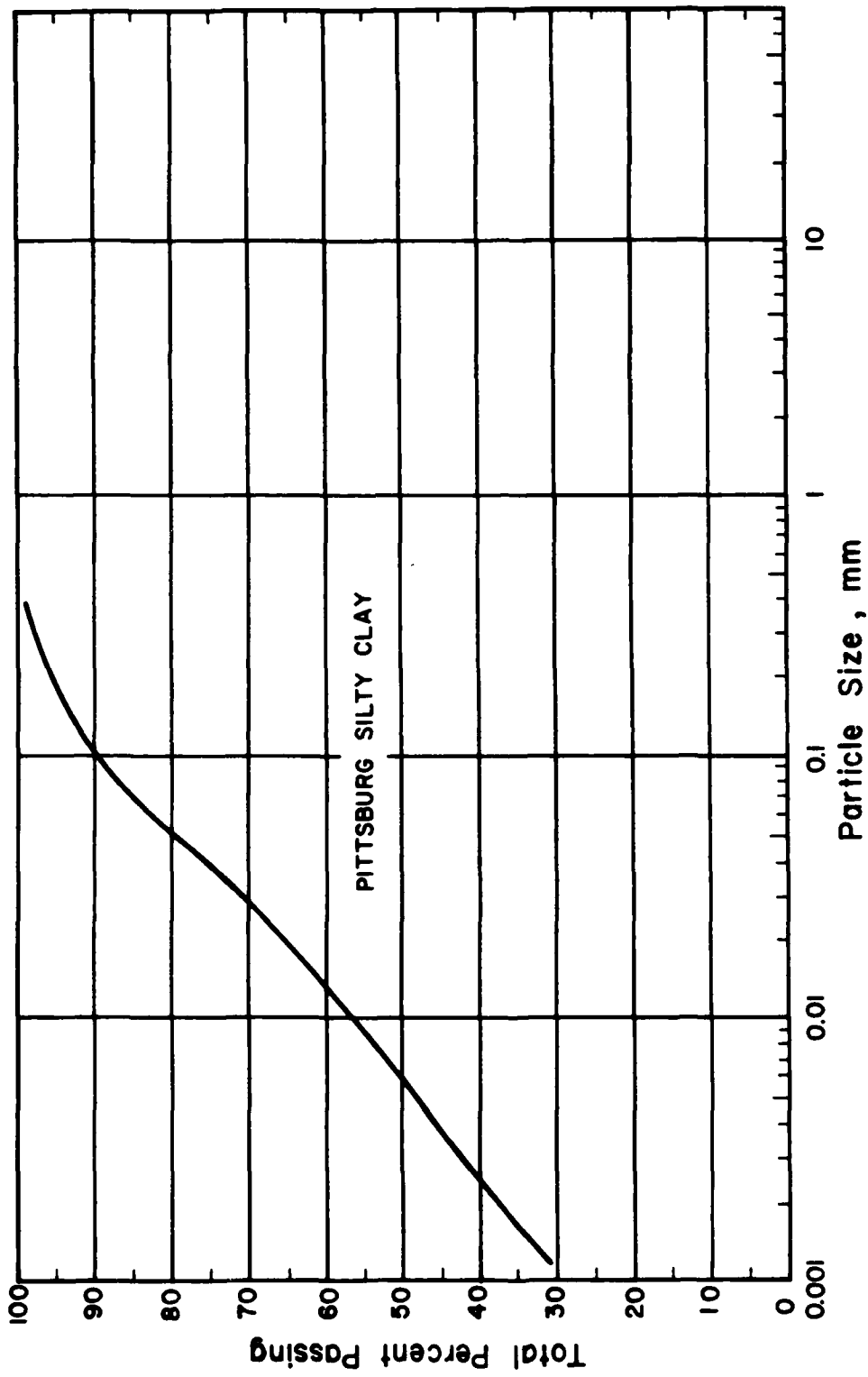


Figure 4.4 Grainsize distribution curve for Pittsburgh silty clay

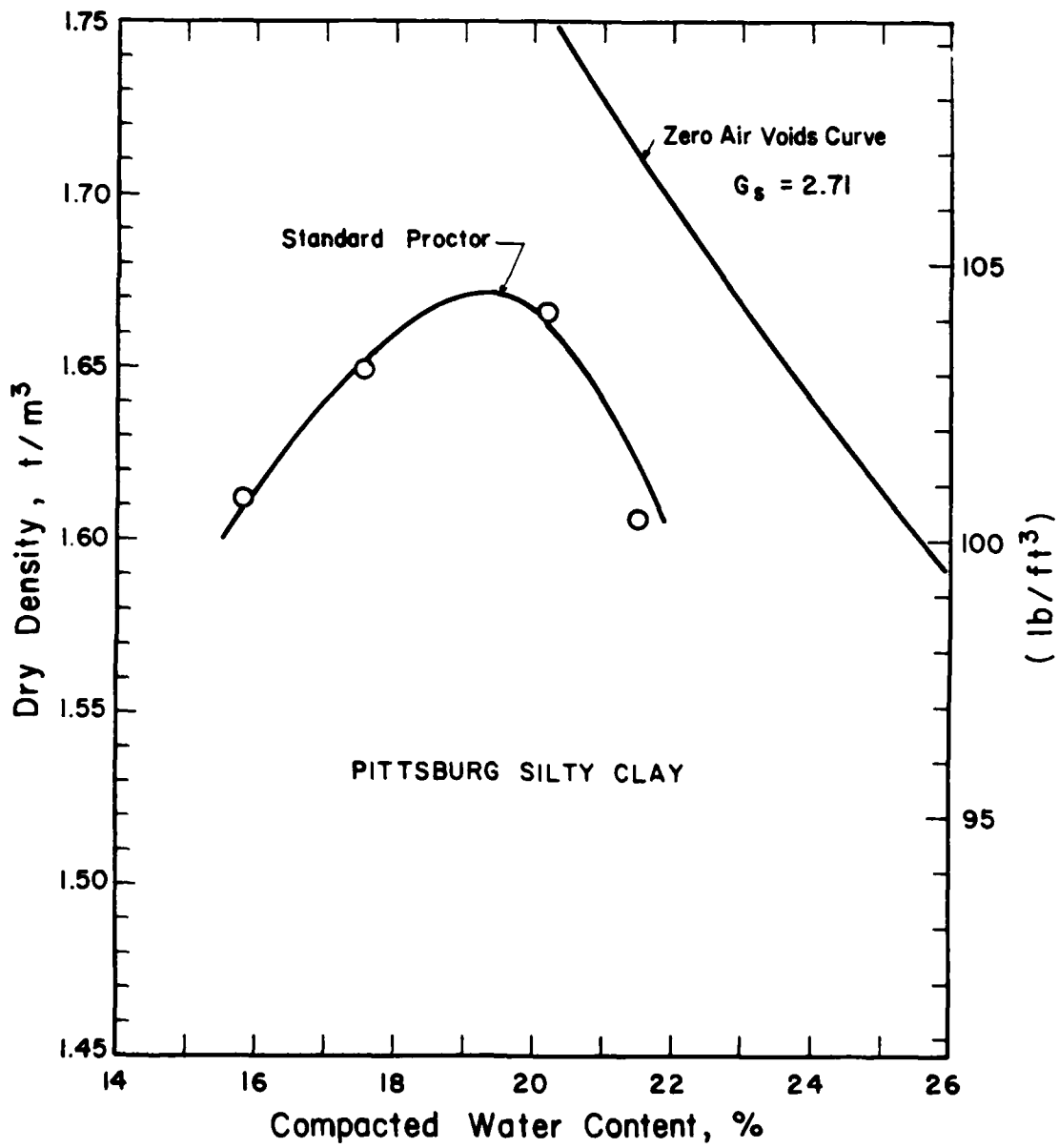


Figure 4.5 Compaction curve for Pittsburg silty clay

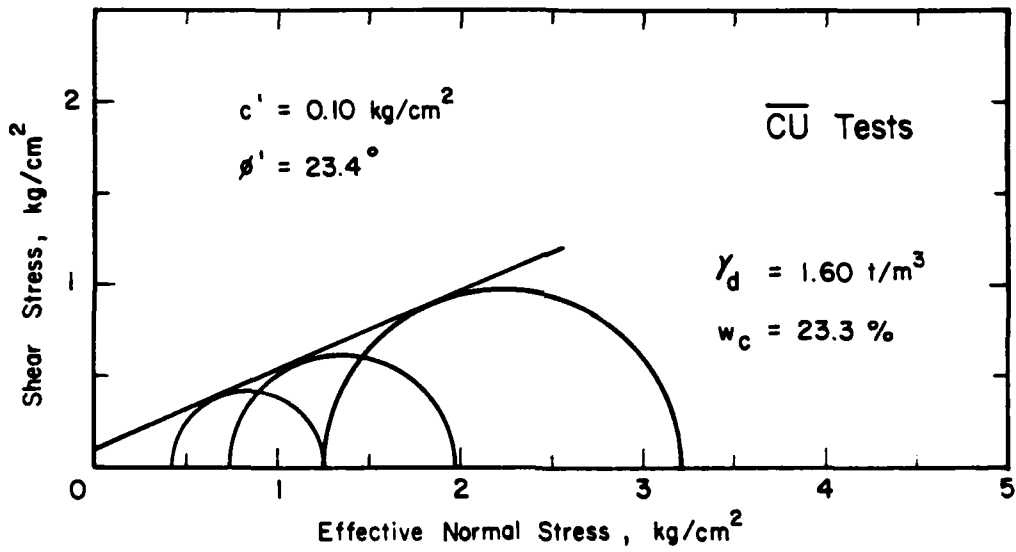


Figure 4.6 Results of consolidated undrained triaxial tests on Pittsburgh silty clay

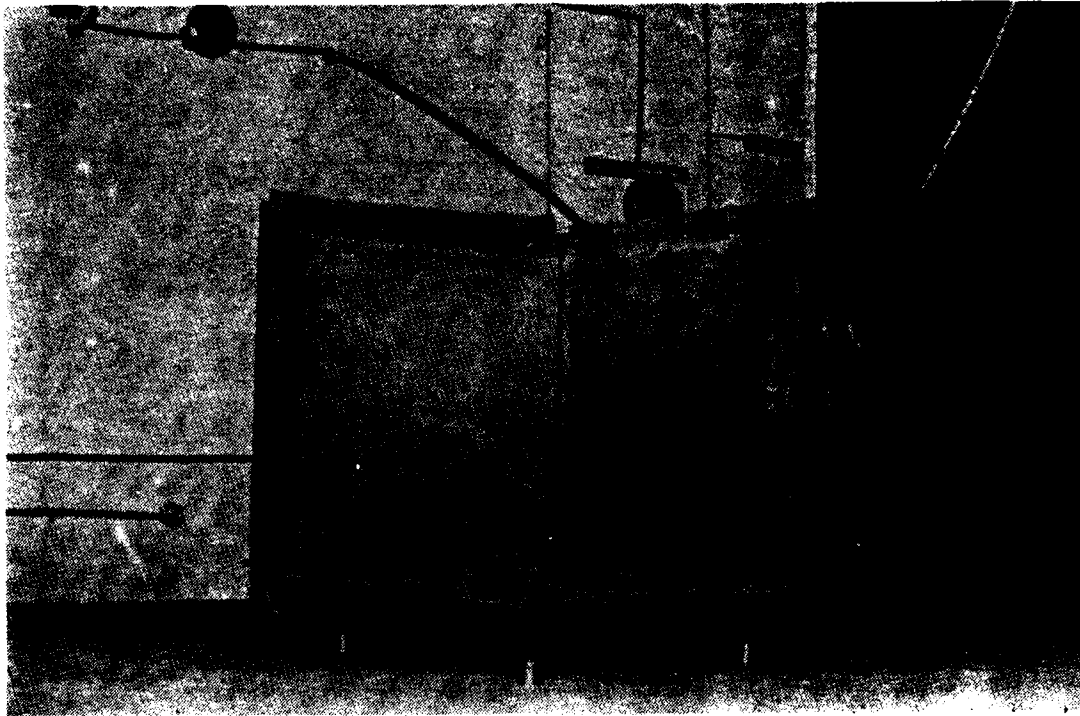


Figure 4.7 Cubical stress apparatus partly dismantled to show the membranes covering three sides of the apparatus

A cross-section through the apparatus is shown in Figure 4.8a. Between the latex membranes and the outside plates, 3.2 mm (1/8 in) movable plates were mounted on screws attached to the outside plates. The outside plates were counter-sunk to allow the movable plates to fit flush within them. The movable plates could be brought out from their counter-sunk position to a position extended 3.2 mm (1/8 in) towards the soil sample. The samples were compacted with two of the movable plates (the ones on the sides) extended. During the test, the movable plates were withdrawn into the counter-sunk position, allowing the sample to expand when fracturing occurred.

The top plate had a 3.2 cm (1-1/4 in) diameter hole for use in bore-hole fracturing tests, and one of the vertical reaction plates had a large circular opening, which could be fitted with one of the several plate inserts shown in Figure 4.8b.

#### Volume Change Measuring Device

The rate at which water flowed into a sample was determined using a volume change measuring device and a timer. Two volume changes devices were used. One of them had a higher sensitivity but lower capacity. This device was used in the beginning of the test. When the capacity of this device was nearly exhausted, the system was switched to a low sensitivity, high capacity device.

The low capacity volume change measuring device consisted of a translucent tubing coiled around a lucite cylinder which had 10 equally spaced divisions along its circumference. The position of the air-water interface was used to monitor the volume of water entering the sample. The capacity of this device was approximately  $100 \text{ cm}^3$  ( $6.1 \text{ in}^3$ ).

The high-capacity volume change measuring device consisted of a vertical lucite cylinder with an inside diameter of 4.45 cm (1-3/4 in) and

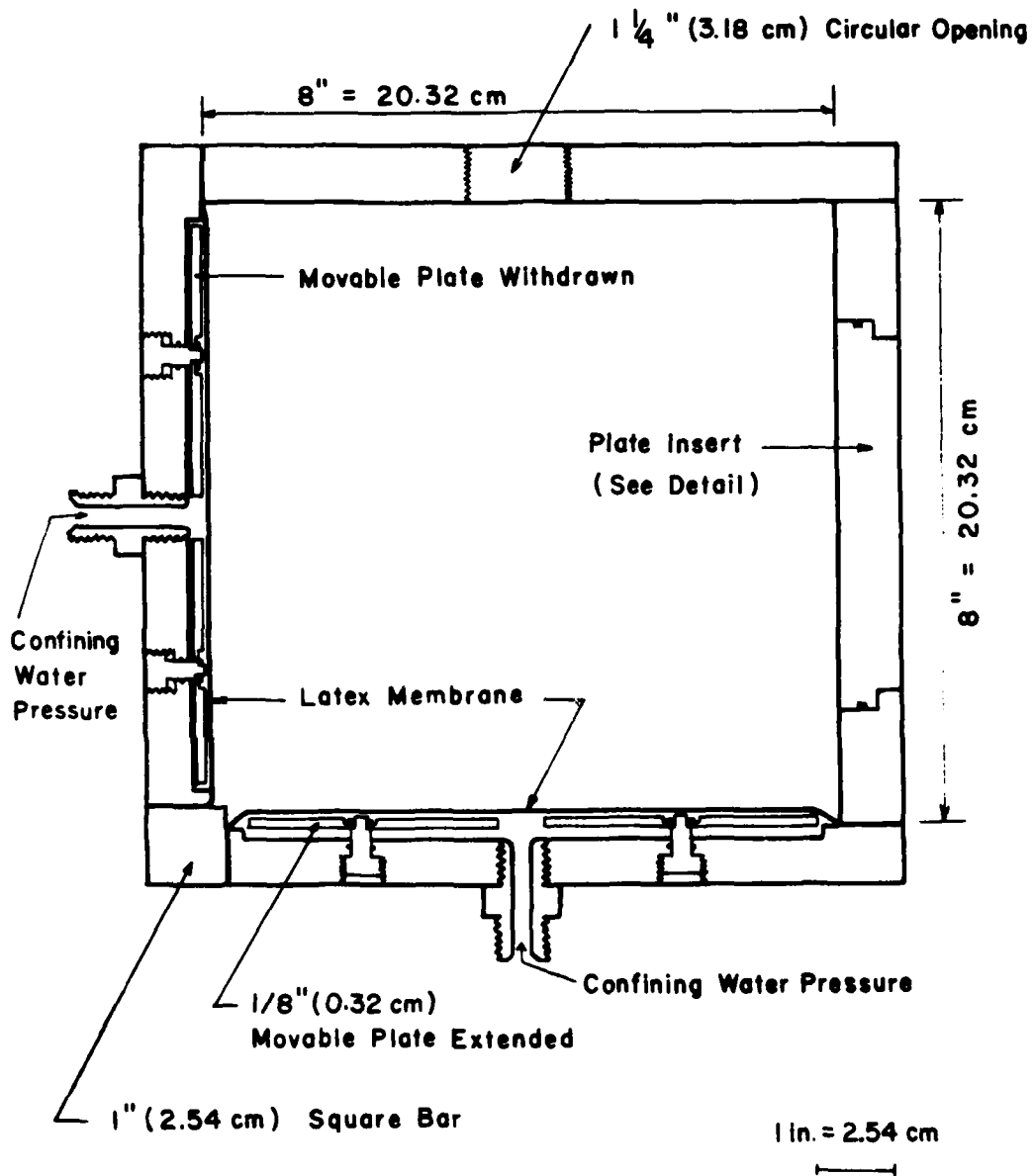
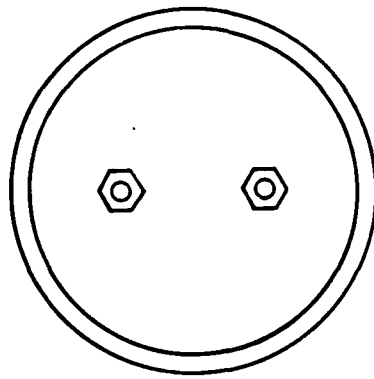
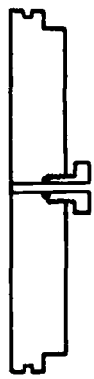
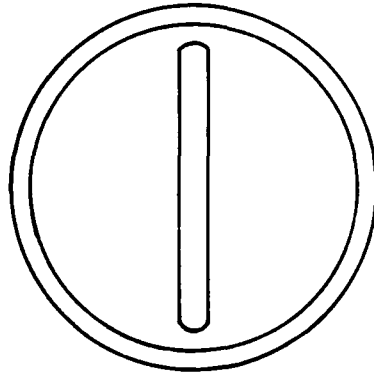
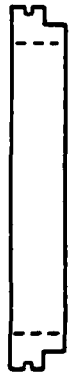


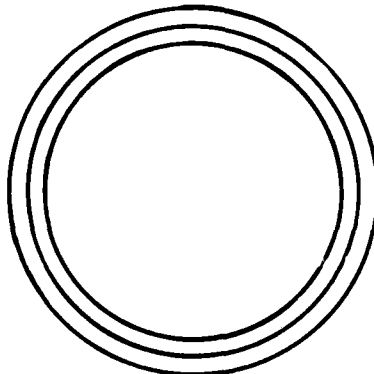
Figure 4.8a Vertical cross section of cubical stress apparatus



1 Solid Plate Insert  
with 2 holes for pore pressure  
measuring tubes



4 Plate Inserts with Slots  
Length of Slots = 4 in. (10.2 cm)  
Width of Slots :  
1/8 in. (0.32 cm)  
1/4 in. (0.64 cm)  
1/2 in. (1.27 cm)  
1 in. (2.54 cm)



1 Plate Insert with 4 in. (10.2 cm)  
Diameter Circular Opening

1 in. = 2.54 cm  


Figure 4.8b Detail of plate inserts

a height of 114 cm (45 in). The capacity of this device was about 1200 cm<sup>2</sup> (73 in<sup>3</sup>).

The water used in the tests was colored with a red dye, rhodamine W.T. Use of the dye made it easier to determine the orientation and extent of the fracture plane after a test. It also improved the visibility of the air-water interface through the translucent tubing of the low capacity volume change measuring device.

#### System Operation

The equipment was mounted on a portable bench with a panel for mounting valves, air pressure regulators, and a pressure gauge. The assembly is shown in Figure 4.9.

At low capacity volume change measuring device is shown at the left side of the cubical stress apparatus, and the high capacity device is on the right side of the back pane. In some of the tests, pore pressures inside the samples were measured using two 3.2 mm (1/8 in) outside diameter tubings with porous stones at their tips and a pore pressure transducer. The strain indicator for the pore pressure readings is shown at the right side of the cubical stress apparatus.

The pressures applied to the membranes of the cubical apparatus were controlled by separate pressure regulators. The pressure from each regulator was applied to the membrane through a water chamber. The use of water instead of air in the membranes allowed easy detection of leaks should they develop. The pressures from the regulators were measured using a Bourdon pressure gauge.

#### PREPARATION OF SAMPLES

##### Teton Dam Silt

A total of five batches of soil were mixed for tests conducted on Teton Dam silt. The soil for each batch was obtained from 5 block samples,

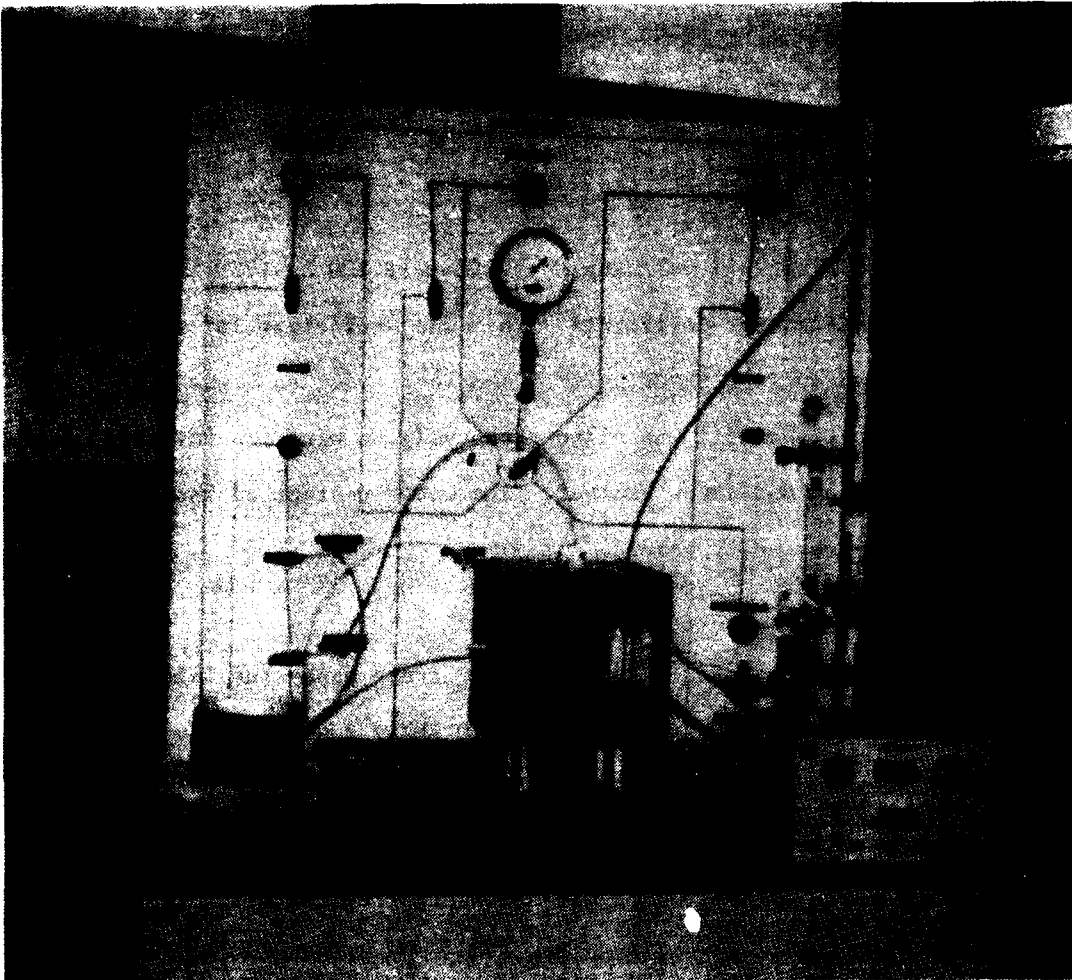


Figure 4.9 Hydraulic fracturing apparatus

which had been broken down into aggregations of particles smaller than 0.95 cm (3/8 in). Particles larger than this size were discarded.

Each batch of soil was used for one to three groups of tests. Before a batch of soil was used for a new test series, it was thoroughly mixed. The water content of the soil was increased or decreased if needed.

Table 4.1 lists the batch numbers, the block sample numbers from which the batches were derived, and the test series numbers for which the batches were used.

#### Pittsburg Silty Clay

A batch of clay soil weighing approximately 120 kg (250 lbs) was obtained from Pittsburg, California. This was sufficient for preparing as many as 7 hydraulic fracturing test samples. When each new test series was begun, the soil was mixed thoroughly to minimize variability in its composition and water content. The water content of the soil was increased or decreased if needed.

#### Compaction

The soil was compacted in the cubical stress apparatus using a California kneading compactor. Figure 4.10 shows a sample being compacted. A rectangular tamper, 5.7 cm (2-1/4 in) by 8.3 cm (3-1/4 in) was used. The density and water content for the silt samples were chosen based on the field values, which were obtained from the block samples (Table 4.1) and the report by the Independent Panel on the failure of the Teton Dam. The density and water content of the clay samples covered a wide range of variation to investigate the effects of density and water content on the hydraulic fracturing pressure.

The compactive effort was controlled by the pressure on the tamper, the number of tamps per layer, and the number of layers. For most of

Table 4.1 List of Block Samples Used in Experimental Study

Batch	Sample No.*	Station ft.*	Offset ft.*	Elevation ft.*	Water Content %	Test Type/ Series
A	84	12+03.2	5.7	5288.1	-	I V/1 V/2
	92	12+51.4	6.1	5269.8	-	
	98	12+17.3	8.0	5271.0	-	
	96	12+30.0	51.3	5271.8	20.4	
	95	12+30.1	49.4	5271.8	20.8	
B	91	12+36.5	2.3	5270.5	20.7	IV/1
	102	12+23.0	42.5	5250.2	29.6	
	108	12+52.6	51.3	5240.8	-	
	101	12+04.3	14.3	5270.8	28.0	
	83	12+30.8	52.7	5284.4	-	
C	133	12+45.5	49.3	5255.6	24.5	BH/1 BH/2 BH/3
	120	12+ 0.8	45.7	5271.7	26.6	
	123	12+03.1	44.7	5266.0	25.2	
	124	12+04.4	14.1	5266.2	21.3	
	125	12+05.2	16.3	5266.2	24.0	
D	114	12+50.2	16.2	5231.6	26.3	IV/2 IV/3
	107	12+52.9	49.4	5340.9	22.2	
	94	12+41.9	54.8	5269.4	22.5	
	128	12+56.4	2.8	5256.3	22.7	
	135	12+32.7	42.1	5256.1	22.7	
E	89	11+87.7	47.7	5279.5	25.2	BH/4 BH/5
	90	12+36.4	1.7	5270.5	19.9	
	88	11+89.1	43.6	5279.4	25.5	
	132	12+46.3	47.5	5255.7	22.9	
	130	12+22.3	15.8	5256.7	22.5	

\*From USBR data on Teton Dam

AD-A144 639

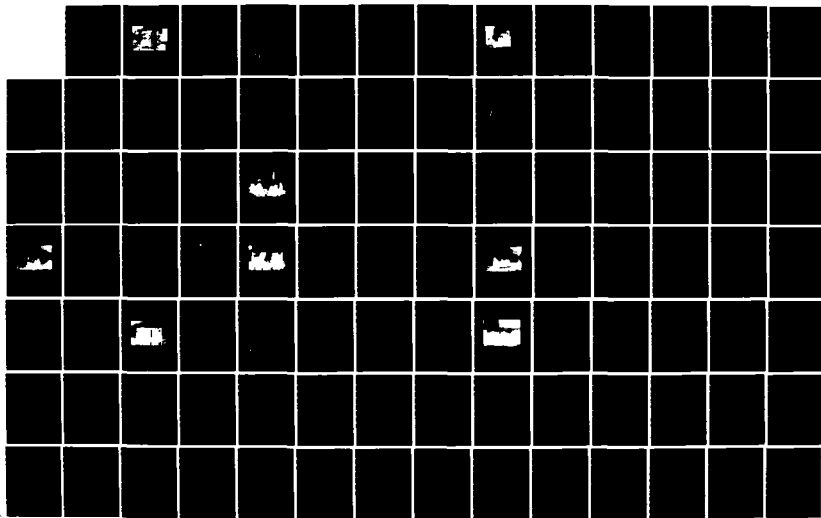
SCALE AND TIME EFFECTS IN HYDRAULIC FRACTURING (U)  
CALIFORNIA UNIV BERKELEY DEPT OF CIVIL ENGINEERING  
H WIDJAJA ET AL. JUL 84 DACW39-81-C-0024

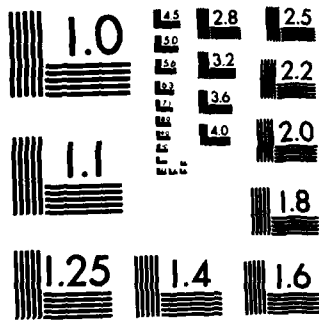
2/3

UNCLASSIFIED

F/G 20/11

NL





MICROCOPY RESOLUTION TEST CHART  
 NATIONAL BUREAU OF STANDARDS-1963-A

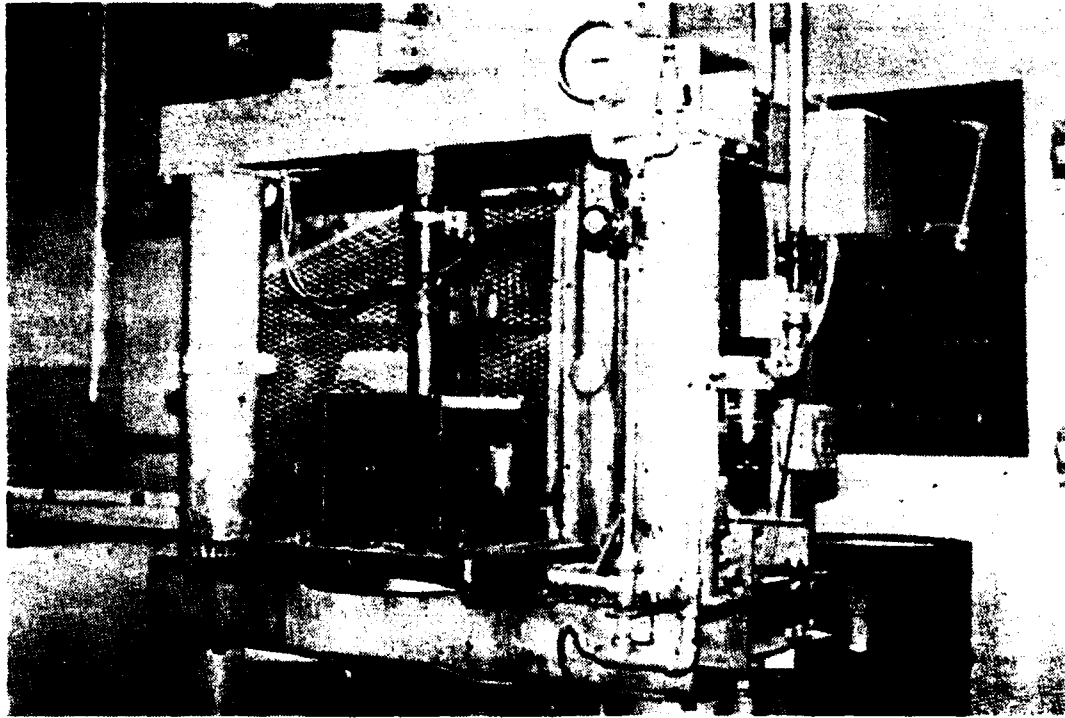


Figure 4.10 California kneading compactor with cubical stress apparatus

the tests, the effort was  $0.7 \text{ kg/cm}^2$  (10 psi) foot pressure, and 24 tamps per layer on 5 layers. The foot pressure of 10 psi was chosen to obtain the required density.

#### TYPES OF TESTS

In addition to borehole fracturing tests, Jaworski et al (1979) conducted five other types of tests. Three of the five types were performed in this study. The test type number designation used in this study followed the system used by Jaworski et al (1979), which is shown in Figure 4.11 and described below:

- Type I: A V-groove was cut on one face of the sample through which water pressure was applied. This is a first-order simulation of the effect of a rock joint.
- Type II: A V-groove was made into the sample, as in Type I tests. At the apex of the groove, a slot was cut into the sample.
- Type III: The sample was compacted in the cubical stress apparatus with one of the vertical reaction plates having a circular hole to simulate compacting soil against an open circular cavity in rock.
- Type IV: The soil was compacted in the cubical stress apparatus, with a vertical slot in one of the vertical reaction plates left open during compaction. These tests simulate compaction against a rock joint somewhat more closely than do Type I tests.
- Type V: A layer of "transitional material" was placed between the soil and the slotted side of the test box. This type of test simulates a transition zone at the upstream face of the core of a dam.

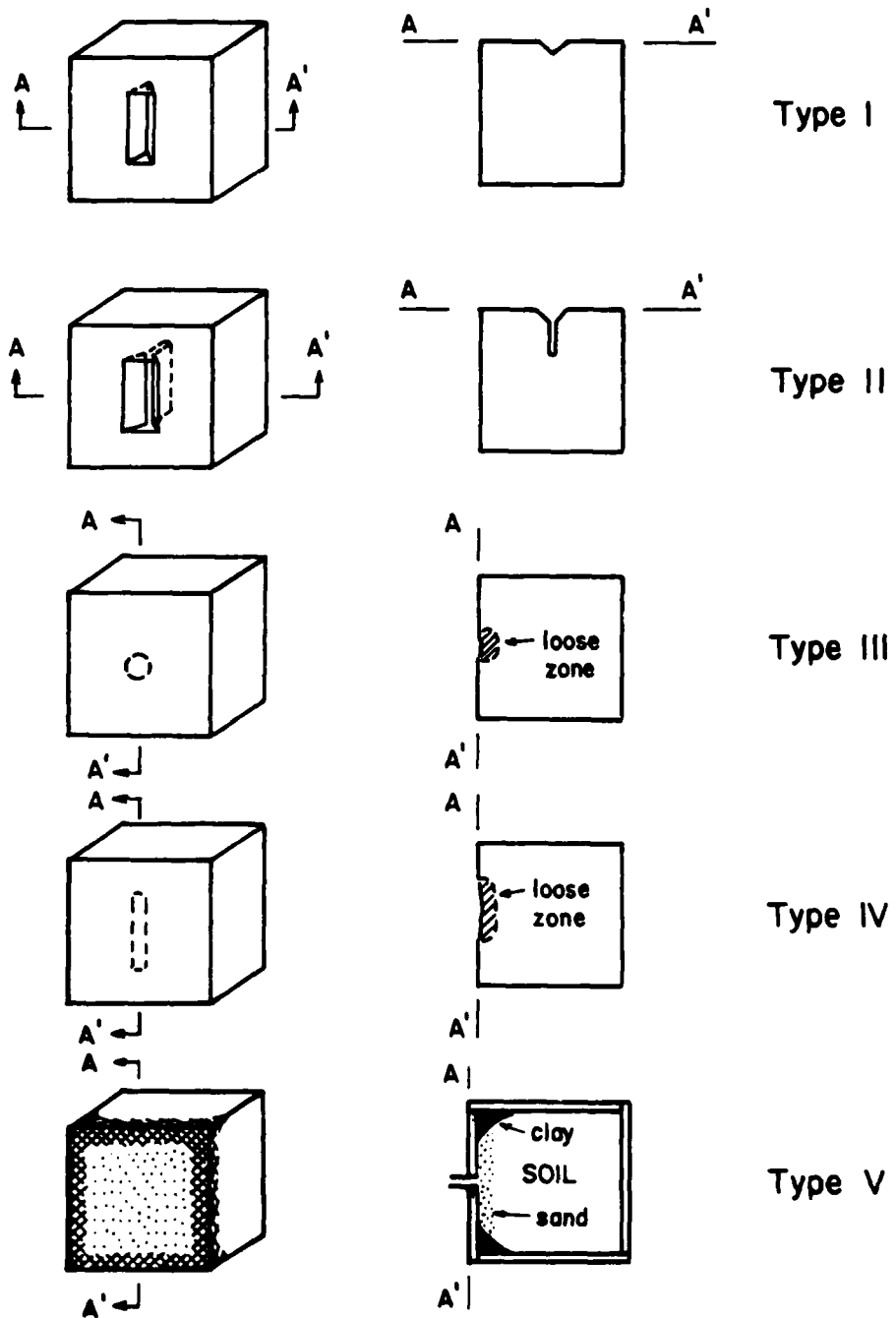


Figure 4.11 Types of tests conducted by Jaworski et al (1979)

In this experimental study, tests of Type I, IV, V and borehole hydraulic fracturing were performed. The procedures used to prepare these samples are described below.

#### Type I Tests

When soil is compacted against a rock mass containing open joints, loose zones would be expected to develop in the vicinity of the rock joints. Type I tests, as illustrated in Figure 4.12, represent a first approximation of this condition. The samples were compacted in the cubical stress apparatus. Then the excess soil was trimmed off with a steel straight-edge, and a V-groove was cut in the sample with a special trimming tool.

The length of the V-groove was 10.2 cm (4 in); the width and the depth were varied as follows:

	Width of V-groove	Depth of V-groove
Smallest	1.27 cm (1/2 in)	0.64 cm (1/4 in)
	2.54 cm (1 in)	1.27 cm (1.2 in)
	5.08 cm (2 in)	2.54 cm (1 in)
Largest	7.62 cm (3 in)	3.81 cm (1-1/2 in)

After the apparatus had been assembled, the confining pressures were applied. These pressures were raised incrementally in a period of one hour or longer. The major principal stress was  $4 \text{ kg/cm}^2$  (4.10 tsf), the intermediate principal stress was  $3 \text{ kg/cm}^2$  (3.07 tsf), and the minor principal stress was  $2 \text{ kg/cm}^2$  (2.05 tsf).

After the samples had been subjected to the confining pressures overnight, water pressure was applied through the opening on the top plate of the apparatus. The pressure was applied incrementally at a rate of  $0.1 \text{ kg/cm}^2$  (0.1 tsf) every 30 seconds.

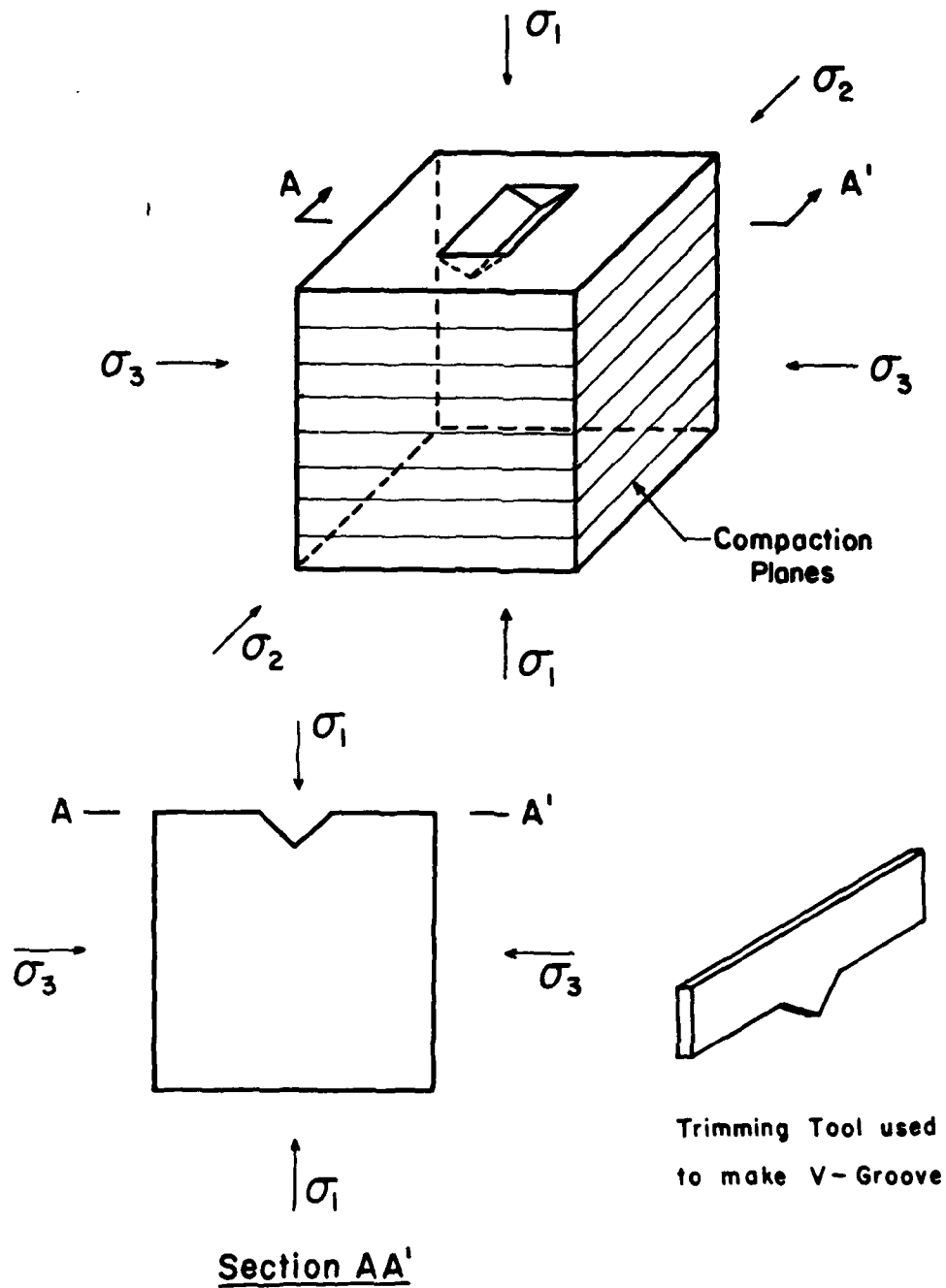


Figure 4.12 Conditions for Type I tests

#### Type IV Tests

In Type IV tests the soil was compacted in the cubical stress apparatus with a vertical slot on one of the vertical reaction plates. The apparatus is shown in Figure 4.13. The slots had lengths of 10.2 cm (4 in) and various widths ranging from 0.32 cm (1/8 in) to 2.54 cm (1 in). During compaction the soil sloughed into the open slot, creating a zone around the opening which was not compacted as well as the remainder of the sample. Thus these tests simulate compaction against an open rock joint somewhat more closely than do Type I tests. After compaction, the slot was covered with a plate through which water pressure was applied.

For testing purposes the cubical stress apparatus was turned over so that the plate with the slot was at the bottom. This is shown in Figure 4.14. The confining pressures, which were the same as in Type I tests, were then applied on the sample. Usually the sample was subjected to the confining pressures overnight, after which water pressure was applied to the sample through the slot. The rate of pressurizing was  $0.1 \text{ kg/cm}^2$  (0.1 tsf) per minute.

#### Type V Tests

In Type V tests the samples were compacted in the cubical stress apparatus with a solid circular plate insert covering the opening on one of the vertical reaction plates; therefore, there was no loose zone in the sample. After compaction the solid plate was removed and replaced with one having a 10.2 cm (4 in) diameter circular opening. This opening was filled with Monterey sand. A cover plate was placed over the sand.

In some of the tests, crushed granite was used instead of sand. The crushed granite passed a sieve with screen openings of 18.85 mm (0.74 in) and was retained on a sieve with screen openings of 13.32 mm (0.52 in). The granite was placed in the 10.2 cm (4 in) circular opening as the soil was compacted.

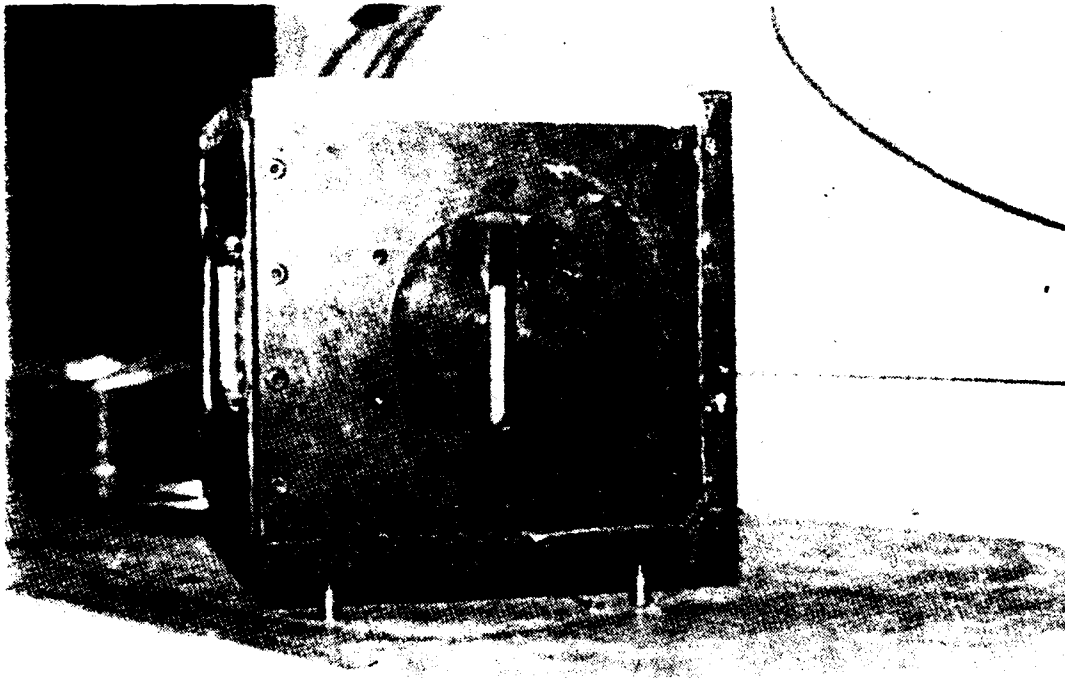
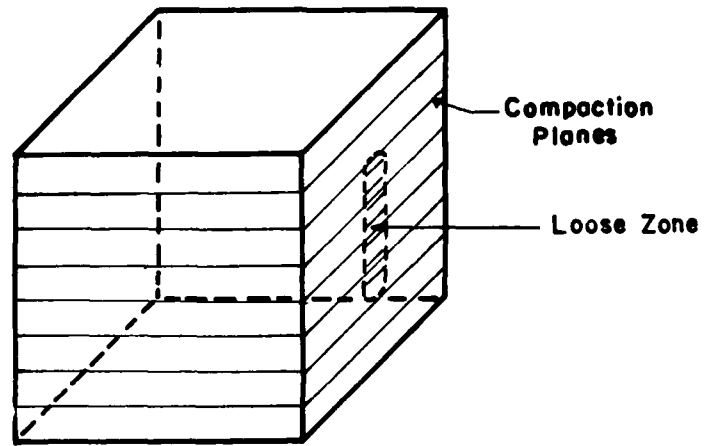
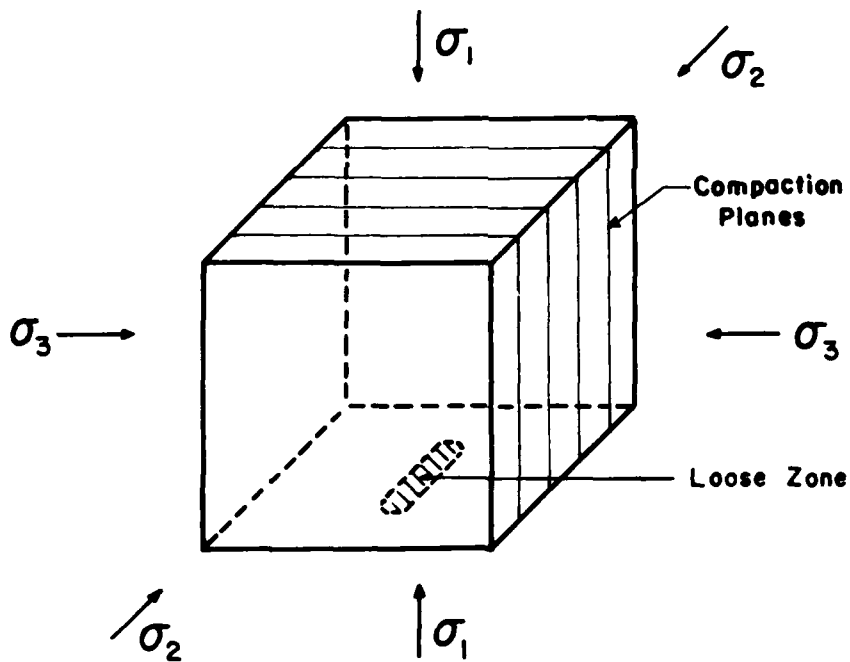


Figure 4.13 Cubical stress apparatus with a slot for a Type IV test



Compaction Condition



Testing Condition

Figure 4.14 Conditions for Type IV tests

The confining pressures used in these tests were the same as in Type I and Type IV tests, except in one test (Test T4) where the intermediate principal stress was equal to the minor principal stress, i.e.  $2 \text{ kg/cm}^2$  (2.05 tsf).

Water pressure was applied to the sample through the transition material. This pressure was raised incrementally at a rate of  $0.1 \text{ kg/cm}^2$  (0.1 tsf) per minute.

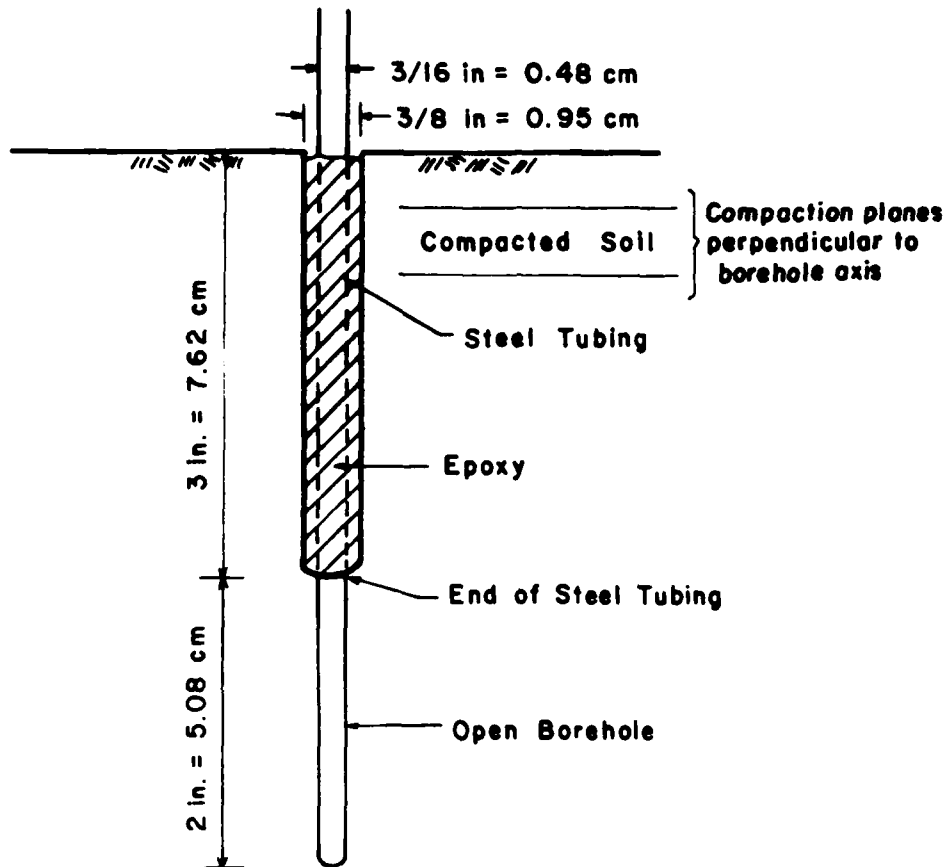
#### Borehole Hydraulic Fracturing Tests

In these tests the water pressure was applied to the sample through a small borehole, which was drilled in the specimen after compaction. Two different borehole lengths were used, 5.1 cm (2 in) and 17.8 cm (7 in), as shown in Figure 4.15.

In these tests the vertical stress was  $4 \text{ kg/cm}^2$  (4.10 tsf) and the horizontal stress was  $2 \text{ kg/cm}^2$  (2.05 tsf), except for tests conducted to investigate the effect of confining stress and the tests on Pittsburgh silty clay. The vertical stress in the tests on Pittsburgh silty clay was  $3 \text{ kg/cm}^2$  (3.07 tsf).

The procedure to install a short borehole is shown in Figure 4.15. A borehole was drilled into the sample through the hole in the top reaction plate using an electric hand drill. Then quick-setting epoxy was placed in the bottom of this hole. Steel tubing, plugged at its tip with soil, was inserted into the wet epoxy, to the bottom of the hole, and was fastened to the top reaction plate. After about 30 minutes, a drill was used to clean out the steel tubing and to extend the hole beyond the bottom of the steel tubing.

To install a long borehole, the hole was drilled to a depth of 17.8 cm (7 in) through the hole in the top reaction plate. The diameter of long boreholes varied from 0.48 cm (3/16 in) to 1.91 cm (3/4 in).



1. 3/8 in. Open Borehole Drilled to 3 in.
2. Epoxy Poured into hole, 3 in. x 3/16 in Tubing  
Inserted before Epoxy Sets.
3. 3/16 in. Open Borehole Advanced 2 in.

Figure 4.15 Two-inch-long borehole setup for hydraulic fracturing tests

## TESTING PROCEDURE

After the sample had been compacted, a vacuum was used to remove most of the air from behind the membranes. If there was a leak in a membrane, it would be indicated by air bubbles continuously rushing to the water surface in the water-filled vacuum chamber.

The confining pressures were applied in 20 equal increments. The time interval between pressure increments was 3 minutes or longer; therefore, the full confining pressures were reached in one hour or longer. Generally, applying water pressures to induce fracturing was begun the day after sample preparation.

The water pressures to induce fracturing were applied in increments of  $0.1 \text{ kg/cm}^2$  (0.1 tsf). The time intervals between pressure increments were generally constant throughout a test. The time increment was also kept constant for all the tests in a group except for the tests conducted to investigate the effect of test duration. The shortest time increment was 30 seconds and the longest was 12 hours.

During pressurizing, the volume change corresponding to each applied pressure was recorded. In four groups of borehole fracturing tests, the pore pressures inside the samples were measured at two locations.

## TESTING PROGRAM

A total of 84 hydraulic fracturing tests of various types were completed; 56 tests were conducted on Teton Dam silt and 28 tests on Pittsburg silty clay.

Table 4.2 and 4.3 list the number of tests conducted for each series, the parameter studied, the soil batch used, and the test numbers.

Table 4.2 List of Fracturing Tests on Teton Dam Silt

Test Type	Series No.	No. of Tests	Test Nos.	Soil Batch	Parameter Study
I	-	5	G2-6	A	Groove size
IV	1	4	S2-5	B	Slot size
	2	5	S17-21	D	Slot size
	3	4	S36,39,41,42	D	Water content
V	1	3	T1,2,4	A	Transition material
	2	4	T3,6,10,11	A	Transition material
BH	1	5	BH1-4,15	C	Test duration
	2	5	BH5-9	C	Test duration
	3	5	BH10-14	C	Test duration
	4*	7	BH23-29	E	Horizontal stress, borehole length, density
	5*	9	BH30-34,36-39	E	Borehole diameter, water content, density

\*With pore pressure measurements

Table 4.3 List of Fracturing Tests on Pittsburgh Silty Clay

Test Type	Series No.	No. of Tests	Test Nos.	Parameter Study
IV	1	4	S12-15	Slot width
	2	4	S22-25	Slot width
	3	4	S30,31,33,34	Water content and density
V	-	5	T7,8,13,15,17	Transition material
BH	1*	4	BH18,20-22	Test duration and aging
	2*	7	BH40-46	Borehole diameter, density, and water content

\*With pore pressure measurements

## V. PRESENTATION AND DISCUSSION OF TEST RESULTS

Eighty-four hydraulic fracturing tests were completed to study the effects of various parameters. Fifty-six tests were performed on Teton Dam silt and 28 tests on Pittsburg silty clay.

### EFFECT OF GROOVE SIZE IN TYPE I TESTS

Five tests of Type I were completed on Teton Dam silt. The results of four tests are shown in Figure 5.1. It can be seen that the flow rate of water entering the sample increased almost linearly with pressure until hydraulic fracturing occurred, at which time the flow rate increased abruptly with no further increase in pressure. Generally, the flow rates of water entering the sample with a larger groove were higher. The fracture planes that developed when fracture occurred were always perpendicular to the direction of minor principal stress.

The results of the tests are summarized in Table 5.1. The care taken in preparing the samples resulted in very small variations in the densities and water contents of the samples. Samples G5 and G6, which had the smallest groove size, did not fracture. When the cubical stress apparatus was disassembled, it could be seen from the stains caused by the red dye in the water that water had flowed around the sample.

Hydraulic fracturing pressures are plotted as a function of groove size in Figure 5.2. It can be seen that the larger the groove size, the lower was the measured fracturing pressure. The theory and finite element analyses described in Chapter III indicated that the size of a discontinuity should have practically no effect on fracturing pressure.

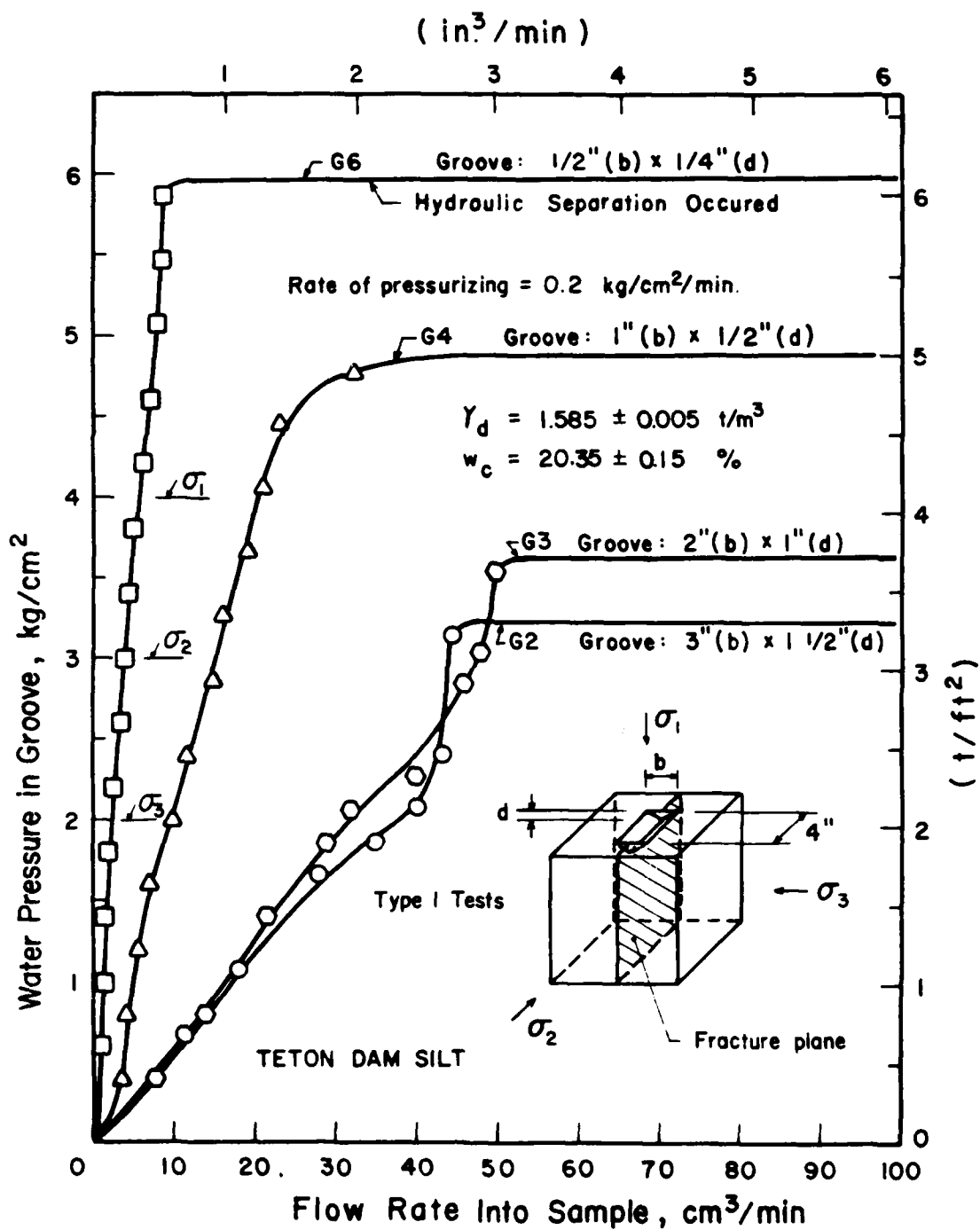


Figure 5.1 Results of Type I tests on Teton Dam silt

Table 5.1 Summary of Type I Test Results on Teton Dam Silt

Test No.	Groove Size		Dry Density t/m <sup>3</sup>	Water Content %	Fracturing Pressure kg/cm <sup>2</sup>
	b in.	d in.			
G2	3.0	1.5	1.59	20.4	3.2
G3	2.0	1.0	1.58	20.5	3.6
G4	1.0	0.5	1.59	20.4	4.9
G5	0.5	0.25	1.59	20.3	*
G6	0.5	0.25	1.59	20.2	**

Note: Rate of pressurizing = 0.1 kg/cm<sup>2</sup> at 30-second interval

Major principal stress = 4 kg/cm<sup>2</sup>

Intermediate principal stress = 3 kg/cm<sup>2</sup>

Minor principal stress = 2 kg/cm<sup>2</sup>

b = width of groove

d = depth of groove

\*Hydraulic separation occurred at a water pressure of 4.0 kg/cm<sup>2</sup>

\*\*Hydraulic separation occurred at a water pressure of 5.9 kg/cm<sup>2</sup>

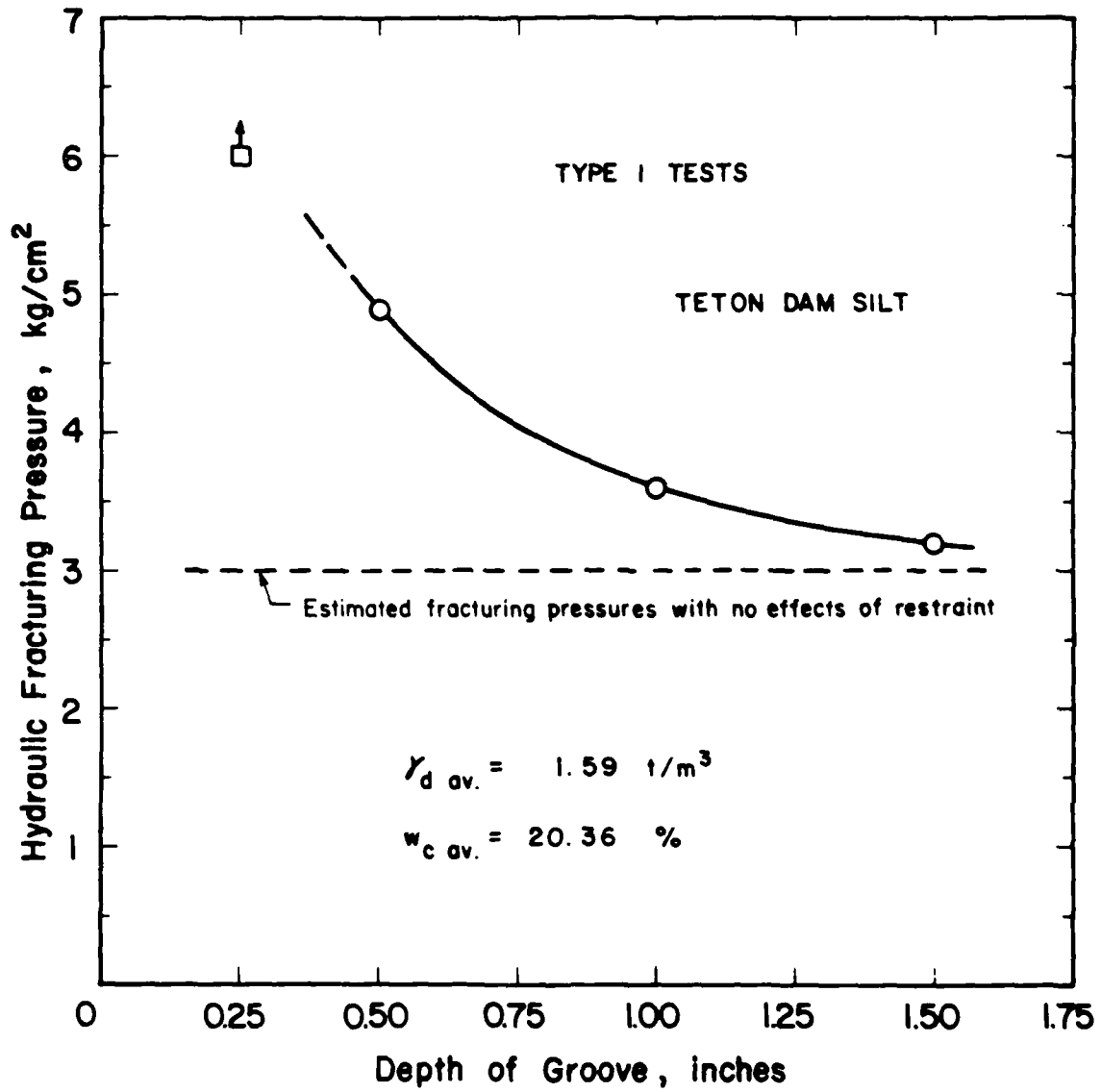


Figure 5.2 Effect of depth of groove in Type I tests on hydraulic fracturing pressure for Teton Dam silt

It is believed that the disagreement between the theoretical and measured fracturing pressure is a result of restraint in the test box. Because the face of the specimen in which the groove was cut was in contact with a solid metal side of the apparatus, there may have been some restraint due to friction between the side of the box and the sample. The tests with larger grooves would be less affected by such restraint because the area of the soil in contact with the metal side was smaller. The fracturing pressures measured in borehole fracturing tests described later in this chapter were practically independent of the borehole diameter because there was no such restraint in borehole tests.

Thus it appears that the fracturing pressures measured in the tests with small grooves were higher than the true fracturing pressures as a result of systematic effects due to wall friction in the test apparatus. Had this friction been completely eliminated, it is believed that the measured fracturing pressures would all have been very nearly equal to the value measured in the tests with the largest groove size.

#### EFFECT OF SLOT SIZE, WATER CONTENT, AND DENSITY IN TYPE IV TESTS

##### Teton Dam Silt

Fifteen tests were completed to study the effects of slot size and water content on hydraulic fracturing in Teton Dam silt. The results are summarized in Table 5.2.

##### Effect of Slot Size

The results of the tests performed to study the effect of slot size in Type IV tests are shown in Figures 5.3 and 5.4. As explained in detail in Chapter IV, the specimens for Type IV tests were compacted with an open slot in the wall of the box, leaving a loose zone through which water pressures were applied.

Table 5.2 Summary of Type IV Test Results on Teton Dam Silt

Series No.	Test No.	Slot Width in.	Dry Density t/m <sup>3</sup>	Water Content %	Fracturing Pressure kg/cm <sup>2</sup>
1	S2	1.0	1.59	23.1	3.5
	S3	0.5	1.60	22.8	3.8
	S4	0.25	1.60	23.1	4.9
	S5	0.125	1.58	23.5	5.3
2	S17	0.125	1.58	22.4	4.3
	S18	0.25	1.58	22.5	3.9
	S19	0.25	1.58	22.5	3.9
	S20	0.5	1.58	22.8	3.5
	S21	1.0	1.58	22.9	3.2
3	S36	0.5	1.58	19.7	3.6
	S39	0.25	1.58	19.7	3.4
	S41	1.0	1.57	20.0	3.3
	S42	0.125	1.59	20.0	4.1

Note: Rate of pressurizing = 0.1 kg/cm<sup>2</sup>/min.

Major principal stress = 4 kg/cm<sup>2</sup>

Intermediate principal stress = 3 kg/cm<sup>2</sup>

Minor principal stress = 2 kg/cm<sup>2</sup>

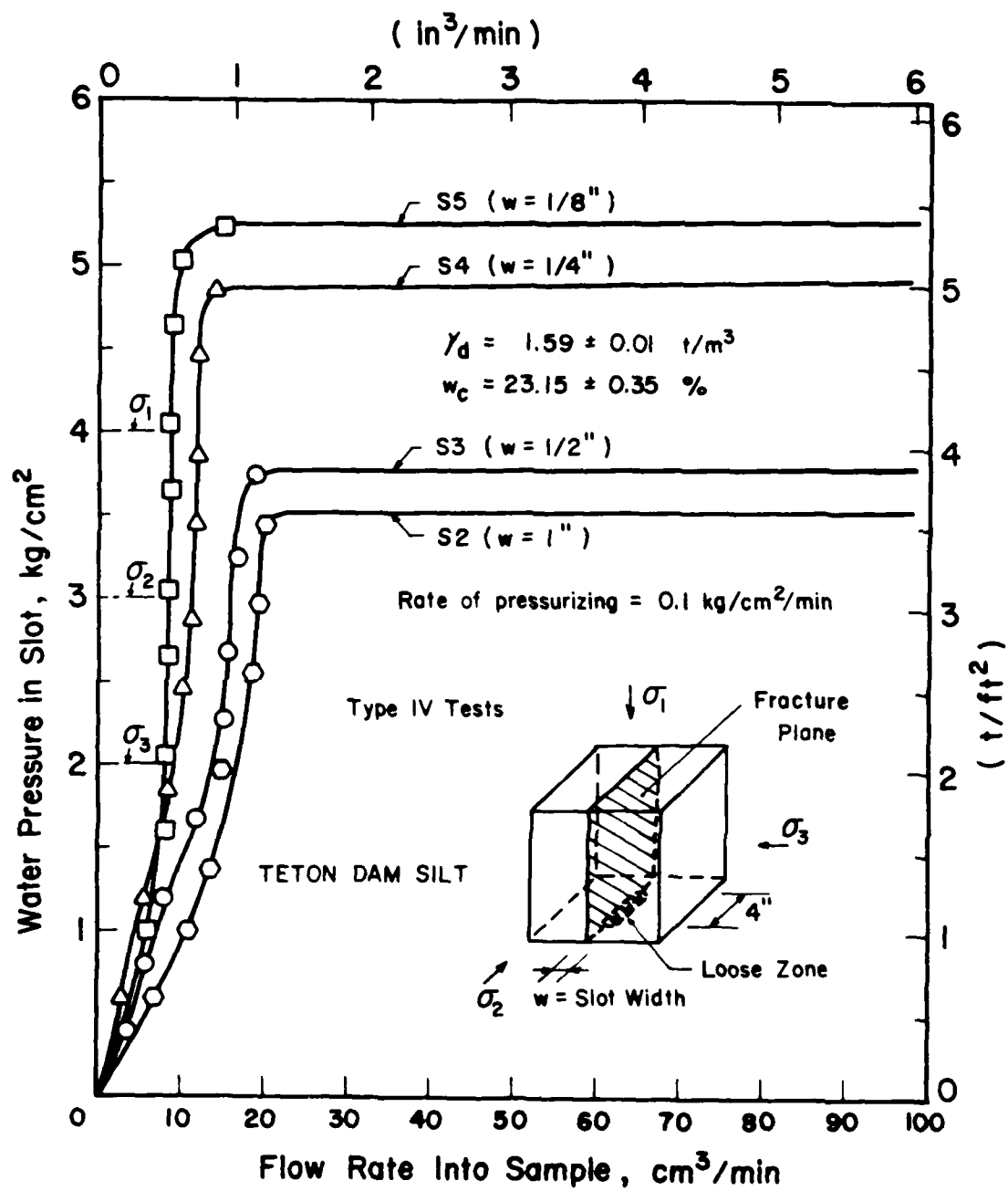


Figure 5.3 Results of Type IV tests, series 1, on Teton Dam silt

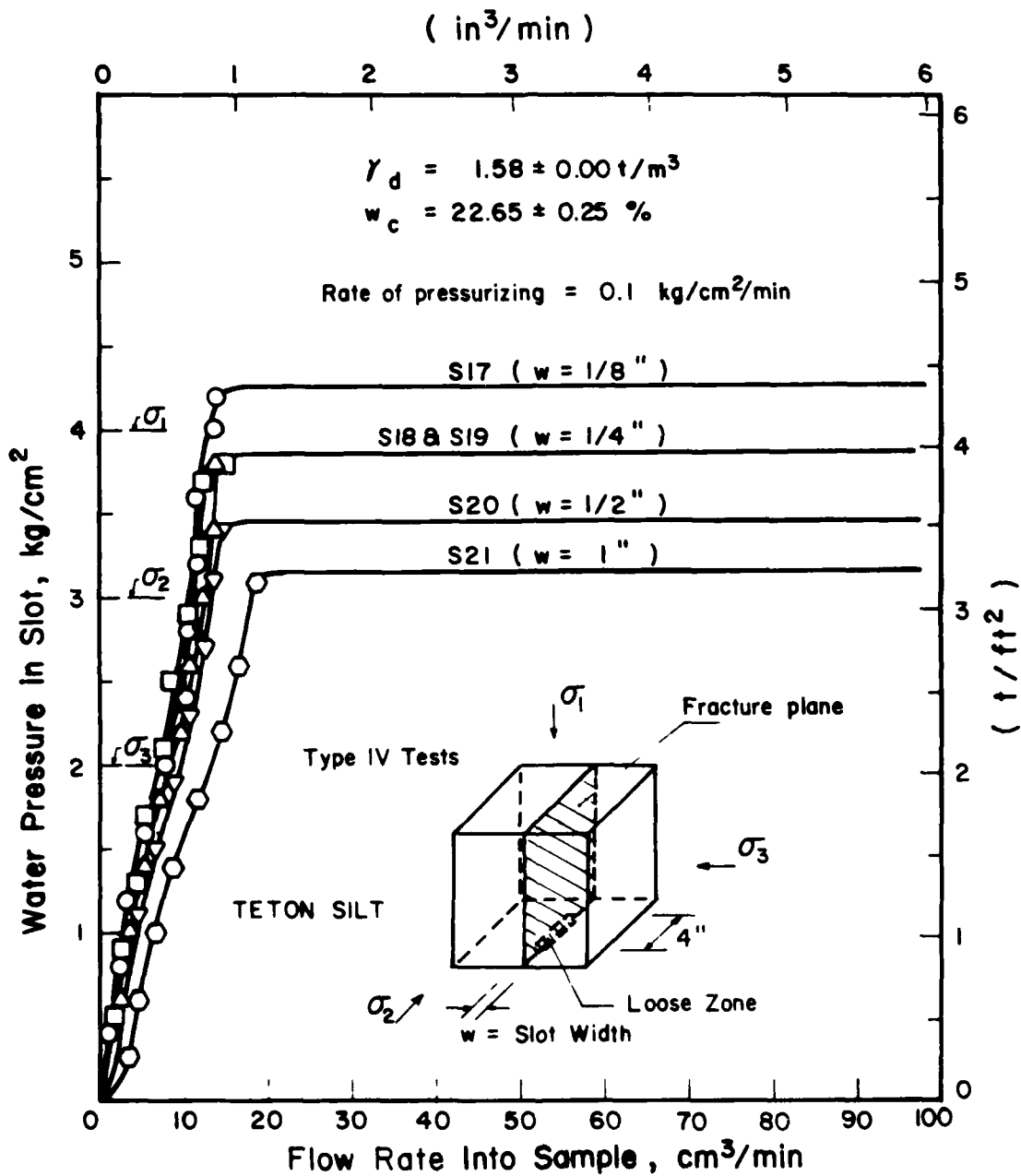


Figure 5.4 Results of Type IV tests, series 2, on Teton Dam silt

The fracturing pressures are plotted as a function of slot size in Figure 5.5, which shows that the fracturing pressures measured in Series 1 tests were consistently higher than those for Series 2. As in Type I tests, it is believed that the test results of Type IV tests were also affected by the restraint due to friction between the soil and the wall of the test box. Had there been no such restraint, it is believed that the measured fracturing pressures would have been very nearly equal in all tests. The higher the density of soil, the larger would be the friction that developed between the soil and the wall of the test box. This is believed to be partly responsible for the higher fracturing pressures measured in Series 1 tests.

The fracture planes in all the tests were perpendicular to the direction of the minor principal stress.

#### Effect of Water Content

The effect of compaction water content was studied in a third series of tests. The soil, which came from the same batch as Series 2, was compacted to the same density but at a lower water content than were the Series 2 specimens.

The results of Series 3 tests are shown in Figure 5.6. Sample S39 fractured at a lower pressure than Sample S36 even though the slot size was smaller. Sample S39 probably had higher permeability than Sample S36, as indicated by the higher flow rates in the test. The theory and finite element analyses described in Chapter III indicate that higher permeability leads to lower hydraulic fracturing pressure, all other things being equal. It is believed that this effect of permeability is the reason why Sample S39 fractured at a lower pressure than Sample S36.

The results of Series 2 and Series 3 tests indicated that the Series 3

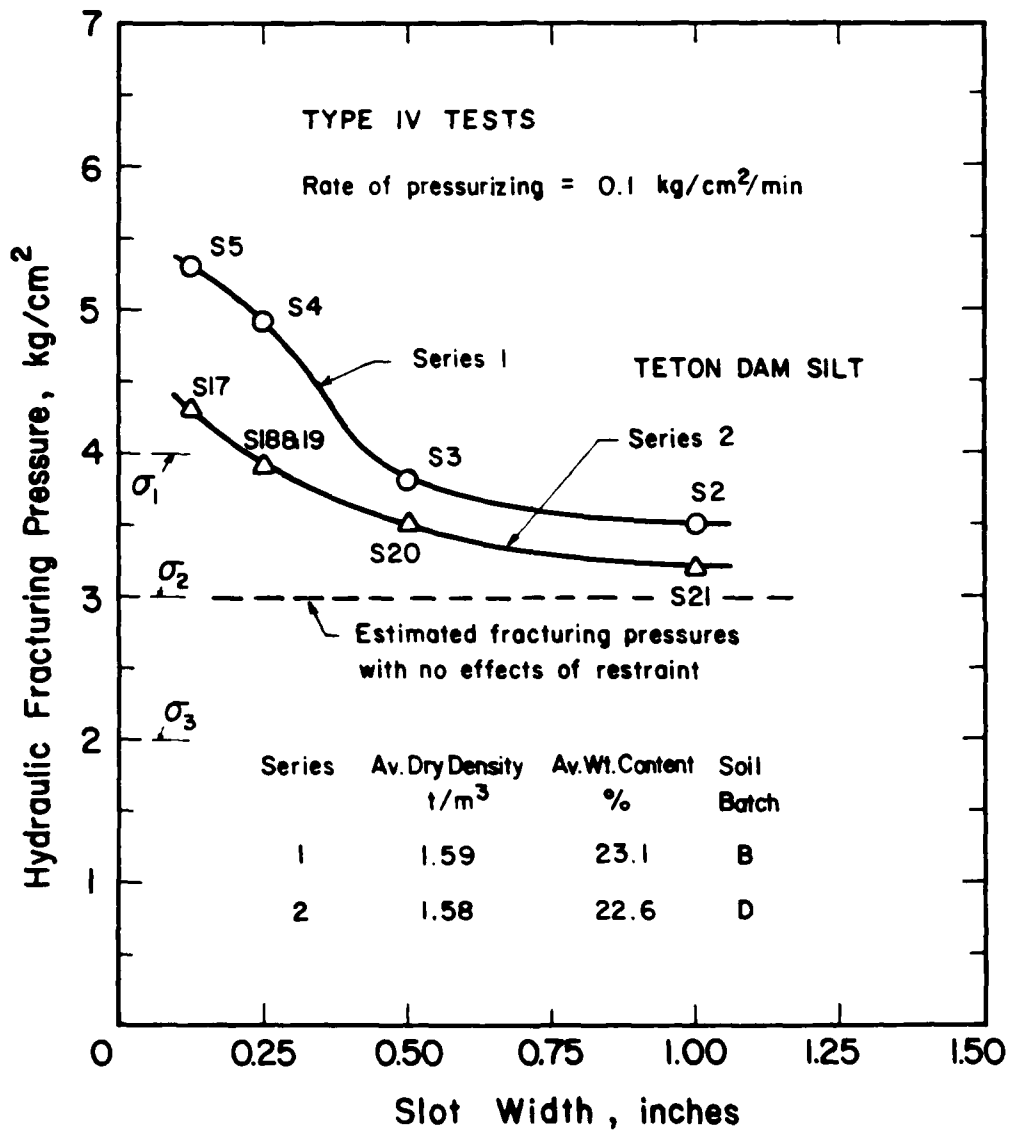


Figure 5.5 Effect of slot width in Type IV tests on hydraulic fracturing pressure for Teton Dam silt

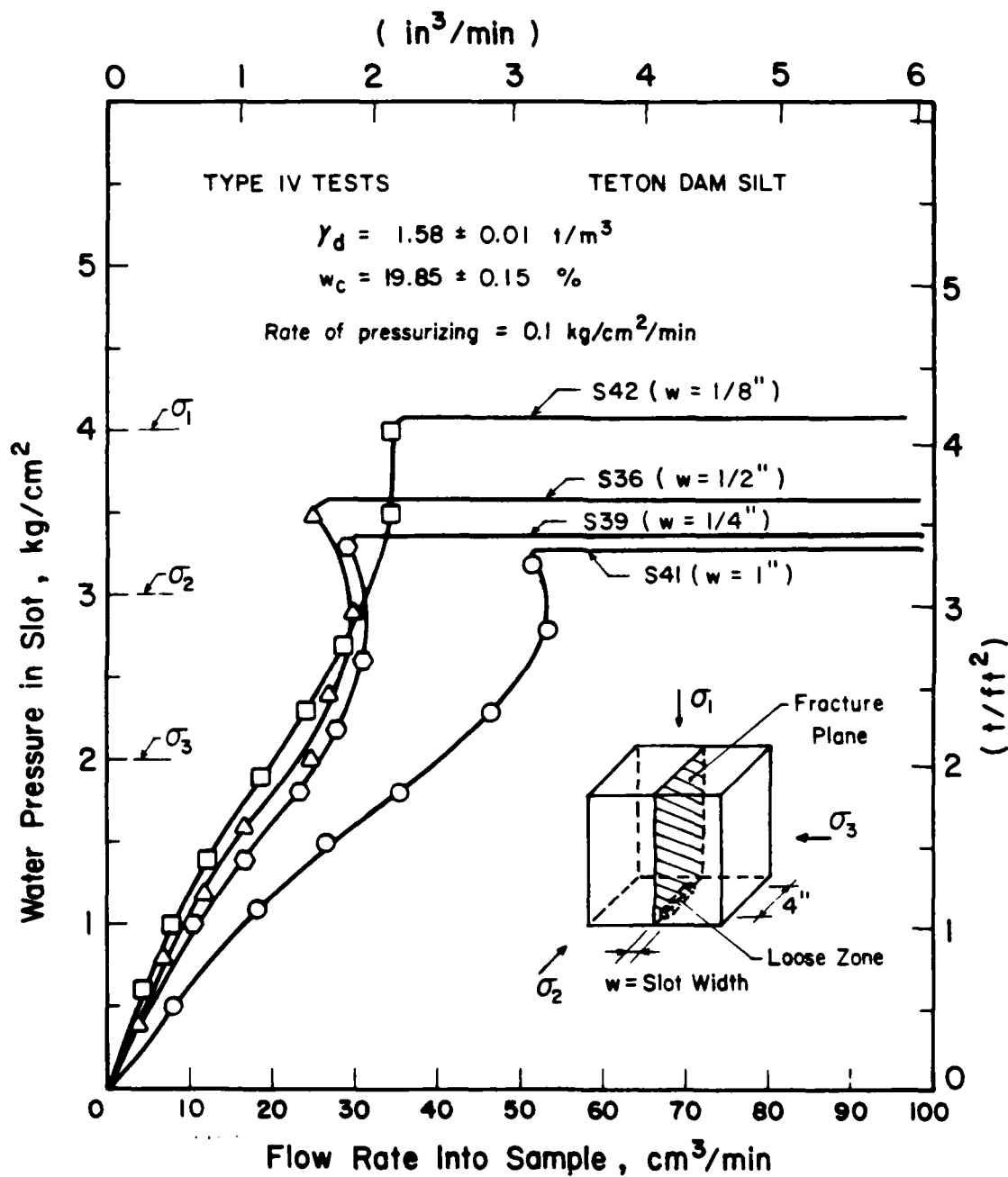


Figure 5.6 Results of Type IV tests, series 3, on Teton Dam silt

samples, which had lower water contents, had higher permeability than Series 2 samples. Series 3 samples probably had higher strength than Series 2 samples because of their lower compaction water content.

The fracturing pressures of Series 3 are compared to those of Series 2 in Figure 5.7, which shows that water content had no consistent effect on the fracturing pressure, probably because of the effects of increased permeability of Series 3 samples and possible higher strength due to lower water contents were essentially in balance.

It is believed that the true fracturing pressures, had there been no restraint, would all have been very nearly equal as shown in Figure 5.7.

#### Pittsburg Silty Clay

Twelve tests were completed to study the effects of slot size, density, and water content on hydraulic fracturing in Pittsburg silty clay. The results are summarized in Table 5.3.

##### Effect of Slot Size

The effect of slot size was studied in Type IV tests, with slot sizes varying from 0.32 cm (1/8 in) to 2.54 cm (1 in). The test results are presented in Figures 5.8 through 5.10. It can be seen that the flow rates were very high initially, and then decreased as the pressures were increased. This was probably due to swelling of the soil around the slot.

The fracture planes were generally perpendicular to the direction of the minor principal stress, except in Tests S30 and S34, shown in Figure 5.10, in which the fracture planes "branched out" at one end of the slot. A typical fracture plane is shown in Figure 5.11.

The hydraulic fracturing pressures are plotted as a function of slot width in Figure 5.12. It can be seen that the measured fracturing pressures decreased with increasing slot size. It is believed that this

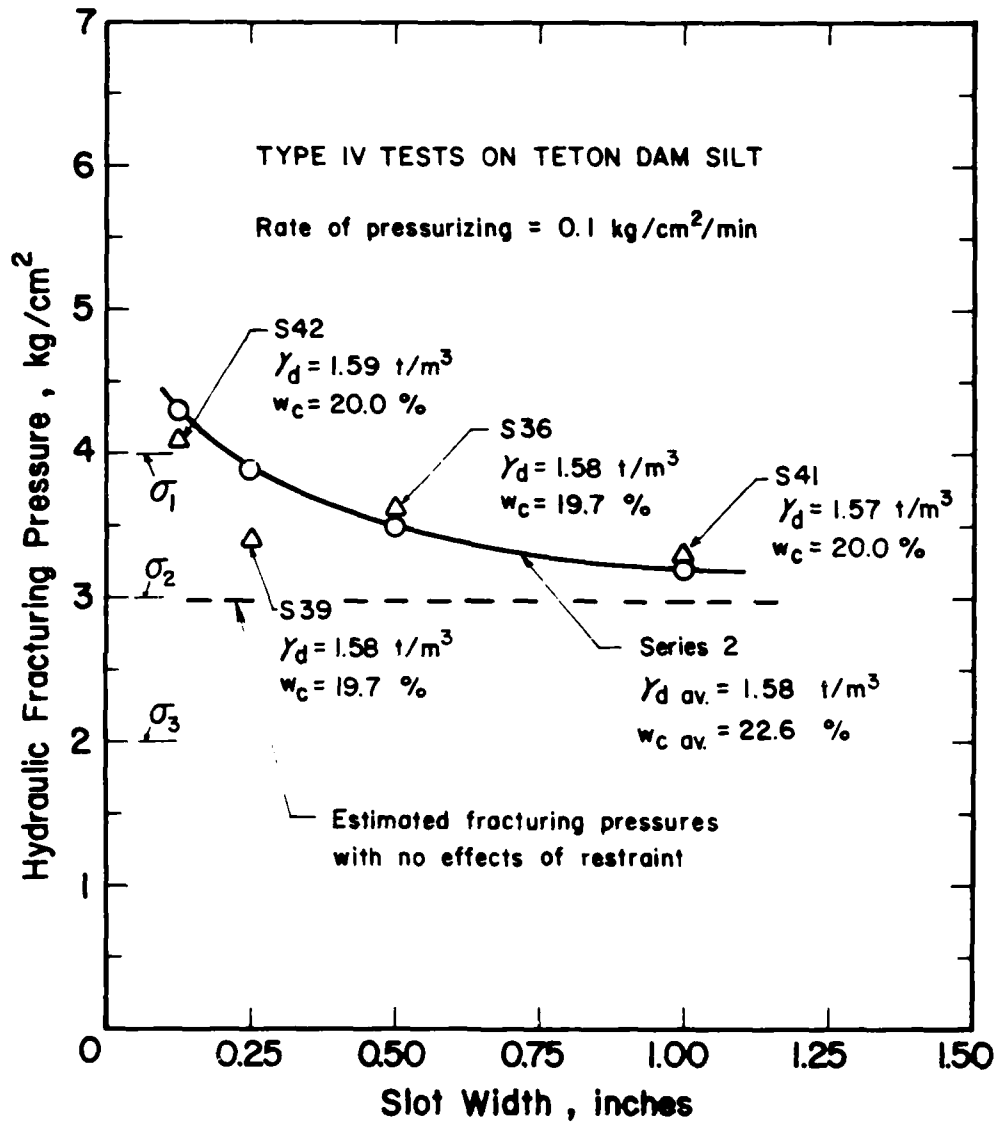


Figure 5.7 Effect of compaction water content on fracturing pressure in Teton Dam silt

Table 5.3 Summary of Type IV Test Results on Pittsburgh Silty Clay

Series No.	Test No.	Slot Width in.	Dry Density $t/m^3$	Water Content %	Fracturing Pressure $kg/cm^2$
1	S12	0.125	1.60	19.1	3.6
	S13	0.25	1.60	19.5	3.9
	S14	0.5	1.61	19.4	2.7
	S15	1.0	1.60	19.4	2.2
2	S22	0.125	1.66	23.5	5.0
	S23	0.25	1.66	23.0	4.8
	S24	0.5	1.66	23.3	4.6
	S25	1.0	1.66	23.4	4.3
3	S30	0.25	1.61	23.9	4.5
	S31	0.5	1.61	24.0	4.2
	S33	1.0	1.60	23.1	4.5
	S34	1.0	1.61	23.3	4.3

Note: Rate of pressurizing =  $0.1 \text{ kg/cm}^2/\text{min}$

Major principal stress =  $4 \text{ kg/cm}^2$

Intermediate principal stress =  $3 \text{ kg/cm}^2$

Minor principal stress =  $2 \text{ kg/cm}^2$

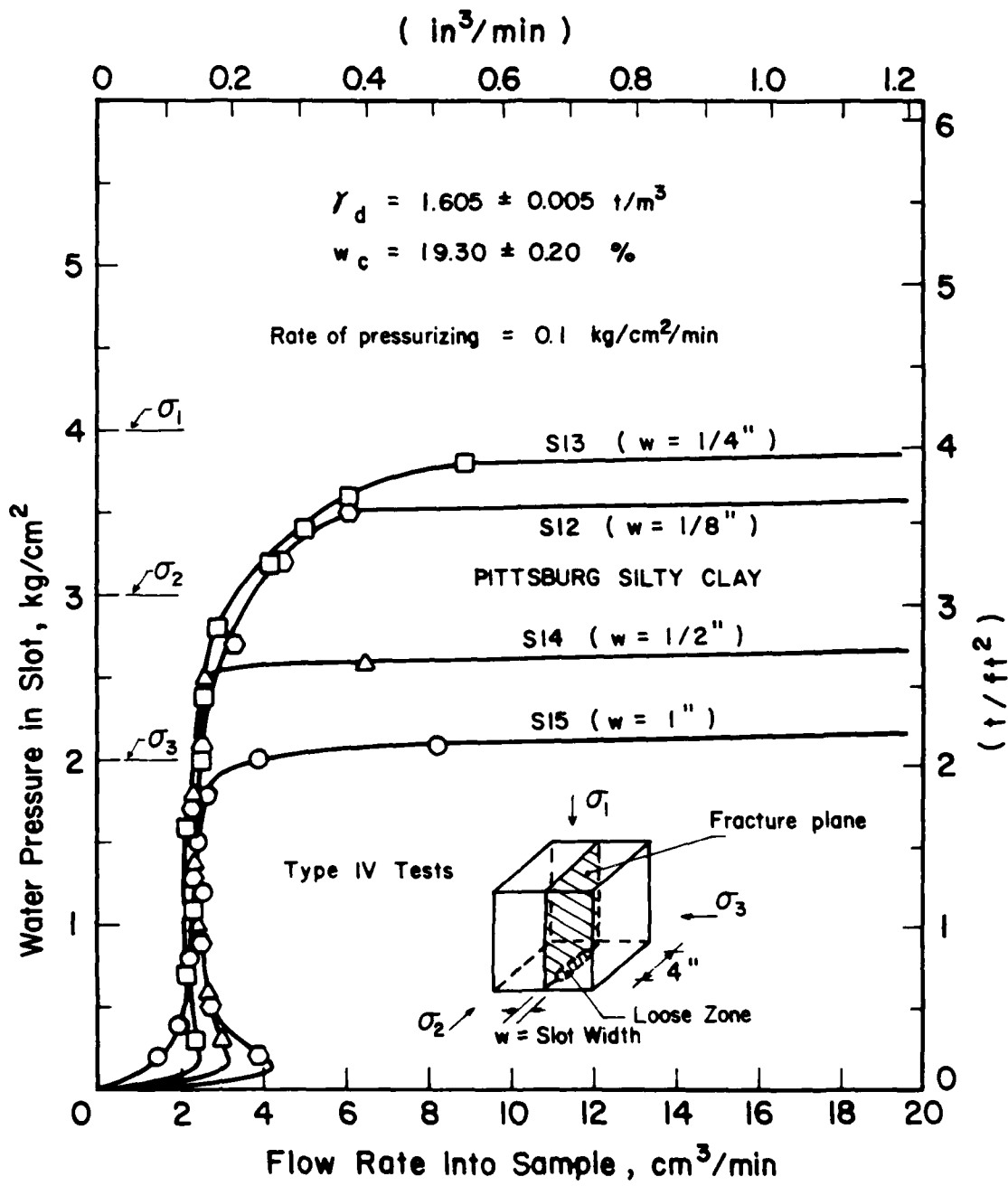


Figure 5.8 Results of Type IV tests, series 1, on Pittsburg silty clay

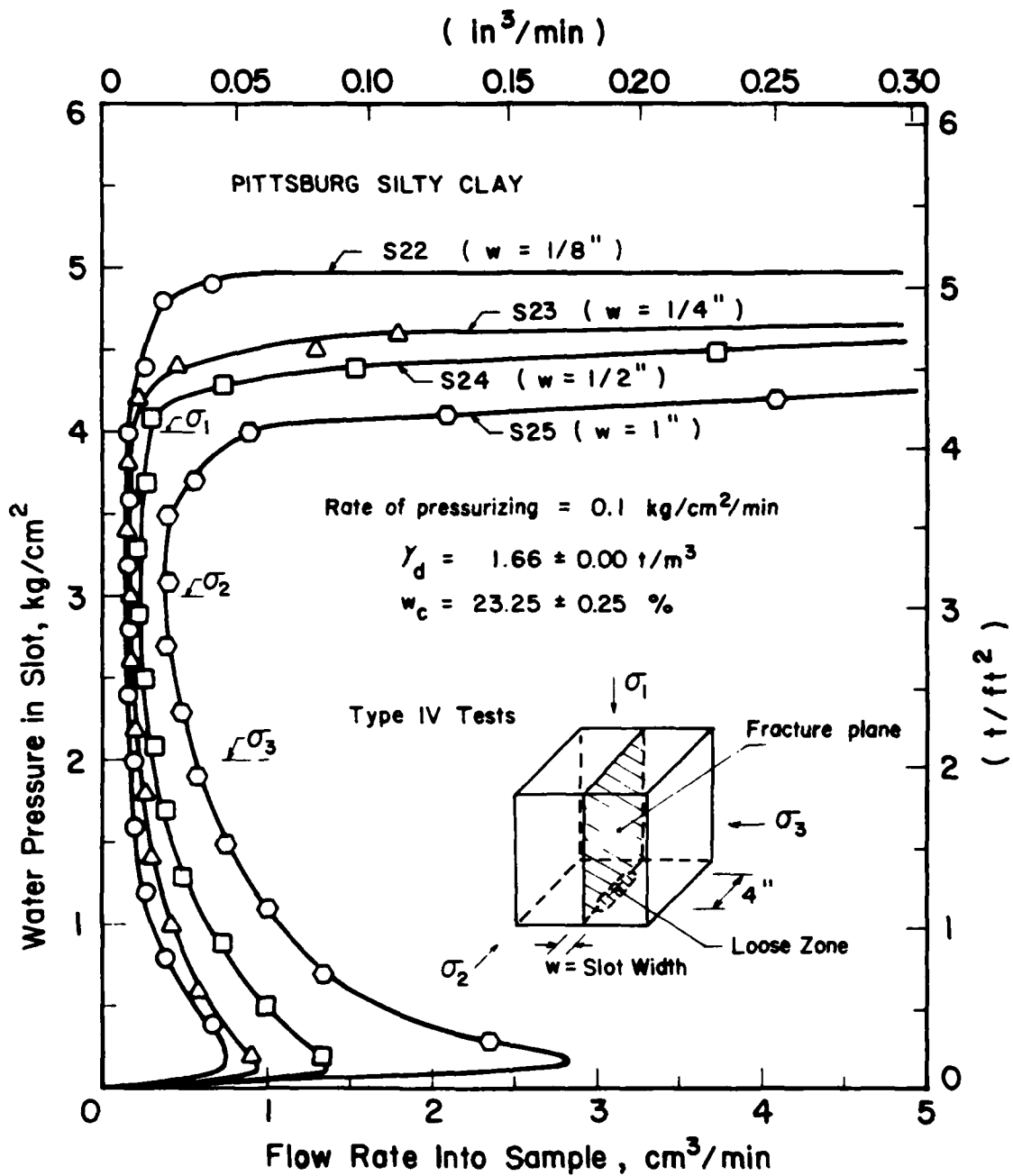


Figure 5.9 Results of Type IV tests, series 2, on Pittsburg silty clay

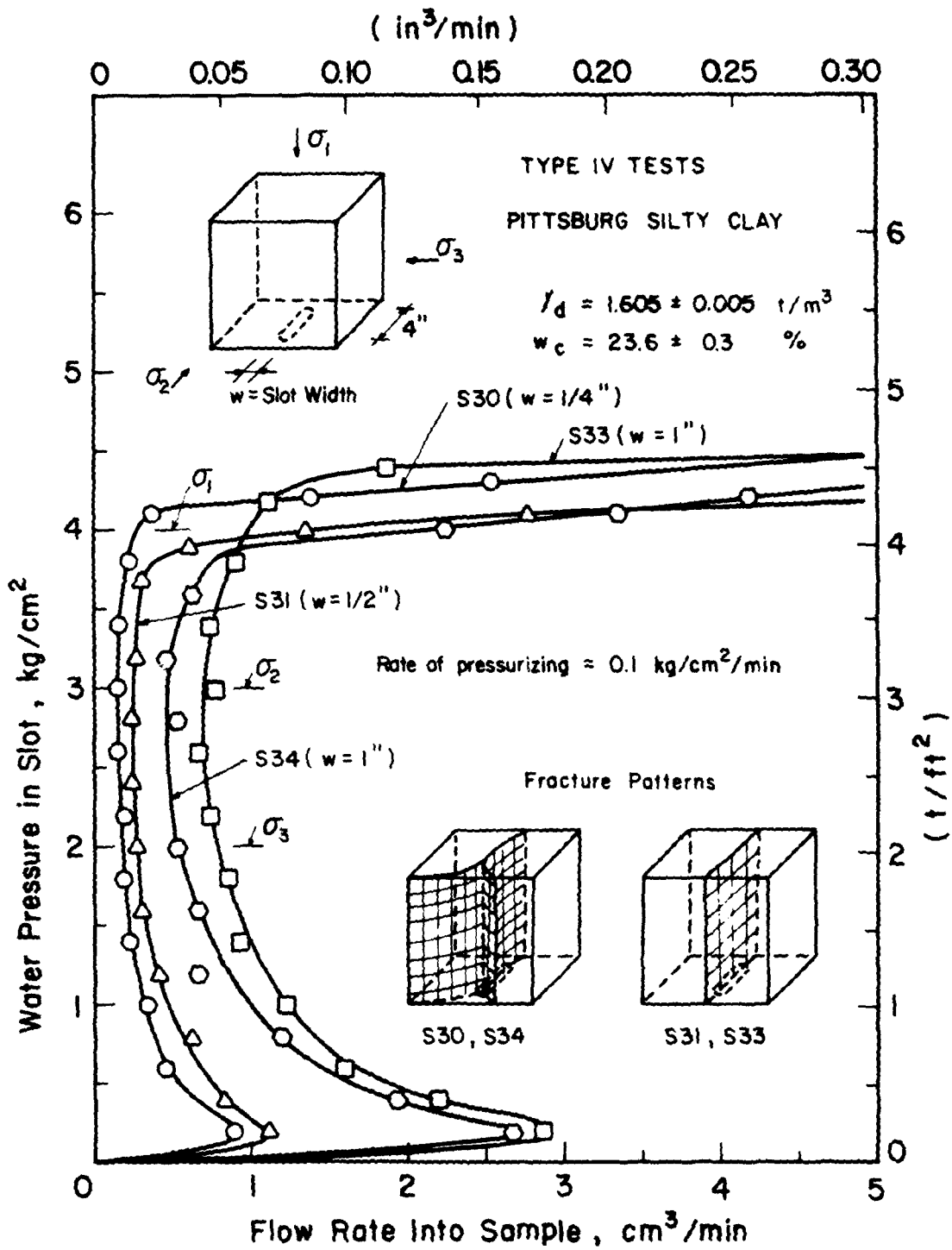


Figure 5.10 Results of Type IV tests, series 3, on Pittsburg silty clay



Figure 5.11 Typical fracture plane in Type IV test specimens

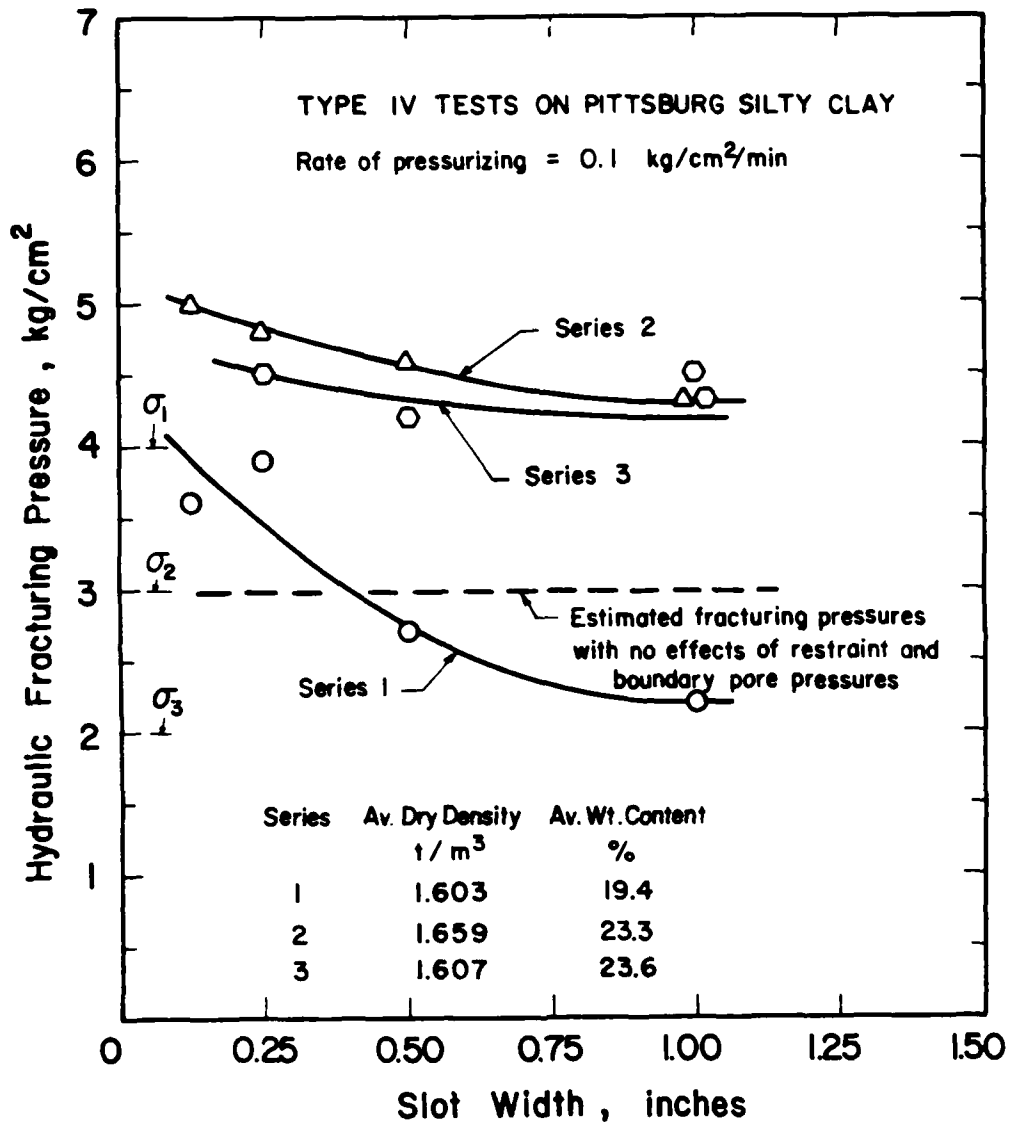


Figure 5.12 Effect of slot width in Type IV tests on hydraulic fracturing pressure for Pittsburgh silty clay

is a result of systematic effects due to wall friction in the test apparatus. It is also believed that the results of Series 1 tests were affected by the boundary pore pressure, which will be discussed in detail in the following section.

#### Effect of Water Content

The effect of water content was studied by comparing the results of Series 1 and Series 3. The water contents of the Series 1 specimens were about optimum, which was about 4% lower than those of the Series 3 specimens, and the densities were the same.

The results are compared in Figure 5.13, which shows that the measured fracturing pressures of samples with higher water contents were higher. The effect of slot size on the measured fracturing pressures was more pronounced in Series 1 samples, which had lower water contents. It is believed that this is due to the higher permeability of the clay samples at lower water contents. By comparing the flow rates of water in the tests, it was deduced that the permeability of the samples with the lower water contents was about one order of magnitude higher. Measurements of pore pressures in borehole fracturing tests showed that when the permeability was high, pore pressures developed at the outer boundary of the samples as a result of insufficient drainage provision at the boundary. The higher the permeability and the groove size, the higher would be the boundary pore pressures. It is believed that the boundary pore pressures, in addition to restraint due to friction in the test box, have affected the fracturing pressures measured in Series 1 samples.

The true effects of water content in these tests cannot be established with certainty due to the difficulties in isolating the effects.

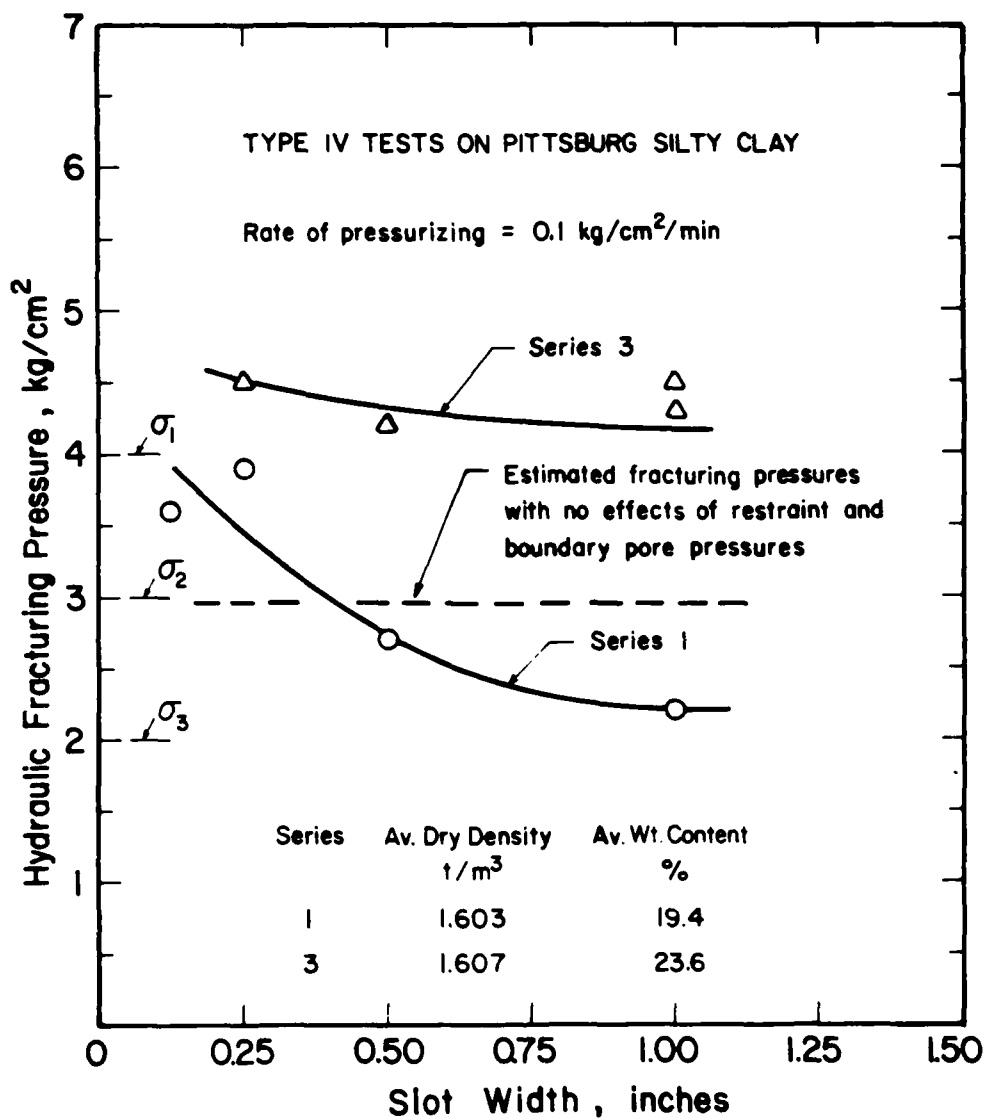


Figure 5.13 Effect of compaction water content on fracturing pressure in Pittsburgh silty clay

### Effect of Density

The effect of density was studied by comparing the results of Series 2 and 3. The water contents of the samples in the two series were essentially the same but the densities differed by about  $0.05 \text{ t/m}^3$  (3 pcf).

The results of the two series are compared in Figure 5.14. It can be seen that the fracturing pressures of Series 2 samples, which had higher densities, were consistently higher than those of Series 3 samples. Because of their higher densities, it could be expected that the friction that developed in the test box would be higher in Series 2 tests. The Series 2 samples may have had higher strength because of their higher densities. Both of these effects may have been responsible for the higher fracturing pressures measured in Series 2 tests. Increased density would be expected to reduce permeability, which would increase the fracturing pressure and increase Poisson's ratio, which would reduce the fracturing pressure.

### EFFECT OF TRANSITION MATERIAL IN TYPE V TESTS

#### Teton Dam Silt

Seven Type V tests were performed on Teton Dam silt. As explained in Chapter III, Type V tests were performed by applying water pressures through a patch of "transition material" in contact with one face of the test specimen. In the first series of tests, the transition material was placed on the  $\sigma_1$ -plane, whereas in a second series of tests the transition material was placed on the  $\sigma_2$ -plane. The results of the tests are summarized in Table 5.4.

#### Results of Series 1

The results of the three Series 1 tests are shown in Figure 5.15. The intermediate principal stress in Tests T1 and T2 was  $3 \text{ kg/cm}^2$  (3.07 tsf), whereas in Test T4 it was the same as the minor principal stress,

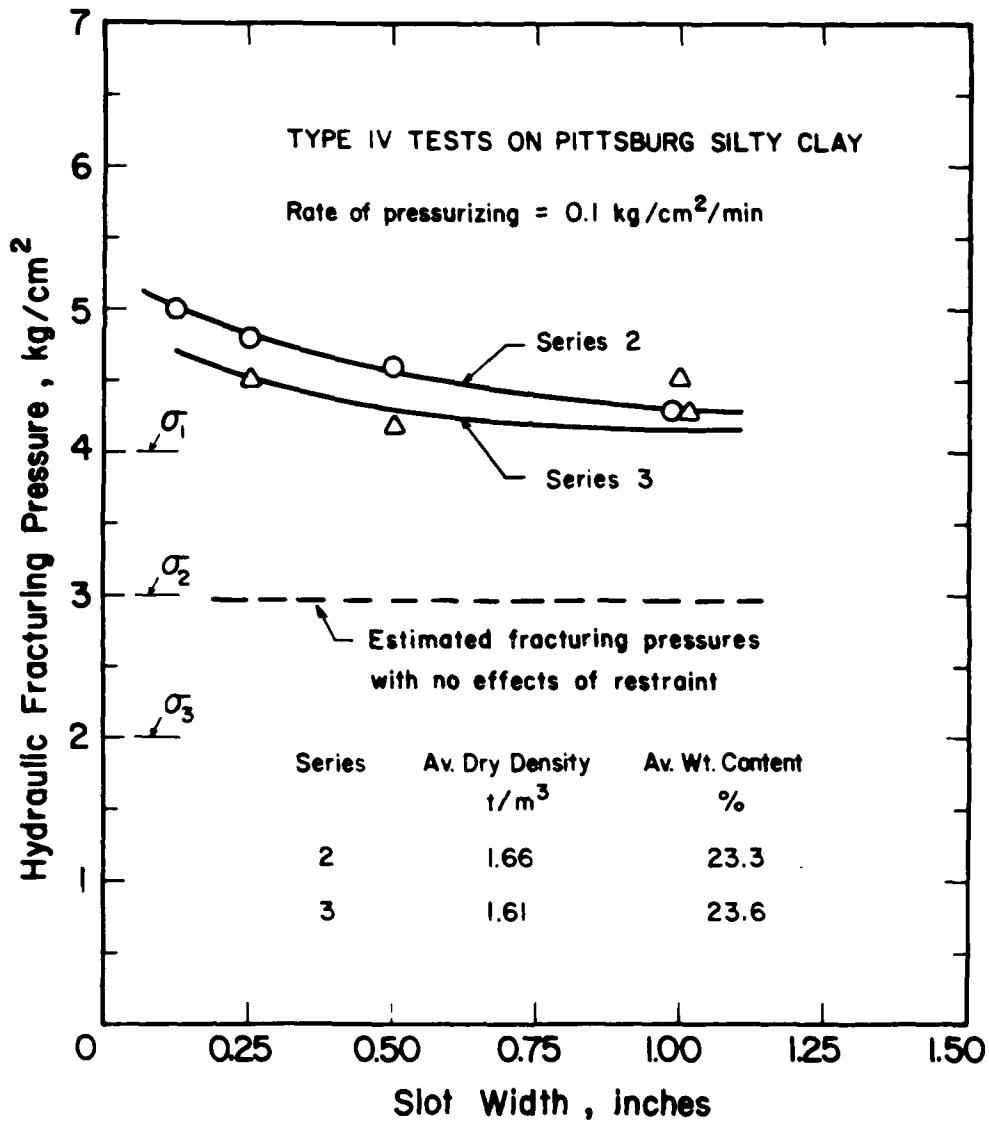


Figure 5.14 Effect of dry density on fracturing pressure in Pittsburgh silty clay

Table 5.4 Summary of Type V Test Results on Teton Dam Silt

Series No.	Position of Filter Material	Test No.	Dry Density t/m <sup>3</sup>	Water Content %	Filter Material	Fracturing Pressure kg/cm <sup>2</sup>
1	$\sigma_1$ -plane	T1	1.62	19.2	Monterey sand	3.2
		T2	1.62	19.3	Monterey sand	3.1
		T4	1.62	19.3	Monterey sand	2.9
2	$\sigma_2$ -plane	T3	1.63	19.5	Monterey sand	3.0
		T6	1.61	19.0	Monterey sand	2.8
		T10	1.62	19.5	Crushed granite	2.5
		T11	1.61	19.7	Crushed granite	2.5

Note: Rate of pressurizing = 0.1 kg/cm<sup>2</sup>/min.

Major principal stress = 4 kg/cm<sup>2</sup>

Intermediate principal stress = 3 kg/cm<sup>2</sup>

Minor principal stress = 2 kg/cm<sup>2</sup>

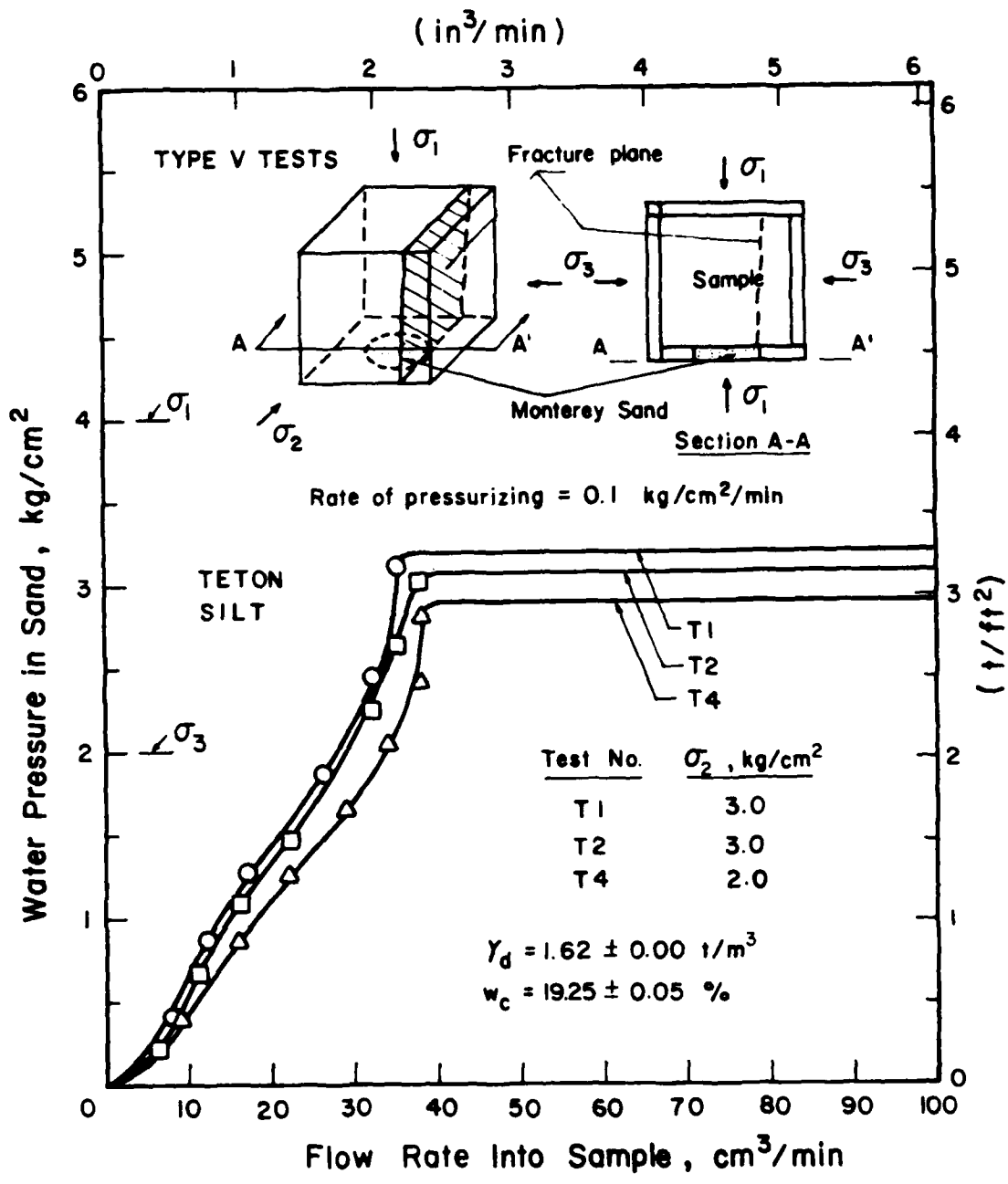


Figure 5.15 Results of Type V tests, series 1, on Teton Dam silt

2 kg/cm<sup>2</sup> (2.05 tsf).

The fracturing pressures of Samples T1 and T2 were 3.2 kg/cm<sup>2</sup> (3.3 tsf) and 3.1 kg/cm<sup>2</sup> (3.2 tsf), respectively. Sample T4 fractured at a lower pressure, 2.9 kg/cm<sup>2</sup> (3.0 tsf). It also had somewhat higher permeability. The lower fracturing pressure of Sample T4 could be due to the lower intermediate stress, which resulted in less dense material with higher permeability. Wall friction may also have influenced the results of these tests to some extent, but seems unlikely to be responsible for the lower fracturing pressure in T4.

The fracture planes were perpendicular to the direction of the minor principal stress and started at the edge of the transition material, as shown in Figure 5.15.

It is believed that the wedging action due to diverging seepage forces caused the samples in Type V tests to fracture.

#### Results of Series 2

Four tests were performed in Series 2. In Tests T3 and T6, Monterey sand was used as the transition material, whereas in Tests T10 and T11, the transition material was crushed granite.

The results of the tests are shown in Figure 5.16, where it can be seen that the fracturing pressures measured in Tests T10 and T11 were lower than those in Tests T3 and T6. This may be due to the fact that compacting the sample against crushed granite resulted in indentations in the face that could promote wedging and develop tensile stresses at an earlier stage.

The fracture plane of Sample T6 is shown in Figure 5.17. When the sample was split to reveal this plane, it was found that the Monterey Sand, which was used as transition material, was washed into the crack after fracturing occurred.

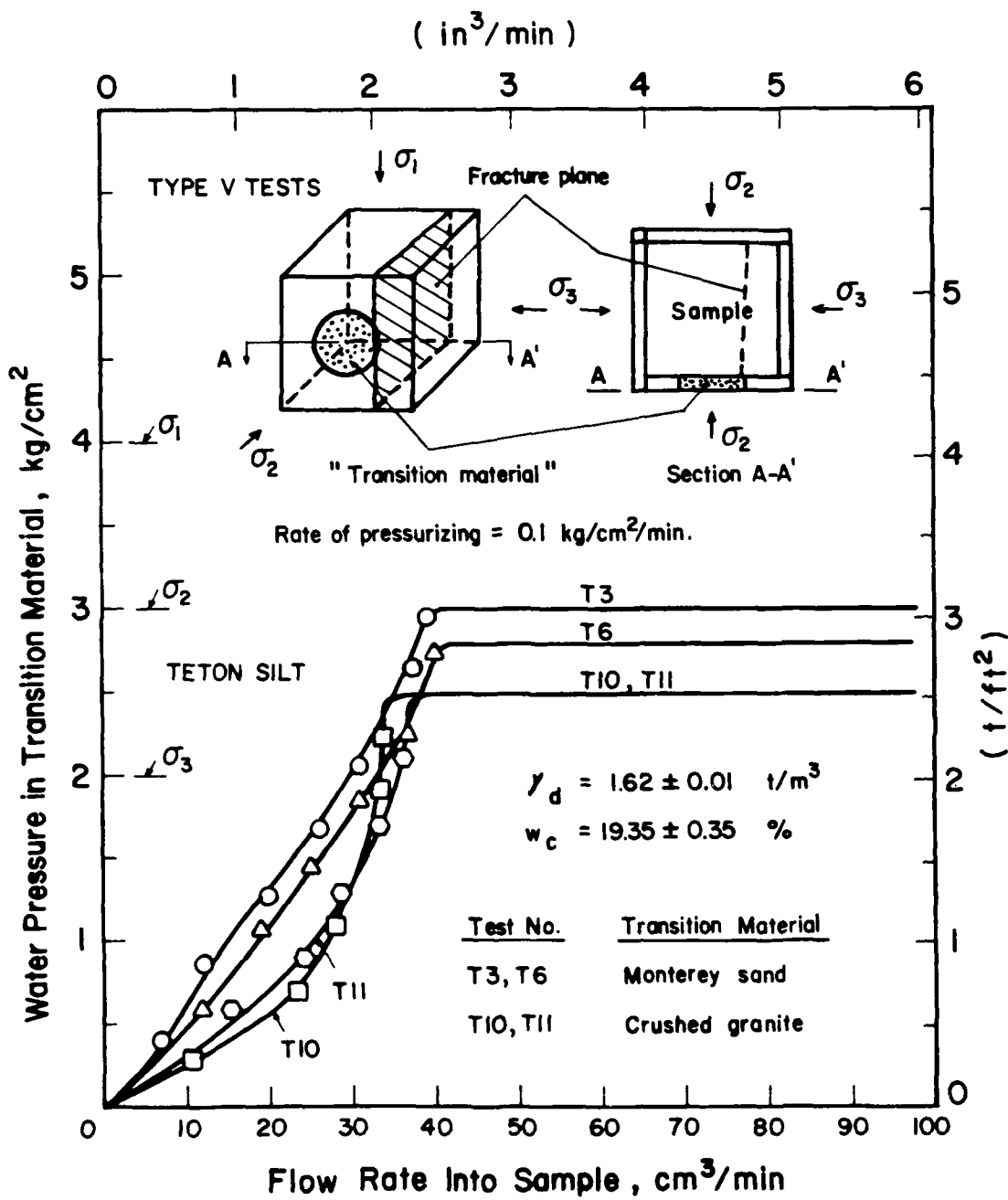


Figure 5.16 Results of Type V tests, series 2, on Teton Dam silt

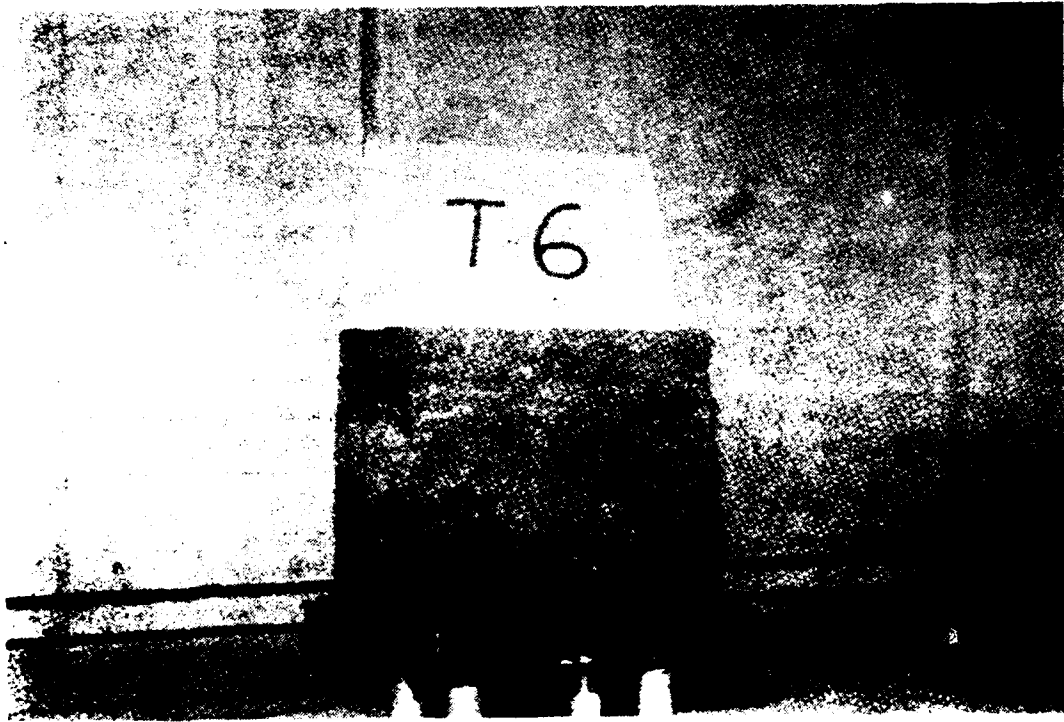


Figure 5.17 Typical fracture plane in Type V test specimens of Teton Dam silt

### Pittsburg Silty Clay

Five Type V tests were performed on Pittsburg silty clay. Monterey sand was used as the transition material in the first three tests (T7, T8, and T9), and crushed granite in the remaining two (T15 and T17).

The results of the tests with sand as the transition material are shown in Figure 5.18, and those with granite in Figure 5.19. The fracturing pressures of all the tests were about  $4 \text{ kg/cm}^2$  (4.1 tsf).

The patterns of the fracture planes were found to be irregular as shown in Figures 5.18 and 5.19. Some of them were horizontal, perpendicular to the direction of the intermediate principal stress. The fracture plane of one Type V test on Pittsburg silty clay is shown in Figure 5.20. The results of all of the Type V tests on Pittsburg silty clay are summarized in Table 5.5.

The hydraulic fracturing pressures measured in the tests on Pittsburg silty clay were higher than those on Teton Dam silt. This is believed to be a result of the lower permeability of the clay as compared to the silt. The theoretical analyses and finite element analyses described in Chapter III showed that lower permeability leads to higher hydraulic fracturing pressure.

#### EFFECT OF TEST DURATION IN BOREHOLE FRACTURING TESTS

##### Teton Dam Silt

Fifteen tests were performed to study the effect of test duration on the hydraulic fracturing pressure in Teton Dam silt. The borehole diameter was 0.48 cm (3/16 in) and its length was 5.1 cm (2 in). The time interval between each  $0.1 \text{ kg/cm}^2$  (0.1 tsf) increase in the borehole water pressure was varied from 30 seconds to 6 hours. The test durations varied from 20 minutes to 11 days.

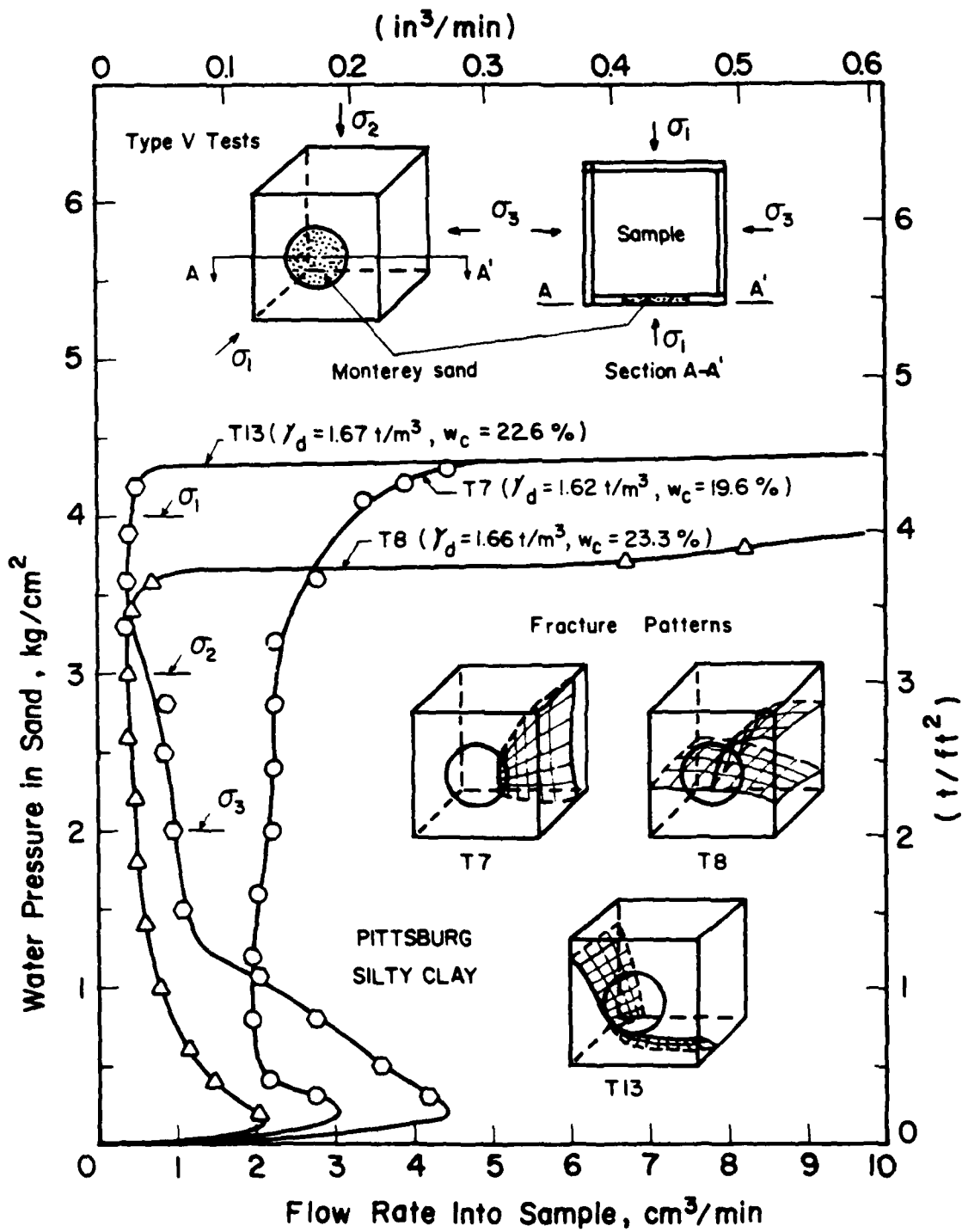


Figure 5.18 Results of Type V tests on Pittsburg silty clay

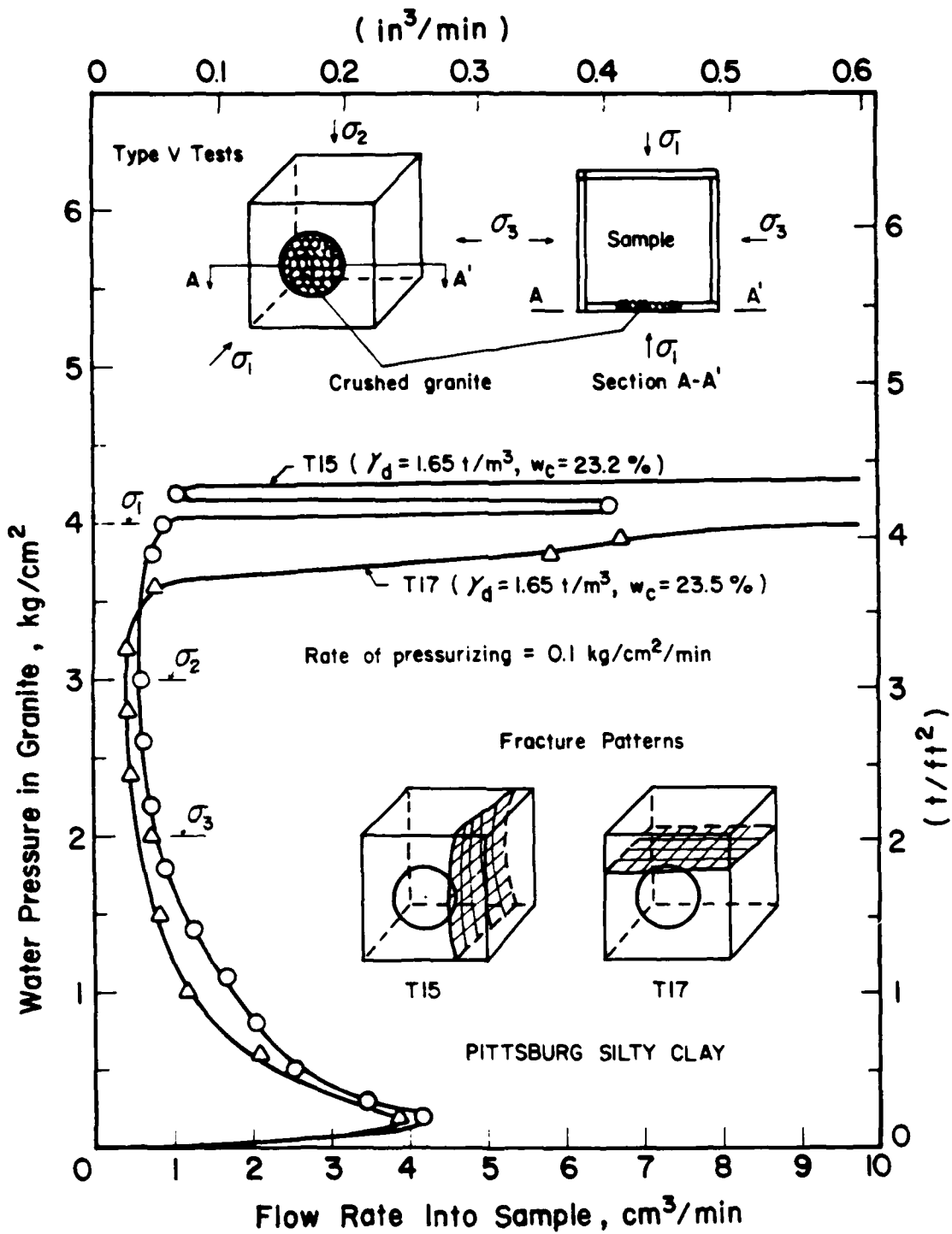


Figure 5.19 Results of Type V tests on Pittsburgh silty clay



Figure 5.20 Fracture plane in a Type v test specimen of Pittsburgh silty clay

Table 5.5 Summary of Type V Test Results on Pittsburgh Silty Clay

Test No.	Dry Density t/m <sup>3</sup>	Water Content %	Filter Material	Fracturing Pressure kg/cm <sup>2</sup>
T7	1.62	19.6	Monterey sand	4.4
T8	1.66	23.3	Monterey sand	3.9
T13	1.67	22.6	Monterey sand	4.4
T15	1.65	23.2	Crushed granite	4.3
T17	1.65	23.5	Crushed granite	4.0

Note: Rate of pressurizing = 0.1 kg/cm<sup>2</sup>/min.

Major principal stress = 4 kg/cm<sup>2</sup>

Intermediate principal stress = 3 kg/cm<sup>2</sup>

Minor principal stress = 2 kg/cm<sup>2</sup>

The hydraulic fracturing pressures are plotted as a function of the time to fracture in Figure 5.21. It can be seen from this figure that (1) the fracturing pressure decreased as the time to fracture increased for times to fracture less than about 500 minutes, (2) the fracturing pressure was essentially unaffected by test duration for tests that lasted longer than about 500 minutes, and (3) the samples with higher densities fractured at higher pressures.

In a slower test more water seeps into the sample, causing a larger seepage zone, which, on the basis of the analytical studies previously discussed, results in more wedging and greater stress change; therefore, lower pressure is required to fracture the sample in a slow test. For tests lasting longer than about 500 minutes, it was noticed that water was leaking out of the box before the samples fractured. This indicated that the seepage zones in these tests extended to the same distance, which is the outer boundary of the samples. It would be expected, therefore, that the fracturing pressures for these long tests would be about the same.

The fracturing planes were generally vertical and parallel to one wall of the box, but in some of the tests they were oriented diagonally. A typical fracture plane is shown in Figure 5.22. The results of all the tests are summarized in Table 5.6.

The permeability of Teton Dam silt was estimated from the test results using Hvorslev's equation (1949):

$$k_h = \frac{q \ln \{mL/D + \sqrt{1 + (mL/D)^2}\}}{2 \pi L H} \quad (5.1)$$

where

q is the flow rate into the sample

$k_h$  is the horizontal permeability

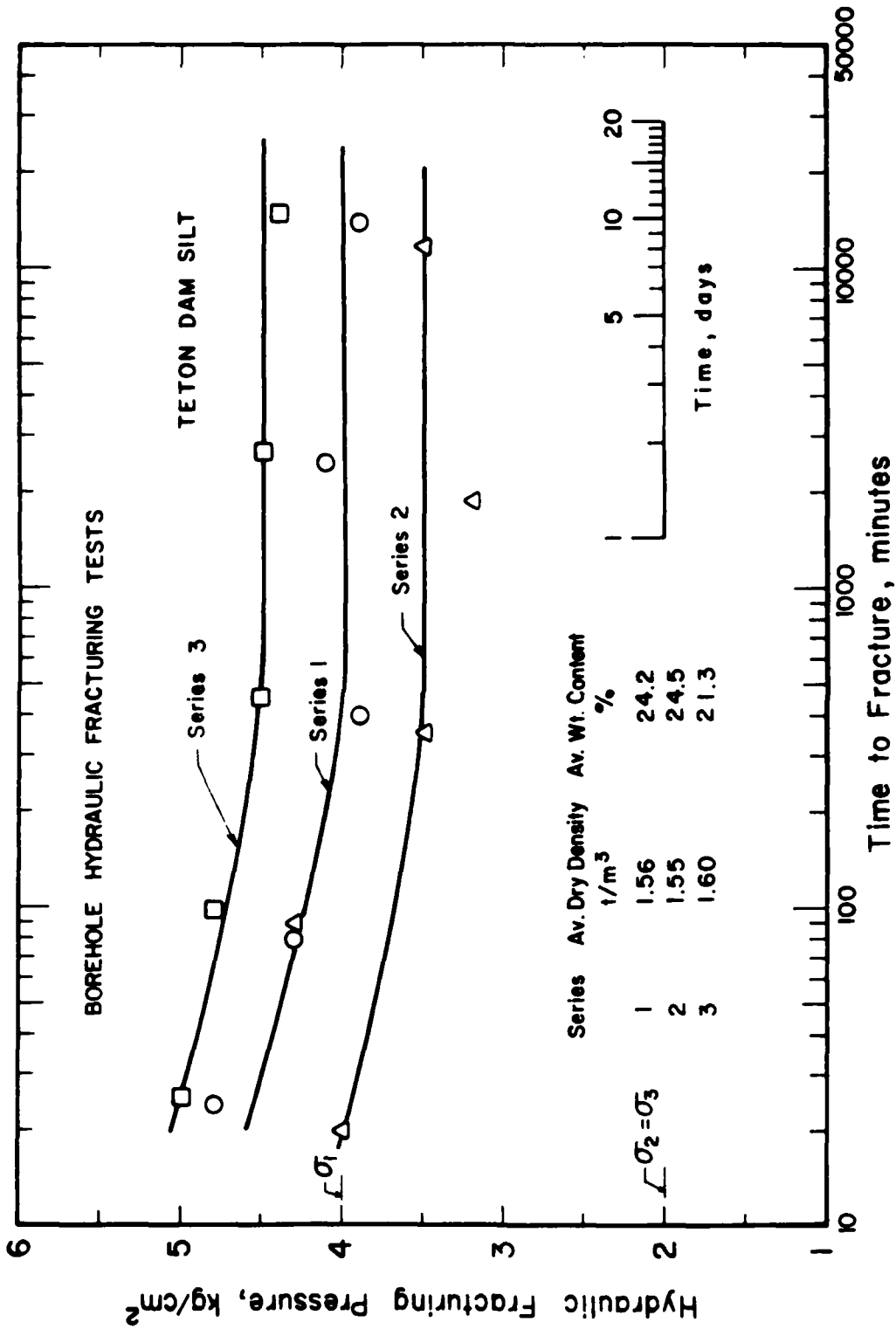


Figure 5.21 Effect of test duration on fracturing pressure in Teton Dam silt

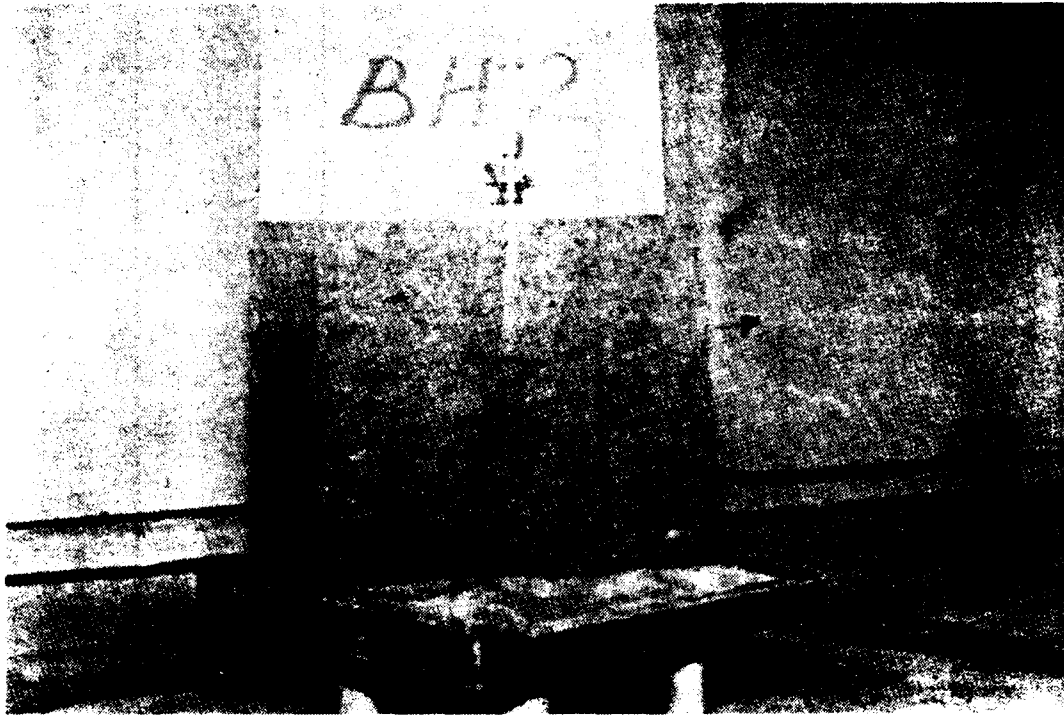


Figure 5.22 Typical fracture plane in borehole fracturing test specimens

Table 5.6 Summary of the Results of Borehole Fracturing Tests,  
Series 1 through 3, on Teton Dam Silt

Series No.	Test No.	Dry Density t/m <sup>3</sup>	Water Content %	Time to Fracture minutes	Fracturing Pressure kg/cm <sup>2</sup>
1	BH1	1.57	24.0	24	4.8
	BH2	1.56	24.2	86	4.3
	BH3	1.56	24.2	390	3.9
	BH4	1.56	24.4	2460	4.1
	BH15	1.57	24.3	13665	4.0
2	BH5	1.55	24.6	11876	3.5
	BH6	1.55	24.7	1870	3.2
	BH7	1.56	23.9	343	3.5
	BH8	1.55	24.8	86	4.3
	BH9	1.55	24.4	20	4.0
3	BH10	1.60	21.4	25	5.0
	BH11	1.60	21.3	96	4.8
	BH12	1.60	21.2	446	4.5
	BH13	1.60	21.3	2650	4.5
	BH14	1.59	21.4	14960	4.4

Note: Vertical stress = 4 kg/cm<sup>2</sup>

Horizontal stress = 2 kg/cm<sup>2</sup>

Borehole diameter = 0.48 cm (3/16")

Borehole length = 5.08 cm (2")

$k_v$  is the vertical permeability

$m$  is  $\sqrt{(k_h/k_v)}$

$D$  is the borehole diameter

$L$  is the borehole length

$H$  is the borehole head

Assuming that  $k_h = k_v$ , the permeability of Teton Dam silt, calculated from the results of 15 borehole tests, ranged from  $1 \times 10^{-7}$  cm/sec ( $3.3 \times 10^{-9}$  ft/sec) to  $2 \times 10^{-6}$  cm/sec ( $6.6 \times 10^{-8}$  ft/sec). The average value was  $5 \times 10^{-7}$  cm/sec ( $1.6 \times 10^{-8}$  ft/sec).

#### Pittsburg Silty Clay

Four tests were performed to study the effect of test duration on the hydraulic fracturing pressures for Pittsburg silty clay. The tests were BH18, BH20, BH21, and BH22.

Sample BH18 was aged under full confining pressures for 11 days. The pore pressures inside the sample were monitored during this time. The pore pressures were measured using two small diameter translucent tubes (OD=1/8 in.) with small porous stones (5mm X 10mm X 10mm) attached on one end. The other end was connected to a pore pressure transducer. These tubes were embedded in the soil during compaction, after being flushed with water. The locations of the porous stones were approximately 4 cm and 7 cm away from the center of the borehole. The soil was not saturated prior to pressurizing the borehole. The pore pressures in the sample at three different times are shown in Figure 5.23. It can be seen that the pore pressures were initially high, and that they decreased with time. The average pore pressure was about  $1.1 \text{ kg/cm}^2$  (1.1 tsf) one day after the confining pressures were applied, decreasing to an average value of about  $0.6 \text{ kg/cm}^2$  (0.6 tsf) after 11 days.

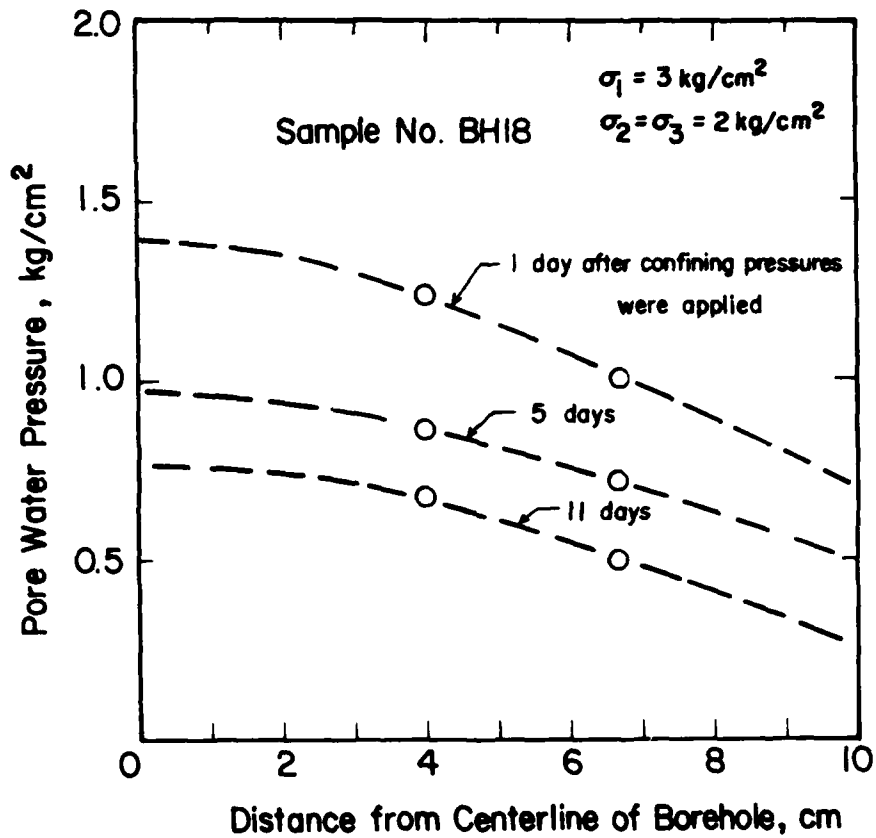


Figure 5.23 Pore water pressures in sample BH18 after confining pressures were applied

Samples BH20, BH21, and BH22 were not aged; the boreholes in these samples were drilled one day after the confining pressures were applied, and pressurizing was begun immediately.

The measured fracturing pressures are plotted as a function of the time to fracture in Figure 5.24. It can be seen that the fracturing pressure increased with test duration. It is believed that this may be due to an increase in effective stress with time, and an increase in strength with age of the samples, a thixotropy effect (Mitchell, 1960).

To explore these explanations of the results shown in Figure 5.24, thixotropic effects in Pittsburg silty clay were studied using triaxial tests. Six samples, which had a diameter of 3.56 cm (1.4 in) and a length of 8.89 cm (3.5 in), were compacted using the Harvard miniature compaction equipment. The samples were sealed in double membranes with a layer of grease between the membranes and allowed to cure in a moist room under water. Three of the samples were tested the following day, and the other three 13 days later. The samples were tested under unconsolidated-undrained conditions using stress-control. The confining pressure was  $0.5 \text{ kg/cm}^2$  (0.5 tsf).

The results of the triaxial tests are summarized in Table 5.7. It can be seen that the samples that were cured for 13 days had higher strengths. Ignoring the results of the test on sample No. 2, which had a somewhat lower water content than the others, it can be concluded that the strength of Pittsburg silty clay increased by about 15% after a period of about 2 weeks, and it was concluded that this could at least partly explain the results shown in Figure 5.24.

The test durations in the borehole fracturing tests BH18 and BH21 were about 5 hours. It may be seen that Sample BH18, which was aged for 11 days, fractured at higher pressure. It is believed that the higher effective stress and the higher strength of Sample BH18 were responsible for the higher fracturing pressure.

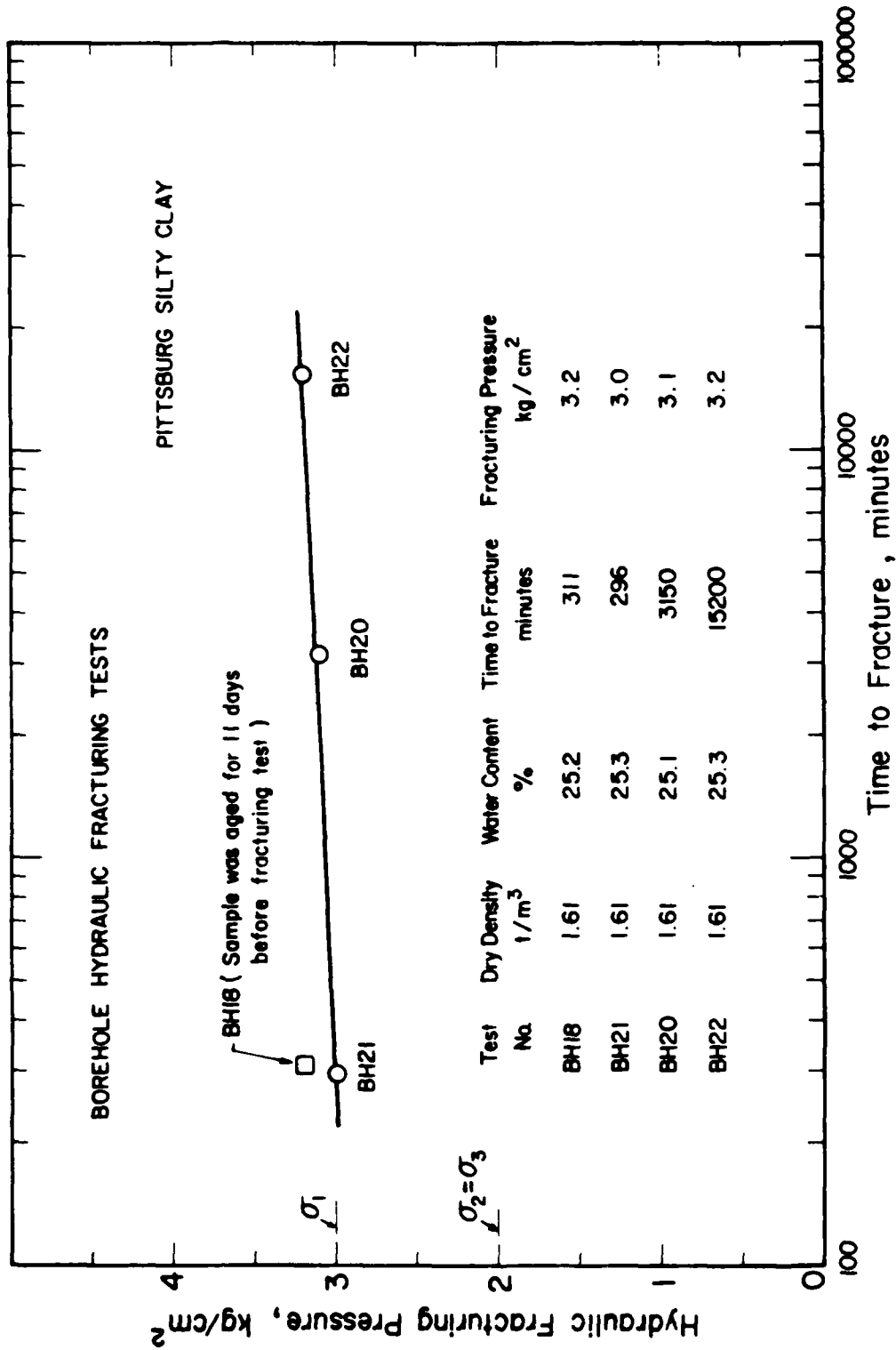


Figure 5.24 Effect of test duration on fracturing pressure in Pittsburg silty clay

Table 5.7 Results of Unconsolidated-Undrained Triaxial Tests on  
Pittsburg Silty Clay

Sample No.	Curing Time days	Dry Density t/m <sup>3</sup>	Water Content %	$(\sigma_1 - \sigma_3)_{\max}$ kg/cm <sup>3</sup>
1	1	1.63	23.4	1.79
3	1	1.63	23.4	1.75
5	1	1.63	23.5	1.77
2	13	1.63	22.4	2.37
4	13	1.63	23.1	2.00
6	13	1.63	23.2	2.03

Note: Confining pressures of all samples = 0.5 kg/cm<sup>2</sup>

The fracturing planes in the sample after fracturing occurred were vertical and were either parallel to one wall of the box or diagonal. The fracturing plane in one of the samples is shown in Figure 5.25. The results of all the tests are summarized in Table 5.8.

The effects of test duration on hydraulic fracturing pressure were different for Teton Dam silt and Pittsburg silty clay. This would seem to be due to the higher pore pressures in the clay samples, which decreased with time, and the effects of thixotropy strength gain in the clay. Together these factors resulted in higher fracturing pressures in tests of long duration on Pittsburg silty clay. The measured fracturing pressures decreased in tests of long duration on Teton Dam silt, which had lower pore pressures and less thixotropy strength gain.

#### EFFECTS OF BOREHOLE LENGTH AND CONFINING PRESSURES

Six tests were performed to study the effects of borehole length and confining pressures on the hydraulic fracturing pressures in Teton Dam silt.

The borehole diameter was 0.48 cm (3/16 in). Borehole length was 5.1 cm (2 in) for the first group of three samples and 17.8 cm (7 in) for the second group. The horizontal stresses in the tests were varied from 1 to 3 kg/cm<sup>2</sup> (1.02 to 3.07 tsf). Vertical stress was twice as large as horizontal stress.

Results of the six tests are shown in Figures 5.26 and 5.27. The figures generally show that increasing the borehole length led to a decrease in fracturing pressure, as expected. However, in Test BH26, which had a long borehole, and in Test BH23, which had a short borehole, fracturing pressures were approximately the same. But in these two tests the flow rate was about the same. Thus, the extent of the seepage zone was greater for the shorter hole (Test BH23). The combination of the increased fracturing pressure due to the short length of hole and the decreased fracturing pressure due to the increased zone of seepage would then tend to cancel, producing about the same fracturing pressures in both samples.



Figure 5.25 Fracture plane in a borehole fracturing test specimen of Pittsburg silty clay

Table 5.8 Summary of the Results of Borehole Fracturing Tests,  
Series 1, on Pittsburgh Silty Clay

Test No.	Dry Density t/m <sup>3</sup>	Water Content %	Time to Fracture minutes	Fracturing Pressure kg/cm <sup>2</sup>
BH18	1.61	25.2	311	3.2
BH20	1.61	25.1	3150	3.1
BH21	1.61	25.3	296	3.0
BH22	1.61	25.3	15200	3.2

Note: Vertical stress = 3 kg/cm<sup>2</sup>

Horizontal stress = 2 kg/cm<sup>2</sup>

Borehole diameter = 0.48 cm (3/16")

Borehole length = 5.08 cm (2")

Sample BH18 was subjected to confining pressures for 11 days before fracturing test was started.

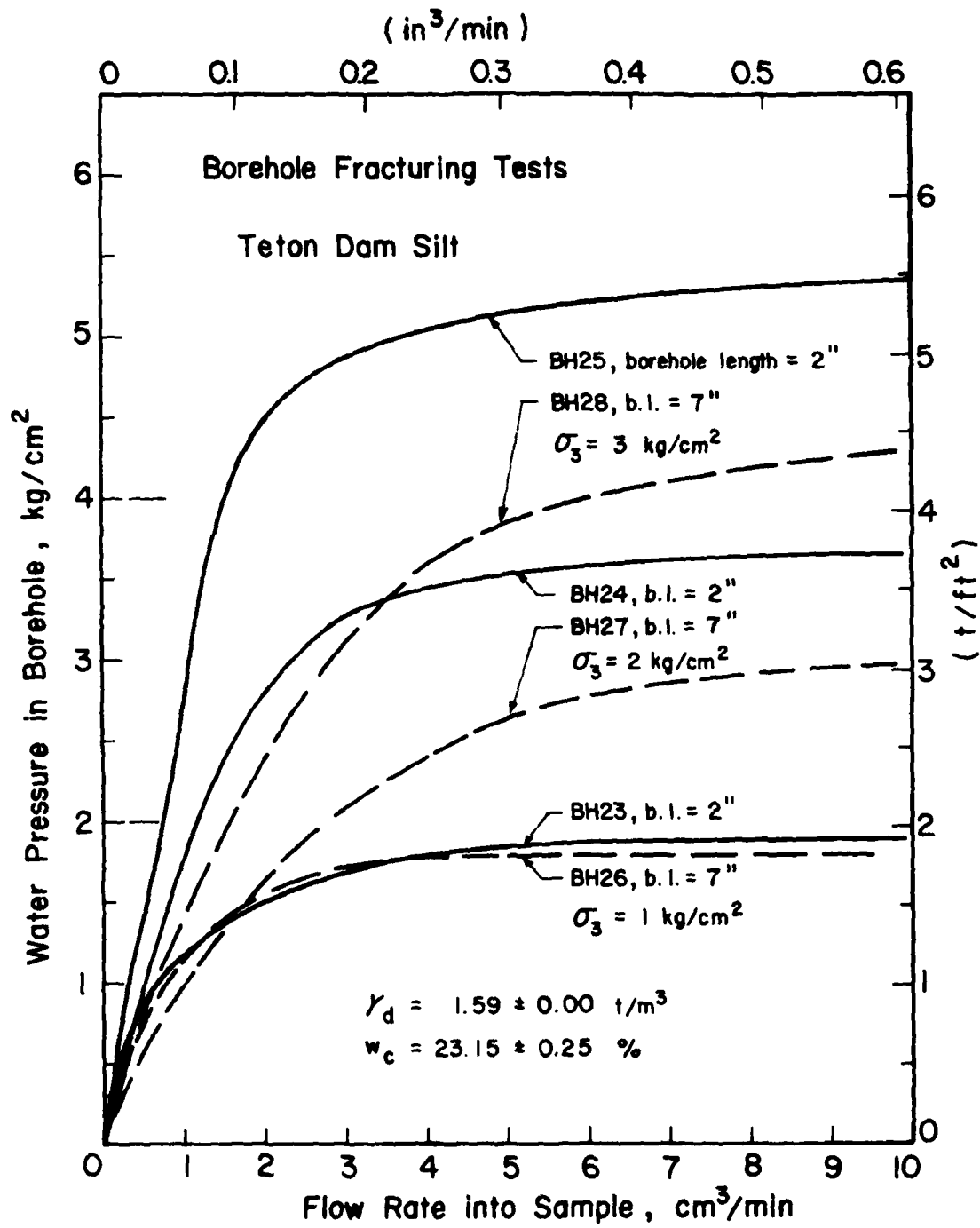


Figure 5.26 Results of borehole fracturing tests, series 4, on Teton Dam silt

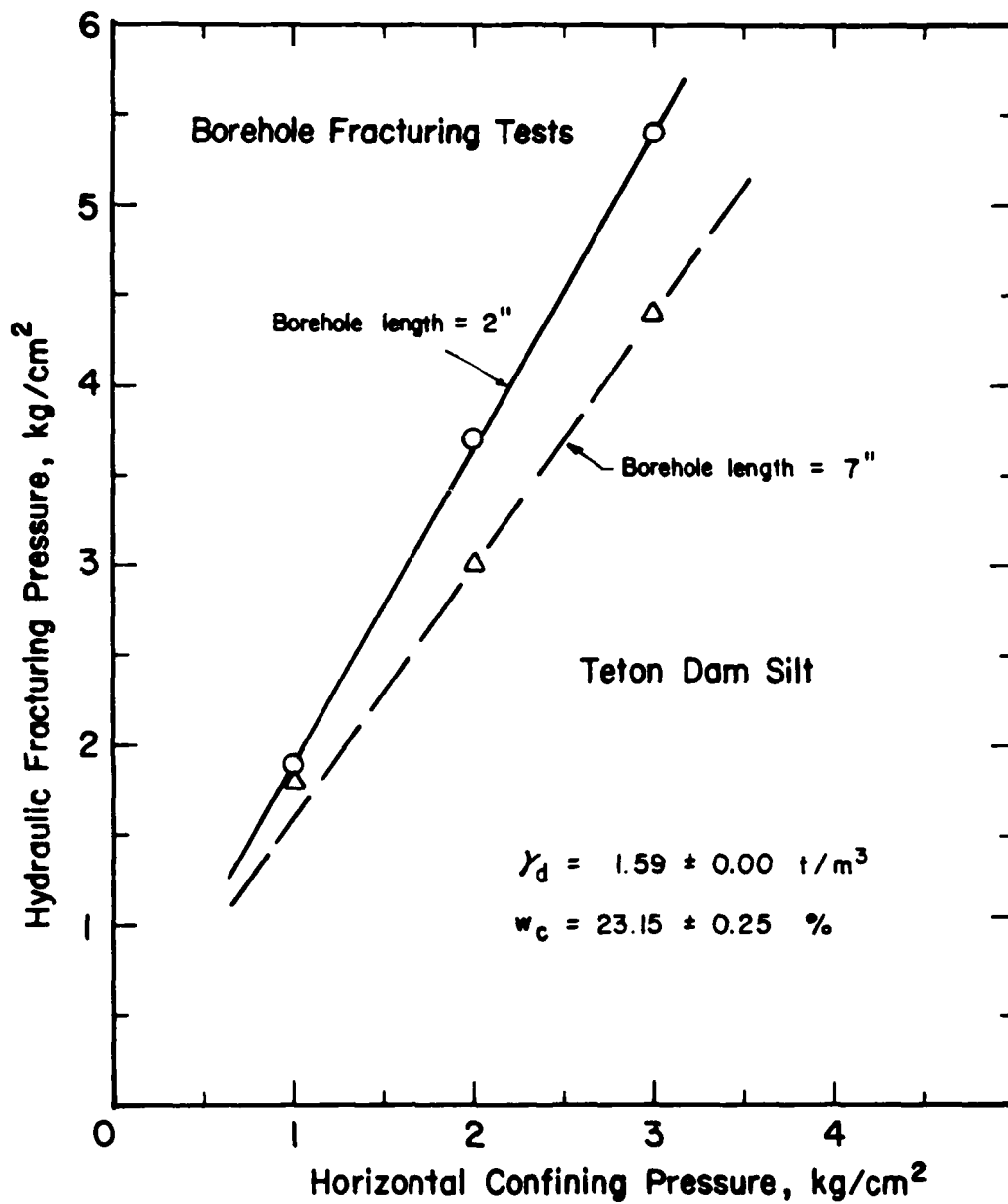


Figure 5.27 Effects of confining pressure and borehole length fracturing pressure in Teton Dam silt

The pore pressures in the samples were measured before and during the tests. It can be seen in Table 5.9 that the initial pore pressures within the samples were approximately zero. The result of Test BH29 will be discussed in another section.

A typical fracture plane for a sample with a long borehole is shown in Figure 5.28.

#### EFFECT OF BOREHOLE DIAMETER

##### Teton Dam Silt

Three tests were performed to study the effect of borehole diameter on hydraulic fracturing pressure in Teton Dam silt. The borehole length was 17.8 cm (7 in). Three borehole diameters were used: 0.48 cm (3/16 in), 0.95 cm (3/8 in), and 1.91 cm (3/4 in).

The results of the tests are shown in Figure 5.29. The fracturing pressures are plotted as a function of borehole diameter in Figure 5.30, which shows that the fracturing pressure decreased slightly with increasing borehole diameter. The results of the tests, numbered BH30, BH31, and BH32, are summarized in Table 5.10.

##### Pittsburg Silty Clay

Three tests were performed to study the effect of borehole diameter on the hydraulic fracturing pressure for Pittsburg silty clay. The borehole length and the variation of the borehole diameter were the same as those in the tests on Teton Dam silt.

The fracturing pressures are plotted as a function of borehole diameter in Figure 5.31. It can be seen that borehole diameter had no significant effect on fracturing pressure, in agreement with the results of the theoretical analyses previously described. The results of the tests, numbered BH40, BH41, and BH42, are summarized in Table 5.11.

Table 5.9 Summary of the Results of Borehole Fracturing Tests,  
Series 4, on Teton Dam Silt

Test No.	Borehole Length in	Horizontal Stress kg/cm <sup>2</sup>	Dry Density t/m <sup>3</sup>	Water Content %	Initial Pore Pressure* kg/cm <sup>2</sup>	Fracturing Pressure kg/cm <sup>2</sup>
BH23	2	1	1.59	23.1	-0.02	1.9
BH24	2	2	1.59	23.0	0.05	3.7
BH25	2	3	1.59	22.9	-0.03	5.4
BH26	7	1	1.59	23.2	-0.05	1.8
BH27	7	2	1.58	23.1	-0.01	3.0
BH28	7	3	1.59	23.4	0.08	4.4
BH29	7	2	1.56	23.4	-0.08	3.6

Note: Rate of pressurizing = 0.1 kg/cm<sup>2</sup> at 5-minute interval

Vertical stress = 2X Horizontal stress

Borehole diameter = 0.48 cm (3/16")

\*Average value of pore pressures at two locations

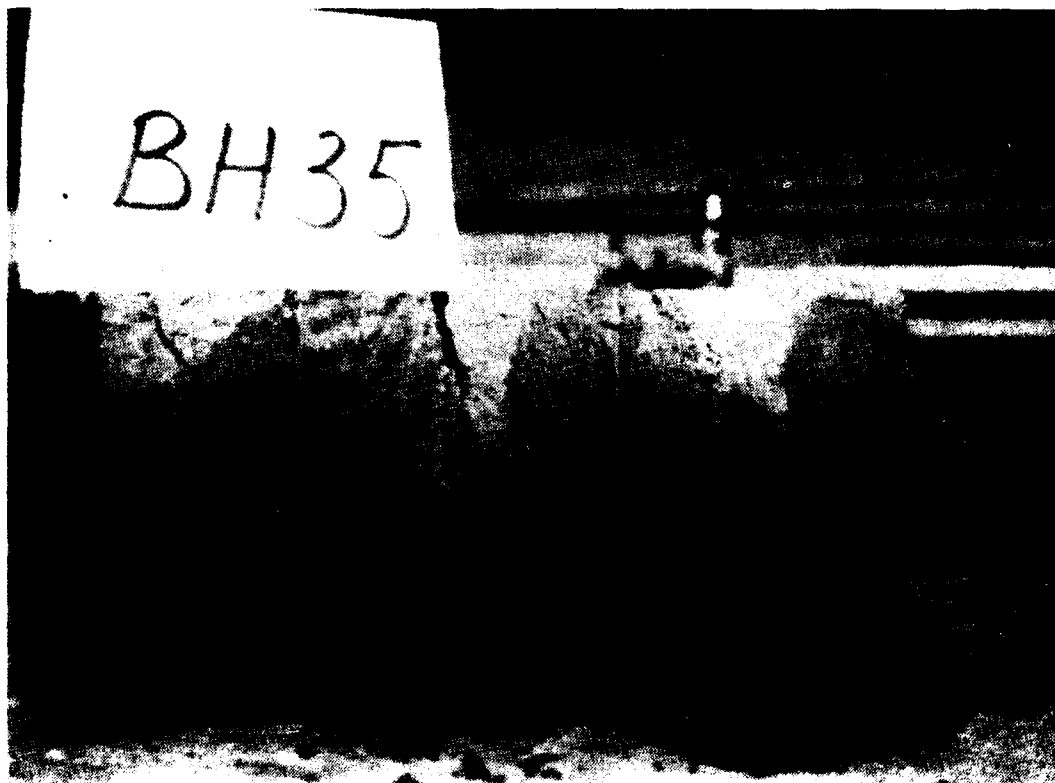


Figure 5.28 Typical fracture plane in fracturing test specimens with long boreholes

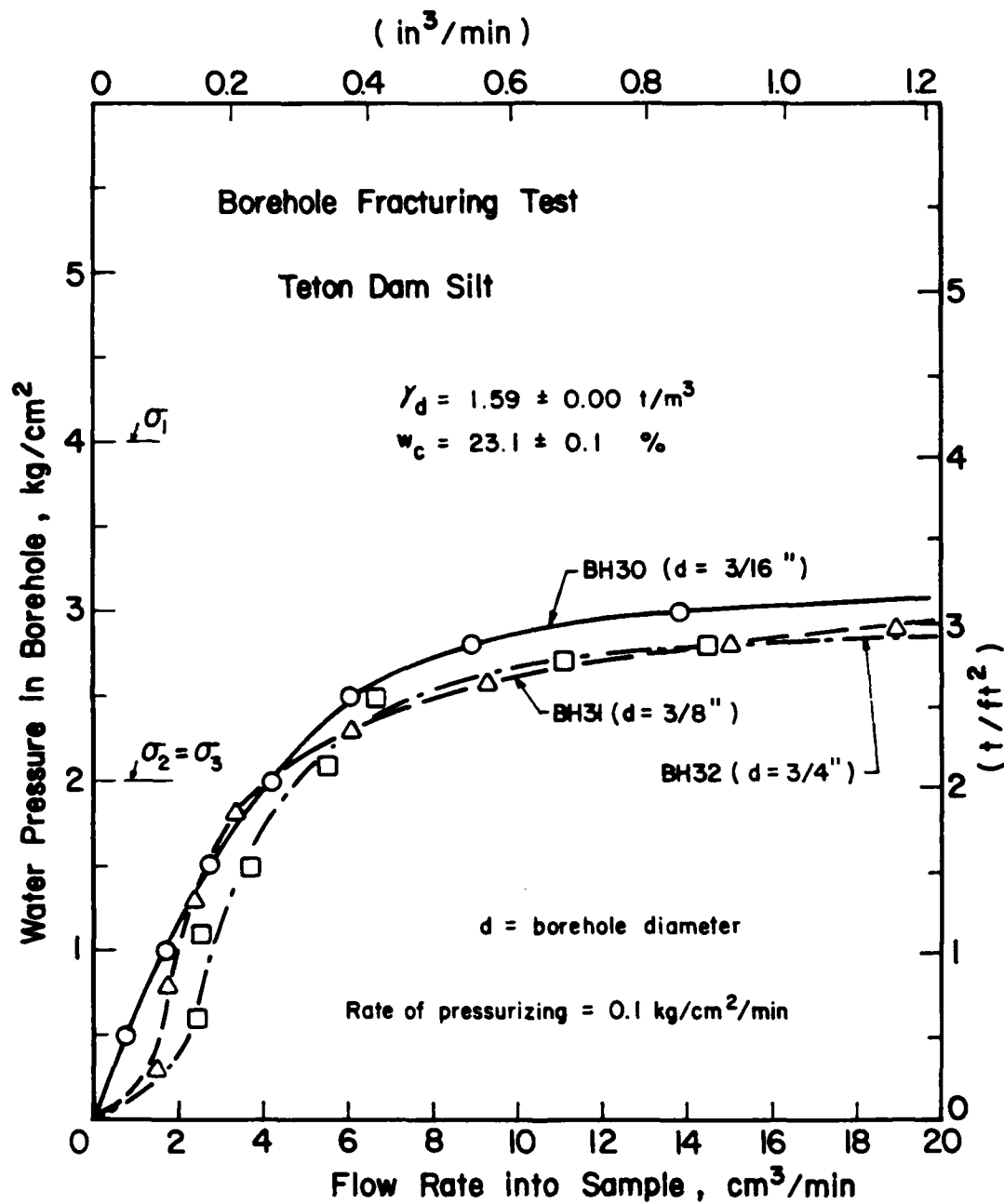


Figure 5.29 Results of borehole fracturing tests with various borehole diameters on Teton Dam silt

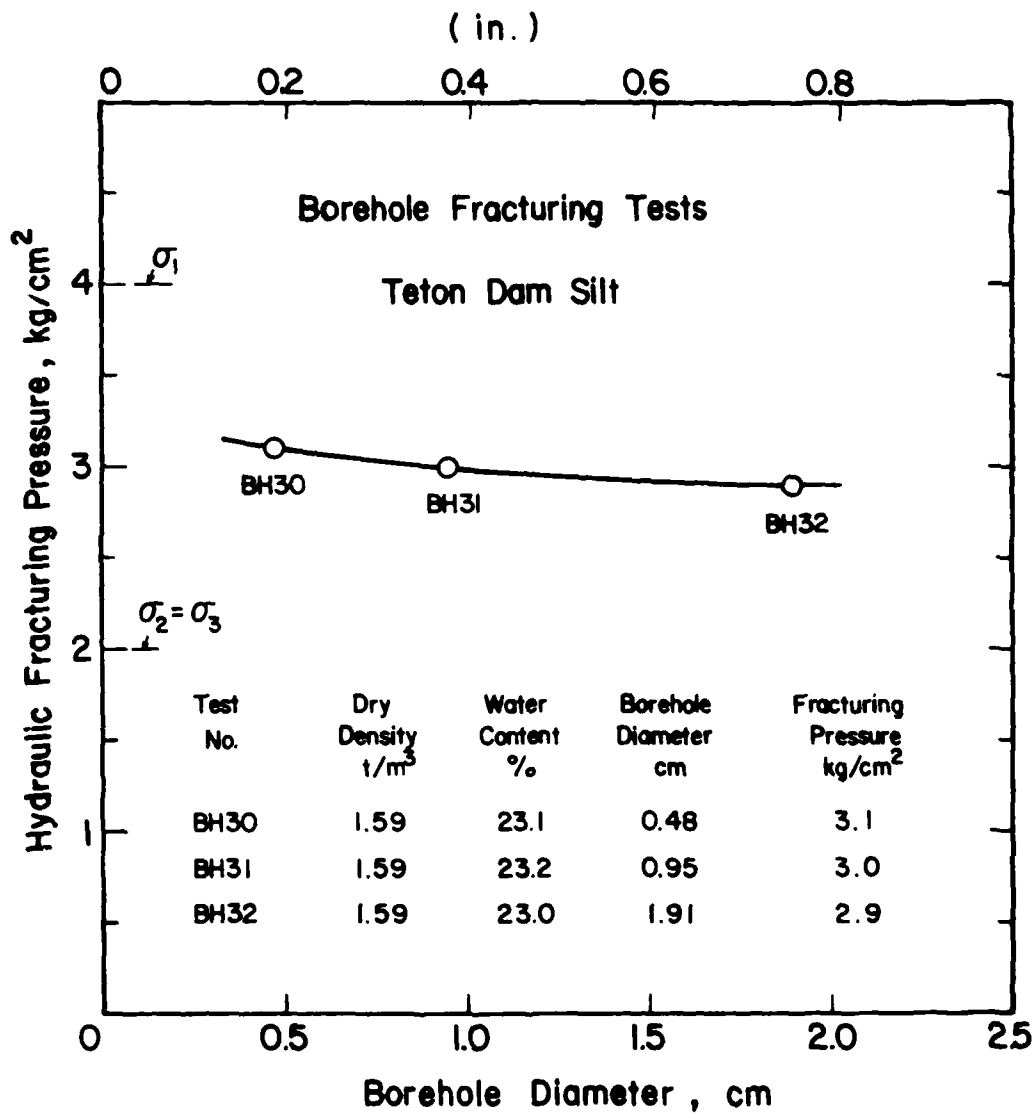


Figure 5.30 Effect of borehole diameter on fracturing pressure in Teton Dam silt

Table 5.10 Summary of the Results of Borehole Fracturing Tests,  
Series 5, on Teton Dam Silt

Test No.	Borehole Diameter cm	Dry Density t/m <sup>3</sup>	Water Content %	Pore Pressure* kg/cm <sup>2</sup>	Fracturing Pressure kg/cm <sup>2</sup>
BH30	0.48	1.59	23.1	0.24	3.1
BH31	0.95	1.59	23.2	0.18	3.0
BH32	1.91	1.59	23.0	0.25	2.9
BH33	0.48	1.59	20.3	0.06	4.0
BH34	0.48	1.59	20.4	-0.12	3.3
BH36	0.48	1.59	23.3	0.14	3.0
BH37	0.48	1.59	23.2	0.05	3.2
BH38	0.48	1.56	23.1	0.02	3.8
BH39	0.48	1.53	23.7	0.00	3.6

Note: Rate of pressurizing = 0.1 kg/cm<sup>2</sup>/min.

Vertical stress = 4 kg/cm<sup>2</sup>

Horizontal stress = 2 kg/cm<sup>2</sup>

Borehole length = 17.8 cm (7")

\*Average value before fracturing test

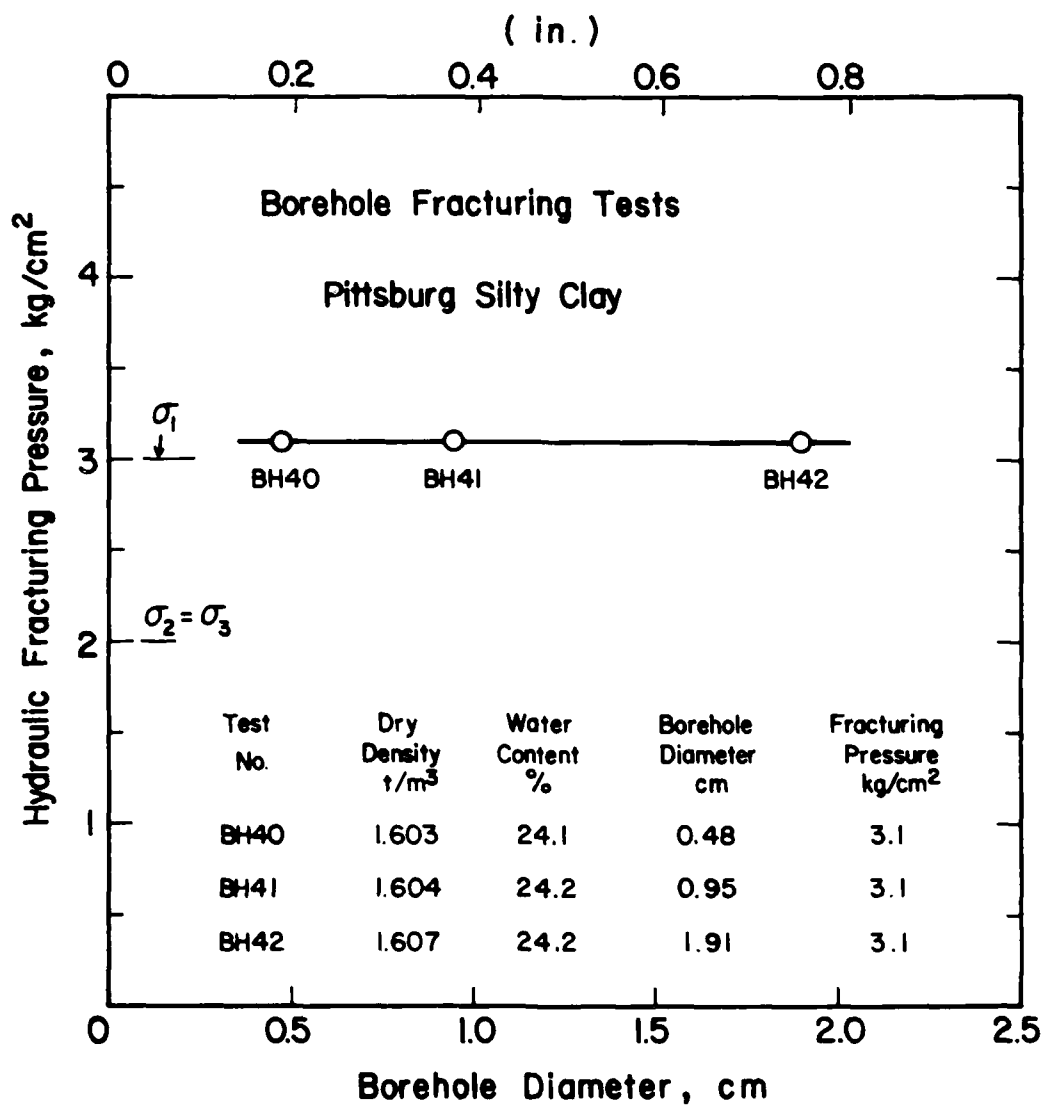


Figure 5.31 Effect of borehole diameter on fracturing pressure in Pittsburg silty clay

Table 5.11 Summary of the Results of Borehole Fracturing Tests,  
Series 2, on Pittsburgh Silty Clay

Test No.	Borehole Diameter cm	Dry Density t/m <sup>3</sup>	Water Content %	Pore Pressure* kg/cm <sup>2</sup>	Fracturing Pressure kg/cm <sup>2</sup>
BH40	0.48	1.603	24.1	0.75	3.1
BH41	0.95	1.604	24.2	0.93	3.1
BH42	1.91	1.607	24.2	0.89	3.1
BH43	0.95	1.636	24.5	1.26	2.7
BH44	0.95	1.527	24.5	0.41	2.9
BH45	0.95	1.612	19.9	0.09	**
BH46	0.95	1.614	20.3	-0.10	***

Note: Rate of Pressurizing = 0.1 kg/cm<sup>2</sup> at 5-minute interval

Vertical stress = 3 kg/cm<sup>2</sup>

Horizontal stress = 2 kg/cm<sup>2</sup>

Borehole length = 17.8 cm (7 in)

\*Average value before drilling borehole

\*\*Water from borehole flowed out of sample rapidly through inter-cluster pores at a pressure of 0.7 kg/cm<sup>2</sup>.

\*\*\*Water from borehole flowed out of sample rapidly through inter-cluster pores at a pressure of 0.4 kg/cm<sup>2</sup>.

In summary, borehole diameter had a slight effect on the hydraulic fracturing pressures in Teton Dam silt, and none in Pittsburg silty clay.

#### EFFECT OF WATER CONTENT IN BOREHOLE

##### FRACTURING TESTS

###### Teton Dam Silt

To study the effect of compaction water content, two samples of Teton Dam silt--BH33 and BH34--were compacted at the same density but lower water contents than that of sample BH30. The borehole diameter was 0.48 cm (3/16 in) and the length was 17.8 cm (7 in).

The water contents for samples BH33 and BH34 were about 3% lower than that for Sample BH30, and as a result the pore pressures in these samples were lower than in Sample BH30. The test results shown in Figure 5.32 indicated that Samples BH33 and BH34 fractured at higher pressures than Sample BH30. The results of all three tests are summarized in Table 5.10.

The initial pore pressures for Samples BH33 and BH34 were lower than for Sample BH30, as shown in Table 5.10. In addition, Samples BH33 and BH34 probably had higher strength because of their lower water contents. These appear to be the reasons why Samples BH33 and BH34 fractured at higher pressures than Sample BH30.

###### Pittsburg Silty Clay

To study the effect of water content on hydraulic fracturing pressure in Pittsburg silty clay, two samples--BH45 and BH46--were compacted at similar densities but lower water contents than Sample BH41. The borehole diameter was 0.95 cm (3/8 in) and the length was 17.8 cm (7 in).

The water contents for Samples BH45 and BH46 were about 4% lower than that for Sample BH41. The water contents for Samples BH45 and BH46

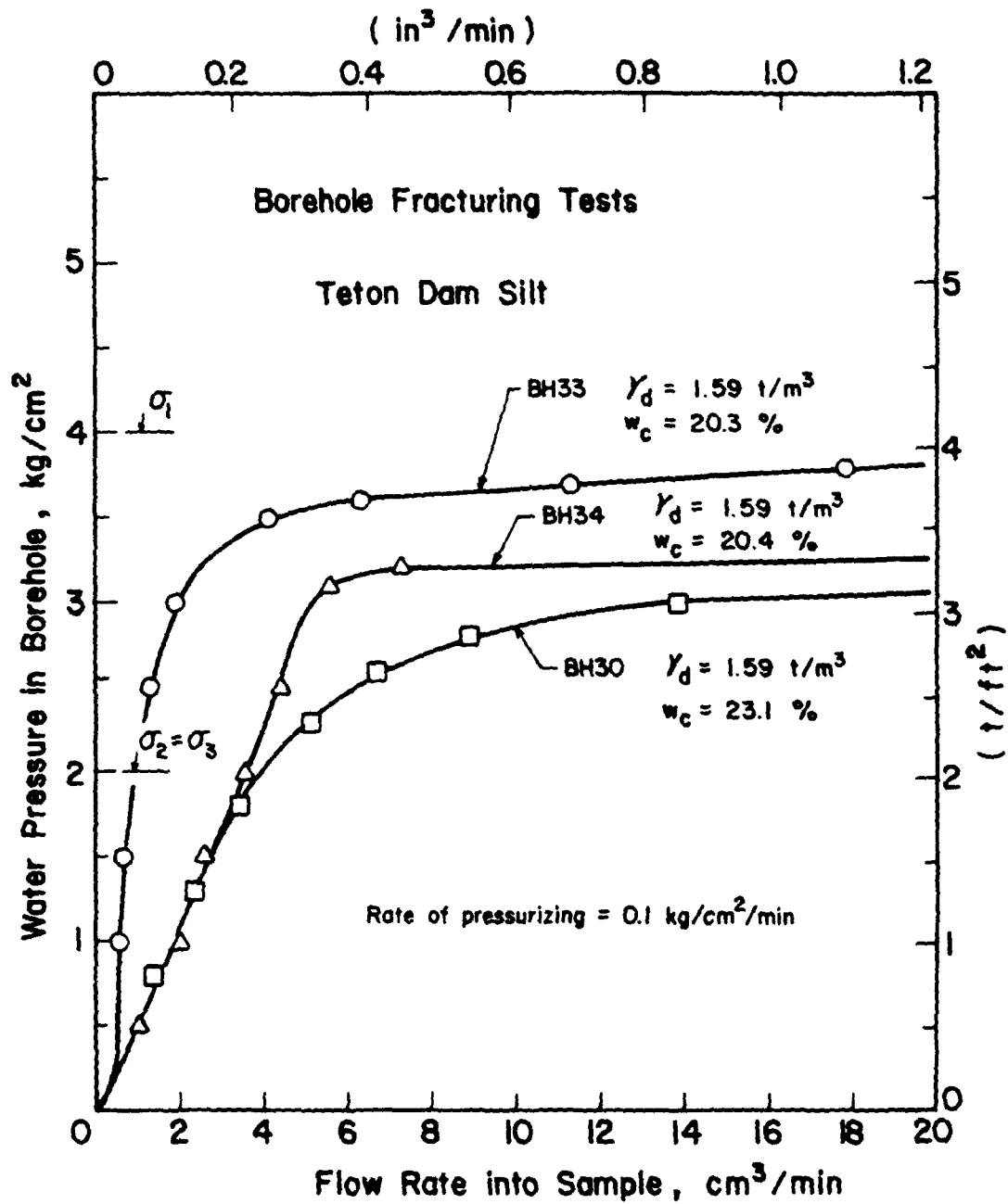


Figure 5.32 Results of borehole fracturing tests BH30, BH33, and BH34 on Teton Dam silt

were reduced by means of evaporating the moisture in the aggregations of clay particles, comparable in size to coarse sand particles (diameter  $\approx$  5 mm) before compaction.

The flow rates are plotted as a function of borehole water pressure in Figure 5.33. It can be seen that at very small pressures the flow rates for Samples BH45 and BH46 increased very abruptly. When the cubical stress apparatus was disassembled, no fracturing planes were found. The stains caused by the dye in the water indicated that water flowed through intercluster pores, and that the high flow rates were simply due to high permeability, not fracturing. The soil for samples BH45 and BH46 was processed from previous test specimens which had higher water contents. The samples were broken down to small aggregations of particles and exposed to air to reduce the water content. Therefore, the water content within the aggregations may not have been uniform; the soil at the surface of the aggregations would be drier and stiffer than the inside. At the compaction effort used, the stiff aggregations formed clusters with large intercluster pores. It seems likely that aggregations of clay particles formed a structure with large intercluster voids and high permeability. The fact that the change in flow rate was abrupt may have been due to some finite water pressure was required for the water to create channels to the outer boundary of the sample.

#### EFFECT OF DENSITY IN BOREHOLE FRACTURING TESTS

##### Teton Dam Silt

The effect of density was investigated in Tests BH27 and BH29 of Series 4 and Tests BH30, BH38, and BH 39 of Series 5.

The results of Tests BH27 and BH 29 are shown in Figure 5.34. The water contents of the two samples were close but the densities differed by about  $0.03 \text{ t/m}^3$  (2 pcf). It may be seen that the more dense sample

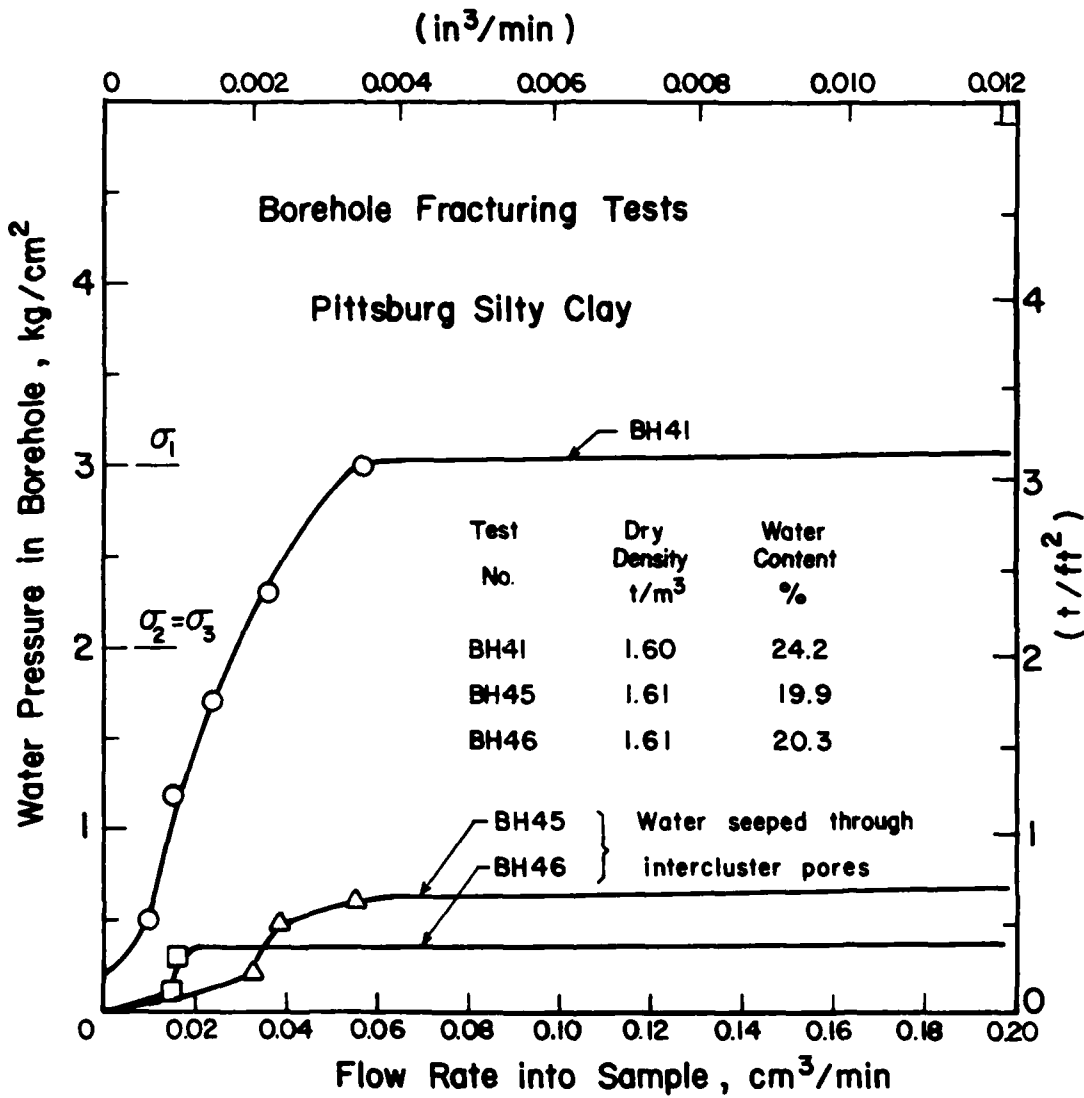


Figure 5.33 Results of borehole fracturing tests BH41, BH45, and BH46 on Pittsburg silty clay

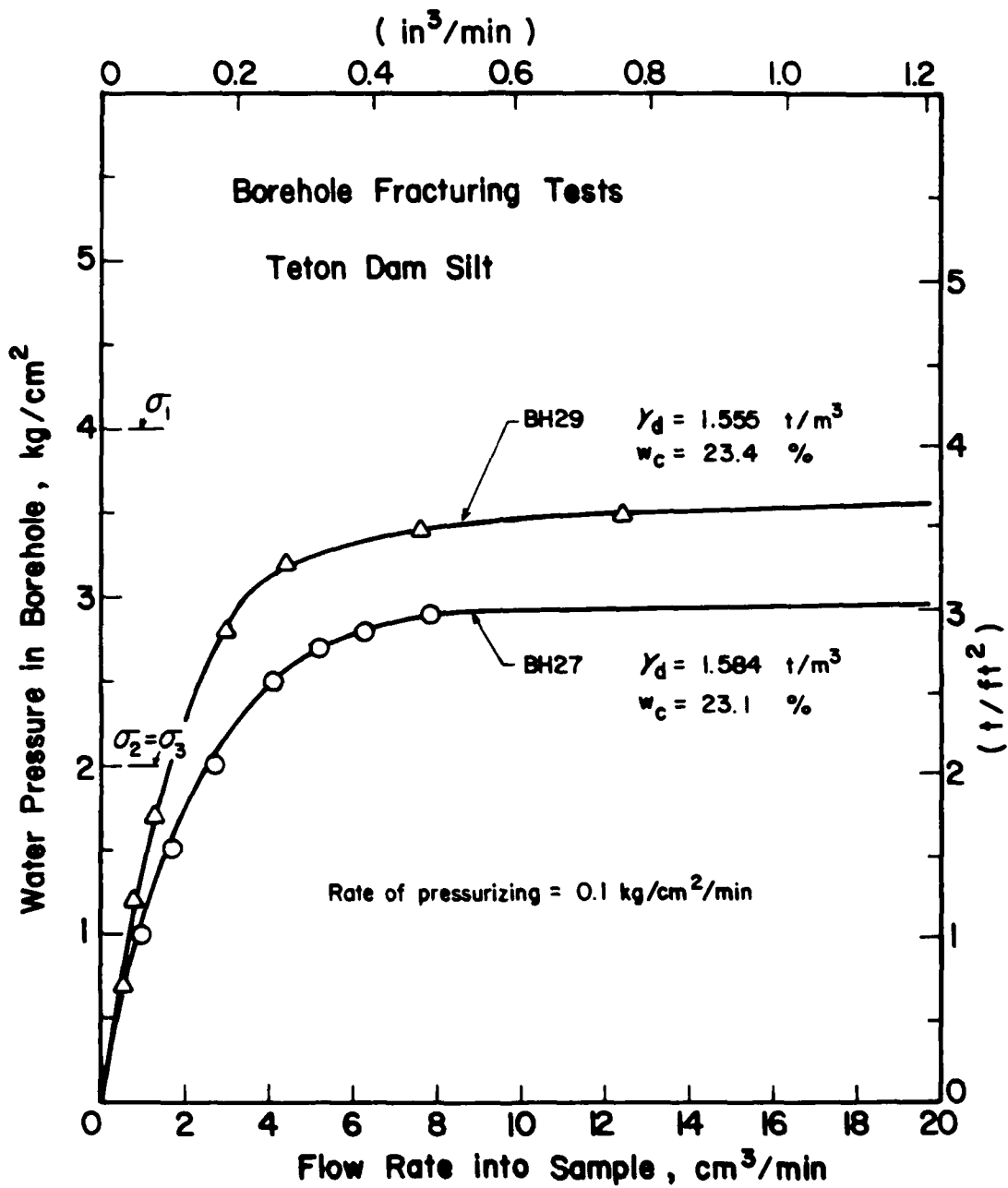


Figure 5.34 Results of borehole fracturing tests BH27 and BH29 on Teton Dam silt

(BH 27) fractured at a lower pressure. Sample BH29 probably had lower tensile strength than Sample BH27 due to its lower density. However, its initial effective stress was higher and its permeability was lower. It is believed that these are the factors that resulted in Sample BH29 fracturing at a higher pressure than Sample BH27.

Similar results are shown in Figure 5.35. Samples GH38 and BH39 had lower densities than Sample BH30, and as a result the compaction pore pressures were lower as shown in Table 5.10. Probably, because Samples BH38 and BH39 had higher effective stresses and lower permeabilities, the fracturing pressures for these tests were higher than for Sample BH30.

Sample BH39, which had lower density than Sample BH38, fractured at a slightly lower pressure. There are two possible reasons for this: (1) the permeability of Sample BH39 was higher as indicated by the higher flow rates, and (2) the tensile strength of Sample BH39 was lower because of its lower density.

#### Pittsburg Silty Clay

The effect of density was studied in Tests BH41, BH43, and BH44, which are summarized in Table 5.11. The water contents of these samples were approximately the same. The borehole diameter was 0.95 cm (3.8 in) and the length was 17.8 cm (7 in).

The results of the tests are shown in Figure 5.36. It can be seen that water did not seep into the sample until pressure was increased to about  $0.3 \text{ kg/cm}^2$  (0.3 tsf). This was because there were positive pore pressures in the samples.

In comparing Tests BH41 to BH43, it may be noted that Sample BH41 had lower pore pressure and higher permeability than Sample BH43. The effect of the higher effective stress probably outweighed the effect of higher permeability, and Sample BH41 fractured at a higher pressure.

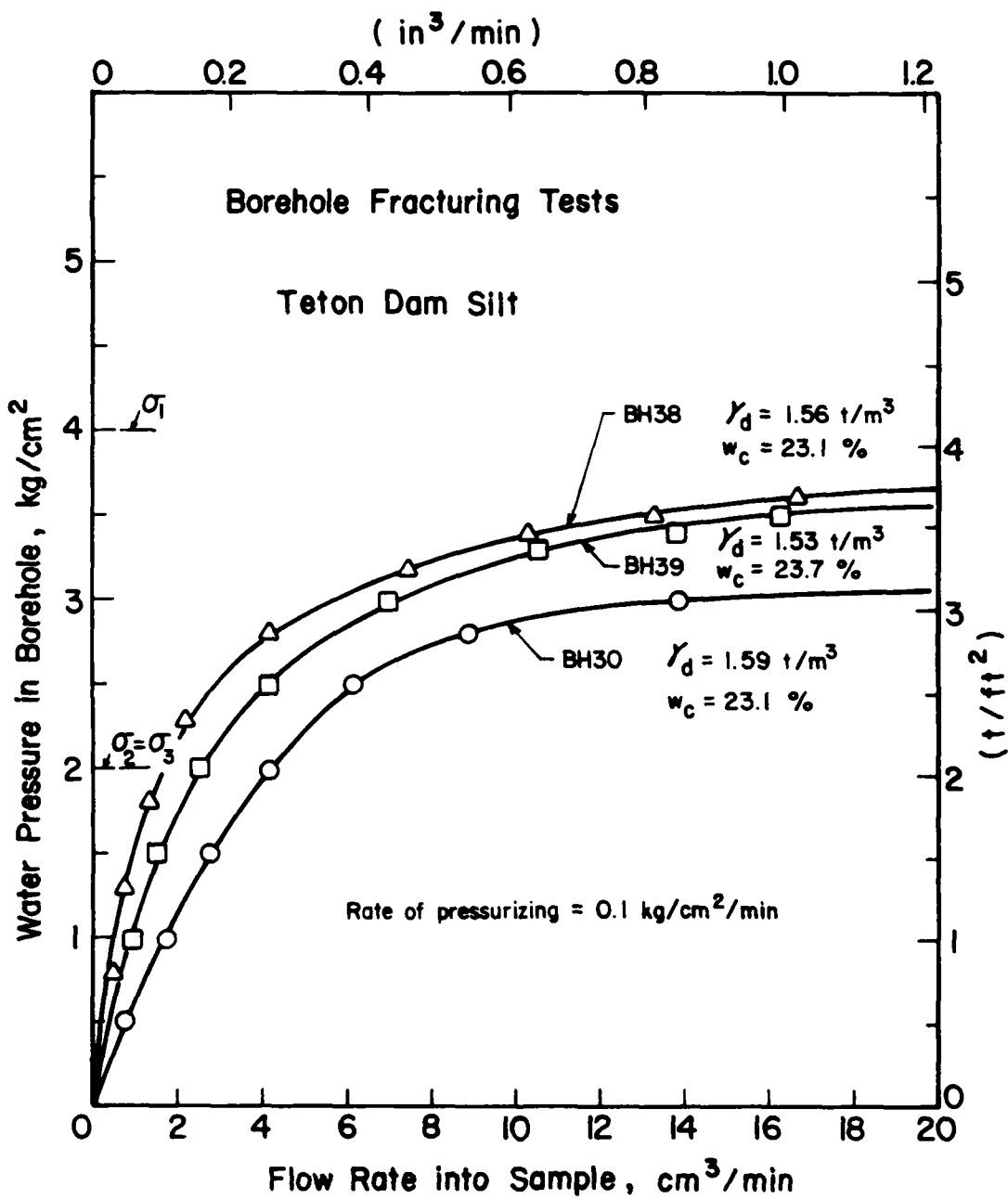


Figure 5.35 Results of borehole fracturing tests BH30, BH38, and BH39 on Teton Dam silt

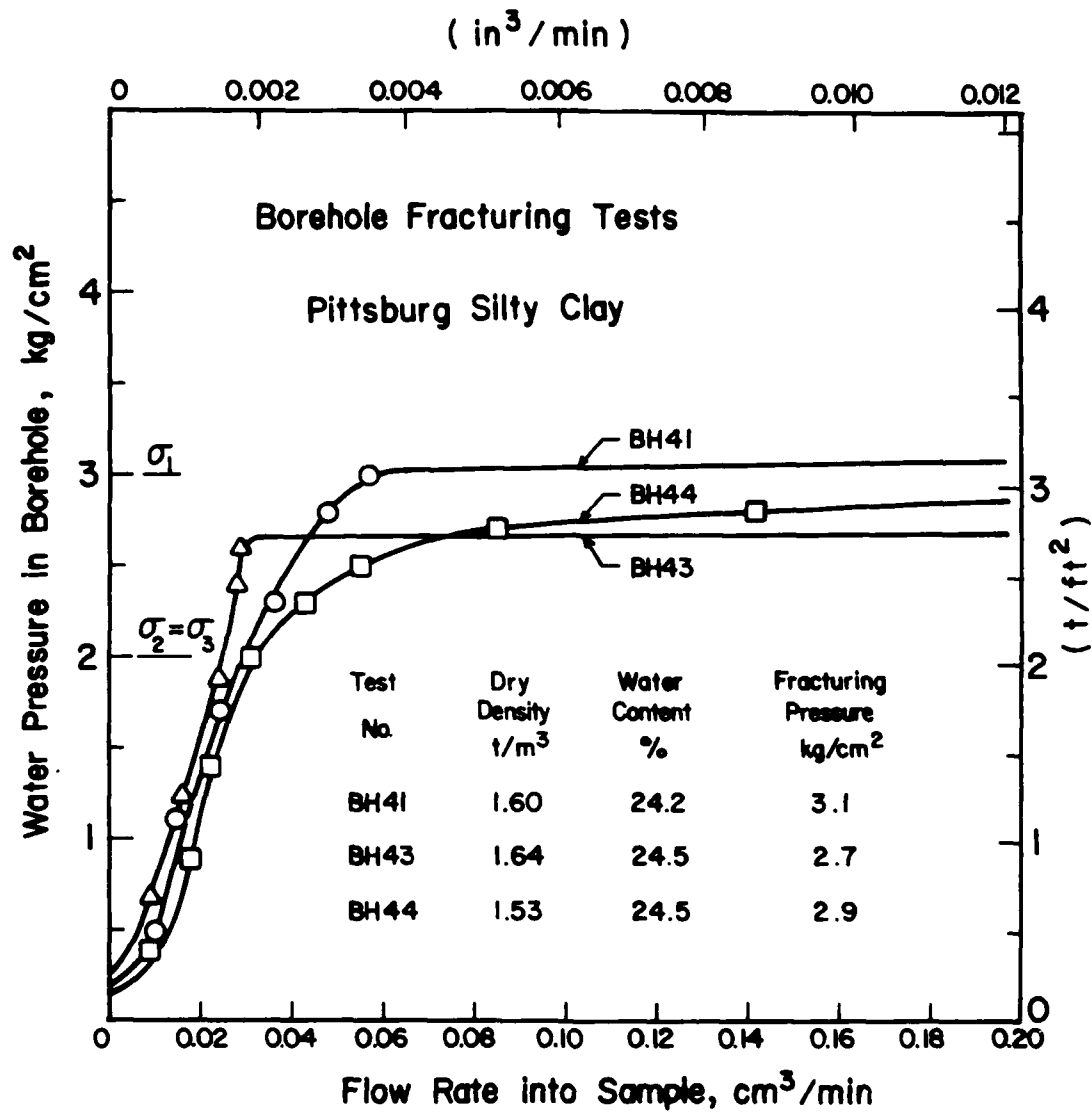


Figure 5.36 Results of borehole fracturing tests BH41, BH43, and BH44 on Pittsburg silty clay

In comparing Test BH41 to BH44, it may be seen that the initial pore pressure in Sample BH41 was higher, the permeability was lower, and the strength was probably higher. The effects of lower permeability and higher strength are believed to be responsible for the higher fracturing pressure in Sample BH41.

Based on these results it may be concluded that a difference in density causes changes in pore pressure, permeability, and tensile strength. A difference in density may increase or decrease the fracturing pressure, depending on how much each of the resulting changes affect the resistance of the soil against hydraulic fracturing.

#### SUMMARY

The results of the hydraulic fracturing tests can be summarized as follows:

(1) Effect of size of discontinuity.

In Type I and Type IV tests the measured fracturing pressure decreased with increasing size of discontinuity. The disagreement with the results of the theory and finite element analyses described in Chapter III is thought to be due to the restraint resulting from the friction that may have developed between the side of the test box and the samples.

In borehole fracturing tests, the fracturing pressure was essentially independent of the borehole diameter for both Teton Dam silt and Pittsburg silty clay.

(2) Hydraulic fracturing at an interface with a transition zone.

The results of Type V tests showed that a geometric discontinuity is not required to induce hydraulic fracturing in soil. Diverging seepage forces can provide the wedging effect required to produce a fracture.

Two types of materials-- fine sand and coarse crushed granite-- were used as transition materials in Type V tests. The type of soil used as transition material had no apparent effect on hydraulic fracturing pressure in Pittsburg silty clay. The fracturing pressure decreased slightly for Teton Dam silt when coarse crushed granite was used as transition material.

(3) Effect of test duration.

A longer test duration led to a somewhat lower hydraulic fracturing pressure in Teton Dam silt. This may be attributed to larger seepage zones in slower tests, resulting in greater wedging and stress change. The fracturing pressure for the tests in Pittsburg silty clay was found to increase in slower tests. This appears to be due to higher effective stresses and increased effects of thixotropy strength gain in tests of longer duration.

(4) Effect of water content.

A decrease in compaction water content in the Teton Dam silt resulted in a decreased permeability, a decreased pore pressure, and an increased tensile strength. As a result, the hydraulic fracturing pressure in the Teton Dam silt increased as the water content decreased.

A decrease in compaction water content in Pittsburg silty clay resulted in increased permeability due to larger intercluster voids formed by aggregations of clay particles. In the fore-hole fracturing tests conducted on samples of Pittsburg silty clay with water contents of about 20%, the flow rates increased abruptly at a pressure much lower than the minor principal stress as the water seeped through the large intercluster pores.

(5) Effect of density.

A change in density may increase or decrease the fracturing pressure, because the change in density is accompanied by changes in pore pressure, permeability, and strength. How a change in density will affect the fracturing pressure depends on how much each of the resulting changes in soil properties affect the resistance of the soil against fracturing.

(6) Direction of fracture plane.

The fracture planes were found to be perpendicular to the direction of minor principal stress in most tests. However, in the type V tests on Pittsburgh silty clay, the orientations of the fracture planes were found to be irregular, and some of them were perpendicular to the direction of the intermediate principal stress.

VI. COMPARISONS OF THEORETICAL WITH EXPERIMENTAL VALUES  
OF HYDRAULIC FRACTURING PRESSURES

In Chapter III, the effects of horizontal stress, borehole diameter, and test duration on hydraulic fracturing pressure were examined using the theory presented in that chapter. The parameters used in the analyses were obtained from tests on Teton Dam silt. In this chapter, the values calculated using the theory are compared with the experimental results.

EFFECT OF HORIZONTAL STRESS

Two series of tests were completed in the laboratory to investigate the effect of horizontal stress. In the first series, the borehole length was 5.1 cm (2 in), while in the second it was 17.8 cm (7 in). In the theory discussed in Chapter III, the sample and the borehole were assumed to be infinitely long. Therefore, the test conditions with long boreholes are closer to the conditions considered in the analyses.

The calculated fracturing pressures are compared with the experimental results in Figure 6.1. It can be seen that the calculated values agree very well with the results of the tests with long boreholes.

EFFECT OF TEST DURATION

Borehole fracturing tests were performed to investigate the effect of test duration on hydraulic fracturing pressure in Teton Dam silt. The borehole length was 5.1 cm (2 in). From the results of the tests to investigate the effect of borehole length, an estimate was made of the

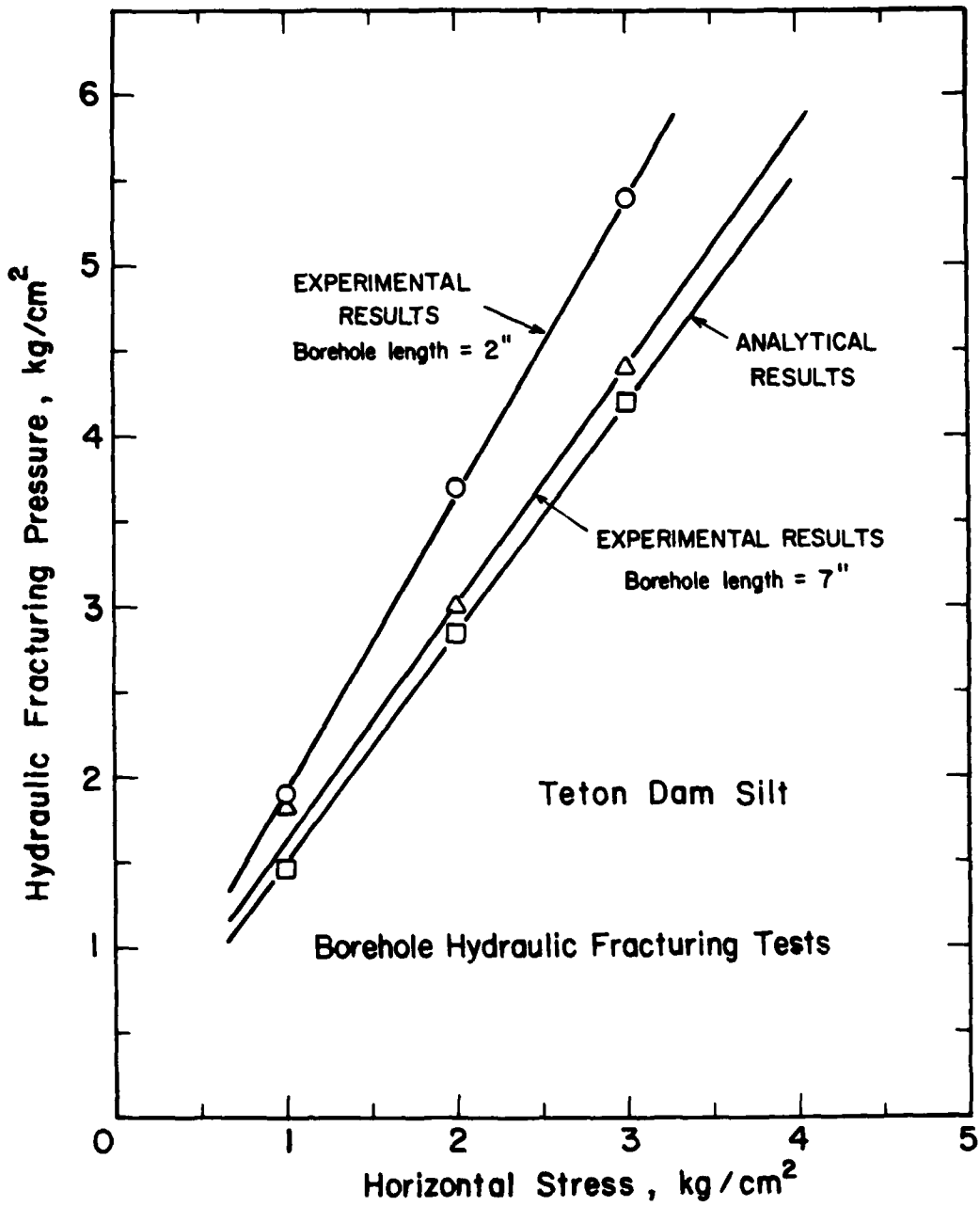


Figure 6.1 Comparison of analytical with experimental results investigating the effect of confining pressure

hydraulic fracturing pressures that would have been measured had the borehole length been the same as the sample length (20.3 cm or 8 in). The analytical results discussed in Chapter III, together with the experimental results and the values estimated for long boreholes, are shown in Figure 6.2. It can be seen from this figure that (1) the calculated hydraulic fracturing pressures are very close to the values estimated for long boreholes, and (2) the calculated and experimental results show no further variation for tests in which the test duration is longer than about 500 minutes.

#### EFFECT OF BOREHOLE DIAMETER

Three tests were completed in the laboratory to investigate the effect of borehole diameter on the hydraulic fracturing pressure in Teton Dam silt. The borehole diameter varied from 0.48 cm (3/16 in) to 1.91 cm (3/4 in). The experimental results are compared with calculated values in Figure 6.3. It can be seen that the theory indicates that borehole diameter should have practically no effect on fracturing pressure, whereas the test results indicate that fracturing pressure decreased slightly with increasing borehole diameter. This slight disagreement is thought to be due to the pore pressures in the sample.

Pore pressures measured in two tests--the ones with the smallest and largest boreholes--are shown in Figure 6.4 for three different borehole water pressures. In the analyses it was assumed that the pore pressures at the outer boundary of the sample were zero. However, in the tests, it can be seen from Figure 6.4 that there were boundary pore pressures, which increased with increasing borehole water pressure and increasing borehole diameter. The boundary pore pressure was increasing because the amount of water that could escape from the box through the cracks at the corners was smaller than the inflow. There would be no boundary

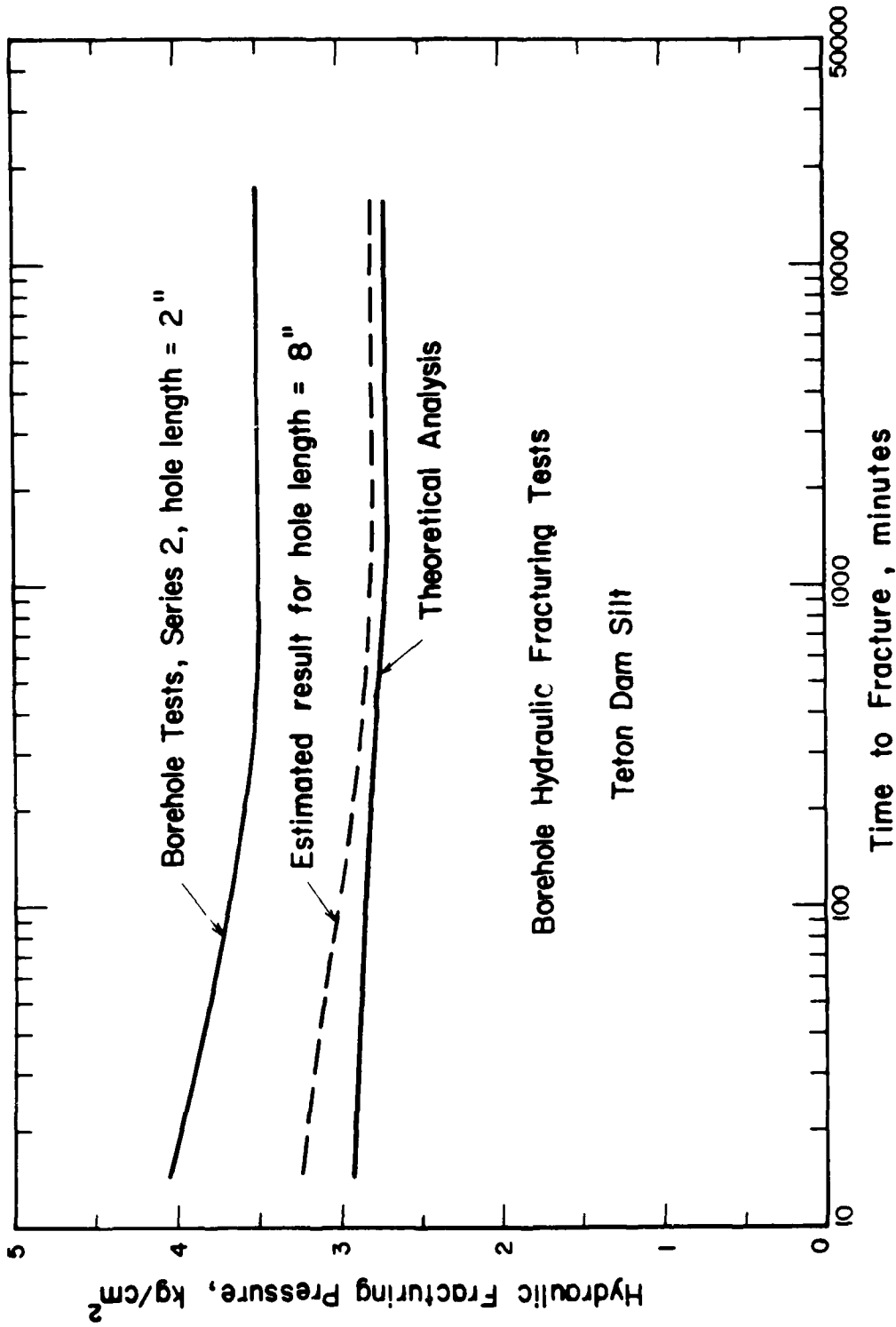


Figure 6.2 Comparison of analytical with experimental results investigating the effect of test duration

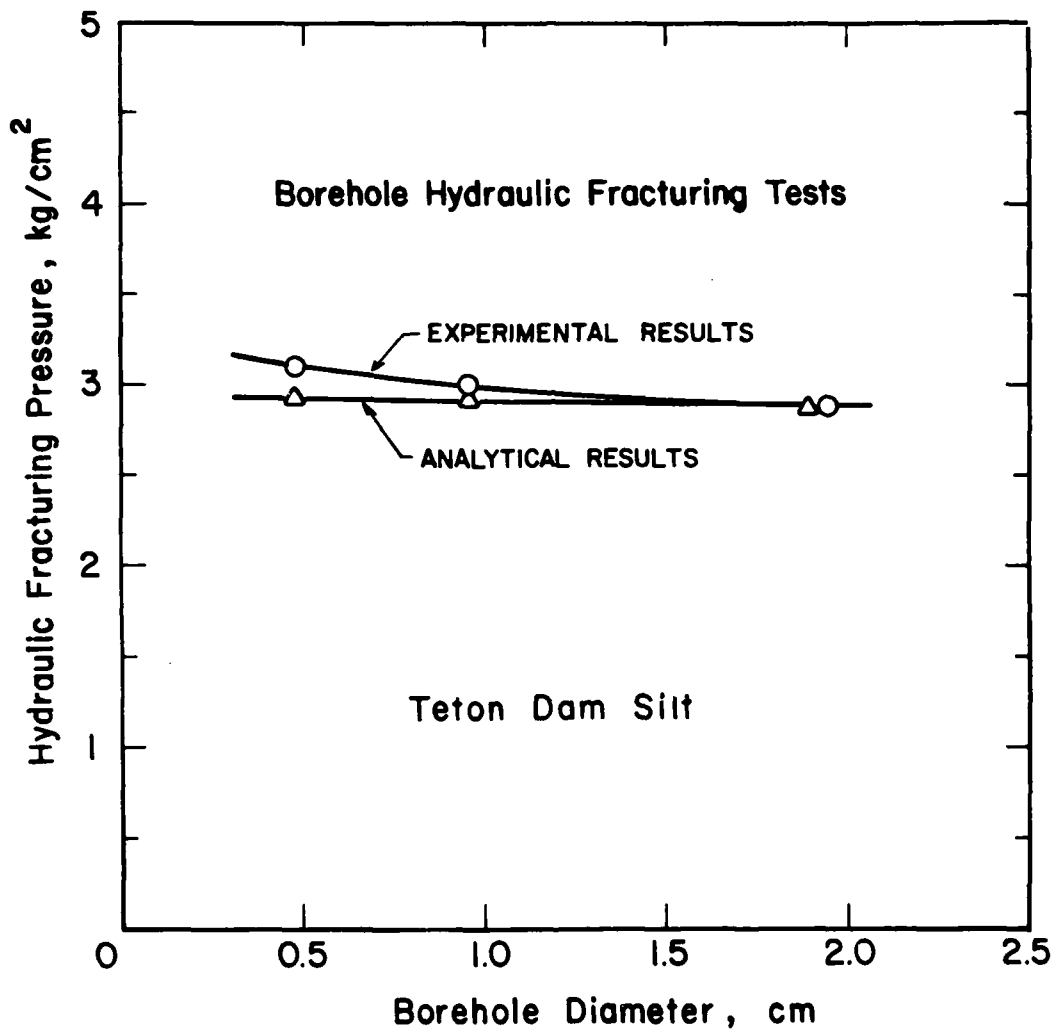


Figure 6.3 Comparison of analytical with experimental results investigating the effect of borehole diameter

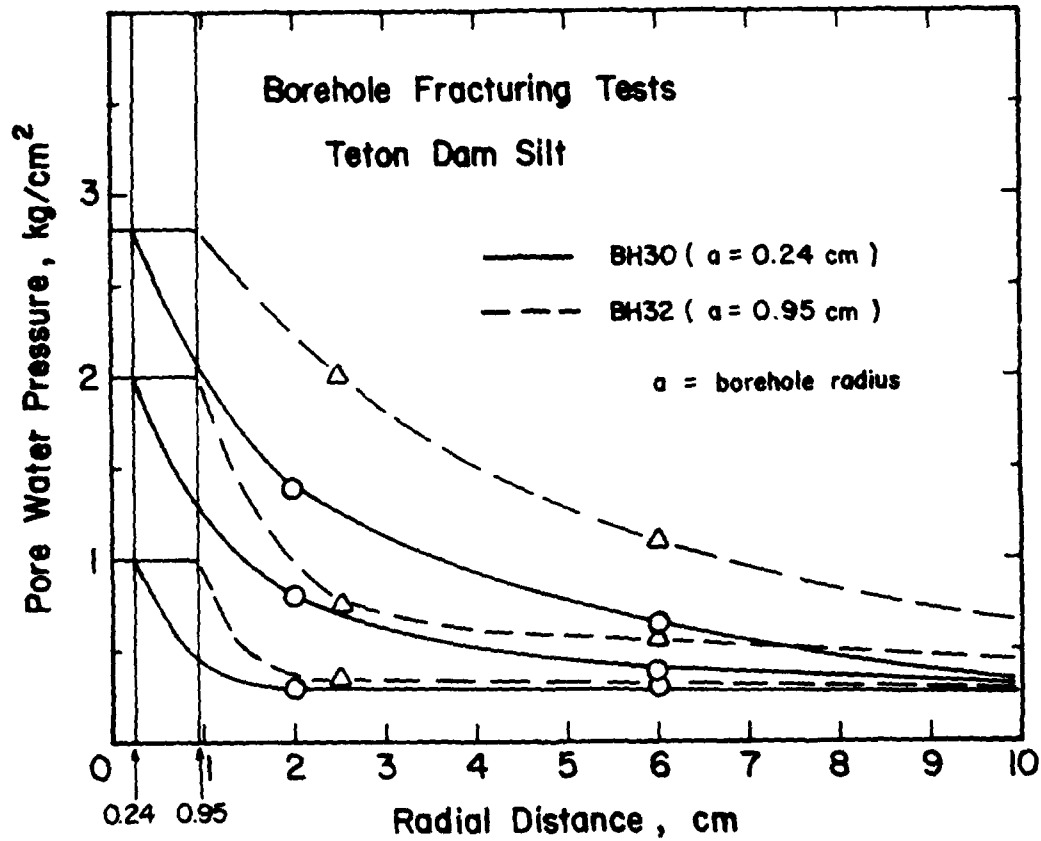


Figure 6.4 Pore water pressures in samples BH30 and BH32 during pressurizing the boreholes

pore pressure if the permeability of the soil was low enough so that the seepage zone did not extend to the boundary of the sample, or if it did, the rate of inflow was lower than the rate that could be drained from the cracks at the corners of the box. To satisfy this condition the sample dimensions would need to be large relative to the borehole diameter, or the permeability of the soil would have to be low. This condition was satisfied in the tests on Pittsburgh silty clay; as a result borehole diameter had no effect on the hydraulic fracturing pressure in Pittsburgh silty clay, as was shown by the test results in Figure 5.31.

Considering the fact that the ratio of the sample dimensions to the groove or slot sizes were small in Type I and Type IV tests, boundary pore pressures may also have developed in these tests on Teton Dam silt, which may have amplified the effect of groove or slot size on the hydraulic fracturing pressure. Unfortunately, pore pressures were not measured in Type I and Type IV tests to verify this.

#### A NOTE ON THE EFFECT OF RATE OF PRESSURIZING

The test results on Teton Dam silt indicated that hydraulic fracturing pressure decreased with increasing test duration. The tests on Pittsburgh silty clay, in which the pore pressures were high and decreased with time, showed that the resistance of this soil against fracturing increased with time. In dams that have developed trouble, e.g. Hyttejuvet Dam and Balderhead Dam, it has been suggested that rapid filling of the reservoir was partly responsible for the trouble.

In the laboratory tests, the water pressures were increased incrementally until the samples fractured. The effect of the rate of pressurizing will be considered in another situation, in which the pressures are kept constant when they reach a certain magnitude which is still below the fracturing pressure under the laboratory condition. This situation

is depicted in Figure 6.5, which shows 2 cases. In Case 1, the pressure is raised at a faster rate  $m_1$ , and then it is kept constant when it reaches the pressure  $p$  in time  $t_1$ . In Case 2, the pressure is raised at a slower rate  $m_2$ , and then it is also kept constant when it reaches the pressure  $p$  in time  $t_2$ . For a time  $t$  greater than  $t_2$ , the seepage zone in Case 1 will be larger than that in Case 2. According to the theory described in Chapter III, the larger the seepage zone, the greater will be the stress change. Therefore, Case 1 (faster rate of pressurizing) is more critical to hydraulic fracturing than Case 2. If, for example, the soil in Case 1 would fracture at time  $t$ , the soil in Case 2 would fracture at a later time.

However, because the time to failure affects the magnitude of the fracturing pressure by a few percent at most, the possible influence of reservoir filling rate on the likelihood of hydraulic fracturing would appear to be negligible for practical purposes. Thus, while there are many reasons that make slow reservoir filling desirable, it does not appear to influence the hydraulic fracturing potential in any significant way.

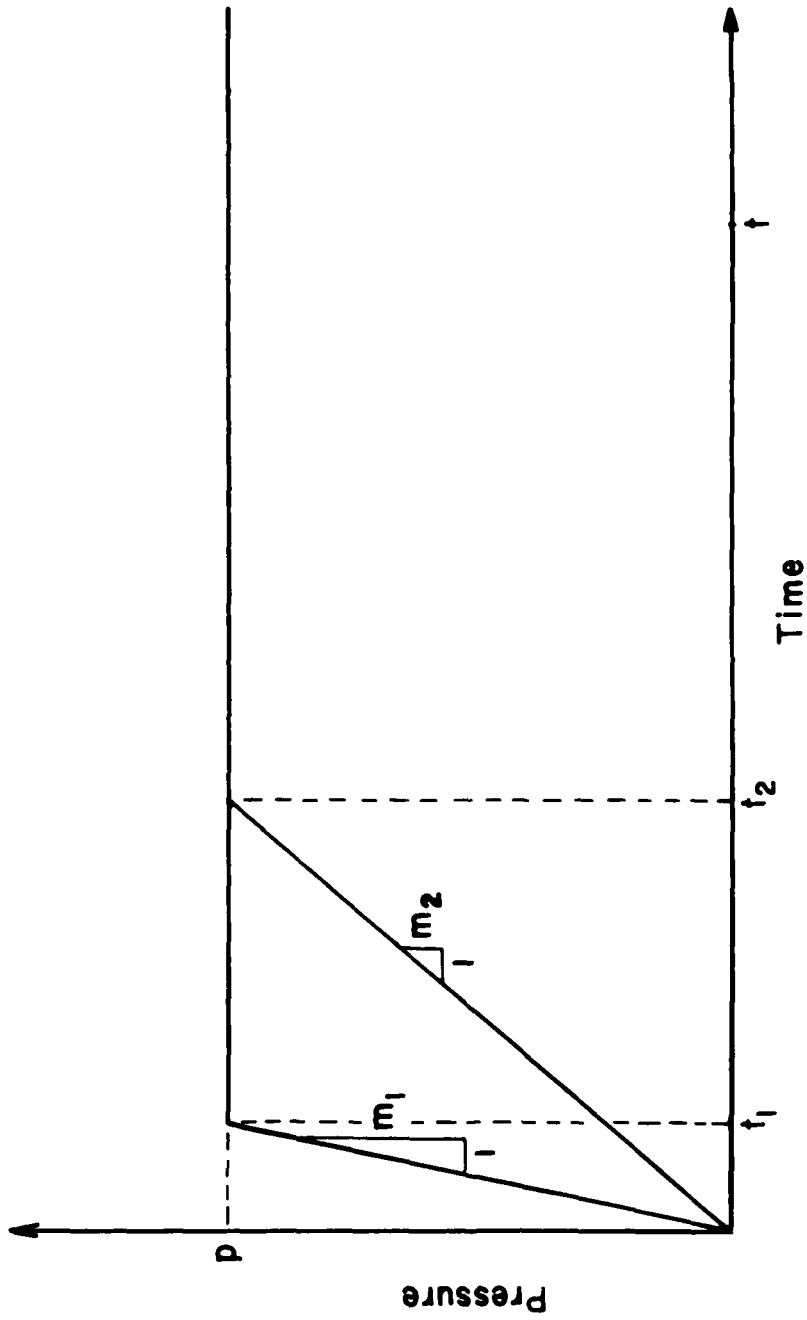


Figure 6.5 Pressure vs time curves

## VII. SUMMARY AND CONCLUSIONS

An extensive experimental study has been conducted to investigate the effects of scale and time on hydraulic fracturing in Teton Dam silt and Pittsburg silty clay. In addition, a new theory has been developed, which is capable of showing how scale, time, and permeability effects are related to the occurrence of hydraulic fracturing, and finite elements analyses have been performed to investigate the possible effects of non-linear soil behavior. Through these studies the factors and conditions which contribute to the occurrence of hydraulic fracturing have been more clearly identified. It now appears possible, therefore, to consider these rationally in the design of embankment dams to minimize the possibility of hydraulic fracturing, and to interpret field data on existing dams rationally, with regard to hydraulic fracturing potential.

The conclusions from this study will be summarized in the following pages.

### PREREQUISITE CONDITIONS FOR HYDRAULIC FRACTURING

The conditions necessary for hydraulic fracturing to occur are:

- (1) The soil must have cohesion and tensile strength. It seems clear that a fracture cannot develop if the soil does not have cohesion and tensile strength. Therefore, cohesionless soils, e.g. clean sands and gravels, cannot undergo hydraulic fracturing.
- (2) Wedging is a necessary condition for hydraulic fracturing. Wedging is an action by the external water pressure or by diverging seepage forces to produce tensile stresses in soil.

Without wedging, no tensile stress can be induced in the soil mass, and fracturing cannot occur. The results of the experimental study showed that wedging and fracturing can occur without a geometric discontinuity in the soil if there are diverging seepage forces in the soil. Figure 7.1 illustrates three cases where wedging can occur as a result of diverging seepage forces.

- (3) The tensile stress on a potential fracture plane must become equal to the soil tensile strength, because hydraulic fracturing involves tensile failure of the soil.

#### THEORETICAL STUDIES

The results of the theoretical studies conducted during this investigation can be summarized as follows:

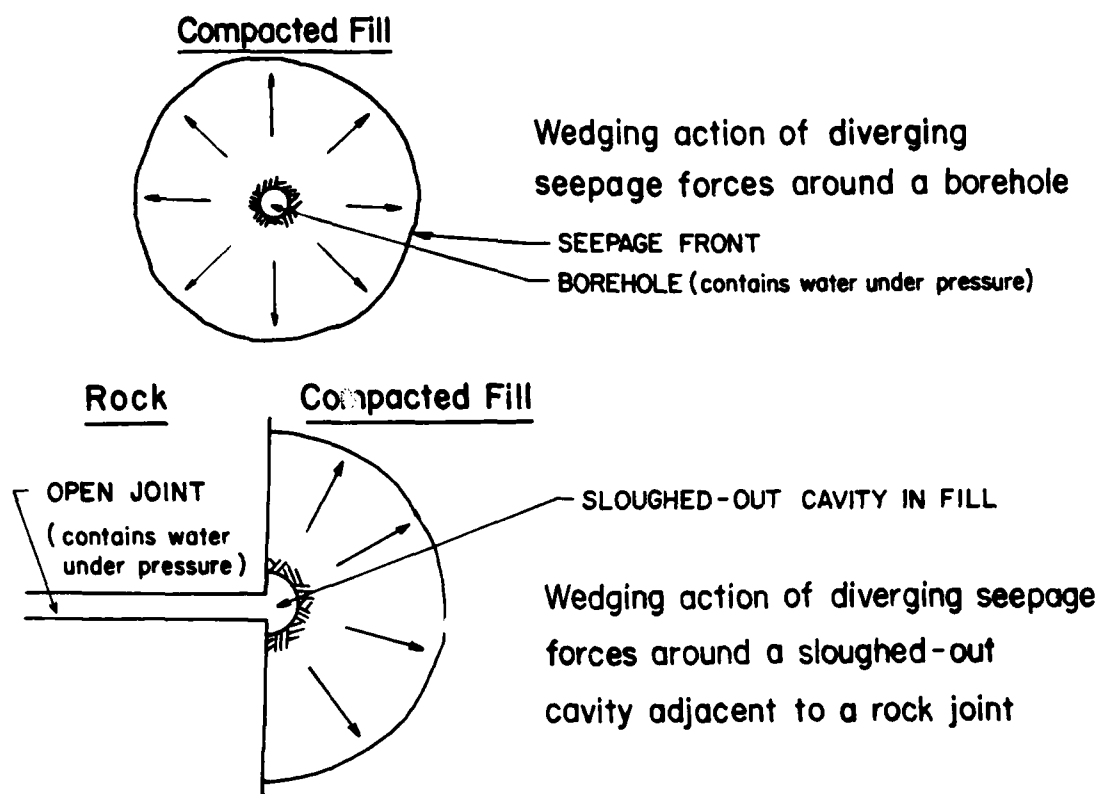
- (1) Other than the value of Poisson's ratio, the only parameter that has a large influence on the value of hydraulic fracturing pressure, calculated using the theory described in Chapter III, is the value of horizontal stress. The excess water pressure required to cause fracturing,  $\Delta u_f$ , can be related to the value of effective horizontal stress,  $\sigma_h'$ , by the following equation:

$$\Delta u_f = C_1 + C_2 \sigma_h' \quad (7.1)$$

where  $C_1$  and  $C_2$  are the intercept and the slope of the line describing the variation of  $\Delta u_f$  with  $\sigma_h'$ , respectively. The values of the coefficients depend on the parameters used in the analyses. The hydraulic fracturing pressure,  $u_f$ , can be expressed by:

$$u_f = C_1 + C_2 \sigma_h' + u_o \quad (7.2)$$

## Geometric Discontinuity in Soil



## Physical Discontinuity in Soil Due to Differential Permeabilities

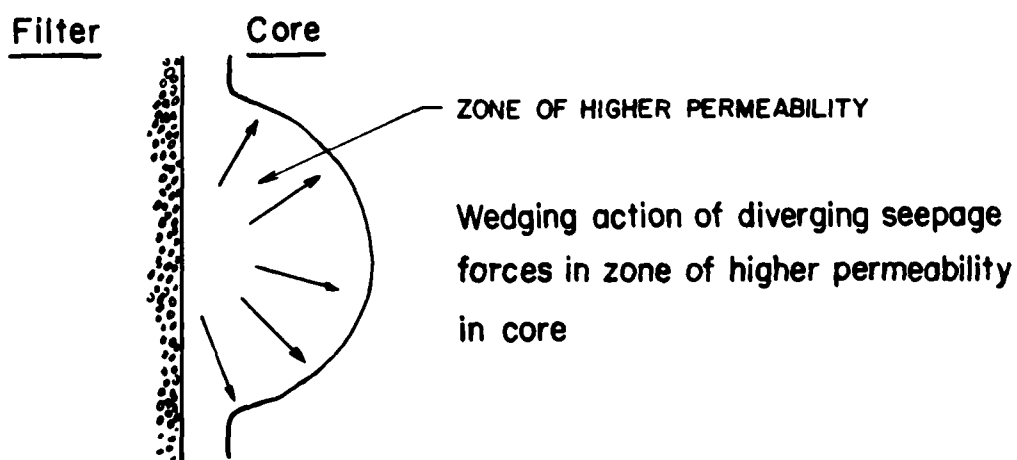


Figure 7.1 Illustrations of wedging action of diverging seepage forces

where  $u_0$  is the initial pore pressure in the soil.

The analysis shown in Figure 3.8 was performed with the values of the parameters obtained from the tests on Teton Dam silt.

The values of the coefficients  $C_1$  and  $C_2$  for this analysis were found to be  $0.1 \text{ kg/cm}^2$  and 1.4, respectively. Equation 7.1 for tests on Teton Dam silt thus becomes:

$$\Delta u_f = 0.1 \text{ kg/cm}^2 + 1.4 \sigma_h' \quad (7.3)$$

This analysis was performed with a value of Poisson's ratio of 0.3. The coefficient  $C_2$  in Equation 7.1 was found to be dependent on the value of Poisson's ratio used in the analysis. If values of Poisson's ratio of 0.4 and 0.2 were used in the analysis, the values of the coefficient  $C_2$  would be 1.2 and 1.6, respectively. The values of fracturing pressures measured in the tests were compared with the analytical results in Figure 6.1, which showed that the analytical results computed using a value of Poisson's ratio of 0.3, agree very well with the experimental results. Thus it appears that a value of 1.4 is reasonable for the coefficient  $C_2$  for Teton Dam silt.

- (2) Borehole diameter, time increment, permeability, and tensile strength all have very little influence on the calculated values of hydraulic fracturing pressure. The calculated pressure is practically independent of borehole diameter, increases slightly with increasing tensile strength of the soil, and decreases slightly with increasing time increment and permeability. With regard to the effect of permeability, however, it should be noted that the most permeable soils, such as sands, gravels, and cohesionless silts cannot be fractured. When the effective stress on some plane in such soils is reduced

to the minimum active earth pressure condition, these soils deform plastically, and no fracture occurs.

#### EXPERIMENTAL STUDY

The conclusions drawn from the results of experimental study conducted during this investigation can be summarized as follows:

- (1) The experimental results confirm the indications of the theoretical analyses that the only parameter that has a large effect on hydraulic fracturing pressure is the minor principal stress.

The results of borehole fracturing tests on Teton Dam silt and Pittsburg silty clay specimens, in which the pore pressures were measured, are shown in Figure 7.2. There is some scatter in the results because of the variations in compaction water content, density, borehole length, and borehole diameter in the tests. The calculated values of hydraulic fracturing pressure, using the values of parameters from tests on Teton Dam silt, are also shown in Figure 7.2. It can be seen that the calculated values provide lower bound fracturing pressures for both Teton Dam silt and Pittsburg silty clay. This shows that the hydraulic fracturing pressures are affected very little by the soil strength characteristics. Therefore, Equation 7.3, or the simpler equation:

$$\Delta u_f = 1.4 \sigma_3' \quad (7.4)$$

can be used as a criterion with regard to hydraulic fracturing potential for compacted clays of low plasticity, if the minor principal effective stress,  $\sigma_3'$ , is known.

- (2) The experimental results showed that borehole diameter and test

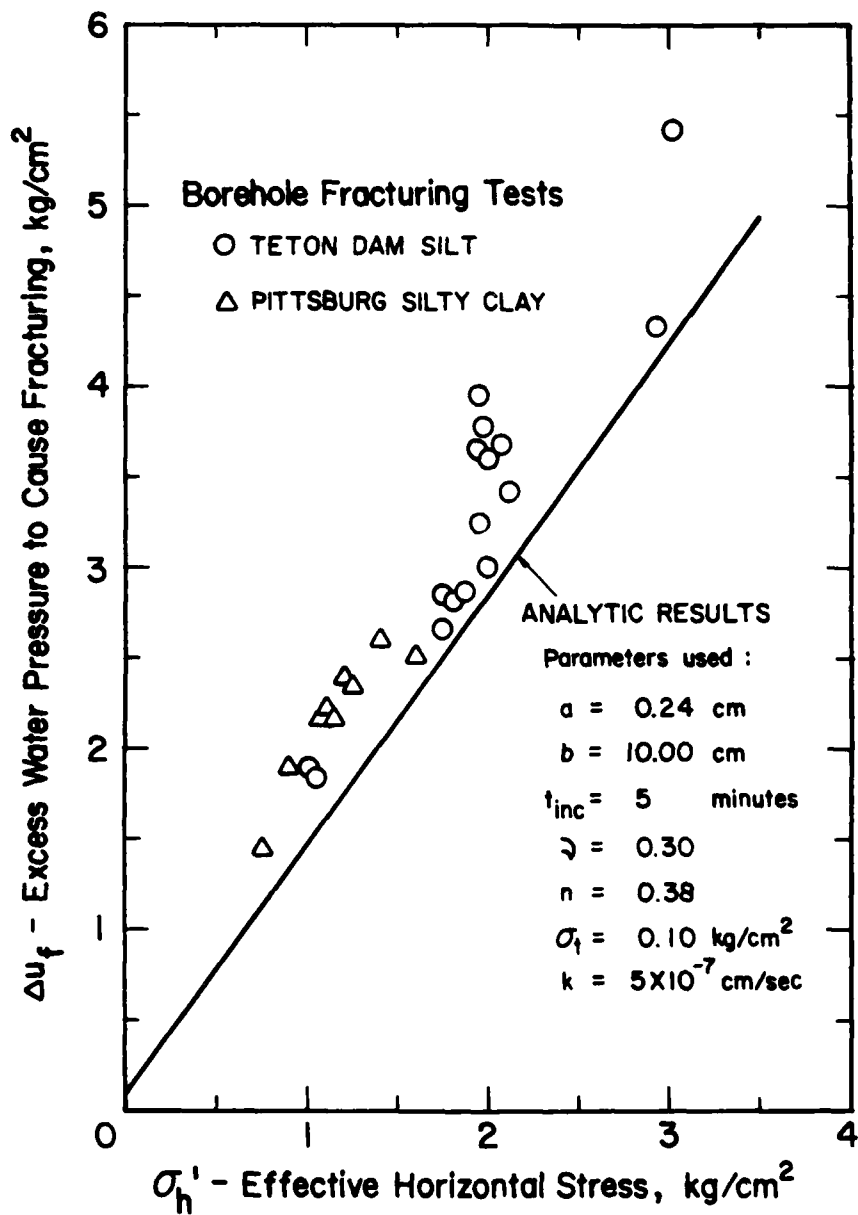


Figure 7.2 Comparison of analytical with experimental results of borehole fracturing tests

duration had small effects on hydraulic fracturing pressure. An increase in borehole diameter by a factor of 2 resulted in a reduction in fracturing pressure of about 3% in Teton Dam silt samples. Borehole diameter did not have any effect on fracturing pressure in Pittsburg silty clay. An increase in test duration by a factor of 10 resulted in a reduction in fracturing pressure of about 7% in Teton Dam silt and an increased fracturing pressure of about 4% in Pittsburg silty clay.

- (3) Changes in compaction water content and density resulted in changes in the values of several parameters that influence the fracturing pressure, i.e. initial pore pressure, permeability, and strength. Therefore, the effects of changes in compaction water content and density depend on how much the values of these parameters are altered.
- (4) It appears that the fracturing pressures measured in Type I and Type IV tests were affected by the restraint due to wall friction in the test apparatus. Had this friction been eliminated, it is believed that the size of groove or slot in these tests would have had negligible effect on the measured fracturing pressure.

#### REFERENCES

- Bjerrum, L. (1953), "Stability and Deformation of Slopes, Earth Dams, and Groundwater Problems," General Report, Proceedings of Third International Conference on Soil Mechanics and Foundation Engineering, Zurich, Vol. 2, pp. 362-371.
- Bjerrum, L. and Andersen, K. H. (1972), "In-Situ Measurement of Lateral Pressures in Clay," Proceedings of the Fifth European Conference on Soil Mechanics and Foundation Engineering, Madrid, Vol. I, pp. 11-20.
- Bjerrum, L., Nash, J. K. T. L., Kennard, R. M., and Gibson, R. E. (1972), "Hydraulic Fracturing in Field Permeability Testing," Geotechnique, Vol. 22, No. 2, London, pp. 1-12.
- Bozozuk, M. (1974), "Minor Principal Stress Measurements in Marine Clay with Hydraulic Fracturing Tests," Proceedings ASCE Specialty Conference on Subsurface Exploration for Underground Excavation and Heavy Construction, Henniker, pp. 333-349.
- Casagrande, A. (1950), "Notes on Design of Earth Dams," Journal of Boston Society of Civil Engineers, Vol. 37, pp. 405-429
- Charles, J. A. (1977), Discussion on "Load Transfer and Hydraulic Fracturing in Zoned Dams," Journal of Geotechnical Engineering Division, ASCE, Vol. 103, No. GT 6, pp. 663-665.
- Clark, J. B. (1949), "A Hydraulic Process for Increasing the Productivity of Wells," Transactions of American Institute of Mining Engineers, Vol. 186, pp. 1-8.
- De Mello, V. F. B. (1977), "Reflections on Design Decisions of Practical Significance to Embankment Dams," Geotechnique, Vol. 27, No. 3, pp. 281-355.
- D'Orazio, T. B. and Duncan, J. M. (1982), "CONSAX: A Computer Program for Axisymmetric Finite Element Analysis of Consolidation," Geotechnical Engineering Report No. UCB/GT/82-01, University of California, Berkeley.
- Haimson, B. (1968), "Hydraulic Fracturing in Porous and Non-Porous Rock and Its Potential for Determining In-Situ Stresses at Great Depth," Technical Report No. 4-68, U. S. Army Corps of Engineers, Missouri River Division, Omaha, Nebraska.
- Hubbert, M. K. and Willis, D. G. (1957), "Mechanics of Hydraulic Fracturing," Transactions of American Institute of Mining Engineers, Vol. 210, pp. 153-168.

AD-A144 639

SCALE AND TIME EFFECTS IN HYDRAULIC FRACTURING(U)  
CALIFORNIA UNIV BERKELEY DEPT OF CIVIL ENGINEERING  
H WIDJAJA ET AL. JUL 84 DACW39-81-C-0024

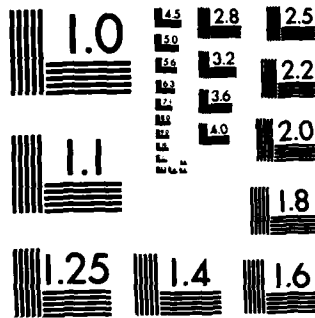
3/3

UNCLASSIFIED

F/G 20/11

NL

END



MICROCOPY RESOLUTION TEST CHART  
NATIONAL BUREAU OF STANDARDS-1963-A

Hvorslev, M. J. (1949), "Time Lag in the Observation of Ground-Water Levels and Pressures," U. S. Army Waterways Experiment Station, Vicksburg, Mississippi.

Independent Panel to Review Cause of Teton Dam Failure (1976), "Report to U. S. Department of the Interior and the State of Idaho on Failure of Teton Dam," Superintendent of Documents, U. S. Government Printing Office, Washington, D. C. 20402.

Jaworski, G. W., Duncan, J. M., and Seed, H. B. (1979), "An Experimental Study of Hydraulic Fracturing," Geotechnical Engineering Report No. UCB/GT/79-02, University of California, Berkeley.

Jaworski, G. W., Duncan, J. M., and Seed H. B. (1981), "Laboratory Study of Hydraulic Fracturing," Journal of the Geotechnical Engineering Division, ASCE, Vol. 107, No. GT6, pp. 713-732.

Kennard, R. M. (1970), "The Measurement of Soil Permeability In Situ by the Constant Head Test," Ph.D. thesis, University of London.

Kjaernsli, B. and Torblaa, I. (1968), "Leakage through Horizontal Cracks in the Core of Hyttejuvet Dam," Norwegian Geotechnical Institute Publication No. 80, Oslo, Norway.

Kulhawy, F. H. and Gurtowski, T. M. (1976), "Load Transfer and Hydraulic Fracturing in Zoned Dams," Journal of Geotechnical Engineering Division, ASCE, GT 9, pp. 963-974.

Lefebvre, G., Philibert, A., Bozozuk, M. and Pare, J-J. (1981), "Fissuring from Hydraulic Fracture of Clay Soil," Proceedings of the Tenth International Conference on Soil Mechanics and Foundation Engineering, Stockholm, pp. 513-518.

Leonards, G. A. and Narain, J. (1963), "Flexibility of Clay and Cracking of Earth Dams," Journal of Soil Mechanics and Foundations Division, ASCE, No. SM 2, pp. 47-98.

Löfquist, B. (1951), "Earth Pressure in a Thin Impervious Core," Transactions of Fourth International Congress on Large Dams, New Delhi, Vol. 1, pp. 99-109.

Löfquist, B. (1957), Discussion on Cracking in Earth Dams, Proceedings of Fourth International Conference on Soil Mechanics and Foundation Engineering, London, Vol. 3, pp. 261-262.

Lowe, J. (1970), "Recent Development in the Design and Construction of Earth and Rockfill Dams," Tenth International Congress on Large Dams, Montreal, Vol. 3, pp. 1-28.

Massarch, K. R., Hotz, R. D., Holm, B. G. and Fredricksson, A. (1975), "Measurement of Horizontal In Situ Stresses," Proceedings of ASCE Specialty Conference on In Situ Measurement of Soil Properties, Raleigh, North Carolina, Vol. 1, pp. 266-286.

Massarch, K. R. and Broms, B. (1976), "Lateral Earth Pressure at Rest in Soft Clay," Journal of Geotechnical Engineering Division, ASCE, GT10, pp. 1041-1047.

Massarch, K. R. (1978), "New Aspects of Soil Fracturing in Clay," Journal of Geotechnical Engineering Division, ASCE, Vol. 104, No. GT8, pp. 1109-1123.

Middlebrooks, T. A. (1952), "Progress in Earth Dam Design and Construction in the United States," Civil Engineering, Vol. 22, No. 9, pp. 702-710.

Mitchell, J. K. (1960), "Fundamental Aspects of Thixotropy in Soils," Journal of the Soil Mechanics and Foundations Division, ASCE, Vol. 86, No. SM3, pp. 19-52.

Mitchell, J. K., Hooper, D. R., and Campanella, R. G. (1965), "Permeability of Compacted Clay," Journal of the Soil Mechanics and Foundations Division, ASCE, Vol. 91, No. SM4, July, pp. 41-65.

Morgenstern, N. R. and Vaughan, P. R. (1963), "Some Observations on Allowable Grout Pressures," Proceedings of Conference on Grouts and Drilling Muds, Institution of Civil Engineers, London.

Nobari, E. S., Lee, K. L. and Duncan, J. M. (1973), "Hydraulic Fracturing in Zoned Earth and Rockfill Dams," Institute of Transportation and Traffic Engineering Report No. TE-73-1, University of California, Berkeley.

Olsen, H. W. (1962), "Hydraulic Flow through Saturated Clays," Proceedings of the Ninth National Conference on Clays and Clay Minerals, pp. 131-161.

Patric, J. G. (1967), "Post-Construction Behavior of Round Butte Dam," Journal of Soil Mechanics and Foundations Division, ASCE, No. SM4, July, pp. 251-263.

Seed, H. B., Leps, T. M., Duncan, J. M. and Bieber, R. E. (1976), "Hydraulic Fracturing and Its Possible Role in the Teton Dam Failure," Appendix D to Report of Independent Panel to Review Cause of Teton Dam Failure, Superintendent of Documents, U. S. Government Printing Office, Washington, D. C. 20402.

Sherard, J. L. (1953), "Influence of Soil Properties and Construction Methods on the Performance of Homogeneous Earth Dams," Technical Memorandum 645, U. S. Bureau of Reclamation, Denver, Colorado.

Sherard, J. L., Decker, R. S., and Ryker, N. L. (1972), "Hydraulic Fracturing in Low Dams of Dispersive Clay," Proceedings of ASCE Specialty Conference on Performance of Earth and Earth Supported Structures, Purdue University, W. Lafayette, Indiana, Vol. 1, pp. 653-689.

Sherard, J. L. (1973), "Embankment Dam Cracking," Embankment Dam Engineering-The Casagrande Volume, John Wiley and Sons, New York.

Timoshenko, S. and Goodier, J. N. (1935), "Theory of Elasticity," McGraw-Hill, New York.

Trollope, D. H. (1957), "The Systematic Arching Theory Applied to the Stability Analysis of Embankments," Proceedings of Fourth International Conference on Soil Mechanics and Foundation Engineering, London, Vol. 2, pp. 382-388.

Vaughan, P. R., Kluth, D. J., Leonard, M. W. and Pradoura, H. H. M. (1970), "Cracking and Erosion of the Rolled Clay Core of Balderhead Dam and the Remedial Works Adopted for Its Repair," Proceedings of the Tenth International Congress on Large Dams, Montreal, Canada, Vol. 3, pp. 73-93.

Vestad, H. (1976), "Viddalsvatn Dam, A History of Leakages and Investigations," Proceedings of Twelfth International Congress on Large Dams, Mexico, Vol. 2, pp. 369-390.

Von Schonfeldt, H. (1970), "An Experimental Study of Open-Hole Hydraulic Fracturing as a Stress Measurement Method with Particular Emphasis on Field Tests," Technical Report MRD 3-70, U. S. Army Corps of Engineers, Missouri River Division, Omaha, Nebraska.

Wilson, S. D. and Squier, L. R. (1969), "Earth and Rockfill Dams," State of the Art Volume, Seventh International Conference on Soil Mechanics and Foundation Engineering, Mexico City, Mexico, pp. 137-223.

## APPENDIX A. DERIVATIONS OF EQUATIONS

The purpose of this appendix is to provide a detailed explanation of the considerations and assumptions on which the theory developed during the course of this investigation are based. Toward this end, the derivations of Equations 3.19 through 3.24 are described in the following sections.

### Derivations of Equation 3.18

This equation defines the radius of the zone of seepage around the borehole.

Water from a borehole seeps radially as the water pressure in the borehole is increased. At time  $t$ , assume that the pressure head is  $h$  and the seepage radius is  $r_s$ , as shown in Figure A.1.

The flow rate,  $q$ , can be calculated using Darcy's Law as follows:

$$q = k i A \quad (A.1)$$

where

$k$  is the soil permeability, cm/sec

$i$  is the hydraulic gradient, dimensionless

$A$  is the area of flow,  $\text{cm}^2$

For a cylinder of unit thickness, the above equation can be written as

$$q = k \left( - \frac{dh}{dr} \right) 2 \pi r \quad (A.2)$$

rearranging,

$$\frac{q}{2\pi k} \frac{dr}{r} = - dh \quad (A.3)$$

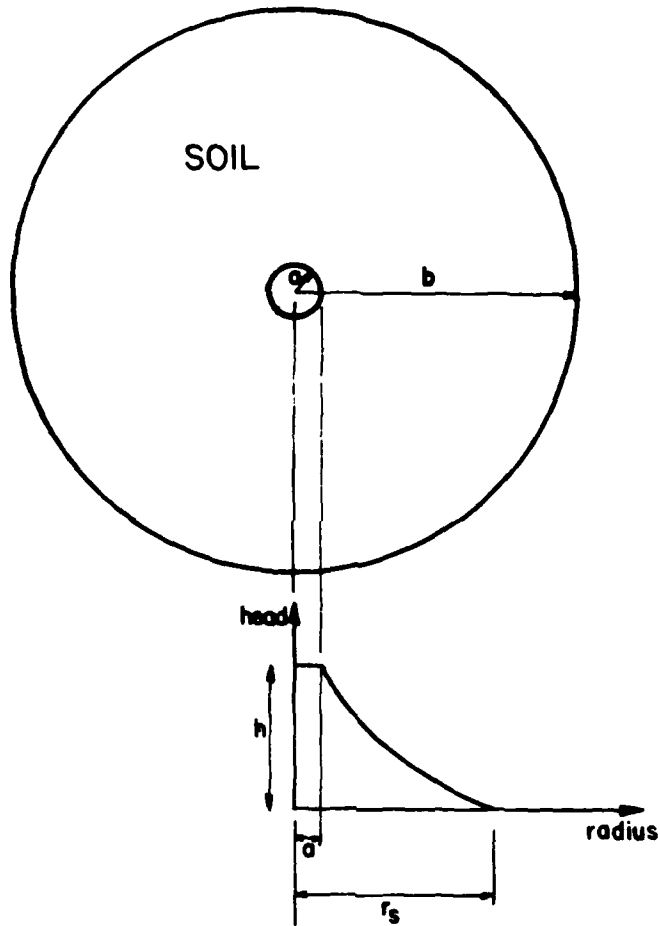


Figure A.1 Pore pressure profile in sample at time T

integrating,

$$\frac{q}{2\pi k} \ln r = -h + C \quad (\text{A.4})$$

where C is a constant to be determined from the boundary conditions,

which are,

$$\text{head} = h \text{ at } r = a \quad (\text{A.5})$$

$$\text{head} = 0 \text{ at } r = r_s \quad (\text{A.6})$$

Substituting these boundary conditions into Equation A.4, the following equation is obtained:

$$q = \frac{2 \pi k h}{\ln(r_s/a)} \quad (\text{A.7})$$

The discharge velocity of the flow,  $v_d$ , is

$$v_d = q/A \quad (\text{A.8})$$

Substituting Equation A.7 into A.8, and substituting  $A = 2 \pi r_s$ ,

$$v_d = \frac{k h}{r_s \ln(r_s/a)} \quad (\text{A.9})$$

The seepage velocity,  $v_s$ , is,

$$v_s = v_d/n \quad (\text{A.10})$$

where n is the porosity of the soil. Substituting Equation A.9 into A.10,

$$v_s = \frac{k h}{n r_s \ln(r_s/a)} \quad (\text{A.11})$$

In time dt, the seepage front advances to a distance  $dr_s$ , where

$$dr_s = v_s dt \quad (\text{A.12})$$

Assuming that the rate of pressurizing is denoted by m, as shown in Figure A.2, the head, h, is related to the previous head,  $h_0$ , by the following equation:

$$h = h_0 + m (t-t_0) \quad (\text{A.13})$$

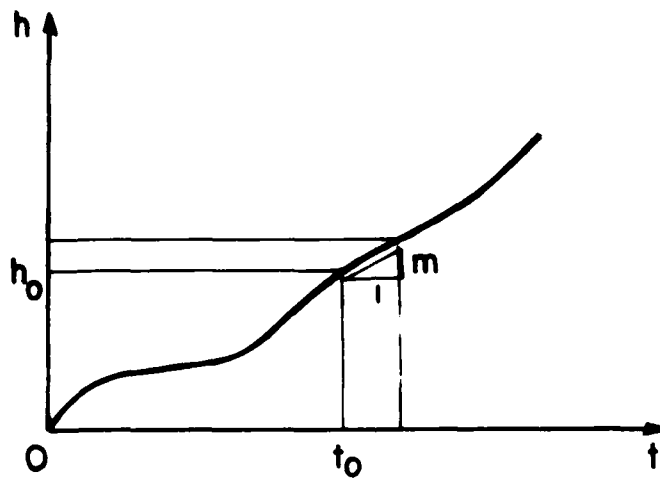


Figure A.2 Pressure head vs time curve

where  $(t-t_0)$  is the elapsed time. Substituting Equations A.12 and A.13 into A.11,

$$dr_s = \frac{k \{h_0 + m (t-t_0)\}}{n r_s \ln(r_s/a)} dt \quad (A.14)$$

rearranging,

$$(r_s \ln r_s - r_s \ln a) dr_s = \frac{k}{n} \{h_0 + m (t-t_0)\} dt \quad (A.15)$$

integrating,

$$\left(\frac{r_s^2}{2} \ln r_s - \frac{r_s^2}{4} - \frac{r_s^2}{2} \ln a\right) = \frac{k}{n} (h_0 t + m \frac{t^2}{2} - m t_0 t) + C \quad (A.16)$$

where C is a constant to be determined from the boundary conditions.

Rearranging Equation A.16,

$$r_s^2 \left\{ \ln(r_s/a) - \frac{1}{2} \right\} = \frac{2k}{n} (h_0 t + m \frac{t^2}{2} - m t_0 t) + C \quad (A.17)$$

The boundary condition is:

$$r_s = r_{s0} \text{ at } t = t_0 \quad (A.18)$$

Substituting the boundary condition into Equation A.17 gives

$$C = r_{s0}^2 \left\{ \ln(r_{s0}/a) - \frac{1}{2} \right\} - \frac{2k}{n} (h_0 t_0 - m t_0^2/2) \quad (A.19)$$

Substituting Equation A.19 into A.17 gives

$$r_s^2 \left\{ \ln(r_s/a) - \frac{1}{2} \right\} - r_{s0}^2 \left\{ \ln(r_{s0}/a) - \frac{1}{2} \right\} - \frac{k}{n} \{2h_0(t-t_0) + m(t-t_0)^2\} = 0 \quad (A.20)$$

#### Derivations of Equations 3.19 and 3.20

These equations define the change of tangential stress in Cylinder 1 and the displacement at the outer boundary of the same cylinder due to seepage forces.

The flow rate of water from the pressurized borehole is given by

Darcy's Law according to Equations A.1 and A.4. Assuming that at time  $t_0$  the pressure head in the borehole is  $h_0$ , the boundary conditions for Equation A.4 are:

$$\text{head} = 0 \quad \text{at } r = r_s \quad (\text{A.21})$$

$$\text{head} = h_0 \quad \text{at } r = a \quad (\text{A.22})$$

The boundary conditions, together with Equation A.4, gives

$$h(r) = h_0 \left\{ 1 - \frac{\ln(r/a)}{\ln(r_s/a)} \right\} \quad (\text{A.23})$$

where  $h(r)$  is the pressure head at radius  $r$ . In terms of the borehole water pressure in excess of initial pressure,  $\Delta u$ , Equation A.23 can be written as

$$u(r) = \Delta u \left\{ 1 - \frac{\ln(r/a)}{\ln(r_s/a)} \right\} \quad (\text{A.24})$$

where  $u(r)$  is the excess pore pressure at radius  $r$ .

The equation of equilibrium in axially symmetrical plane polar co-ordinates is:

$$\frac{d\sigma_r}{dr} + \frac{\sigma_r - \sigma_\theta}{r} = 0 \quad (\text{A.25})$$

where  $\sigma_r$  and  $\sigma_\theta$  are the radial and tangential stresses, respectively.

Equation A.25 can be written in terms of effective stresses using Equation A.24:

$$\frac{d\sigma_r'}{dr} + \frac{\sigma_r' - \sigma_\theta'}{r} - \frac{\Delta u}{r \ln(r_s/a)} = 0 \quad (\text{A.26})$$

where  $\sigma_r'$  and  $\sigma_\theta'$  are the effective radial and tangential stresses, respectively. Assuming plane strain condition holds, Equation A.26 gives the following general results (Bjerrum et al, 1972):

$$\sigma_r' = C_1 + C_2 r^{-2} + \frac{\Delta u \ln r}{2(1-\nu) \ln(r_s/a)} \quad (\text{A.27})$$

$$\sigma_{\theta}' = C_1 - C_2 r^{-2} + \frac{\Delta u (1 + \ln r)}{2(1-\nu) \ln(r_s/a)} - \frac{\Delta u}{\ln(r_s/a)} \quad (\text{A.28})$$

$$\delta_r = \frac{r(1+\nu)(1-2\nu)}{E} \left\{ -C_1 + \frac{C_2}{r^2(1-2\nu)} - \frac{\Delta u \ln r}{2(1-\nu) \ln(r_s/a)} + \frac{\Delta u}{2 \ln(r_s/a)} \right\} \quad (\text{A.29})$$

where

$C_1$  and  $C_2$  are constants to be determined from boundary conditions

$E$  is Young's modulus

$\delta_r$  is the radial displacement

$\nu$  is Poisson's ratio

According to Equation 3.14, the radial stress at  $r = r_s$ , after the borehole is drilled, is

$$(\sigma_r')_{r_s} = \frac{1 - a^2/r_s^2}{1 - a^2/b^2} \sigma_h' \quad (\text{A.30})$$

where  $\sigma_h'$  is the initial effective horizontal stress.

Because the strains and displacements arise from changes in effective stresses, the problem can be analyzed in terms of the increments of stress, regarding the state after the borehole is drilled as the reference state.

The boundary conditions for Equations A.27 through A.29 are:

$$\Delta\sigma_r' = 0 \quad \text{at } r = a \quad (\text{A.31})$$

$$\Delta\sigma_r' = -\frac{1 - a^2/r_s^2}{1 - a^2/b^2} \sigma_h' \quad \text{at } r = r_s \quad (\text{A.32})$$

These boundary conditions, together with Equations A.27 through A.29

give

$$\Delta\sigma_{\theta_{1s}}' = -\frac{1+a^2/r^2}{1-a^2/b^2} \sigma_h' - \frac{\Delta u(1+a^2/r^2)}{2(1-\nu)(1-a^2/r_s^2)} + \frac{\Delta u \{1+\ln(r/a)\}}{2(1-\nu) \ln(r_s/a)} - \frac{\Delta u}{\ln(r_s/a)} \quad (\text{A.33})$$

$$\begin{aligned}
(\delta_{1s})_{r_s} = & \frac{r_s(1+\nu)(1-2\nu)}{E} \left\{ \frac{\sigma_h'}{1-a^2/b^2} + \frac{\Delta u}{2(1-\nu)(1-a^2/r_s^2)} + \frac{\sigma_h'(a^2/r_s^2)}{(1-2\nu)(1-a^2/b^2)} \right. \\
& \left. + \frac{\Delta u(a^2/r_s^2)}{2(1-\nu)(1-2\nu)(1-a^2/r_s^2)} - \frac{\Delta u}{2(1-\nu)} + \frac{\Delta u}{2 \ln(r_s/a)} \right\} \quad (A.34)
\end{aligned}$$

where

$\Delta\sigma_{\theta}'_{1s}$  is the change in tangential stress in Cylinder 1 due to seepage forces

$(\delta_{1s})_{r_s}$  is the displacement at the outer boundary of Cylinder 1 due to seepage forces

#### Derivations of Equations 3.21 and 3.22

These equations define the change in tangential stress in Cylinder 1 and the deformation at the outer boundary of the same cylinder due to restraint pressure  $p$ .

The boundary conditions are:

$$\Delta\sigma_r' = 0 \quad \text{at} \quad r = a \quad (A.35)$$

$$\Delta\sigma_r' = p \quad \text{at} \quad r = r_s \quad (A.36)$$

The boundary conditions, together with Equations A.27 through A.29, without the pore pressure terms, give

$$\Delta\sigma_{\theta}'_{lp} = p \frac{1 + a^2/r^2}{1 - a^2/r_s^2} \quad (A.37)$$

$$(\delta_{lp})_{r_s} = -\frac{r_s(1+\nu)(1-2\nu)}{E} \left\{ \frac{p}{1-a^2/r_s^2} + \frac{p(a^2/r_s^2)}{(1-2\nu)(1-a^2/r_s^2)} \right\} \quad (A.38)$$

where

$\Delta\sigma_{\theta}'_{lp}$  is the change in tangential stress in Cylinder 1 due to restraint pressure  $p$

$(\delta_{lp})_{r_s}$  is the displacement at the outer boundary of Cylinder 1 due to restraint pressure  $p$ .

Derivations of Equations 3.23 and 3.24

These equations define the change in tangential stress in Cylinder 2 and the displacement at the inner boundary of the same cylinder due to restraint pressure  $p$ .

According to Equation 3.14, the radial stress at  $r = r_s$ , after the borehole is drilled, is

$$(\sigma_r')_{r_s} = \frac{1 - a^2/r_s^2}{1 - a^2/b^2} \sigma_h' \quad (\text{A.39})$$

Because the initial stress is released and restraint pressure  $p$  is applied on the inner boundary of Cylinder 2, the boundary conditions are:

$$\Delta\sigma_r' = p - \frac{1 - a^2/r_s^2}{1 - a^2/b^2} \sigma_h' \quad \text{at } r = r_s \quad (\text{A.40})$$

$$\Delta\sigma_r' = 0 \quad \text{at } r = b \quad (\text{A.41})$$

The above boundary conditions, together with Equations A.27 through A.29 give

$$\Delta\sigma_{\theta 2p}' = -\frac{r_s^2/b^2 + r_s^2/r^2}{1 - r_s^2/b^2} \left( p - \frac{1 - a^2/r_s^2}{1 - a^2/b^2} \sigma_h' \right) \quad (\text{A.42})$$

$$(\delta_{2p})_{r_s} = \frac{r_s(1+\nu)(1-2\nu)}{E} \left\{ \frac{1 + (1-2\nu)r_s^2/b^2}{(1-2\nu)(1-r_s^2/b^2)} p - \right.$$

$$\left. \frac{1+(1-2\nu)r_s^2/b^2}{(1-2\nu)(1-r_s^2/b^2)} \frac{1 - a^2/r_s^2}{1 - a^2/b^2} \sigma_h' \right\} \quad (\text{A.43})$$

where

$\Delta\sigma_{\theta 2p}'$  is the change in tangential stress in Cylinder 2 due to restraint pressure p

$(\delta_{2p})_s$  is the displacement at the inner boundary of Cylinder 2 due to restraint pressure p

APPENDIX B. LIST OF SYMBOLS

English Letters

a	borehole radius
A	area
A	Skempton's pore pressure parameter
b	sample radius
B	Skempton's pore pressure parameter
c'	effective cohesion intercept
C	constant
C <sub>b</sub>	material bulk compressibility
CD	consolidated-drained
C <sub>r</sub>	material matrix compressibility
CU	consolidated-undrained
D	diameter
e <sub>o</sub>	initial void ratio
E	Young's modulus
G <sub>s</sub>	specific gravity
h, H	pressure head
h <sub>o</sub>	previous pressure head
i	hydraulic gradient
k	permeability
k <sub>h</sub> , k <sub>v</sub>	horizontal and vertical permeabilities, respectively
k <sub>s</sub>	saturated permeability
K	slope of isotropic rebound or recompression curve
K <sub>o</sub>	coefficient of earth pressure at rest
L	length
m	transformation ratio

m	rate of pressurizing
M	strength parameter, slope of line describing variation of $q_f$ with $p'$
n	porosity
p	pressure
p	restraint pressure
$p'$	effective mean normal stress
$p_r$	reference pressure
$p_o'$	effective overburden pressure
$p_o'$	effective stress where yield surface intersects the $p'$ axis
q	flow rate
$q_f$	value of generalized deviatoric stress at failure
r	radial distance from center of borehole
$r_s$	radius of seepage zone
$r_{so}$	radius of previous seepage zone
S	degree of saturation
$S_o$	initial degree of saturation
$S_f$	threshold degree of saturation at which water in pores begins to flow freely
t	time
$t_{inc}$	time increment
$t_o$	previous time
$u_f$	hydraulic fracturing pressure
$u_o$	initial pore pressure
$v_d$	discharge velocity
$v_s$	seepage velocity
$w_c$	compaction water content

### Greek Letters

$\alpha$	porous elastic parameter
$\alpha$	stress factor
$\beta$	stress factor
$\gamma$	total density
$\gamma_d$	dry density
$\lambda$	slope of virgin isotropic consolidation curve
$\nu$	Poisson's ratio
$\sigma_1, \sigma_2, \sigma_3$	major, intermediate, and minor principal total stresses, respectively
$\sigma_1', \sigma_2', \sigma_3'$	major, intermediate, and minor principal effective stresses, respectively
$\sigma_r', \sigma_\theta'$	effective radial and tangential stresses, respectively
$\sigma_t$	tensile strength
$\sigma_v, \sigma_h$	total vertical and horizontal stresses, respectively
$\sigma_v', \sigma_h'$	effective vertical and horizontal stresses, respectively
$\sigma_x, \sigma_y, \sigma_z$	total stresses in x, y, and z directions, respectively
$\phi'$	effective friction angle
$\delta$	displacement
$\Delta u$	excess water pressure
$\Delta u_f$	excess water pressure required to cause hydraulic fracturing
$\Delta\sigma_r', \Delta\sigma_\theta'$	changes in radial and tangential effective stresses, respectively

**END**

**FILMED**

**DTIC**